Magnetic Fields inside Extremely Fast Shock Waves

Jorrit Wiersma
2007

ISBN 978-90-393-4532-0

Magnetic Fields inside Extremely Fast Shock Waves

Magnetische velden in extreem snelle schokgolven

(met een samenvatting in het Nederlands)

Proefschrift

ter verkrijging van de graad van doctor aan de Universiteit Utrecht
op gezag van de rector magnificus, prof.dr. W.H. Gispen,
ingevolge het besluit van het college voor promoties
in het openbaar te verdedigen op
dinsdag 29 mei 2007 des ochtends te 10.30 uur

door
Jorrit Wiersma
geboren op 7 mei 1977
te de Bilt

Promotor: Prof.dr. A. Achterberg

Dit proefschrift werd (mede) mogelijk gemaakt met financiële steun van de Nederlandse Onderzoekschool voor Astronomie (NOVA).

Preface

The world around us is made up of microscopic particles. Solid objects may appear solid and the air we breath may appear intangible, but both are made up of atoms and molecules, the only difference being how strongly they are held together. It has always fascinated me how almost all physical phenomena can be explained as the interaction between particles. How even the light of the Sun is produced from the energy that is freed as particles deep inside the Sun fuse together.

This fascination is the reason why the subject of my PhD research appeals to me. My research also concerns the interaction of particles, although the particles considered here have extraordinary properties. They travel almost with the speed of light, something that Earthly particles do not do outside of man-made laboratories. And they are part of a plasma: a gas of electrically charged particles, such as the gas inside a fluorescent lamp or in the Earth's upper atmosphere.

But what really makes these particles interesting is that, together, they form a shock wave, whose interaction with the interstellar material produces so much radiation that, although they can be billions of light years distant, they briefly become the brightest sources of gamma-rays in our sky. I have spent five years at the University of Utrecht investigating how these particles would interact according to the theories of modern-day physics to help explain how they produce the radiation that we see.

In this thesis [99][1] I present the results of my research. I have tried to structure it in a convenient way for you, the reader. There are three parts. The first part contains an introduction, in which I explain the physical principles that are important for the subject matter of the rest of my thesis. I have tried

[1] Numbers in square brackets refer to entries in the bibliography included near the end of this thesis.

to keep it understandable for everyone, even if you do not have a background in physics or astronomy. If you do have a background in astronomy then it may serve as a refresher. The second part contains the results of my research. Most of the chapters in this part are also published in (or submitted to) the professional European astronomy journal Astronomy & Astrophysics. Therefore, the text is aimed at astronomers who are at home with the subject matter. I have preceded each chapter with a short summary of its contents and an indication of its relation to the other chapters. This should provide you with enough information to skim these chapters and to just read the details you are interested in. The third and last part contains a discussion of the conclusions that I draw from the results of my research. It also contains a summary in Dutch and a curriculum vitae.

The five years at the 'Sterrekundig Instituut Utrecht' have been very pleasant and I would like to use this opportunity to thank everyone for the good time. In particular, I would like to thank Bram for his guidance as my promotor. Whenever I had a question he was available to help and as far as I can remember he could always point me to some article or a chapter in some book to provide me with more information. I would also like to thank Marc, Pui Kei, Jeroen and Sung-Chul, who were my roommates during (part of) my time at the Institute. Thanks also go to Marion for doing so much for the institute, especially organizing the social activities such as Sinterklaas and the game evenings. And also thanks to Rob Rutten, for being a fun professor to assist in his courses and for keeping me, a little bit, involved with the solar physics research. Thanks to Selma, Evert, Cees and Gemma for the good times at the game evenings and to Axel for the good times in general.

Most thanks of all and a lot of love go to my wife Saskia. I can imagine that sitting next to me when I was working on my thesis with my laptop on the couch wasn't the most romantic thing imaginable. Yet you did so much to give me the time I needed to finish it.

The illustration on the cover was made by my five-year-old daughter Silke on 24 February 2007 and is a *Zon die kapot is* ('Sun that is broken'), which is how we tried to describe the subject of my research to her.

Contents

Part I

Introduction

Chapter 1

Overview

During my period as a PhD student (2001–2006) my promotor Bram Achterberg and I have investigated the predictions that current physical theories give about the properties of shock waves that move almost with the speed of light. These shocks are produced in the tenuous gas that pervades deep space (the *interstellar medium*) by catastrophic events such as exploding massive stars. We have looked at how strong electrical currents can form in such shocks through the magnetic interaction of charged particles. This thesis presents the results of this research.

This first part introduces the subject, starting with chapter 2 in which I explain why the subject of my thesis is important.

In chapter 3 I summarize the basic physics needed the understand the rest of my thesis: the physics of shock waves, relativity theory, electricity and magnetism and the Weibel plasma instability.

In chapter 4 I give an introduction to Gamma-ray Bursts, an astronomical phenomenon that is probably produced by the kind of shock waves that I describe in this thesis.

In part II I present the results of my research. I start with the large-scale structure of extremely fast shock waves (chapter 5). The rest of my research has focused on the Weibel plasma instability, a mechanism that generates magnetic fields inside extremely fast shock waves. We have investigated this mechanism by solving the mathematical equations that describe the dynamics of the particles in the shock front analytically (chapters 6–9) and by simulating the dynamics of the particles in the shock wave, and their associated electromagnetic fields, with the help of computers (chapter 10).

In part III I discuss the conclusions that we draw from our research, summarizing how electrical currents and magnetic fields are spontaneously generated in the shock wave by the interaction of charged particles and what this means

for models that try to explain how Gamma-ray Bursts are formed. I also discuss the limitations of our research and how future research can advance the field.

Part III also contains a summary of this thesis in Dutch and a Curriculum Vitae.

Chapter 2

Relativistic Shock Waves and Magnetic Fields

Fast shock waves occur in the tenuous gas that pervades deep space (the *interstellar medium*) around catastrophic events such as exploding massive stars. When the shock waves are so strong that they reach speeds close to the speed of light we call them *relativistic* shock waves because the effects described by Relativity Theory become important for their dynamics. Such extremely fast shock waves form an important part of the favored explanation for the high-energy radiation (X rays and gamma rays) and particles (cosmic rays) produced in and around several astronomical phenomena, such as Gamma-ray Bursts, Pulsar Winds, and Active Galactic Nuclei.

Because relativistic shock waves occur around sources at great distances from the Earth and the solar system, much is still unclear about the physical processes in and near them. The typical length scale[1] on which the processes that I have studied take place is more than a kilometer, making them too large to study directly in the laboratory. Theoretical research such as my PhD research provides predictions about the physical processes in relativistic shocks. These predictions can then be tested by astronomical observations or by laboratory experiments on a smaller scale.

Relativistic shocks will form when a very fast outflow of matter interacts with material surrounding the object. Such a very fast outflow can be produced, for example by an exploding massive star or by a very compact, rapidly spinning energetic object like a pulsar or a black hole.

At the front of the shock wave a violent change in pressure and temperature takes place. It causes the material that it leaves behind to glow brightly,

[1] Here, with *typical length scale* I mean the plasma skin depth.

producing among others high-energy radiation like X rays and gamma rays. Although the interstellar medium is very tenuous, and the compressed gas left behind by the shock is as well, the effect of relativistic shocks is strong enough to produce radiation that is visible on Earth even from the distant universe.

The gas in the shock front consists of atoms, ions and electrons. These particles are very small, and because the gas is so tenuous the particles rarely collide with each other. Instead, they interact through electromagnetic forces because they are electrically charged. Therefore, we refer to such shock waves as *collisionless shocks*. Because the force between individual particles is very weak, relativistic shocks must form by the collective interaction of large groups of these particles. This thesis is mostly concerned with these collective interactions.

Observations of astronomical objects that involve relativistic shocks show that magnetic fields play a key role. Due to the large speed of the shock, concentrations of charged particles produce strong electrical currents and magnetic fields. The magnetic fields act as a catalyst allowing the particles in the shock to use the outflow energy to produce radiation and particle emissions.

To investigate the formation of these electrical currents I have looked at the collective behavior of the different particle populations in a shock front: shocked and unshocked electrons and protons. This can, eventually, give a complete description of the formation and the structure of the shock, but with current techniques it is impossible to create complete models for the whole shock transition from interstellar medium to post-shock medium. Our models apply to the very start of the shock transition, and serve as a starting point for further investigations into the rest of the structure of relativistic shock waves.

We have found that the generation of magnetic fields through the formation of electrical currents is a general phenomenon in the initial phase of the shocks. The electrical currents that produce the magnetic fields can consist of electrons and of heavier charged particles such as protons, but when both kinds of particles are present, the strength of the proton currents is limited by the presence of the electrons.

Much remains unclear, however. Astronomical observations only provide indirect clues about these shock waves because we can only compare them to *models* for the sources of high energy radiation and cosmic rays. Laboratory experiments cannot reach the scale of astronomical phenomena. Theoretical research, such as the research that I present in this thesis, can provide the glue needed to make further progress, by connecting results from these two fields[2].

[2]This has also recently been discussed by Medvedev [57].

Chapter 3

Basic Physics

In this chapter I introduce the basic physical concepts concerning shock waves, relativity theory and electromagnetism. At the end of this chapter (section 3.4) I give an introduction to the Weibel plasma instability, which is a mechanism that can generate magnetic fields in relativistic shock waves. In the rest of my thesis I work out the properties of the Weibel instability in relativistic shock waves in more detail.

3.1 Shock waves

> [A shock wave is a] strong pressure wave in any elastic medium such as air, water, or a solid substance, produced by supersonic aircraft, explosions, lightning, or other phenomena that create violent changes in pressure. Shock waves differ from sound waves in that the wave front, in which compression takes place, is a region of sudden and violent change in stress, density, and temperature. Because of this, shock waves propagate in a manner different from that of ordinary acoustic waves. In particular, shock waves travel faster than sound, and their speed increases as the amplitude is raised; but the intensity of a shock wave also decreases faster than does that of a sound wave, because some of the energy of the shock wave is expended to heat the medium in which it travels.
>
> From: *Encyclopaedia Britannica*

Waves are collective motion: they only exist through the collective behavior of a large amount of particles. Take the example of the wave that travels through a rope when you flick one of its ends. The disturbance travels from the end that you flicked to the other because each part of the rope passes the disturbance on to the next. In this sense, wave motion is very different from the motion of a projectile or the flow of water: as long as the wave's amplitude is small, the rope itself will not have moved once the wave has passed. Rather, it is the disturbance that moved through it.

Sound and shock waves are examples of pressure waves. Some source, such as the human vocal cords or an explosion, produces a disturbance of the local pressure in an elastic medium (such as air) and this disturbance is passed on to the surrounding medium, thus traveling outwards. Although this disturbance travels very fast (the speed of sound is of the order of a thousand kilometers per hour) the particles in the air barely move (during normal speech, the typical flow velocity of the involved air is only one fiftieth of a centimeter per second). Therefore, when a typical sound wave has passed it leaves the properties of the air practically unchanged.

However, when the intensity of a sound wave is very high (well above the human pain threshold), the effect on the air it passes through becomes noticeable, typically in the form of what is called *radiation pressure* pushing away from the source of the sound (this phenomenon is often exaggerated for humorous effect in TV ads or in music videos in which huge loudspeakers blow away everything in front of them).

When the source of the waves involves an even stronger pressure disturbance (for example, due to an explosion) it produces a *shock wave* that causes a noticeable change in the medium through which it travels. Instead of having a smooth wave profile, a shock wave consists of a sharp change in pressure in a narrow region.

Such a sharp change is formed in strong waves because they involve very strong disturbances of the pressure. Because the velocity of each part of a wave depends on the pressure, it influences its own velocity. The points of the wave where the pressure is highest move faster than the rest of the wave causing a pile-up of wave fronts. The result is that the pressure and temperature increase sharply at the front of the wave. As stated in the quote at the start of this section, such shock waves have higher velocities than normal sound waves, with stronger waves traveling faster. The shock waves that I discuss in this thesis are so extremely strong that they even approach the light speed.

3.2 The theory of relativity

The speed of light (or of any electromagnetic wave) is special in the sense that the speed of light is a universal constant. Normally, the perceived velocity of a wave (or any velocity) will depend on the velocity of the observer: when you are surfing near some tropical island, the waves will seem to be almost at rest with respect to your surfboard, even though they are crashing on to the beach with high velocities. The big exception are light waves: the speed of light in free space is a constant, independent of the velocity of the observer. When Einstein formulated his relativity theory this was one of his postulates and it has since been confirmed by physical experiments like the Michelson–Morley experiment and subsequent work[1].

Considerations of whether and how the laws of physics change when you compare observations of observers moving relative to each other, are what is denoted by the term *relativity theory*. In 1905 Einstein worked out the consequences of the fact that the velocity of light is independent of the motion of the observer if you assume that all physical laws should be the same for all observers that move inertially (without being accelerated). This theory is usually referred to as the *special* theory of relativity[2]. Some of its consequences are counter-intuitive. For example: events that happen simultaneously for one observer do not necessarily happen simultaneously for another; no matter how

[1] For a historical perspective see [71]

[2] Einstein also formulated a *general* theory of relativity in 1915, which connects the phenomenon of gravitational attraction with the structure of space and time

much energy you give to an object, it can never go faster than light; and mass and energy turn out to be interchangeable quantities.

The fact that the speed of light is constant means that if a surfer turns on a flash light, then he sees the light flying away from him with *exactly* the same velocity as someone who is at rest on the beach. Even though these two observers move relative to each other they assign equal velocities with respect to themselves to the *same* light beam. In everyday life we do not notice such curious effects because the speed of, say, a typical surfer (of the order of 10 to 20 kilometers per hour) is much smaller than the speed of light (of the order of a billion kilometers per hour). In the case of a shock wave moving almost at the speed of light, however, the effects become significant. From the point of view of the shock wave any light emitted by the particles in the shock wave is flying away from it with the speed of light, but to a distant observer who is at rest the relative speed between the shock and the light emitted by it seems to be very small. The perception of space and time is very different from the point of view of someone moving with the shock and from the point of view of a distant observer.

The rest of this section discusses some of the consequences of the relativity of space and time to keep in mind when considering the physics of relativistically moving shock fronts.

3.2.1 The light cone

In any system of particles (for example, the particles in a shock front), the velocity of light is an upper bound on both the velocities of the particles and on the speed at which physical interactions between particles can take place. This means that, given a certain time span into the future, only a certain region of space around each particle is causally connected to it: within that time span a particle can only influence other particles that fall within this region. Similarly, given a time span into the past, only a certain region of space around a particle can have influenced it. These regions are called the *light cone* of a particle (because they are cone-shaped in a space–time diagram).

The light cone puts a limit on the size of a fluctuating phenomenon. Because it is unlikely that parts of an object fluctuate in the same way unless they are causally connected, the object cannot be larger than the distance light travels on the timescale of the fluctuations. We use this, for example, to estimate the size of the source of Gamma-ray Bursts in chapter 4.

3.2.2 Proper time and proper density

One of the consequences of the relativity of space and time is *time dilation* (or *time dilatation*). A relativistically moving particle experiences time differently from observers at rest. At each instantaneous point in time the rate of the particle's clock is different from the observer's clock. Time as it is experienced by the particle itself is called the *proper time* of the particle. At each point in time the observer will see the proper time of the particle running slow with respect to the observer's own clock by a factor equal to the instantaneous Lorentz factor, denoted by γ and defined by

$$\gamma = \frac{1}{\sqrt{1 - v^2/c^2}}, \tag{3.1}$$

where v/c is the ratio of the speed of the particle and the light speed. The physical processes that happen in a frame of reference that moves with respect to the observer therefore occur in slow-motion from the point of view of the observer.

I should note, however, that the *observed* effect is different if the source is moving directly towards the observer with a speed close to the light speed. The source then moves towards the observer with about the same speed as the light it emits. Because each subsequent photon travels a shorter distance to the observer, the light emitted over a certain time-span arrives at the observer in a much shorter time span. After correcting for the time dilation mentioned in the previous paragraph, the net effect is that the observed fluctuations in the light from a relativistic shock moving towards us happen *faster* than in the rest frame of the shock.

Another relativistic effect is that lengths along the direction of movement are compressed. If two particles are at a certain distance L from each other along their direction of movement (as perceived by the particles) then to a stationary observer they will seem to be closer to each other by the Lorentz factor in equation (3.1):

$$L_{\text{observed}} = L/\gamma. \tag{3.2}$$

Distances perpendicular to the direction of movement are not compressed.

This also means that the number density (the number of particles per unit volume) of a group of particles with a certain average velocity will seem to be larger by a Lorentz factor than the number density in the frame of reference in which their average velocity is zero, which we call the *proper density*. After all, smaller apparent distance between the particles means higher apparent density.

3.2.3 Relativistic Doppler shift

The fact that space and time are different for particles with different velocities means that they also see the wavelength and frequency of (light) waves differently.

The cause of the classic Doppler effect is that if you move with respect to the source of a wave then you will see the wave crests passing you with a different frequency than the source frequency. This is what causes the siren of an ambulance to appear to change pitch as the vehicle passes you by.

If the relative velocity between the observer and the source of the wave is large enough, relativistic effects will happen on top of these classical Doppler effects. The number of wave crests in a wave is an absolute quantity, but since time and space are different for observers with different velocities, this absolute number of wave crests must fit in a different time or length span for different observers. In particular, the time difference means that the frequency of the wave is even different if the observer is moving perpendicularly to the wave.

These effects on the appearance of a wave are called the *relativistic Doppler shift* and will affect the observed spectral energy distribution of the radiation from relativistic shocks.

3.2.4 Relativistic momentum and energy

Conservation of momentum and energy is a basic postulate of physics. Energy measures the capacity of an object to do work and depends (among other things) on the velocity of the object: a fast moving car has the potential of causing a more catastrophic accident than a slow moving car[3]. Momentum is a measure of the direction and magnitude of the motion of an object. In particular, it measures how much force would be needed to be applied for how long in which direction to bring the object to rest[4].

Because energy and momentum depend on the velocity of a particle and therefore on the space–time reference frame of the observer (because velocity measures the distance traveled by an object through space during a certain time) the definitions of energy and momentum have to be adapted in situations where relativity theory applies to make sure that conservation of energy and momentum still holds for all observers. Both theory and experiment show that the momentum of a relativistically moving particle is like the momentum of

[3]One could even say (like the author of the entry on *energy* in the Encyclopaedia Britannica) that all energy is associated with some kind of motion, either potentially or actually.

[4]In mathematical terms, energy is the spatial integral of the force applied to a particle (along the path of the particle), and momentum is the temporal integral of the force.

a non-relativistic particle but that its mass m seems to be larger than its rest mass m_0 by a Lorentz factor. Its energy E is given by the famous equation

$$E = mc^2 = \gamma m_0 c^2, \tag{3.3}$$

where c is the light speed and again its mass m is larger than its rest mass m_0 by a Lorentz factor (see equation 3.1). The particle always possesses a certain amount of energy, even when it is at rest. This energy m_0c^2 is called the *rest energy* of the particle.

Note that the Lorentz factor, and therefore also the energy and momentum of a particle, become infinite as the particle's velocity approaches the speed of light. This means that it costs more and more force to change a particles velocity or its direction of motion as it approaches the speed of light.

3.3 Electricity and Magnetism

> Electricity is the phenomenon associated with positively and negatively charged particles of matter at rest and in motion, individually or in great numbers. [...] Because every atom contains both positively and negatively charged particles, electricity cannot be divorced from the physical properties of matter, which include such diverse phenomena as magnetism, conductivity and crystal structure; from chemical reaction; or from the waves of electromagnetic radiation, which include visible light.
>
> From: *Encyclopaedia Britannica*

The particles making up the shocks that I discuss in this thesis are charged, and their behavior is dominated by electromagnetic effects.

Electricity concerns the attractive or repelling force between charged (electrified) bodies. Separating opposite charges requires work resulting in potential energy (*electric energy*) that can be released by bringing the charges together again. This can happen in the form of a spark jumping between the charged bodies or in the form of a flow of charges through a conducting material connecting the bodies. The tendency of an electric charge to attract opposite charges (or to repel same charges) is often represented as a force field around the charge: the *electric field*.

Magnetism concerns the force between electrical currents. However, most people will be more familiar with the magnetic forces working between magnetic dipoles such as the Earth magnetic field and a compass needle. The magnetic force tends to (anti-)align magnetic dipoles (or rather, it tends to align a (small) magnetic dipole with the local direction of the *magnetic field*) causing a compass needle to always point to the (magnetic) north pole of the Earth. Magnetic dipoles involve rotating charges (that is, closed electrical current loops) and the forces between these current loops cause the magnetic effects. The magnetic force causes parallel currents to attract one another and anti-parallel currents to repel.

One of the most important experimental discoveries in the field of electromagnetism, by Michael Faraday (1791–1867), was that just as electrical currents produce magnetic effects, changing magnetic fields produce electrical effects that can drive an electrical current (this phenomenon forms the basis of simple dynamos). In addition, it was found that a changing electric field (often referred to as a *displacement current*) also produces magnetic effects, a phenomenon that was first hypothesized by Maxwell in 1865 to complete his theory of electromagnetism. These two discoveries showed the strong connection

between electric and magnetic phenomena and led to the theory of electromagnetic energy conservation (known as Poynting's Theorem, 1884), which led to the conclusion that both electricity and magnetism are forms of energy. The sum of all the effects just described ensures that charged particles and their associated electric and magnetic fields form an energy conserving system.

Because electric and magnetic phenomena are associated with charged particles respectively at rest or in motion, we have to be especially careful about frames of reference when discussing electromagnetic interactions. The charge of a particle is independent of its velocity as far as experiments have been able to determine[5]. But a particle that is at rest with respect to one observer will be seen to be in motion by another observer who moves with respect to the first. As a result, even for observers moving non-relativistically the electromagnetic fields they see will be different.

3.3.1 Light

Light is a form of energy that travels freely[6] through empty space (with a constant speed of 299 792 458 m/s).

It was Maxwell (in 1865) who presented a theory that light and radiant heat are electromagnetic disturbances in the form of waves. The laws Maxwell developed prescribed that in empty space a change in the electric field strength must always be accompanied by a change in magnetic field strength in such a way that an electromagnetic disturbance can propagate freely through (empty) space. This opened the possibility of self-sustaining electromagnetic waves in free space with exactly the same wave velocity as the experimentally determined velocity of light. Since then it is generally accepted that light is simply a particular form of electromagnetic radiation.

3.3.2 Charged Particles in electromagnetic fields

Much of my thesis is concerned with the behavior of charged particles in electromagnetic fields (which are formed by the surrounding particles).

The effect of an electric field on a charged particle is to accelerate (or decelerate) it. This way, an electric field also increases (or decreases) the kinetic energy of charged particles.

[5] Whereas the (effective) mass of a particle depends on its velocity (relative to the observer). See the previous section.

[6] Most other forms of energy can only be transported by transport of the matter associated with them.

The effect of a magnetic field on a charged particle is to change its direction of motion. However, magnetic fields do not change the speed of the particle and therefore do not (directly) influence its energy. The way in which a magnetic field deflects the trajectory of a charged particle is such that in a *homogeneous, constant* magnetic field the particle will spiral around magnetic field lines (but its velocity parallel to the field lines is not influenced).

A (moving) charged particle will induce electric and magnetic fields around it. This way, charged particles can interact. When the particles move with respect to each other with a relativistic velocity one has to take into account that these electromagnetic fields propagate with the finite velocity of light. Therefore the fields at one particle depend on the position of the other particle at an earlier time. This contrasts with the non-relativistic interaction, which can be considered to be instantaneous. (See also the discussion of the *light cone* in section 3.2.1).

3.3.3 Interaction of particles and electromagnetic radiation

One of the basic properties of charged particles is that they emit electromagnetic radiation when they are accelerated. Every charged particle causes electromagnetic fields in its surroundings, but the electromagnetic field of an *accelerated* charge becomes an electromagnetic wave far away from the particle. Through this emission of radiation the accelerated particle loses energy. This happens both when their velocity is increased or decreased (acceleration along the direction of the particle's motion) and when their trajectory is deflected (acceleration perpendicular to the particle's motion).[7]

The radiation is emitted roughly perpendicularly to the direction of acceleration for a particle that moves non-relativistically. When a particle moves relativistically, the transformation of space-time from its rest frame to the observer frame causes the emission to be skewed towards its direction of motion. When the Lorentz factor is noticeably larger than unity, this relativistic effect dominates the emission pattern and practically all the emission is concentrated within a narrow angle (in radians of the order of one divided by the Lorentz factor) with the direction of motion.

Also, for a relativistic particle the power radiated for a force applied perpendicularly to the particle's direction of motion is the square of the Lorentz factor larger than for the same force applied in parallel. So for *very* relativistic particles the acceleration perpendicular to the direction of motion is the determining factor for the emitted radiation.

[7] Jackson [41], chapter 14 discusses radiation by moving charges in more depth.

We can observe relativistic shock waves through the radiation that the particles in the shock wave emit as they are accelerated by their interaction. Especially when the particles produce the radiation through their collective electromagnetic interaction (groups of particles interacting; see the next section) will the emitted radiation be visible.

When charged particles interact with electromagnetic waves that were generated by some other source, they will scatter these waves. The wave fields coming from the external source will cause the particle to oscillate so that the particle absorbs energy. The corresponding acceleration of the particle will, however, cause it to emit radiation and the particle loses part or all of the absorbed energy again. This also happens in shock waves when the radiation from particles behind the shock front is scattered by the particles inside the shock front.

3.4 The Weibel or filamentation instability

In a shock wave moving almost with the speed of light, the magnetic interaction of the particles will be more important then their electric interaction. There are two reasons for this. Firstly, electrical currents induce magnetic fields and charged particles moving at such large velocities can produce strong electrical currents. Secondly, the magnetic force (Lorentz force) on a charged particle is also proportional to its speed. In other words, the charged particles in an extremely fast shock wave can produce strong electrical currents that will interact strongly through their magnetic fields.

This strong magnetic interaction will cause the plasma to become unstable. The starting situation may be in equilibrium, but a small perturbation of the plasma will quickly grow much stronger. This is similar, for example, to a ball on top of a hill. As long as the ball lies still, nothing will happen, but if you give the ball a small push it will quickly roll down the hill faster and faster. As I will explain below, in a fast moving shock front in outer space a small disturbance of the magnetic field will quickly grow in strength in the same way.

This unstable magnetic interaction can provide a way for the particles to dissipate energy in the shock front. As a shock front plows through the material in front of it, its kinetic energy forms a source of free energy. Random interactions of the particles in the shock front can dissipate this energy, causing the gas in the shock front to heat up, to become magnetically charged and to emit radiation.

This phenomenon is known as equipartition of energy: initially, all the energy is in the movement of the particles along the propagation direction of the

shock wave, but random processes have the tendency to distribute this energy over all the available degrees of freedom of the system. In a system of charged particles these degrees of freedom are thermal motions of the particles and the electromagnetic field.

To reach conditions with a magnetic energy density that is comparable to the total energy density in the shock wave the charged particles in the shock must generate magnetic fields *collectively*. Whether, and how, this might be possible is the main subject of this thesis. The main idea is that the charged particles (collectively called a *plasma*) in the shock wave are unstable in such a way that a small concentration of the charged particles will quickly grow. Because of the high velocity of the particles, this charge concentration will produce a strong electrical current, which deflects more and more charges towards it through the magnetic field that it generates.

The electrical currents that correspond to the random concentrations of charge in the plasma merge because parallel currents attract each other. This process cannot go on indefinitely: at some point the magnetic forces become so strong that they would disrupt the motion of the particles that make up the electrical currents themselves if they were to grow stronger. The end result of the whole process is that plasma in the shock breaks up into filaments, each carrying a strong electrical current. You can see this clearly in the computer simulations in chapter 10.

This mechanism is known as the filamentation instability (often also called the Weibel instability) and can cause the magnetic field to quickly grow in strength. The strength of the magnetic field produced by the instability depends on the size of these filaments. We can make a simple estimate by using the Biot-Savart law for magnetic fields: this law states that the magnetic field strength B produced by an electrical current I that is contained in a filament of size d will be

$$B = \frac{2I}{cd}, \tag{3.4}$$

here c is the speed of light. When the number density of relativistically moving charged particles with charge q is n then the electrical current contained within a cylinder of radius d is $I = qn\pi d^2 c$ so that the magnetic field at the edge of the cylinder is

$$B = 2\pi qnd. \tag{3.5}$$

Although this is a very coarse estimate of the strength of the magnetic field that can be produced, we can see that, in theory, larger filaments (larger d) can produce stronger magnetic fields (larger B). In chapters 8 and 9 we give more

sophisticated estimates of the magnetic field strength and we show how the plasma in the shock wave (the electrons in particular) determines the maximum size of the filaments.

In 1959 Erich S. Weibel proved the existence of this kind of self-excited transverse electromagnetic waves in plasmas having velocity distributions that deviate from an isotropic distribution, and Burton D. Fried explained the mechanism of their formation [98, 25]. In the 1970s the first computer simulations of these mechanisms were presented, for example by Davidson *et al.* [16], who showed that the amplitude of the instability is limited by magnetic trapping of the particles taking part in the instability, and by Lee & Lampe [52], who showed that the instability causes filamentation of plasma beams and subsequent recombination into larger filaments. These results were confirmed in more detail by Yang *et al.* [104] in 1994. The first fully 3D computer simulations of the Weibel instability were done by Fonseca *et al.* at the start of this century [21] and after that Frederiksen *et al.* simulated how the Weibel instability can develop in a (relativistic) shock front [24]. In their PhD theses Hededal [35] and Haugbølle [34] present larger computer experiments that are working towards covering the full shock ramp.

The Weibel instability is also of interest to laboratory experiments involving a high-power laser that produces a relativistic beam of electrons. Although Silva *et al.* [89] showed that the effect in practical applications is probably low, Wei *et al.* [97] detected the filamentation of electron beams in an actual experiment.

In astrophysics, there are several applications of the Weibel instability: in pulsar winds [45], in the jets of active galactic nuclei (AGN) [69], and in cold fronts [70] and shocks [87, 26] in galaxy clusters. Medvedev & Loeb [58] and Brainerd [9] suggested that the Weibel instability can also help to explain the radiation mechanisms responsible for Gamma-ray Bursts and their afterglows (see also the next chapter). The role of the Weibel instability in this scenario is to produce magnetic fields, and the rest of my thesis discusses this subject in more detail. I should note that it is still unclear whether these magnetic fields can survive long enough to really explain Gamma-ray Bursts. For example, Gruzinov [31] presented arguments why they might not, but Jaroschek *et al.* [42] presented arguments in favor.

In chapter 6 we discuss how the Weibel instability starts with the spontaneous generation of magnetic fields. In chapter 7 we show that the associated electrical currents will mainly be directed perpendicularly to the shock front. In chapter 8 we estimate that the magnetic energy density will reach about 0.01 % of the total energy density in a typical shock wave (see section 8.3.3). In

chapter 9 we explain that the attainable magnetic field strength is limited as a result of two mechanisms: firstly, the particles become trapped in the magnetic fields that they generate themselves, and secondly the electrons in the plasma tend to shield the magnetic fields that the protons produce. These effects limit the scale of the magnetic fields that the Weibel instability can produce, basically because the length-scale d in equation (3.5) cannot become very large. We confirm the validity of these results with computer simulations of the behavior of the particles in chapter 10.

The importance of this research is to determine how (the particles in) shock waves moving almost with the speed of light can lose their energy, aided by the Weibel instability, producing radiation with a non-thermal energy distribution. This is known as *collisionless dissipation* because the particles lose their energy not through collisions with each other but through their electromagnetic interaction. In most astrophysical plasmas this is the only way to dissipate energy because the particle densities are so low that collisions between particles are very rare.

A large fraction of the literature concerning relativistic shock waves has concentrated on the application in models for Gamma-ray Burst sources. This is probably attributable to the large amount of astronomical observations of Gamma-ray Bursts (see the next chapter), to which we can compare the theoretical predictions about the evolution of relativistic shock waves. Although much of my thesis discusses general results about relativistic shock waves I will mainly compare my results to what we know from Gamma-ray Bursts for the same reason. Unfortunately, we can draw no firm conclusions yet, and it remains unclear whether the estimate for the magnetic field strength that follows from our results is sufficient to explain the brightness of Gamma-ray Burst sources (see the discussion in chapter 11).

Chapter 4

Gamma-ray Bursts

At the moment, the most important application of the theory of relativistic shock waves is in explaining the radiation from Gamma-ray Burst sources. I will briefly introduce the phenomenon of Gamma-ray Bursts, what we know about them from observations and then discuss the role that relativistic shocks play in the models for the source of Gamma-ray Bursts.

Gamma radiation is a form of light that consists of photons carrying about a million times as much energy as the photons that make up visible light. Because the earth's atmosphere is relatively opaque to gamma radiation (compared to visible light) the detection of gamma radiation from outer space became possible only recently, in the 1970s, through the launch of satellites with gamma-ray detectors on board. Today, special-purpose astronomical satellites detect exceptionally bright bursts of gamma radiation about once a day (usually outshining for a brief time all other sources of gamma radiation in the sky) that seem to come from completely arbitrary directions. We call these strong, one-time bursts *Gamma-ray Bursts* (often abbreviated to GRB). Although it is hard to investigate such an unpredictable phenomenon, there is strong evidence that these Gamma-ray Bursts are formed by the relativistic shocks produced by very strong explosions in the distant universe[1]. In this chapter I will discuss some of the relevant observational evidence and theoretical considerations pointing in this direction[2].

There are several classes of short-lived gamma-ray sources in the sky. As I mentioned in the previous paragraph the strongest of these are the Gamma-

[1]The most distant known Gamma-ray Burst originated from a redshift distance (see footnote 6) $z \sim 6.5$, which means that it was produced when the universe was just one sixth of the age that it is today.

[2]Peter Mészáros wrote a review about this subject in Science [64]. Tsvi Piran wrote two, more technical, reviews [76, 75].

ray Bursts, which are strictly one-time events. There seem to be two classes of Gamma-ray Bursts: *long* ones that typically last longer than a few seconds and *short* ones that last shorter than a few seconds. Although the division between the two classes is not very sharp (and the explanation for both involves relativistic shocks), there is evidence that they are formed by distinct classes of sources. I will come back to this point in section 4.3 below[3]. Another class of transient gamma-ray sources is known as *soft gamma-ray repeaters*. These can sometimes be confused with Gamma-ray Bursts but, unlike Gamma-ray Bursts, are recurring events. The evidence is strong that soft gamma-ray repeaters are neutron stars and therefore quite different from the sources of Gamma-ray Bursts but the possibility exists that they very rarely emit giant flares of gamma radiation that do actually *look like* short Gamma-ray Bursts [39, 51]. Lastly there are, of course, also transient gamma-ray sources that are unexplained. Most of this chapter applies to the class of *long* Gamma-ray Bursts.

[3] Also, Nature recently reported a breakthrough in the observations of short bursts [77, 22].

4.1 Observational facts

We cannot predict when and where a Gamma-ray Burst will occur. Therefore, special purpose satellites have been built that can observe a large part of the (gamma-ray) sky. Examples of such satellites are HETE 2 [48] and SWIFT [29].

Gamma-ray detectors are not very accurate at determining the position of the source of the radiation. However, sources of gamma rays typically also emit a certain amount of X rays. Therefore, these satellites also carry X-ray detectors (and in the case of SWIFT also a telescope that observes ultra-violet light) that are automatically pointed in the (general) direction of any bursts of gamma-rays in order to determine the position of the source more accurately. The positioning information of the detectors is quickly transmitted to Earth so that telescopes on the Earth's surface can try to detect other forms of radiation from the source, such as visible light and radio waves.

Gamma-ray Bursts come from all directions in the sky (Piran [75], section II.C.3). Current detectors typically observe fewer than one Gamma-ray Burst per day, and they are conveniently named after the day they were observed: for instance, the gamma-ray burst observed on 29 March 2003 is named GRB030329.

The initial burst of gamma rays and high energy X rays (the prompt emission) is sometimes followed by an afterglow that can be detected much longer (hours, days or even months after the initial burst) in other wavelength bands (visible light and radio, for example).

During the prompt emission phase most observed Gamma-ray Bursts are, for a fraction of a second to a few seconds, the brightest source in the sky. To be visible from such a large distance, the energy output at the source must be so large that they are the most luminous objects known to exist. The prompt emission can vary wildly, peaking repeatedly on a timescale of fractions of a second. Typically the intensity during each peak rises quickly and falls off more gradually (fast-rise, exponential decay). There is, however, great variety in variability: some Gamma-ray Bursts are just a single (long) peak, whereas others can consist of hundreds of sub-peaks, sometimes interspersed with quiescent periods. The total duration of the Gamma-ray Burst (excluding the afterglow) ranges from a few milliseconds to hundreds of seconds.

The spectral energy distribution of the prompt radiation clearly points to a radiation mechanism that is not thermal: it comprises X and gamma rays spanning a large range of photon energies. For thermal emission the amount of (high-energy) photons falls off exponentially[4] with increasing photon en-

[4]Proportional to $\exp(-\beta E)$ with some constant β.

ergy E, but the high-energy spectrum of Gamma-ray Bursts typically falls off as a (broken) power-law[5] instead. This spectrum quickly deviates many orders of magnitude from the thermal energy distribution.

X-ray satellites and optical and radio telescopes detected Gamma-ray Burst afterglows for the first time in 1997, when the technology became available for pinpointing the Gamma-ray Burst sources quickly [14, 94, 23]. Although X-ray afterglows are practically always detected when a Gamma-ray Burst is located quickly enough, not all Gamma-ray Bursts have a detectable optical afterglow. The reason for this is still unclear (Piran [75], section II.B.3).

When an afterglow is detected, the X-ray afterglow is the strongest signal. The optical (visible light) and radio afterglow are weaker (and therefore harder to detect). The optical afterglow sometimes reaches its peak intensity only a day after the burst, and can typically be detected for a few weeks or longer before it becomes dimmer than the galaxy in which the Gamma-ray Burst source is located. The radio afterglow typically only reaches its peak intensity after a number of weeks, and the brightest afterglows remain visible in radio waves for more than a year.

We usually describe this evolution of the afterglow at different wavelengths as a signature of the progressive cooling of the source: although the total luminosity becomes smaller, a cooler light source will emit more light in low-energy radiation (such as radio waves). However, *cooling* is not really the right word because the spectral energy distribution of the afterglow is distinctly non-thermal (again with a power-law dependence on photon energy that differs widely from a thermal distribution [103, 102]). As I will explain below, we think that the afterglow is produced by shock waves from a large explosion, and that the afterglow fades and 'cools' because the shock wave becomes less vigorous over time.

4.2 Properties derived from observations

With the detection of the optical (visible light) afterglow of Gamma-ray Bursts their location in the sky became known much more accurately than before. In many cases observations showed that the position of the Gamma-ray Burst overlapped with a distant galaxy. Most likely the sources of those Gamma-ray Bursts are located inside those distant galaxies: the chance that the Gamma-ray Bursts are actually in front of the host galaxy and that the superposition is purely coincidental is very small. In a number of cases these galaxies were

[5] Proportional to $E^{-\alpha}$ with some constant α.

bright enough to determine their distance, which then also yields the distance of the Gamma-ray Burst.

The distance of the host galaxy can be determined by an identification of certain features in the spectral energy distribution of its light. When objects are very far away then these features are shifted towards longer wavelengths with respect to their normal position, which is known as *redshift*. This shift is an effect of the expansion of the universe because the light takes a certain time to travel from the source to us[6]. Host galaxies of (long) Gamma-ray Bursts can be very far away: a distance of ten billion light years is not uncommon[7]. Gamma-ray Bursts sources are detected from such great distances so often because of their brightness: there is simply much more space far away from us than close to us. The typical distance of short Gamma-ray Bursts is not well known because they are harder to detect, but evidence is mounting that they are intrinsically dimmer than long Gamma-ray Bursts, and are therefore only detected from relatively smaller distances[8].

The location of the Gamma-ray Burst sources inside their host galaxies indicates that they mostly appear in regions where new stars are forming. However, the evidence is not conclusive yet (Piran [75], section II.C.1).

When the distance of a Gamma-ray Burst is known, we can also calculate how much energy was emitted by the source (in the form of radiation) from the detected flux. However, because we do not know whether the Gamma-ray Burst emitted its radiation in all directions equally, this is only an estimate and probably an upper limit.

These energy estimates are similar to or larger than the energy emitted by a typical supernova, sometimes up to a thousand times larger. The difference with a supernova is that a Gamma-ray Burst lasts much shorter (seconds instead of weeks) and involves much more energetic photons. This means that either the sources of Gamma-ray Bursts are much shorter lived than supernovae, or that the light is produced by something moving towards us with an extremely large velocity as explained on page 23. In the following section I will explain that we believe that the latter is the case.

Long Gamma-ray Bursts do seem to be associated with supernovae. There are two definite cases in which a supernova was detected at the same position

[6]The redshift is measured by a parameter z, which indicates that the universe has expanded by a factor $1 + z$ since the emission of the radiation. Nearby sources have $z \simeq 0$ but many Gamma-ray Burst host galaxies have $z > 1$ [75, section II.C].

[7]A distance of a lightyear indicates that the source is so far away that the light from it had to travel a year to reach us. A lightyear is approximately 10 trillion kilometers (10^{12} km).

[8]A number of articles on the subject recently appeared in Nature [77, 22].

in the sky as a Gamma-ray Burst when the much faster fading afterglow allowed the light from the supernova to be seen[9]. At least a number of the long Gamma-ray Bursts are therefore associated with the death of massive stars[10] (Piran [75], section II.C.4).

A last important clue about the nature of Gamma-ray Burst sources came from the afterglow of GRB970508. The radio waves in this afterglow were observed to twinkle in the first four weeks after the burst. This phenomenon is similar to the twinkling of stars in the night sky, which is caused by the Earth's atmosphere. However, the twinkling of radio waves can only be caused by material in outer space between us and the source and it only occurs when the source of the radio waves is smaller than a certain size, so Frail *et al.* [23] were able to determine that the Gamma-ray Burst source had to be smaller than 10^{12} kilometers in the first four weeks after the burst and larger than this size after that. This is the only direct estimate of the size of Gamma-ray Burst sources independent of any model for their formation.

4.3 The sources of Gamma-ray Bursts

Based on the observational properties of Gamma-ray Bursts that I have described so far we can make some guesses about the possible sources of these interesting phenomena. The most general property seems to be that they are explosive: they are very bright for a very short period of time[11]. This also means that the source is *compact*: it is physically impossible to light up a large object in such a short time because of the finite speed of light (see section 3.2.1). The sources of Gamma-ray Bursts that show variability on a timescale of milliseconds cannot be larger than (a few) thousand kilometers, which is quite small for an astronomical object: the Sun is about a million kilometers across and even the Earth is ten thousand kilometers across. Apparently, Gamma-ray Bursts involve an object smaller than the Earth producing, in a few seconds, more energy than the Sun produces in its lifetime[12].

Another constraint is the energy requirement. I mentioned earlier that the total emitted energy inferred from observations is of the same order as (or larger than) the energy involved in a supernova. Not many phenomena could

[9] These cases are GRB980425 [27] and GRB030329 [37].

[10] At least ten times more massive than the Sun.

[11] Although explosive models are favored by current theories, other models have also been proposed that are based on a central engine that emits strongly over a longer period of time, but is only pointing in our direction for the duration of the 'burst.'

[12] Gamma-ray Bursts seem to emit a total amount of energy of around 10^{51-52}erg, whereas the Sun has produced around 10^{50}erg in radiation during its lifetime.

produce so much energy in such a short time. Most likely a Gamma-ray Burst involves the destruction of a massive star, just like a supernova.

In view of these considerations the most popular model for *long* Gamma-ray Bursts involves the destruction of a very massive star by the collapse of its core into a black hole[13]. As we will see below, the 'fireball' model for the mechanism that produces the Gamma-ray Burst emission and its afterglow requires that the source expels matter at almost the speed of light, causing strong shock waves in its surroundings[14].

The most popular model for *short* Gamma-ray Bursts involves a binary star consisting of two neutron stars (or a neutron star and a black hole) that is destroyed when the neutron stars collide with each other[15]. Such an event would also produce strong, extremely fast shock waves in its surroundings.

Something that puzzled astronomers when Gamma-ray Bursts were just discovered is the non-thermal spectrum of the radiation. Although several radiation mechanisms can explain the shape of the spectral distribution of the radiation, this can only explain Gamma-ray Burst spectra if the light can escape rapidly from the source. The problem is that the maximum size derived from the time variability of the bursts is so small and the involved energy is so large that one would expect a very dense, hot, and opaque 'fireball' to form. The radiation from such a fireball should carry a thermal signature that is very different from the observed radiation (figure 4.1). This problem is known as the *compactness problem*.

A solution was suggested by Martin Rees and Peter Mészáros [79]. The fireball is so dense that radiation can hardly escape from it, and instead it expands with almost the speed of light sending shock waves into its surroundings. Rees and Mészáros suggested that these shock waves could produce the observed Gamma-ray Burst and its afterglow instead. The shock waves would be slowed down by the material surrounding the source and processes inside the shock would convert its kinetic energy into radiation[16].

These shock waves are probably not emitted isotropically in all directions. The evolution in time of the afterglow radiation indicates that the ejected material that causes the shock wave to form is initially confined to a jet. In particular, the decline in the intensity of the radiation indicates that the material spreads out as it travels away from the source [83].

[13] See Piran [75, section IX] for more information about Gamma-ray Burst progenitors.

[14] For other models based on a similar idea, see for example [15].

[15] This would happen because such a binary loses energy to gravitational waves, causing it to collapse inevitably.

[16] Mészáros wrote a short overview of the model recently [64].

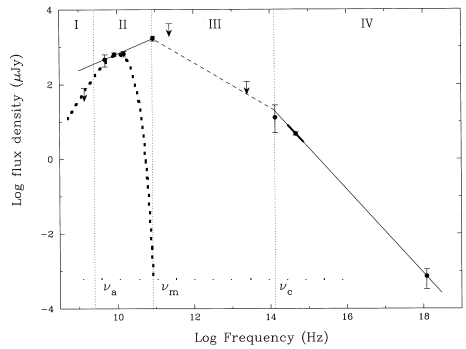

Figure 4.1: The solid line is a synchrotron spectrum fit to GRB970508 (data indicated with points with error bars) taken from an article by Wijers and Galama [102]. The dotted line is my addition: a Planck spectrum that shows that only the low energy part can be fitted by a thermal spectrum.

The material in the shock waves (and the material that they encounter) consists of charged particles (ions, electrons and positrons) because the density is very low and the temperature is very high. If the magnetic interaction of these particles is strong enough then the resulting acceleration of the particles causes them to radiate their kinetic energy through the synchrotron process [79]. Under the right conditions, the spectral energy distribution of this radiation will correspond to the spectrum of Gamma-ray Bursts. Especially the afterglows agree quite well with the synchrotron mechanism (figure 4.1). Regarding the prompt Gamma-ray Burst emission there are some indications that the spectrum is modified in some way, for example by scattering of the radiation on the energetic particles (synchrotron self-Compton scattering [96]).

Because of the difference in characteristics of the prompt Gamma-ray Burst and the subsequent afterglow we distinguish two types of shock waves in the outflow from the source: internal and external shock waves. The great variation in fluctuations of the prompt Gamma-ray Bursts arises from internal shock waves in the outflow that flare up when parts of the outflow overtake each other due to differences in speed. The afterglow emission is produced by the shock wave that is formed as the outflow encounters the interstellar material around the source[17]. Most of the results in my thesis apply to the external shock waves that produce the afterglow radiation.

[17]See the review by Mészáros and references therein for more information [64].

Although we now have solid observational grounds for the hypothesis that the synchrotron process produces the Gamma-ray Burst and afterglow radiation, we are still left with the question whether it is theoretically possible that the synchrotron process occurs in these shock waves.

The models that can reproduce the synchrotron spectrum (as in figure 4.1) require a population of charged particles with a power-law distribution for their kinetic energy that extends to much higher energies than a thermal distribution. This, in turn, requires some kind of mechanism in the shock waves that accelerates the particles to such high energies. Particle acceleration in shocks is a hairy subject, but the consensus of researchers seems to be that particles do get accelerated in shocks to a power-law energy distribution. The details of the mechanism responsible for the acceleration is still the subject of debate in the literature (Piran [75], section V.B).

A second requirement for explaining the synchrotron spectrum is a strong magnetic interaction of the charged particles in the shock wave[18]. In chapter 5 I will discuss how the compression of plasma in the shock front will always boost the magnetic field strength by a certain factor. However, this boost is not enough to explain the synchrotron spectra of Gamma-ray Burst afterglows. As I described earlier in section 3.4 we do however expect that the magnetic interaction in the shock front is strong because of plasma instabilities. Therefore, in the rest of my thesis I investigate these processes in more detail.

To summarize, Gamma-ray Bursts have only been known for a short time and form an important test for modern physics. To observe them we depend on modern techniques to detect high-energy radiation and cosmic rays with satellites and with detectors on Earth. To explain them we use modern physical theories like the Special Theory of Relativity (physics at velocities approaching the speed of light), plasma physics (physics of charged particles and their interactions) and particle physics (the physics of particles at large energies). This thesis discusses an important part of their explanation: the magnetic interaction of charged particles in relativistic shocks.

[18]The strength of the magnetic interaction is generally measured through the ratio of magnetic energy density to total energy density in the shock wave. The synchrotron model requires this ratio to be at least 1–10 % [96, 32].

Part II

Research

Chapter 5

Relativistic Shock Conditions

Like all physical phenomena a shock wave must obey certain conservation laws such as conservation of energy and momentum. This restricts the possible ways in which a shock wave can change the gas that passes through it: for each quantity that is conserved, the same amount must come out of the shock transition as goes into it. In this chapter I use this fact to derive relations between the properties of the material behind the shock and the properties of the material in front of the shock. We call these relations 'shock conditions.'

In relativistic collisionless shock waves we have to take into account that processes such as plasma instabilities inside the shock wave can use part of the available energy to produce electromagnetic fields. The *total* energy is conserved, but the division into kinetic, thermal and electromagnetic energy depends on the processes that work inside the shock transition. In this chapter, this introduces an uncertainty into the properties of the material behind the shock wave: based purely on the conservation laws we cannot say how large the magnetic energy density behind the shock is, so this quantity is left as a free parameter ε_B. In later chapters (such as chapters 8 and 9) we will see how a study of the Weibel instability can yield an estimate for this parameter.

5.1 Introduction

Relativistic shock waves in astrophysical plasmas are considerably more complex than classical shock waves in gases. Apart from relativistic effects and the influence of electromagnetic fields, processes inside the shock transition can include particle creation [73] and magnetic field generation [58], so that mass and magnetic flux conservation might no longer apply across the shock front. In this chapter I will analyze how this affects the properties of the shocked material.

A shock is a location of sudden change in flow properties such as density, pressure, temperature, and magnetic field strength. A transition occurs from an unshocked flow to a shocked flow. In this chapter I will discuss the problem of finding the properties of the shocked material if the properties of the unshocked material and the shock speed are given.

In astrophysical shocks, the change in plasma properties across the shock front and the internal structure of the shock front is controlled by plasma instabilities rather than by collision-dominated processes such as viscosity and heat conduction. The plasma is so tenuous that particle collisions are unimportant (collisionless plasma). Exchange of energy and momentum with electromagnetic fields plays a much larger role (see [92] for a book on non-relativistic collisionless shocks). Medvedev and Loeb [58] have shown that this can involve the generation of magnetic fields, particularly when relativistic speeds are involved (see also [11]).

Jump conditions give the properties of a shock transition independent of its internal structure in the limit of an infinitesimally thin shock. In that case, the state of the shocked plasma is related to the state of the unshocked plasma through conservation laws: when a quantity is conserved, the same amount must flow out of the shock front as flows into it.

Relativistic shock conditions have been studied in the literature. Blandford & McKee [8] have given an explicit form of the hydrodynamical shock conditions for strong relativistic shocks (without a magnetic field). Kennel & Coroniti [46] have given shock conditions in the presence of a magnetic field in the ideal MHD approximation and Lichnerowicz [53] has given a covariant formulation for ideal MHD shock conditions. Kirk & Duffy [47] have written a review of the theory of relativistic shocks.

In this chapter I will give a derivation of the shock conditions that leaves open the possibility of magnetic field generation in the shock so that magnetic flux conservation does not apply. The derivation starts with the conservation laws of magnetohydrodynamics (section 5.2.1), which can be simplified us-

ing suitable approximations. The most important approximation is to take the magnetic field perpendicular to the direction in which the shock moves. I will solve the shock conditions in this case and give a justification for the approximation of a perpendicular magnetic field (section 5.3). In the last section I discuss the assumptions made and the general properties of the results (section 5.4).

5.2 Theory: Magnetohydrodynamics

5.2.1 MHD description of the plasma

I will examine the plasma on a length-scale that is much larger than the length-scale associated with the plasma instabilities in the shock transition. In this limit we can view the plasma as an ideally conducting, compressible fluid. Its properties are described by the theory of relativistic magnetohydrodynamics (MHD) [53].

MHD treats the collection of charged particles that makes up the plasma as a continuum. The flow velocity $\mathbf{v}$ is then the bulk velocity of the particles (measured throughout this chapter in units of the light-speed) and the proper mass density ρ is measured in the frame where the velocity $\mathbf{v}$ is zero (the 'fluid rest frame'). The velocity field has an associated Lorentz factor $\gamma = 1/\sqrt{1-|\mathbf{v}|^2}$, four-velocity $u^\alpha = (\gamma, \gamma\mathbf{v})$ and mass flux ρu^α.

The proper internal energy density e consists of the rest mass energy density and the kinetic energy density in thermal motions. The pressure P denotes the momentum flux density in thermal motions. The associated energy-momentum tensor in the fluid rest frame is (*e.g.*, [49])

$$T^{\text{gas}} = \text{diag}(e, P, P, P). \qquad \text{(fluid rest frame)} \tag{5.1}$$

The electromagnetic properties of the plasma are described through macroscopic electromagnetic fields. In an ideal (infinitely good conducting) plasma the electric field vanishes in the fluid rest frame. This is the MHD assumption. The magnetic field $\mathbf{B}$ does not vanish and has an associated four-vector $\mathcal{B}^\alpha = (0, \mathbf{B})$ in the fluid rest frame.

The total energy momentum tensor (gas plus electromagnetic fields) for such a plasma can be written as (see Lichnerowicz [53], section 33):

$$T^{\alpha\beta} = (w + \frac{B^2}{4\pi})u^\alpha u^\beta - (P + \frac{B^2}{8\pi})g^{\alpha\beta} - \frac{\mathcal{B}^\alpha \mathcal{B}^\beta}{4\pi}, \tag{5.2}$$

where $g^{\alpha\beta} = \text{diag}(1, -1, -1, -1)$ is the Minkowski metric tensor, w is the enthalpy density in the fluid rest frame, and B is the magnetic field strength in

the fluid rest frame:

$$B = |\mathbf{B}| = \sqrt{-\mathcal{B}^\alpha \mathcal{B}_\alpha}. \tag{5.3}$$

I will use subscript 1 for the upstream (unshocked) plasma, *e.g.*, ρ_1, v_1, *etc.*, and subscript 2 for the properties of the downstream (shocked) plasma. The plasma flow speeds v_1 and v_2 are measured in the rest frame of the shock.

The shock front is (locally) a flat surface. It moves in the rest frame of the upstream plasma along the shock-normal with a velocity v (with corresponding Lorentz factor $\gamma_{\rm sh}$ and four-velocity $u^\alpha_{\rm sh}$). The vector $\mathbf{l}$ will denote the shock-normal. I define a corresponding four-vector $\ell^\alpha = (0, \mathbf{l})$ in the shock rest frame.

5.2.2 Physics of MHD Plasmas

Conservation laws (for mass, energy, and momentum), Maxwell's equations, thermodynamics and relativity theory determine the properties of the plasma (see the book by Lichnerowicz [53], which treats much of this section in more detail).

Plasmas obey conservation of energy and momentum and, if particle creation plays no role, also mass conservation. In ideal fluids (in which collisions and radiation losses are not important) the sum of bulk kinetic, internal, and electromagnetic energy is conserved. Similarly, the sum of bulk, thermal, and electromagnetic momentum is conserved. This is expressed by the non-divergence of the energy-momentum tensor:

$$\partial_\alpha T^{\alpha\beta} = 0, \tag{5.4}$$

where $\partial^\alpha = (\partial/\partial t, \partial/\partial x, \partial/\partial y, \partial/\partial z)$. Mass conservation can be expressed as non-divergence of the mass flux:

$$\partial_\alpha (\rho u^\alpha) = 0. \tag{5.5}$$

For infinitesimally thin shocks the conservation laws require that the flux of a conserved quantity into the shock must equal the flux out of the shock: what goes in must come out; the internal structure of the shock is stationary. Nevertheless, different contributions (magnetic, kinetic, and thermal energy) to a conserved quantity can be converted into each other.

A common way of expressing flux continuity across shocks is (see [53], section 47b):

$$\ell_\alpha (\rho_2 u_2^\alpha - \rho_1 u_1^\alpha) = 0, \qquad \ell_\alpha (T_2^{\alpha\beta} - T_1^{\alpha\beta}) = 0, \tag{5.6}$$

which ensures that the flux along the shock-normal is continuous. These equations are a restraint on the jump in density, pressure, energy density and flow speed across the shock and are therefore called the *jump conditions*.

The electromagnetic fields are constrained by Maxwell's equations. For *ideal* MHD these can be reduced to one covariant equation which expresses conservation of magnetic flux:

$$\partial_\alpha (u^\alpha \mathcal{B}^\beta - \mathcal{B}^\alpha u^\beta) = 0. \tag{5.7}$$

We can apply this equation across the shock:

$$\ell_\alpha (u_2^\alpha \mathcal{B}_2^\beta - \mathcal{B}_2^\alpha u_2^\beta) = \ell_\alpha (u_1^\alpha \mathcal{B}_1^\beta - \mathcal{B}_1^\alpha u_1^\beta). \qquad \text{(frozen)} \tag{5.8}$$

However, this assumes that the ideal MHD approximation applies across the *whole* shock front. I will indicate equations that depend on this assumption with the keyword 'frozen' since it means that the magnetic field lines are frozen to the plasma.

Mass and magnetic flux conservation might not apply if particle creation and magnetic field generation play a role in the shock transition. One way to drop these two conservation laws is to consider the mass density and magnetic field strength behind the shock to be given quantities instead of variables. Alternatively, to take particle creation into account, a parameter $\eta = \rho_2^{\text{cons}}/\rho_2$ can be introduced that gives the ratio of conserved number of particles to total number of particles behind the shock (see Kirk and Duffy [47]). For the magnetic field I will show in section 5.3.2 how to find shock conditions assuming that the ratio of magnetic to internal energy $\varepsilon_B \equiv B_2^2/(8\pi e_2)$ is a given quantity. However, these are ad hoc solutions and a full solution requires a theory for the internal shock structure that gives ρ_2 and B_2 as a function of the shock parameters (see also the discussion in section 5.4).

The density, pressure, and internal energy are thermodynamic quantities that can be related through an equation of state. A simple equation of state, which I will use here, is:

$$P = (\Gamma - 1)(e - \rho), \tag{5.9}$$

where Γ is the specific heat ratio, which is equal to $5/3$ for a cold plasma and $4/3$ for a relativistically hot plasma (see the the next subsection for the definition of hot and cold plasma). For intermediate cases another equation of state should be used (Kirk and Duffy [47] discuss how to use a Synge equation of state).

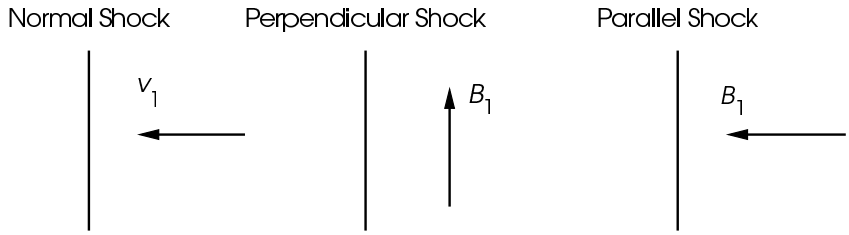

Figure 5.1: Different shock configurations. The term 'normal shock' applies to the direction of the flow. The terms 'perpendicular' and 'parallel' apply to the direction of the magnetic field.

Several frames of reference are important to the problem: the shock rest frame (SRF), and the fluid rest frames of the shocked and unshocked plasma: the downstream rest frame (DRF) and the upstream rest frame (URF) respectively. The representations of (four-)vectors and tensors in different frames are related through Lorentz transformations, see for example Chapter 11 of Jackson [41].

5.2.3 Approximations

I will make use of a number of different approximations to simplify the calculations. I do not use all of these everywhere, so I will indicate when they are used (see also the discussion in section 5.4).

When the total energy is much larger than the rest mass energy of the plasma, the shock will be *ultra-relativistic*, *i.e.*, the shock Lorentz factor will be very large: $\gamma_{\rm sh} \gg 1$. When flow speeds are very close to the speed of light it is convenient to describe them by means of their Lorentz factor, which can be used as an ordering parameter in an asymptotic expansion. Expressions that are only valid for ultra-relativistic shocks will be labeled with the abbreviation 'UR'.

A shock is *strong* when the upstream pressure can be neglected compared to the downstream pressure. As we will see below, this is always the case for ultra-relativistic shocks. Expressions only valid for strong shocks will be labeled with the word 'strong'.

A shock is *normal* when its direction of propagation is along the normal to the shock front ($v_1 \parallel \mathbf{l}$ in the SRF; figure 5.1). In this chapter I will mostly consider normal shocks, since a shock can always be made normal locally through

a change of reference frame.

When magnetic fields are involved, important classes of shocks are those of *perpendicular* and *parallel* shocks (figure 5.1). When the magnetic field is parallel to the propagation direction of the shock ($\mathbf{B} \parallel \mathbf{l}$ in the SRF) a shock is *parallel*. When the magnetic field is perpendicular to this direction it is *perpendicular* ($\mathbf{B} \perp \mathbf{l}$ in the SRF). I will show below that ultra-relativistic shocks can almost always be considered to be perpendicular.

Certain approximations can also be made regarding the properties of the up- or downstream plasma. The plasma is said to be *cold* when the thermal motions of the particles are negligible. This means that the pressure and thermal energy density are not important for the dynamics: $P \ll \rho, e \simeq \rho$. A plasma is relativistically *hot* when its thermal energy density is much larger than its rest mass density: $e \gg \rho$. In this case the adiabatic constant is $\Gamma = 4/3$ and the equation of state (5.9) can be approximated by $P \simeq e/3$. Lastly, the plasma is said to be *unmagnetized* when the influence of the magnetic field can be neglected (*i.e.*, when the Larmor radius of the particles is much larger than any relevant length scale of the problem).

5.3 Shock conditions and their solutions

5.3.1 General situation

The goal of this chapter is to find the properties of the shocked plasma given the properties of the unshocked plasma and the shock (figure 5.2). To do this analytically I will simplify the situation by assuming that the shock is ultra-relativistic ($\gamma_{\rm sh} \gg 1$).

For ultra-relativistic shocks the magnetic field can almost always be considered to be perpendicular to the shock-normal. I will prove this in section 5.3.3 but it can be anticipated because of the following. In general, the magnetic field in the unshocked material will be at an inclination angle i to the shock-normal with parallel and perpendicular components $B_\parallel = B\cos i$ and $B_\perp = B\sin i$ (I will put the x-axis along $B_\parallel$, and the y-axis along $B_\perp$). A Lorentz transformation with boost v gives the situation in the shock rest frame (*e.g.*, Jackson [41], Section 11.10):

$$B_\perp^{\rm srf} = \gamma_{\rm sh} B \sin i, \quad B_\parallel^{\rm srf} = B\cos i. \tag{5.10}$$

The perpendicular component is amplified by a Lorentz factor, whereas the parallel component remains unchanged. Therefore we can expect the perpendicular component to dominate unless $\sin i \lesssim 1/\gamma_{\rm sh}$.

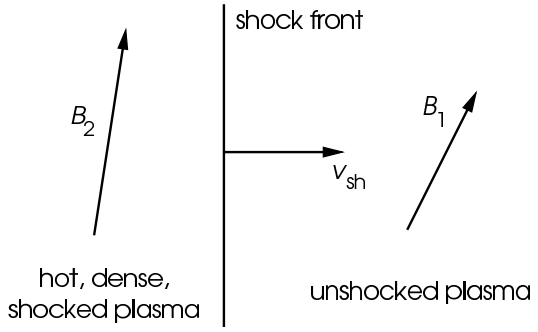

Figure 5.2: Shock moving through unshocked plasma leaving behind shocked plasma.

In view of this, I will first give derivations and results for perpendicular shocks, neglecting the parallel component of the magnetic field. After that, I will give an explicit proof that the effect of the parallel component is small.

5.3.2 Perpendicular Shocks

I will derive expressions for the jump conditions of perpendicular shocks in different reference frames. After that I will solve for the plasma properties for a number of different situations.

When the magnetic field is perpendicular to the flow direction, as in perpendicular, normal shocks, the influence of the magnetic field can be represented through an effective pressure $\bar{P}$ and energy density $\bar{e}$ along the flow direction defined by

$$\bar{P} = P + B^2/8\pi \quad \text{and} \quad \bar{e} = e + B^2/8\pi. \tag{5.11}$$

The energy-momentum tensor (5.2) then has the form

$$T^{\alpha\beta} = \bar{w} u^\alpha u^\beta - \bar{P} g^{\alpha\beta} - \frac{\mathcal{B}^\alpha \mathcal{B}^\beta}{4\pi}, \tag{5.12}$$

where $\bar{w} = \bar{e} + \bar{P} = w + B^2/(4\pi)$ is the effective enthalpy density.

The effective pressure and energy density do not obey the gas equation of state, but we can construct an 'effective' equation of state of the same form:

$$\bar{P} = (\bar{\Gamma}_B - 1)(\bar{e} - \rho). \tag{5.13}$$

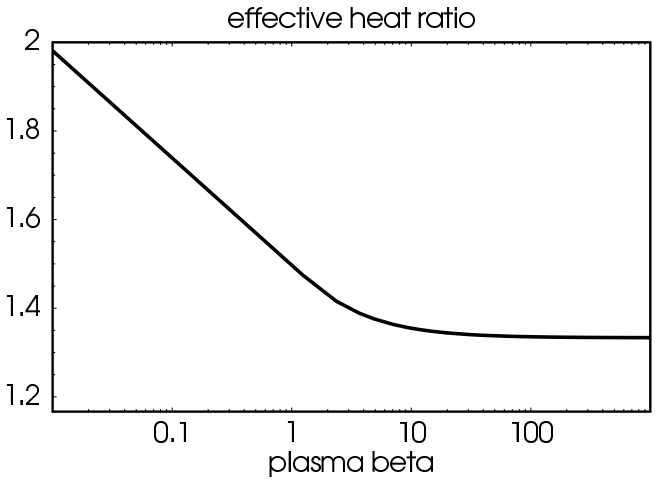

Figure 5.3: Log-linear plot of the effective specific heat ratio $\bar{\Gamma}_B$ against the plasma beta β for a relativistically hot plasma with $\Gamma = 4/3$. See equation (5.14).

The effective specific heat ratio $\bar{\Gamma}_B$ depends on the magnetization of the plasma. If the gas obeys the equation of state (5.9) it is a function of the plasma beta $\beta \equiv 8\pi P/B^2$:

$$\bar{\Gamma}_B = \frac{\beta\Gamma + 2(\Gamma - 1)}{\beta + (\Gamma - 1)}. \tag{5.14}$$

For an unmagnetized plasma $\beta \to \infty$ and $\bar{\Gamma}_B \to \Gamma$. For a strongly magnetized plasma $\beta \to 0$ and $\bar{\Gamma}_B \to 2$ (which expresses that the magnetic pressure and energy density are equal). A parameter often used in gamma-ray burst models to measure the magnetization is $\varepsilon_B \equiv B_2^2/(8\pi e_2)$, the ratio of magnetic energy to internal energy in the shocked plasma. If the plasma is relativistically hot ($\Gamma = 4/3$), we find $\beta = (3\varepsilon_B)^{-1}$ and

$$\bar{\Gamma}_B = \frac{4 + 6\varepsilon_B}{3 + 3\varepsilon_B}. \qquad \text{(hot)} \tag{5.15}$$

The jump conditions in covariant form (5.6) and (5.8) are shock conditions as is, but to solve for the shocked plasma properties I will use the non-covariant form. To do this we have to choose a reference frame. Three velocities are important to the problem: the shock velocity v and the up- and downstream

Table 5.1: Velocities in different reference frames

	shock front	upstream plasma	downstream plasma
SRF	0	$-v_1$	$-v_2$
URF	v_1	0	$v_{\rm rel}$
DRF	v_2	$-v_{\rm rel}$	0

Table 5.2: Four-vectors in different reference frames

	ℓ^α	$u^\alpha_{\rm sh}$	u^α_1	u^α_2
SRF	$(0,1,0,0)$	$(1,0,0,0)$	$(\gamma_1,-\gamma_1 v_1,0,0)$	$(\gamma_2,-\gamma_2 v_2,0,0)$
URF	$(\gamma_1 v_1,\gamma_1,0,0)$	$(\gamma_1,\gamma_1 v_1,0,0)$	$(1,0,0,0)$	$(\gamma_{\rm rel},\gamma_{\rm rel} v_{\rm rel},0,0)$
DRF	$(\gamma_2 v_2,\gamma_2,0,0)$	$(\gamma_2,\gamma_2 v_2,0,0)$	$(\gamma_{\rm rel},-\gamma_{\rm rel} v_{\rm rel},0,0)$	$(1,0,0,0)$

velocities v_1 and v_2. We can always eliminate one of these by studying the problem in the right reference frame: the shock rest frame (SRF), the upstream rest frame (URF) or the downstream rest frame (DRF) (Table 5.1). The relative velocity between the up- and the downstream plasma $v_{\rm rel}$ and the associated Lorentz factor $\gamma_{\rm rel}$ are

$$v_{\rm rel} = \frac{v_1 - v_2}{1 - v_1 v_2}, \qquad \gamma_{\rm rel} = \gamma_1\gamma_2(1 - v_1 v_2). \tag{5.16}$$

The representations of the four-vectors are listed in table 5.2. The magnetic four-vectors are $\mathcal{B}^\alpha_{1,2} = (0,0,0,B_{1,2})$ in all three frames (recall that B denotes the magnetic field strength in the fluid rest frame). Conservation of magnetic flux (5.8) reduces to

$$\gamma_2 v_2 B_2 = \gamma_1 v_1 B_1. \qquad \text{(frozen)} \tag{5.17}$$

In the shock rest frame the jump conditions (5.6) result in symmetric equations that express conservation of mass, momentum and energy:

$$\textbf{Mass:} \qquad \rho_2\gamma_2 v_2 = \rho_1\gamma_1 v_1, \tag{5.18}$$

$$\textbf{Momentum:} \quad \bar{w}_2\gamma_2^2 v_2^2 + \bar{P}_2 = \bar{w}_1\gamma_1^2 v_1^2 + \bar{P}_1, \qquad \text{(SRF)} \tag{5.19}$$

$$\textbf{Energy:} \qquad \bar{w}_2\gamma_2^2 v_2 = \bar{w}_1\gamma_1^2 v_1. \tag{5.20}$$

(see equations (5.30–5.32) for the equivalent equations in the DRF). Each equation contains on the right hand side the flux of the given quantity into the shock and on the left hand side the flux out of the shock.

For a perpendicular, normal shock there is only one equation for conservation of momentum. We will see in section 5.3.3 that for non-perpendicular shocks the flow can pick up a component along the shock surface and two equations for conservation of momentum are needed; see equations (5.66–5.69).

If magnetic flux is conserved, the magnetic field is compressed by the same factor as the plasma (see equations 5.17 and 5.18):

$$\boxed{\frac{B_2}{B_1} = \frac{\rho_2}{\rho_1}. \qquad \text{(frozen)}} \tag{5.21}$$

We can use the conservation laws (5.18–5.20) to find relations between the plasma speeds and the effective pressure and energy density. First write (5.19) as

$$\bar{P}_2 - \bar{P}_1 = \bar{w}_1\gamma_1^2 v_1^2 - \bar{w}_2\gamma_2^2 v_2^2. \tag{5.22}$$

From (5.20) the first term on the right-hand side is $\bar{w}_1\gamma_1^2 v_1^2 = \bar{w}_2\gamma_2^2 v_2 v_1$ and mutatis mutandis for the second term. This results in

$$\bar{P}_2 - \bar{P}_1 = (\bar{w}_2\gamma_2^2 - \bar{w}_1\gamma_1^2) v_1 v_2. \tag{5.23}$$

Now write (5.19) as $\bar{w}_2\gamma_2^2 - \bar{w}_1\gamma_1^2 = \bar{e}_2 - \bar{e}_1$ using the identity $\gamma^2 v^2 = \gamma^2 - 1$, which follows from the definition of the Lorentz factor. Use this in (5.23) to find

$$v_1 v_2 = \frac{\bar{P}_2 - \bar{P}_1}{\bar{e}_2 - \bar{e}_1}. \tag{5.24}$$

I will show below that ultra-relativistic shocks have $\bar{P}_2 \gg \bar{P}_1$, $\bar{e}_2 \gg \bar{e}_1$, and $\bar{e}_2 \gg \rho_2$ so that (with $v_1 \simeq 1$ and equation of state (5.13)):

$$\boxed{v_2 = \bar{P}_2/\bar{e}_2 = \bar{\Gamma}_B - 1. \qquad \text{(UR)}} \tag{5.25}$$

For a hot downstream plasma equation (5.15) gives $\bar{\Gamma}_B$ and the downstream flow speed varies from $v_2 = 1/3$ for an unmagnetized plasma to $v_2 \to 1$ for a strongly magnetized plasma (in a strongly magnetized plasma the shock is an electromagnetic wave and propagates at the speed of light in all reference frames).

Returning to the general case, we can now eliminate v_1 or v_2. For example, start again with equation (5.22), and use $\bar{w}_2\gamma_2^2 v_2^2 = \bar{w}_1\gamma_1^2 v_2 v_1$ (see equation 5.20) to find

$$\begin{aligned} \bar{P}_2 - \bar{P}_1 &= \bar{w}_1\gamma_1^2(v_1^2 - v_2 v_1) \\ &= \bar{w}_1\gamma_1^2\Big(v_1^2 - \frac{\bar{P}_2 - \bar{P}_1}{\bar{e}_2 - \bar{e}_1}\Big). \end{aligned} \tag{5.26}$$

Eliminating the Lorentz factor through $\gamma_1^2 = (1 - v_1^2)^{-1}$ we find an equation that can be solved for v_1:

$$v_1 = \sqrt{\frac{(\bar{P}_2 - \bar{P}_1)(\bar{e}_2 + \bar{P}_1)}{(\bar{e}_2 - \bar{e}_1)(\bar{e}_1 + \bar{P}_2)}}. \tag{5.27}$$

Because of the symmetry of the jump conditions under the exchange of the indices 1 and 2 we also find

$$v_2 = \sqrt{\frac{(\bar{P}_2 - \bar{P}_1)(\bar{e}_1 + \bar{P}_2)}{(\bar{e}_2 - \bar{e}_1)(\bar{e}_2 + \bar{P}_1)}}. \tag{5.28}$$

We can use these results to express the Lorentz factor $\gamma_{\rm rel}$ of the relative velocity between the up- and downstream plasma in $\bar{P}$ and $\bar{e}$. Equation (5.16) yields after some algebra:

$$\gamma_{\rm rel} = \sqrt{\frac{(\bar{e}_2 + \bar{P}_1)(\bar{e}_1 + \bar{P}_2)}{(\bar{e}_1 + \bar{P}_1)(\bar{e}_2 + \bar{P}_2)}}. \tag{5.29}$$

Now I will derive the jump conditions in the rest frame of the downstream plasma. The equations in the upstream rest frame are the same, but with subscripts 1 and 2 interchanged. Note that these equations are equivalent to those in the shock rest frame, equations (5.18–5.20). The jump conditions (5.6) yield in the downstream rest frame:

$$\textbf{Mass:} \quad \rho_2 v_2 = \rho_1 \gamma_{\rm rel} v_2 + \rho_1 \gamma_{\rm rel} v_{\rm rel}, \tag{5.30}$$

$$\textbf{Momentum:} \quad \bar{P}_2 = \bar{w}_1 \gamma_{\rm rel}^2 v_{\rm rel} v_2 + \bar{w}_1 \gamma_{\rm rel}^2 v_{\rm rel}^2 + \bar{P}_1, \qquad \text{(DRF)} \tag{5.31}$$

$$\textbf{Energy:} \quad \bar{e}_2 v_2 = (\bar{e}_1 + \bar{P}_1 v_{\rm rel}^2)\gamma_{\rm rel}^2 v_2 + (\bar{e}_1 + \bar{P}_1)\gamma_{\rm rel}^2 v_{\rm rel}, \tag{5.32}$$

where a factor γ_2 has been eliminated from all three equations. The equations contain on the left hand side the flux of each quantity out of the shock. The downstream plasma is at rest and v_2 enters the equations not as a flow speed but as the speed of the shock. The movement of the shock front causes a flux of density $\times$ shock speed, *e.g.*, the mass flux is $\rho_2 v_2$. The only contribution to the momentum flux out of the shock is the effective pressure $\bar{P}_2$ because the bulk momentum density behind the shock is zero in this reference frame. Both the movement of the shock and the movement of the upstream plasma contribute to the flux *into* the shock on the right hand side (the first and second terms respectively). The momentum flux also has a contribution from the pressure $\bar{P}_1$.

The equations contain the downstream quantities ρ_2, $\bar{e}_2$ and $\bar{P}_2$ in a simple way and we can work out some properties of these quantities.

We can write mass conservation as

$$\boxed{X \equiv \frac{\rho_2}{\gamma_{\rm rel}\rho_1} = 1 + \frac{v_{\rm rel}}{v_2}.} \tag{5.33}$$

The quantity X plays an important role in later calculations. For ultra-relativistic shocks $v_{\rm rel} \to 1$ and $1/3 \lesssim v_2 \lesssim 1$ (see above) so that $2 \lesssim X \lesssim 4$. The compression ratio ρ_2/ρ_1 will be of order $\gamma_{\rm rel}$ because X is of order 1.

To get a relation between the Lorentz factor $\gamma_{\rm rel}$ of the relative velocity between the up- and downstream plasma and the Lorentz factor $\gamma_{\rm sh}$ of the shock velocity we can use mass conservation in the URF:

$$\rho_1 v = \rho_2 \gamma_{\rm rel}(v - v_{\rm rel}). \qquad \text{(URF)} \tag{5.34}$$

Rewriting this as $(\gamma_{\rm rel}\rho_2 - \rho_1)v = \rho_2 \gamma_{\rm rel} v_{\rm rel}$ and squaring both sides to eliminate the velocities in favor of the Lorentz factors, we find after some straight-

forward algebra

$$\gamma_{\rm sh}^2 = \frac{(X\gamma_{\rm rel}^2 - 1)^2}{(X-2)X\gamma_{\rm rel}^2 + 1}. \tag{5.35}$$

For ultra-relativistic shocks both $\gamma_{\rm sh}$ and $\gamma_{\rm rel}$ are large and provided $X \neq 2$ we get the approximate expression

$$\boxed{\gamma_{\rm sh}^2 = \frac{X}{X-2}\gamma_{\rm rel}^2. \qquad \text{(UR)}} \tag{5.36}$$

For ultra-relativistic shocks $\gamma_{\rm rel}$ will therefore be of the same order as $\gamma_{\rm sh}$. This enables us to find the order of the downstream plasma properties from the DRF equations (5.30–5.32): the density ρ_2 is of order $\gamma_{\rm rel}$, the energy density and pressure are of order $\gamma_{\rm rel}^2$, and a frozen-in magnetic field is of order $\gamma_{\rm rel}$, see equation (5.21).

Now I will solve for the downstream plasma properties v_2, ρ_2, e_2, P_2, and B_2. For a unique solution we need five equations. The conservation laws of mass, momentum, energy, and magnetic flux provide four equations and the downstream equation of state the fifth.

First I will give a derivation for the strong unmagnetized shock solution given by Blandford and McKee [8]. Then I will give a derivation for magnetized ultra-relativistic shocks with conserved magnetic flux (similar to solutions found in [46] and [30]). Finally, I will give a solution for a fixed $\varepsilon_{\rm B}$.

Unmagnetized shocks. Blandford & McKee [8] have given an analytic solution for strong unmagnetized shocks. I will derive their results (see table 5.3 for notational differences).

The idea is to find a relation for e_2/ρ_2 and to use this with the equation of state to eliminate e_2 and P_2. The resulting equation can be solved to find ρ_2 as a function of $\gamma_{\rm rel}$. The last step is to relate $\gamma_{\rm rel}$ to the shock Lorentz factor.

The jump conditions (5.30–5.32) give

$$\rho_2 = \gamma_{\rm rel}\rho_1(1 + v_{\rm rel}/v_2), \tag{5.37}$$

$$P_2 - P_1 = \gamma_{\rm rel}^2 w_1 v_{\rm rel}(v_2 + v_{\rm rel}), \tag{5.38}$$

$$(e_2 + P_1) = \gamma_{\rm rel}^2 w_1(1 + v_{\rm rel}/v_2), \tag{5.39}$$

Table 5.3: Notation used by Blandford & McKee [8]

	This chapter	Blandford & McKee
adiabatic const.	Γ	$\hat{\gamma}_2$
shock Lorentz factor	$\gamma_{\rm sh}$	Γ
relative L. factor	$\gamma_{\rm rel}$	γ_2
mass density	ρ	$m\,n$

where I have dropped the $^-$ accents. The only non-trivial change is in the last equation where I used the identity $\gamma_{\rm rel}^2 v_{\rm rel}^2 = \gamma_{\rm rel}^2 - 1$. Equations (5.37) and (5.39) yield

$$\boxed{\frac{e_2 + P_1}{\rho_2} = \gamma_{\rm rel}\frac{w_1}{\rho_1}.} \tag{5.40}$$

Note that this equation is *exact* and that it is also valid with the subscripts 1 and 2 interchanged. For strong shocks $P_2 \gg P_1$ and therefore $e_2 \gg P_1$ so that we can approximate equation (5.40) with

$$\boxed{\frac{e_2}{\rho_2} = \gamma_{\rm rel}\frac{w_1}{\rho_1}. \qquad \text{(strong)}} \tag{5.41}$$

This is equation (3) of Blandford and McKee [8]. It expresses that the energy per unit mass behind the shock is equal to the energy per unit mass in front.

To derive equations (4) and (5) of Blandford and McKee [8] we need the extra assumption that the upstream plasma is cold, $P_1 \ll \rho_1$ (Blandford & McKee do not mention this explicitly). In a cold plasma we have $w_1 \simeq e_1 \simeq \rho_1$ so that $e_2 \simeq \gamma_{\rm rel}\rho_2$ and (5.38) becomes

$$P_2 = \gamma_{\rm rel}^2 \rho_1 v_{\rm rel}(v_2 + v_{\rm rel}). \qquad \text{(strong)} \tag{5.42}$$

After some manipulation, mass conservation (5.37) gives

$$v_2 + v_{\rm rel} = \frac{\rho_2 v_{\rm rel}}{(\rho_2 - \gamma_{\rm rel}\rho_1)}. \tag{5.43}$$

and (5.42) becomes:

$$\begin{aligned} P_2 &= \frac{\gamma_{\rm rel}^2 v_{\rm rel}^2 \rho_1 \rho_2}{(\rho_2 - \gamma_{\rm rel}\rho_1)} \\ &= \frac{(\gamma_{\rm rel}^2 - 1)\rho_1 \rho_2}{(\rho_2 - \gamma_{\rm rel}\rho_1)}. \end{aligned} \qquad \text{(strong)} \tag{5.44}$$

The equation of state is

$$P_2 = (\Gamma - 1)(e_2 - \rho_2) = (\Gamma - 1)(\gamma_{\rm rel} - 1)\rho_2. \qquad \text{(strong)} \tag{5.45}$$

Now we can eliminate P_2 from (5.44) and (5.45) and solve for ρ_2/ρ_1. The result is equation (4) of [8]:

$$\boxed{\frac{\rho_2}{\rho_1} = \frac{\Gamma\gamma_{\rm rel} + 1}{\Gamma - 1}. \qquad \text{(strong)}} \tag{5.46}$$

Finally, this relation can be used to eliminate X from equation (5.35) for the shock Lorentz factor. Some tedious manipulation yields equation (5) of [8]:

$$\boxed{\gamma_{\rm sh}^2 = \frac{(\gamma_{\rm rel} + 1)[\Gamma(\gamma_{\rm rel} - 1) + 1]^2}{\Gamma(2 - \Gamma)(\gamma_{\rm rel} - 1) + 2}. \qquad \text{(strong)}} \tag{5.47}$$

The two Lorentz factors scale almost linearly; see figure 5.4. This means that the density ρ_2, in equation (5.46), also scales approximately linearly with $\gamma_{\rm sh}$.

For ultra-relativistic shocks ($\gamma_{\rm sh} \to \infty$) the results can be approximated. The jump conditions (5.30–5.32) show that the energy density and pressure behind the shock are an order $\gamma_{\rm rel}$ larger than the mass density. The shocked plasma

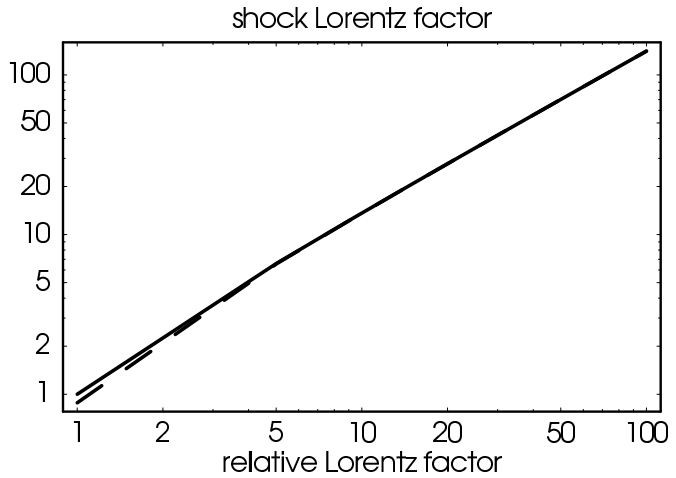

Figure 5.4: Shock Lorentz factor $\gamma_{\rm sh}$ against Relative Lorentz factor $\gamma_{\rm rel}$ for strong shocks. The solid line is the full solution (5.47), the dashed line the approximation $\gamma_{\rm sh} = \sqrt{2}(\gamma_{\rm rel} - 3/8)$.

will be hot ($e_2 \gg \rho_2$) and we can set $\Gamma = 4/3$. The asymptotic results are:

$$\boxed{\begin{aligned} \gamma_{\rm rel} &= \sqrt{\tfrac{2-\Gamma}{\Gamma}}\gamma_{\rm sh} &&= \tfrac{1}{2}\sqrt{2}\gamma_{\rm sh}, \\ \rho_2 &= \tfrac{\Gamma}{\Gamma-1}\gamma_{\rm rel}\,\rho_1 &&= 2\sqrt{2}\gamma_{\rm sh}\,\rho_1, \\ e_2 &= \gamma_{\rm rel}\,\rho_2 &&= 2\gamma_{\rm sh}^2\,\rho_1, \qquad \text{(UR)} \\ P_2 &= (\Gamma-1)e_2 &&= \tfrac{2}{3}\gamma_{\rm sh}^2\,\rho_1, \\ v_2 &= (\Gamma-1) &&= 1/3. \end{aligned}} \tag{5.48}$$

The upstream density ρ_1 and the shock Lorentz factor $\gamma_{\rm sh}$ completely determine the properties of the shocked plasma for strong, unmagnetized shocks in a cold plasma.

Magnetized shocks with magnetic flux conservation. The solution of [8] does not include a magnetic field. Blandford & McKee remark that a perpendicular

magnetic field can be included by replacing e_2 and P_2 with $\bar{e}_2$ and $\bar{P}_2$ respectively, but they do not mention that, in addition, Γ has to be replaced with $\bar{\Gamma}_B$, which is a function of the magnetic field strength; see equation (5.14) or (5.15). The resulting equations are more difficult to solve than equations (5.37–5.39) plus the normal equation of state (5.9).

It is easier to use the ultra-relativistic limit $\gamma_{\rm sh} \gg 1$ to simplify the jump conditions and to solve these simplified equations. If the shocked plasma is not extremely magnetized, equation (5.36) tells us that $\gamma_{\rm rel}$ and $\gamma_{\rm sh}$ are of the same order. We can set $v_{\rm rel} = v = 1$ (the differences $1 - v$ and $1 - v_{\rm rel}$ do not occur in the calculations). The asymptotic form of the conservation laws (5.30–5.32) is

$$\rho_2 = \rho_1 \gamma_{\rm rel}(1 + 1/v_2), \tag{5.49}$$

$$\bar{P}_2 = \bar{w}_1 \gamma_{\rm rel}^2 (1 + v_2), \qquad \text{(UR)} \tag{5.50}$$

$$\bar{e}_2 v_2 = \bar{w}_1 \gamma_{\rm rel}^2 (1 + v_2). \tag{5.51}$$

Equations (5.50) and (5.51) yield

$$v_2 = \bar{P}_2/\bar{e}_2 = \bar{\Gamma}_B - 1, \qquad \text{(UR)} \tag{5.52}$$

and (5.49) gives

$$X \equiv \frac{\rho_2}{\gamma_{\rm rel}\rho_1} = \frac{v_2 + 1}{v_2} = \frac{\bar{\Gamma}_B}{\bar{\Gamma}_B - 1}. \qquad \text{(UR)} \tag{5.53}$$

Equations (5.49) and (5.51) combine to give the effective version of (5.41):

$$\frac{\bar{e}_2}{\rho_2} = \gamma_{\rm rel}\frac{\bar{w}_1}{\rho_1} \qquad \text{(UR)} \tag{5.54}$$

Eliminate v_2 from equation (5.50) to find

$$\frac{\bar{P}_2}{\rho_2} = \gamma_{\rm rel}\frac{\bar{w}_1}{\rho_1}\frac{1}{X - 1} \qquad \text{(UR)} \tag{5.55}$$

If magnetic flux is conserved, we can now solve for the shocked plasma properties. Introduce the non-relativistic Alfvén speed $v_{\rm A}$ in the unshocked plasma as a measure of the magnetic field strength:

$$v_{\rm A} \equiv \frac{B_1}{\sqrt{4\pi\rho_1}} \tag{5.56}$$

and eliminate B_2 through equation (5.8) to find

$$\begin{aligned}
\frac{\bar{w}_1}{\rho_1} &= \frac{w_1}{\rho_1} + v_{\rm A}^2, \\
\frac{B_2^2}{8\pi\rho_2} &= \frac{\rho_2}{\rho_1}\frac{B_1^2}{8\pi\rho_1} = \tfrac{1}{2}\gamma_{\rm rel} X v_{\rm A}^2, \\
\frac{\bar{e}_2}{\rho_2} &= \frac{e_2}{\rho_2} + \tfrac{1}{2}\gamma_{\rm rel} X v_{\rm A}^2, \\
\frac{\bar{P}_2}{\rho_2} &= \frac{P_2}{\rho_2} + \tfrac{1}{2}\gamma_{\rm rel} X v_{\rm A}^2.
\end{aligned} \qquad \text{(frozen)} \tag{5.57}$$

Equations (5.54) and (5.55) become

$$\begin{aligned}
\frac{e_2}{\rho_2} &= \gamma_{\rm rel}\big(\tilde{w}_1 + v_{\rm A}^2(1 - \tfrac{1}{2}X)\big), \\
\frac{P_2}{\rho_2} &= \gamma_{\rm rel}\Big(\frac{\tilde{w}_1 + v_{\rm A}^2}{X-1} - \tfrac{1}{2}v_{\rm A}^2 X\Big),
\end{aligned} \qquad \text{(UR, frozen)} \tag{5.58}$$

where $\tilde{w}_1 = w_1/\rho_1$. The downstream plasma is relativistically hot so that $P_2 \simeq e_2/3$. The two equations (5.58) then lead to a quadratic equation for X with positive root (figure 5.5):

$$\boxed{X = \frac{1}{2v_{\rm A}^2}\Big(\sqrt{\tilde{w}_1^2 + 16v_{\rm A}^2\tilde{w}_1 + 16v_{\rm A}^4)} - \tilde{w}_1\Big). \qquad \text{(UR, frozen)}} \tag{5.59}$$

Now we know X and this gives $\gamma_{\rm rel}$ as a function of $\gamma_{\rm sh}$, see equation (5.36), and ρ_2 as a function of $\gamma_{\rm sh}$ and ρ_1, see equation (5.53). Finally, we can find P_2 and e_2 by inserting the expressions for X, ρ_2, and $\gamma_{\rm rel}$ in equations (5.58). In other words, for an ultra-relativistic shock in which magnetic flux is conserved, the complete solution is a function of $\gamma_{\rm sh}$, w_1, ρ_1, and $v_{\rm A}$ (or B_1). This solution is similar to the solutions given by Kennel and Coroniti [46] and Granot and Königl [30].

Magnetized shocks without magnetic flux conservation. Now I turn to the situation where magnetic flux is not conserved. Instead, let us assume that the ratio of magnetic to internal energy $\varepsilon_{\rm B} = B_2^2/(8\pi e_2)$ is a known quantity. Then

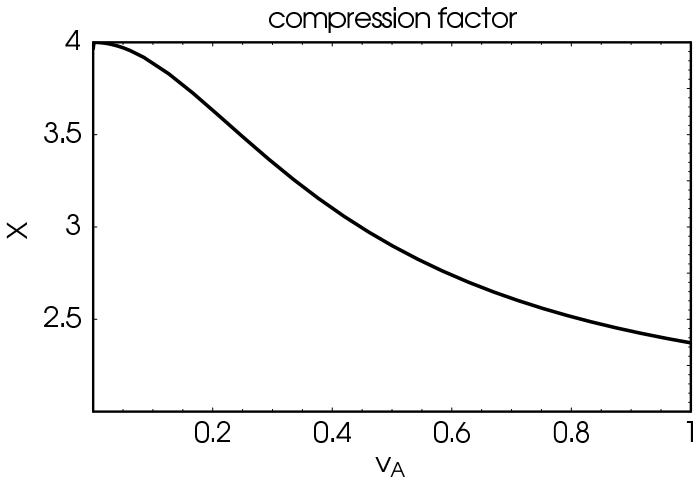

Figure 5.5: The compression factor $X \equiv \rho_2/(\gamma_{\rm rel}\rho_1)$ as a function of the Alfvén speed in the upstream plasma $v_{\rm A} \equiv B_1/\sqrt{4\pi\rho_1}$ for an ultra-relativistic shock in a cold upstream plasma ($w_1 = \rho_1$).

we have $\bar{e}_2 = e_2(1+\varepsilon_{\rm B})$ and since the downstream plasma is hot for ultra-relativistic shocks, we can use the effective adiabatic constant given in (5.15). The result is:

$$\boxed{\begin{aligned} v_2 &= \frac{1+3\varepsilon_{\rm B}}{3+3\varepsilon_{\rm B}}, \\ X &= \frac{4+6\varepsilon_{\rm B}}{1+3\varepsilon_{\rm B}}, \\ \gamma_{\rm rel} &= \frac{\gamma_{\rm sh}}{\sqrt{2+3\varepsilon_{\rm B}}}, \\ \frac{e_2}{\rho_2} &= \gamma_{\rm rel}\frac{\tilde{w}_1 + v_{\rm A}^2}{1+\varepsilon_{\rm B}}. \end{aligned} \qquad \text{(UR)}} \tag{5.60}$$

Note that the expression for $\gamma_{\rm rel}$ is not valid for $\varepsilon_{\rm B} \to \infty$; see equation (5.35). The equations above give the properties of the downstream plasma as a function of $\gamma_{\rm sh}$, w_1, ρ_1, $v_{\rm A}$ and $\varepsilon_{\rm B}$.

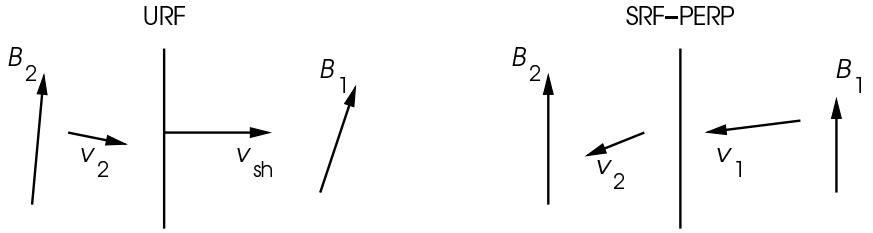

Figure 5.6: Left: shock moving through medium with a non-perpendicular magnetic field (seen from the upstream rest frame URF). Right: same situation in another reference frame where the magnetic field lines run perpendicular to the shock-normal.

5.3.3 Non-perpendicular shocks

So far I have ignored any parallel component of the magnetic field. I will now show that the effect of a parallel component will in general be small. Recall that i denotes the inclination angle of the magnetic field in the URF: $B_\perp = B_1 \sin i$ and $B_\parallel = B_1 \cos i$.

A parallel component of the magnetic field leads to many extra terms in the conservation laws that greatly complicate the calculations. However, it is possible to eliminate the parallel component of the magnetic field by transforming to a reference frame that moves perpendicularly to the shock-normal (in the y-direction). The price we pay for this is that all the velocities in the problem pick up a perpendicular component (figure 5.6).

We will first find the Lorentz transformation that eliminates the parallel field. The magnetic field in the shock rest frame is (see equation (5.10))

$$B_z^{\rm srf} = \gamma_{\rm sh} B_1 \sin i, \quad B_x^{\rm srf} = B_1 \cos i. \tag{5.61}$$

The ideal MHD condition in the upstream plasma tells us that there is an electric field along the y-axis ${E_y}^{\rm srf} = v_x B_z = -v\gamma_{\rm sh} B_1 \sin i$. Now do a Lorentz transformation with a boost $v_\perp$ in the z-direction. The parallel magnetic field (along the x-axis) in the new frame is

$$\gamma_\perp (B_x^{\rm srf} + v_\perp {E_y}^{\rm srf}) = \gamma_\perp B_1 \cos i (1 - v_\perp \gamma_{\rm sh} v \tan i), \tag{5.62}$$

where $\gamma_\perp = (1 - v_\perp^2)^{-1/2}$. The parallel magnetic field will be zero if we choose

$$\boxed{v_\perp = \frac{1}{\gamma_{\rm sh} v \tan i}.} \tag{5.63}$$

Note that this is only possible if $\gamma_{\rm sh} v > 1/\tan i$.

We can now calculate the shock conditions in this new frame of reference. To do this, we must use two Lorentz transformations (one to the SRF and one in the perpendicular direction) on the relevant four-vectors. For example, the upstream four-velocity becomes

$$u_1^\alpha = (\gamma_\perp \gamma_{\rm sh}, -\gamma_{\rm sh} v, 0, \gamma_{\rm sh}\gamma_\perp v_{\perp)} \tag{5.64}$$

and the magnetic four-vector becomes

$$\mathcal{B}_1^\alpha = (-\gamma_\perp \gamma_{\rm sh} B_1 \cos i/v, \gamma_{\rm sh} B_1 \cos i, 0, \gamma_\perp B_1/\sin i). \tag{5.65}$$

In the ultra-relativistic limit $\gamma_{\rm sh} \to \infty$, $v \to 1$, $v_\perp \to 0$, and $\gamma_\perp \to 1$. The jump conditions (5.6) yield

$$\textbf{Mass:} \qquad \rho_1 \gamma_1 v_{\parallel 1} = \rho_2 \gamma_2 v_{\parallel 2}, \tag{5.66}$$

$$\textbf{Par. momentum:} \qquad \bar{w}_1 \gamma_1^2 v_{\parallel 1}^2 + \bar{P}_1 = \bar{w}_2 \gamma_2^2 v_{\parallel 2}^2 + \bar{P}_2, \tag{5.67}$$

$$\textbf{Perp. momentum:} \qquad w_1 \gamma_1^2 v_{\perp 1} v_{\parallel 1} = w_2 \gamma_2^2 v_{\perp 2} v_{\parallel 2}, \qquad \text{(UR)} \tag{5.68}$$

$$\textbf{Energy:} \qquad \bar{w}_1 \gamma_1^2 v_{\parallel 1} = \bar{w}_2 \gamma_2^2 v_{\parallel 2}, \tag{5.69}$$

where $v_\parallel$ is the parallel velocity in this special frame with $v_{\parallel 1} = v/\gamma_\perp$. The perpendicular component $v_{\perp 1} = v_\perp$ is given in equation (5.63). The result only differs from the jump conditions (5.18–5.20) for perpendicular shocks through the extra conservation law of perpendicular momentum.

I will now relate $v_{\perp 2}$ to $v_\perp$ to show that $v_{\perp 2}$ is small for ultra-relativistic shocks. Conservation of perpendicular momentum gives

$$\frac{v_{\perp 2}}{v_{\perp 1}} = \frac{w_1 \gamma_1^2 v_{\parallel 1}}{w_2 \gamma_2^2 v_{\parallel 2}}. \tag{5.70}$$

Eliminate the parallel velocities using energy conservation to find:

$$\frac{v_{\perp 2}}{v_{\perp 1}} = \frac{\bar{w}_2}{\bar{w}_1} \times \frac{w_1}{w_2}. \tag{5.71}$$

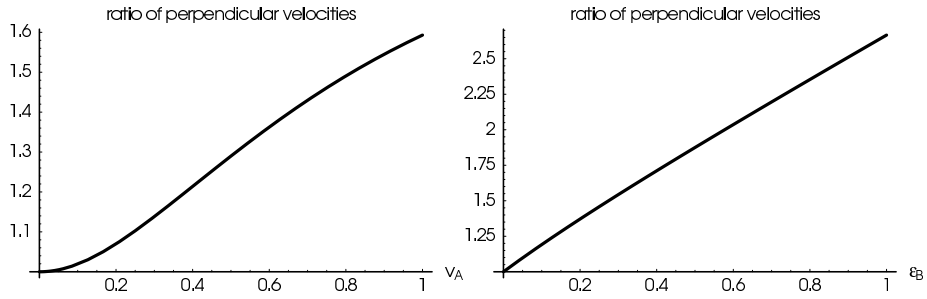

Figure 5.7: The ratio $v_{\perp 2}/v_{\perp 1}$. Left: for shocks with a frozen-in magnetic field as given in equation (5.73). Right: as given in equation (5.74) for negligible $v_{\rm A}$. The plots are made for a cold upstream plasma, $w_1 = \rho_1$ and a hot downstream plasma, $\Gamma = 4/3$.

Note that $v_{\perp 2}/v_{\perp 1} \to 1$ when $B_2^2/(4\pi w_2) \to 0$.

The result (5.54) for the energy density is still valid and we can use it to eliminate the enthalpies. In the ultra-relativistic limit $\bar{w}_2 \simeq \bar{\Gamma}_B \bar{e}_2$ and $w_2 \simeq \Gamma e_2$, and we find

$$\frac{v_{\perp 2}}{v_{\perp 1}} = \frac{\bar{\Gamma}_B}{\Gamma} \frac{\bar{e}_2/\rho_2}{e_2/\rho_2} \frac{w_1}{\bar{w}_1} = \frac{\bar{\Gamma}_B}{\Gamma} \frac{\tilde{w}_1}{e_2/(\gamma_{\rm rel}\rho_2)}. \qquad \text{(UR)} \tag{5.72}$$

We know from the analysis of perpendicular shocks, *e.g.*, equation (5.58), that the quantity $e_2/(\gamma_{\rm rel}\rho_2)$ is of order one so that $v_{\perp 2}$ will be of the same order as $v_{\perp 1}$, *i.e.*, small and of order $1/\gamma_{\rm sh}$ unless $\tan i \lesssim 1/\gamma_{\rm sh}$.

To find an explicit equation for $v_{\perp 2}$ insert the ultra-relativistic results for $\bar{\Gamma}_B$ and $e_2/(\gamma_{\rm rel}\rho_2)$. For a frozen-in magnetic field we can use equation (5.58) to find (figure 5.7)

$$\frac{v_{\perp 2}}{v_{\perp 1}} = \frac{\bar{\Gamma}_B}{\Gamma} \frac{\tilde{w}_1}{\tilde{w}_1 - v_{\rm A}^2(\frac{1}{2}X - 1)}. \qquad \text{(UR, frozen)} \tag{5.73}$$

Note that $\bar{\Gamma}_B = X/(X-1)$ and the value of X lies in the range 2–4; see equation (5.59). For a non-conserved magnetic flux we can use the $\varepsilon_{\rm B}$ notation to rewrite relation (5.72) using expression (5.15) for $\bar{\Gamma}_B$ and the relations for the downstream quantities (5.60) (figure 5.7):

$$\frac{v_{\perp 2}}{v_{\perp 1}} = \frac{1 + 4\varepsilon_{\rm B} + 3\varepsilon_{\rm B}^2}{1 + 2\varepsilon_{\rm B}} \frac{\tilde{w}_1}{\tilde{w}_1 + v_{\rm A}^2}. \qquad \text{(UR)} \tag{5.74}$$

The last step is to transform back to the shock rest frame where the upstream plasma flows along the shock-normal. Since $v_{\perp 1}$ is small we can use a Galilean transformation instead of a Lorentz transformation and simply subtract $v_{\perp 1}$ from $v_{\perp 2}$:

$$v_{\perp 2}^{\mathrm{srf}} = \left(\frac{v_{\perp 2}}{v_{\perp 1}} - 1\right) \frac{1}{\gamma_{\mathrm{sh}} v \tan i} \qquad \text{(UR, SRF)} \tag{5.75}$$

where $v_{\perp 2}/v_{\perp 1}$ follows either from equation (5.73) or (5.74).

The conclusion is that the difference between perpendicular and non-perpendicular shocks is that in non-perpendicular shocks the downstream plasma picks up a velocity in the direction perpendicular to the shock-normal. This velocity is of order $1/(\gamma_{\mathrm{sh}} \tan i)$ and will be small if $\gamma_{\mathrm{sh}} \gg 1/\tan i$.

5.4 Discussion of the results

5.4.1 General results

Conservation laws constrain the change in plasma properties across a shock front. I have formulated these constraints in the previous section for ultra-relativistic shocks as relations between the up- and downstream plasma properties (equations (5.18–5.20), (5.30–5.32) or (5.66–5.69)) and as solutions for the downstream plasma properties (equations (5.48), (5.59), or (5.60)). The solutions give the downstream plasma properties (energy density, mass density, flow speed, and magnetic field strength) as a function of the upstream plasma properties (mass density, enthalpy density, magnetic field strength) and the shock Lorentz factor.

I have shown that we can consider the magnetic field to be perpendicular to the shock-normal except when the shock moves almost parallel to the upstream magnetic field lines.

The downstream plasma is hot so that the equation of state is well approximated by one with a ratio of specific heats $\Gamma = 4/3$, because the internal energy density is an order of the Lorentz factor larger than the mass density.

The shock is strong ($P_2 \gg P_1$) because the downstream pressure is at least two orders of the Lorentz factor larger than the upstream pressure.

5.4.2 Internal structure of the shock

These shock properties result from conservation of mass, momentum, energy and magnetic flux. This large scale treatment does not specify the internal processes that are responsible for the dissipation of bulk kinetic energy to inter-

nal energy in the shock transition. These processes might involve particle creation and magnetic field generation and could influence the properties of the shocked plasma.

If particle creation plays a role in the shock transition the mass density behind the shock is higher. Nevertheless, many of the results do not depend on conservation of mass and therefore still apply.

It is likely that the assumption of magnetic flux conservation is also incorrect because plasma instabilities that violate the MHD assumption occur in the shock transition.

The processes that involve such particle creation or plasma instabilities require a closer look at the internal structure of the shock. A first study of the influence of plasma instabilities on the magnetic field in relativistic shocks was given, *e.g.*, by Medvedev & Loeb [58] and by Brainerd [9]. In this chapter the magnetic energy density was treated as a free parameter ε_B; see equations (5.60). In the following chapters we investigate the plasma instabilities that determine this parameter ε_B in more depth.

Chapter 6

Linear theory of the Weibel instability

As the pre- and post-shock particles mix in the shock front they form a plasma with wildly differing particle velocities: seen from the point of view of the shock, the pre-shock particles will move into the shock front with a high velocity. Such a situation is unstable and because of the Weibel instability the particles will arrange themselves into separated electrical currents. These currents will generate a small-scale magnetic field.

In this chapter we show how the initial growth of the Weibel instability only depends on how diffuse the velocity distribution is and on the strength of the incoming plasma flow compared to the (shocked) background plasma.

Because a relativistic collisionless shock wave is formed by electromagnetic interaction instead of particle collisions the previous chapter introduced the question of how much energy will end up in electromagnetic energy. In chapters 8 and 9 we will see how the growth of the magnetic field strength will be stopped, which will lead to an estimate of the magnetic energy density.

This chapter has been submitted to Astronomy & Astrophysics [3].

6.1 Introduction

The Weibel instability is an electromagnetic instability of low-frequency perturbations in a plasma where one (or more) of the particle species has an anisotropic momentum distribution. In its original form, as discussed by Weibel [98], this anisotropy is caused by different values of the kinetic temperature of the particles in two mutually orthogonal directions. More recent astrophysical applications, see for instance [32], [31], [58] and [24], have concentrated on the anisotropy caused by the presence of bulk plasma motions in the form of beams in a (thermal) background plasma.

In relativistic shocks, which propagate into a cold medium with bulk speed $V_{\rm sh} \sim c$, this version of the instability could be important as the collisionless relaxation mechanism in the 'transition layer' where the shock-heated and incoming (unshocked) plasma mix. As this instability has its most rapid growth in the low-frequency regime, so that $|\omega| \ll kc$ with $k = 2\pi/\lambda$ the wave number, it generates an electromagnetic field ($\delta\mathbf{E}$, $\delta\mathbf{B}$) that is dominated by the magnetic component: $|\delta\mathbf{B}| \gg |\delta\mathbf{E}|$.

Generation of magnetic fields is a necessary ingredient in those models that explain the prompt gamma-rays, and the broad-band afterglow emission from Gamma Ray Bursts as (Lorentz-boosted) synchrotron radiation. These synchrotron models must assume that the magnetic field is strong in the sense that the ratio of magnetic to internal energy is of order $B^2/8\pi e \approx 0.01 - 0.1$. Here B the magnetic field strength with corresponding energy density $e_{\rm B} = B^2/8\pi$, and e is the internal energy density of the radiating plasma. Details of the arguments leading to this estimate can be found in the reviews by Piran [74, 75] and Mészáros [65, 66], and in the references therein.

The compression of existing interstellar (or circumstellar) magnetic fields by a relativistic shock leads to an insufficient field strength, with $\epsilon_{\rm B} \ll 1$. In fact, without additional field amplification one finds that the pre- and post-shock values of $\epsilon_{\rm B} \equiv B^2/8\pi e$ are of similar magnitude, see equation (6.4) below. For an exterior shock, propagating into a cold astrophysical plasma with proper mass density ρ, the upstream energy density is dominated by the rest energy density of the hadrons: $e \simeq \rho c^2$. Therefore, the pre-shock value of the equipartition parameter $\epsilon_{\rm B1}$ is small:

$$\epsilon_{\rm B1} \approx B_1^2/8\pi\rho_1 c^2 = \left(V_{\rm A}^2/2c^2\right)_1 \ll 1\,. \tag{6.1}$$

Here $V_{\rm A} = B/\sqrt{4\pi\,\rho}$ is the (non-relativistic) Alfvén velocity. Here (and in what follows) we use the subscript 1 (2) to denote the pre-shock (post-shock) values of physical quantities.

In the best possible case, where the pre-shock magnetic field is tangential to the shock surface with strength $B_{\rm t}$, the shock jump conditions (in particular mass conservation and magnetic flux conservation) imply that the pre- and post shock magnetic fields are related by

$$\frac{B_{\rm t1}}{\rho_1} = \frac{B_{\rm t2}}{\rho_2} \, . \tag{6.2}$$

Since the upstream magnetic field is dynamically unimportant (equation 6.1), one can apply the approximate *hydro*dynamic jump conditions of Blandford and McKee [8]. For an ultra-relativistic shock with $\gamma_{\rm sh} = 1/\sqrt{1 - V_{\rm sh}^2/c^2} \gg 1$, propagating into a cold medium with mass density ρ_1 and pressure $P_1 \ll \rho_1 c^2$, the relativistically hot post-shock gas has a proper mass density ρ_2, pressure P_2 and a thermal energy density e_2 given by:

$$\frac{\rho_2}{\rho_1} = 2\sqrt{2}\,\gamma_{\rm sh} \;\; , \;\; e_2 = 3P_2 = 2\gamma_{\rm sh}^2 \rho_1 c^2 \, . \tag{6.3}$$

Relations (6.2) and (6.3) imply that the post-shock ratio of magnetic and thermal energy densities is

$$\epsilon_{\rm B2} \equiv \frac{B_{\rm t2}^2}{8\pi e_2} \approx \frac{B_{\rm t1}^2}{2\pi\rho_1 c^2} \approx 4\epsilon_{\rm B1} \ll 1 \, . \tag{6.4}$$

This shows that the pre- and post shock values are of similar magnitude. Clearly an additional mechanism is needed to generate a post-shock magnetic field with $\epsilon_{\rm B2} \sim 0.1$–$1$.

This chapter is concerned with the linear stage of the Weibel instability, where the electromagnetic field amplitudes grow exponentially, $|\delta\mathbf{E}| \, , \, \delta|\mathbf{B}| \propto \exp(\tilde{\sigma} t)$, with $\tilde{\sigma} = \mathrm{Im}(\omega)$ the growth rate. We present a detailed analysis of the dispersion relation that determines the growth rate starting from first principles of the fluid description of the plasma and of a kinetic *waterbag* description of the plasma. These results are important for the analysis of the non-linear stage of the relativistic Weibel instability, which depends sensitively on the dispersion in the plasma; see chapter 9. From the dispersion relation we derive expressions for the growth rate $\tilde{\sigma}$ using various approximations: non-relativistic and ultrarelativistic; with and without a background magnetic field. The aim is to determine the basic parameters that characterize the solution.

In section 6.2 we introduce the covariant formalism employed here and the general form of the plasma response. In section 6.3 we derive the linear dispersion relation for the beam-driven Weibel instability from two points of view: a

fully relativistic fluid plasma version and a kinetic version, both for two counterstreaming beams. In the latter case we employ a mathematically convenient model for the momentum distribution of the beam particles: the *waterbag distribution*. In section 6.4 we consider the case of cold relativistic beams and the non-relativistic limit, showing that our results agree with those available for these two cases in the literature. In section 6.5 we discuss the Weibel instability driven by two symmetric, counterstreaming beams. There we show that the fluid and kinetic results are closely related and are characterized by only two parameters: the ratio of effective plasma frequencies of beams and background plasma and an effective Mach number of the beam plasma with respect to the background plasma. In section 6.6 we consider the ultra-relativistic limit where the beam velocity is close to c and the beam Lorentz factor satisfies $\gamma_{\rm b} \gg 1$. In section 6.7 we consider the effect of anomalous dispersion that occurs when the background plasma is relativistically hot, and in section 6.8 we discuss the magnetized Weibel instability for beams aligned with the magnetic field. There we show that in the ultra-relativistic case the influence of the background magnetic field is small for typical parameters. In section 6.9 we briefly discuss the asymmetric case, where the instability is driven by relativistic beams of unequal density. Conclusions are presented in section 6.10. The Appendices 6.11 through 6.14 contain the necessary mathematical details.

6.2 Covariant formulation of plasma dispersion

Anticipating our application to relativistic shocks, we use a fully relativistic (covariant) formulation that is valid in any (conveniently chosen) reference frame. This has the advantage that we can decompose the dispersion tensor of the plasma into normal modes based on a set of polarization vectors, postponing considerations of the choice of a specific reference frame as long as possible (see below). Co- and contravariant vector and tensor components are related in the usual fashion, e.g. $\tilde{J}_\mu = \eta_{\mu\nu}\tilde{J}^\nu$ and $\alpha^\mu_{\ \nu} = \eta^{\mu\sigma}\,\alpha_{\sigma\nu}$, with $\eta_{\mu\nu} = \eta^{\mu\nu} \equiv \mathrm{diag}(1\,,\,-1\,,\,-1\,,\,-1)$ the Minkowski metric tensor of flat spacetime, which satisfies $\eta^\mu_{\ \nu} = \delta^\mu_{\ \nu}$.

The covariant description employed here (and by others, see the references below) expresses the linear electromagnetic response of the plasma in terms of the wave four-current $\tilde{J}^\mu(k) = (\tilde{\rho}\,,\,\tilde{\mathbf{J}}(k))$ and the wave four-potential $\tilde{A}^\mu(k) = (\tilde{\Phi}(k)\,,\,\tilde{\mathbf{A}}(k))$ in the Fourier domain through a tensorial relation of the form [e.g. 61]

$$4\pi\tilde{J}^\mu(k) = \alpha^\mu_{\ \nu}(k)\,\tilde{A}^\nu(k)\ . \tag{6.5}$$

The polarization tensor $\alpha^{\mu}_{\nu}(k)$ contains all information about the plasma response. Here, and in what follows, we employ a tilde ($\sim$) to denote the four-potential and four-current density in the Fourier domain (see definition 6.92 in Appendix 6.11), which depend on the wavenumber four-vector $k^{\mu} = (\omega/c\,,\,\mathbf{k})$. Greek indices are used to denote the components of four-vectors.

The dispersion relation for the linear electromagnetic wave modes in the plasma follows from using (6.5) in the covariant set of Maxwell equations, equation (6.90) of Appendix 6.11. The resulting set of linear relations in the Fourier domain takes the form $D^{\mu\nu}(k)\,\tilde{A}_{\nu}(k) = 0$, with $D^{\mu\nu}(k) \equiv (k\cdot k)\,\eta^{\mu\nu} - k^{\mu}k^{\nu} + \alpha^{\mu\nu}(k)$, see Appendix 6.12. This leads to three independent physical wave modes. It is convenient to expand the four-potential of the three physical degrees of freedom in terms of three mutually orthogonal polarization vectors: $\tilde{A}^{\mu}(k) = \tilde{A}^{i}(k)\,e^{\mu}_{i}$, with $i = 1\,,\,2\,,\,3$. The dispersion relation, which is the solution condition for the system of equations, then takes the form $\mathcal{D}(\omega\,,\,K) = \det(\mathcal{D}_{ij}) = 0$, where the 3×3 matrix $\mathcal{D}_{ij}$ is defined in terms of α^{μ}_{ν}, k^{μ} and the three polarization vectors e^{μ}_{i} of the linear wave modes, see Appendix 6.12, equation (6.134). If one chooses a Lorentz gauge for the electromagnetic fields, $k^{\mu}\tilde{A}_{\mu} = 0$, $\mathcal{D}_{ij}$ takes the form:

$$\mathcal{D}_{ij}(k) = (k\cdot k)\,g_{ij} + \alpha_{ij}(k)\;. \tag{6.6}$$

Here we employ the notation $A\cdot B \equiv \eta_{\mu\nu}\,A^{\mu}B^{\nu}$ for the scalar product of two four-vectors, and introduce the quantities $g_{ij} \equiv (e_i\cdot e_j)$, and $\alpha_{ij} \equiv e^{\mu}_{i}\,\alpha_{\mu\nu}\,e^{\nu}_{j}$. We also adhere to the Einstein summation convention for double indices.

This covariant formulation of the linear electromagnetic response of the plasma is based on the work of Melrose [62], see also [61] and [18], and is very convenient for this problem. As it is not commonly used, we provide a full set of definitions together with the necessary mathematical details in the Appendices 6.11 and 6.12. Appendix 6.13 contains full expressions for the dispersion tensor for the different approaches presented below.

6.2.1 Polarization tensor in the fluid approximation

Many of the properties of the beam-driven Weibel instability can be understood from a simple fluid model. Consider a plasma consisting of several particle species, with charge q_{s}, rest mass m_{s} and four-velocity $U^{\mu}_{s} \equiv (\gamma_{\mathrm{s}}\,,\,\gamma_{\mathrm{s}}\mathbf{V}_{\mathrm{s}})$ for each particle species s. The proper density of species s is n_{s}, the rest mass density is $\rho_{\mathrm{s}} = n_{\mathrm{s}}m_{\mathrm{s}}$, the thermal energy density is e_{s} and the pressure is P_{s}. We will use units with $c = 1$ so that the Lorentz factor is $\gamma_{\mathrm{s}} = 1/\sqrt{1-|\mathbf{V}_{\mathrm{s}}|^2}$.

However, we will retain c in some expressions for clarity. For the moment, we will neglect the influence of an ambient magnetic field, in effect treating an unmagnetized plasma. The magnetized case will be considered briefly in section 6.8.

The calculation of the linear response of each species involves the linearization of the covariant equation of motion for species s in a charged fluid,

$$(\rho + e + P)_{\rm s}\ (U_{\rm s}\cdot\partial)\, U^\mu_{\rm s} = h^{\mu\nu}_{\rm s}\,\partial_\nu P_{\rm s} + n_{\rm s} q_{\rm s} F^{\mu\nu} U_{{\rm s}\nu}\ . \tag{6.7}$$

Here $h^{\mu\nu}_{\rm s} \equiv \eta^{\mu\nu} - U^\mu_{\rm s} U^\nu_{\rm s}$ is the tensor that projects onto the hyperplane perpendicular to the four-velocity $U^\mu_{\rm s}$. $F^{\mu\nu} = \partial^\mu A^\nu - \partial^\nu A^\mu$ is the Faraday tensor of the electromagnetic field. Equation of motion (6.7) is supplemented by the continuity equation and an equation of state,

$$\partial_\mu \left(n_{\rm s} U^\mu_{\rm s} \right) = 0 \ \ , \ \ P_{\rm s} \propto n_{\rm s}^{\Gamma_{\rm s}}\ . \tag{6.8}$$

This procedure leads to a polarization tensor $\alpha^\mu_\nu = \sum_s (\alpha^\mu{}_\nu)_{\rm s}$, where the contribution from species s takes the form (see equation (6.112) in the appendix):

$$\left(\alpha^\mu{}_\nu\right)_{\rm s} = -\tilde{\omega}^2_{\rm ps}\, \mathcal{P}^\mu_{{\rm s}\alpha} \left(\delta^\alpha{}_\beta - \frac{C_{\rm s}^2\, k^\alpha k_\beta}{(k\cdot U_{\rm s})^2 - K^2_{{\rm s}\perp} C_{\rm s}^2} \right) \mathcal{P}^{\dagger\beta}_{{\rm s}\nu}\ . \tag{6.9}$$

The projection tensor $\mathcal{P}^\mu_{{\rm s}\nu} \equiv \delta^\mu_\nu - U^\mu_{\rm s} k_\nu/(k\cdot U_{\rm s})$ and its transpose appear as a result of charge conservation and the invariance of the current density $\tilde{J}^\mu$ under electromagnetic gauge transformations [18], see Appendix 6.11 for a full discussion. From here onwards $U^\mu_{\rm s}$ is the unperturbed four-velocity of species s.

The relativistic plasma frequency $\tilde{\omega}_{\rm ps}$ and the sound speed $C_{\rm s}$ of species s are respectively defined by:

$$\tilde{\omega}^2_{\rm ps} \equiv \frac{4\pi n_{\rm s}^2 q_{\rm s}^2}{(\rho + e + P)_{\rm s}} \ \ , \ \ C_{\rm s}^2 \equiv \frac{\Gamma_{\rm s} P_{\rm s}}{(\rho + e + P)_{\rm s}}\ . \tag{6.10}$$

The quantity $K^2_{{\rm s}\perp}$ is the absolute value of the length of the space-like four-vector $k^\mu_{{\rm s}\perp} \equiv h^{\mu\nu}_{\rm s} k_\mu = k^\mu - (k\cdot U_{\rm s}) U^\mu_{\rm s}$:

$$K^2_{{\rm s}\perp} \equiv -k_{{\rm s}\perp}\cdot k_{{\rm s}\perp} = (k\cdot U_{\rm s})^2 - k\cdot k\ . \tag{6.11}$$

Choosing the manifestly covariant Lorentz gauge $k_\mu \tilde{A}^\mu = 0$ and using the resulting properties of the three polarization vectors $e_1 - e_3$ (see Appendix 6.12,

equations (6.129–6.131), it follows from expression (6.9) that the contribution of species s to $\alpha_{ij} \equiv e_i^\mu \, \alpha_{\mu\nu} \, e_j^\nu$ is

$$\left(\alpha_{ij}\right)_{\rm s} = -\tilde{\omega}_{\rm ps}^2 \left\{ g_{ij} + \frac{(k\cdot k)\left(1-C_{\rm s}^2\right)\, U_{{\rm s}i} U_{{\rm s}j}}{(k\cdot U_{\rm s})^2 - K_{{\rm s}\perp}^2 C_{\rm s}^2} \right\} , \tag{6.12}$$

where $U_{{\rm s}i} \equiv U_{\rm s}\cdot e_i$ and $g_{ij} = e_i \cdot e_j$.

6.2.2 Polarization tensor in the kinetic description

Although the fluid approach of the previous section is mathematically easier, a more adequate description of the waves and oscillations in the plasma is given by the kinetic approach. This is especially relevant since we will consider plasmas with a finite temperature in the following sections. We will compare results for the two approaches in section 6.5.

In the kinetic description, one describes the multi-species plasma using the covariant Vlasov equation for the phase-space distribution function $\mathcal{F}_{\rm s}(x^\mu\,,\, p^\mu)$ of each species in the plasma:

$$\frac{{\rm d}\mathcal{F}_{\rm s}}{{\rm d}\tau} \equiv \frac{{\rm d}x^\mu}{{\rm d}\tau}\,\frac{\partial \mathcal{F}_{\rm s}}{\partial x^\mu} + \frac{q_{\rm s}}{m_{\rm s}}\, F^{\mu\nu} p_\nu \,\frac{\partial \mathcal{F}_{\rm s}}{\partial p^\mu} = 0 \,, \tag{6.13}$$

cf. equations (6.113) and (6.114) of Appendix 6.11. As before, $F^{\mu\nu} = \partial^\mu A^\nu - \partial^\nu A^\mu$ is the Faraday tensor of the electromagnetic field. The position four vector x^μ and momentum four vector p^μ satisfy ${\rm d}x^\mu/{\rm d}\tau = p_\mu/m_{\rm s}$, with τ the proper time.

Linearizing the Vlasov equation in the Fourier domain, and calculating the four-current density $\tilde{J}^\mu$ resulting from the linear perturbation, one can calculate the polarization tensor $(\alpha^\mu_{\ \nu})_{\rm s}$ for each species.

As was the case in the fluid description, it is convenient to work with the representation α_{ij} of the polarization tensor in the Lorentz gauge. The contribution to this tensor from species s, $(\alpha_{ij})_{\rm s}$, can be written as (see Appendix 6.13, equations 6.143 and 6.144):

$$\left(\alpha_{ij}\right)_{\rm s} = -\tilde{\omega}_{\rm ps}^2 \int \frac{{\rm d}^3\mathbf{p}}{\gamma(\mathbf{p})}\, f_{0{\rm s}}(\mathbf{p}) \,\left(g_{ij} + \frac{(k\cdot k)\, p_i p_j}{(k\cdot p)^2} \right) . \tag{6.14}$$

Here $f_{0{\rm s}}(\mathbf{p})$ is the ordinary Vlasov distribution of the particles in three-momentum space, normalized to unity, and $\overline{n}_{\rm s}$ is the density of the particle species s in the lab frame, so that $\overline{n}_{\rm s} f_{0{\rm s}}(\mathbf{p})\,{\rm d}^3\mathbf{p}$ is the lab-frame number density of particles

with their three-momentum in an infinitesimal momentum space volume $\mathrm{d}^3\mathbf{p}$ around $\mathbf{p}$. The frequency $\bar{\omega}_{\mathrm{ps}}$ is defined by

$$\bar{\omega}_{\mathrm{ps}}^2 = \frac{4\pi q_{\mathrm{s}}^2 \overline{n}_{\mathrm{s}}}{m_{\mathrm{s}}} \ , \tag{6.15}$$

and is the plasma frequency based on the density of species s in the lab frame. As before $g_{ij} \equiv e_i \cdot e_j$ and we define $p_i = p \cdot e_i$, with $p^\mu = (E\,,\,\mathbf{p})$ the four-momentum vector.

6.2.3 The cold plasma limit

Because cold plasmas are already well-studied in the literature we will check our results in later sections by taking the cold limit. In this section we will give an expression for the polarization tensor in the cold limit.

It is well-known [e.g. 63] that the fluid approach and the kinetic approach yield the same answer for a cold plasma. Our expressions for α_{ij} satisfy this simple requirement. The cold plasma assumption corresponds to putting $C_{\mathrm{s}} = 0$ in expression (6.12), and to putting $f_{0\mathrm{s}}(\mathbf{p}) = \delta^3(\mathbf{p} - \mathbf{p}_{\mathrm{s}})$ in expression (6.14). Here $\mathbf{p}_{\mathrm{s}} \equiv \gamma_{\mathrm{s}} m_{\mathrm{s}} \mathbf{V}_{\mathrm{s}}$ is the bulk momentum of particle species s, where we still allow for relativistic bulk motion with Lorentz factor $\gamma_{\mathrm{s}} = 1/\sqrt{1 - V_{\mathrm{s}}^2} \gg 1$. In that case one has $\overline{n}_{\mathrm{s}} = \gamma_{\mathrm{s}} n_{\mathrm{s}}$ due to Lorentz-contraction, and the two plasma frequencies defined above are related by:

$$\tilde{\omega}_{\mathrm{ps}}^2 = \frac{\bar{\omega}_{\mathrm{ps}}^2}{\gamma_{\mathrm{s}}} = \frac{4\pi q_{\mathrm{s}}^2 n_{\mathrm{s}}}{m_{\mathrm{s}}} \ . \tag{6.16}$$

The cold plasma polarization tensor is then given by

$$\left(\alpha_{ij}\right)_{\mathrm{cold}} = -\sum_{\mathrm{s}} \tilde{\omega}_{\mathrm{ps}}^2 \left(g_{ij} + \frac{(k \cdot k)\, U_{\mathrm{s}i} U_{\mathrm{s}j}}{(k \cdot U_{\mathrm{s}})^2} \right) \ , \tag{6.17}$$

where the sum is over all plasma species, and $U_{\mathrm{s}}^\mu = p_{\mathrm{s}}^\mu / m_{\mathrm{s}} = \gamma_{\mathrm{s}}(1\,,\,\mathbf{V}_{\mathrm{s}})$ is the four-velocity of the bulk motion of species s.

6.3 The beam-driven Weibel instability

We now consider the case of a plasma with the following components: a (multi-species) 'background' plasma at rest in the lab frame with bulk four-velocity

$U_s^\mu = (1\,,\,0\,,\,0\,,\,0)$, and two counterstreaming beams of charged particles moving along the z-axis, with an associated four-velocity

$$U_\pm^\mu = \gamma_b\ (1\,,\,0\,,\,0\,,\,\pm V_b)\ . \tag{6.18}$$

The beam Lorentz factor is $\gamma_b = 1/\sqrt{1 - V_b^2}$. The beam particles have a rest mass m_b and a charge q_b. The two beams have a proper density

$$n_\pm = \frac{1 \pm \Delta}{2}\, n_b\ . \tag{6.19}$$

The parameter $\Delta \leq 1$ measures the asymmetry in the strength of the two counterstreaming beams, with the symmetric case of two equal density beams corresponding to $\Delta = 0$. For simplicity we assume that the beams consist of a single particle species, and that the temperature of the two beams, quantified by the sound speed C_b of the beam plasma in the fluid description or by the velocity dispersion in the kinetic description (see below), is identical. The case of beams consisting of more than one particle species is a straightforward generalization of the results presented here.

We limit the discussion to the case of waves with a wave vector $\mathbf{k} = K\hat{\mathbf{x}}$ perpendicular to the beam direction, corresponding with a wave four-vector $k^\mu = (\omega\,,\,K\,,\,0\,,\,0)$ in the lab frame. This choice implies that, for species belonging to the background plasma, one has $k \cdot U_s = \omega$, and $K_{s\perp} = |K|$. In this case the three polarization vectors can be chosen as $e_1^\mu = (K\,,\,\omega\,,\,0\,,\,0)/\sqrt{|k \cdot k|}$, $e_2^\mu = (0\,,\,0\,,\,1\,,\,0)$ and $e_3^\mu = (0\,,\,0\,,\,0\,,1)$, see Appendix 6.12. These three vectors all satisfy $k \cdot e_i = 0$, ensuring that $\tilde{A}^\mu(k) = \sum_i \tilde{A}^i(k)\, e_i^\mu$ satisfies the Lorentz gauge.

For this choice of $\mathbf{k}$, the only non-zero components of the tensor $\mathcal{D}_{ij}$ as defined in equation (6.6) are: $\mathcal{D}_{11}$, $\mathcal{D}_{22}$, $\mathcal{D}_{33}$ and $\mathcal{D}_{13} = \mathcal{D}_{31}^*$. The dispersion relation $\mathcal{D}(\omega\,,\,K) \equiv \det(\mathcal{D}_{ij}) = 0$ factors into

$$\mathcal{D}(\omega\,,\,K) = \mathcal{D}_{22}\ \left(\mathcal{D}_{11}\mathcal{D}_{33} - |\mathcal{D}_{31}|^2\right) = 0\ . \tag{6.20}$$

Here $|\mathcal{D}_{31}|^2 = \mathcal{D}_{31}\mathcal{D}_{31}^* = \mathcal{D}_{31}\mathcal{D}_{13}$. The explicit expressions for the non-zero components of $\mathcal{D}_{ij}$ are listed in Appendix 6.13.

The solution $\mathcal{D}_{22} = 0$ corresponds to a stable, purely electromagnetic mode with $\tilde{\mathbf{E}} \perp \mathbf{k}$ and $\tilde{\mathbf{E}} \perp \mathbf{V}_b$ in the lab frame, with $\mathbf{V}_b = \pm V_b\hat{\mathbf{z}}$ the beam velocity. This mode is unaffected by the bulk motion of the forward and backward beam. It will not be considered further.

The remaining two modes, which follow from $\mathcal{D}_{11}\mathcal{D}_{33} - |\mathcal{D}_{31}| = 0$, are mixed in the sense that the wave electromagnetic field in the rest frame of the background plasma is -in general- not purely transverse, with $\tilde{\mathbf{E}} \perp \mathbf{k}$ in the lab frame, or purely longitudinal, with $\tilde{\mathbf{E}} \parallel \mathbf{k}$ in the lab frame. Physically, this is due to the fact that the bulk motion of the beams leads to an 'advection current' in addition to the usual 'conduction current'. The advection current arises as charge density perturbations in the beam plasma are dragged along by the beams, whereas the conduction current is due to the perturbations in the velocity of the beam particles. This couples the transverse (current-driven) and longitudinal (charge-driven) response of the beam plasma. However, in the symmetric case of equal beams, $\Delta = 0$, the charge density perturbations of the two beams are opposite and cancel each other, but the associated advection currents are equal due to the opposite sign of the velocity of the two beams. The charge density cancellation results in $\mathcal{D}_{13} = \mathcal{D}_{31} = 0$. In that symmetric case the Weibel instability is purely transverse, with $\tilde{\mathbf{E}} \perp \mathbf{k}$ and $\tilde{\mathbf{E}} \parallel \mathbf{V}_\mathrm{b}$ in the lab frame. We will mostly consider this symmetric case, where the Weibel instability is the unstable solution branch of the much simplified dispersion relation

$$\mathcal{D}_{33}(k) = K^2 - \omega^2 + \sum_s (\alpha_{33})_s = 0 \,. \tag{6.21}$$

The asymmetric case with $\mathcal{D}_{31} \neq 0$ will be briefly considered in the next section for the case of cold beams in a cold background plasma, and in section 6.9 for the hot case.

6.4 The limit of a cold beam and the non-relativistic limit

As a check on our results, we briefly consider the limit of a cold beam and cold background plasma, and the non-relativistic limit, for which results are available in the literature. For ease of comparison we reinstate c in this section. As before we assume $\mathbf{k} = K\hat{\mathbf{x}}$ and $\mathbf{V}_\mathrm{b} = \pm V_\mathrm{b}\,\hat{\mathbf{z}}$ in the laboratory frame, which is the rest frame of the background plasma. Using (6.6) and (6.17), the dispersion relation (6.20) can be written as:

$$|k \cdot k| \left\{ \left(1 - \sum_\mathrm{s} \frac{\tilde{\omega}_\mathrm{ps}^2}{\omega^2} \right) \left(K^2c^2 - \omega^2 + \sum_\mathrm{s} \frac{\tilde{\omega}_\mathrm{ps}^2}{\omega^2} \left[1 - \frac{V_\mathrm{s}^2}{c^2} + \frac{K^2 V_\mathrm{s}^2}{\omega^2} \right] \right) \right. \tag{6.22}$$

$$\left. - \left(\sum_\mathrm{s} \frac{\tilde{\omega}_\mathrm{ps}^2}{\omega^2} K V_\mathrm{s} \right)^2 \right\} = 0 \,.$$

Here the sum extends over *all* species in the plasma: beams and stationary background. The background plasma has $V_\mathrm{s} = 0$, and the 'cold' plasma frequency is $\tilde{\omega}_\mathrm{ps}^2 = 4\pi q_\mathrm{s}^2 n_\mathrm{s}/m_\mathrm{s}$ for species s, with the density of the two individual beams given by equation (6.19). This dispersion relation agrees with the more general result of Akhiezer et al. [6] for cold relativistic beams in the case $\mathbf{k} \perp \mathbf{V}_\mathrm{b}$, and with the dispersion relation of Alexandrov et al. [7], Ch. 6.3.1., for $\mathbf{k} \perp \mathbf{V}_\mathrm{b}$ and zero magnetic field.

In the non-relativistic limit, where $V_\mathrm{s} \ll c$ for all species, the unstable solution branch has $|\omega^2| \ll \sum_\mathrm{s} \tilde{\omega}_\mathrm{ps}^2$. The same holds for weak beams in the relativistic case, i.e. when the plasma frequency associated with the beams satisfies $\tilde{\omega}_\mathrm{pb}^2 = 4\pi q_\mathrm{b}^2 n_\mathrm{b}/m_\mathrm{b} \ll \sum_\mathrm{s} \tilde{\omega}_\mathrm{ps}^2$. If either of these two inequalities applies one can make the approximation $1 - \sum_\mathrm{s} \tilde{\omega}_\mathrm{ps}^2/\omega^2 \approx -\sum_\mathrm{s} \tilde{\omega}_\mathrm{ps}^2/\omega^2$, and the dispersion relation (6.22) reduces to

$$K^2c^2 - \omega^2 + \sum_\mathrm{s} \tilde{\omega}_\mathrm{ps}^2 \left(\frac{1}{\gamma_\mathrm{s}^2} + \frac{K^2 V_\mathrm{s}^2}{\omega^2} \right) - \frac{K^2 \left(\sum_\mathrm{s} \tilde{\omega}_\mathrm{ps}^2 V_\mathrm{s} \right)^2}{\omega^2 \sum_\mathrm{s} \tilde{\omega}_\mathrm{ps}^2} = 0 \,. \tag{6.23}$$

Here $\gamma_\mathrm{s} = 1/\sqrt{1 - V_\mathrm{s}^2/c^2}$. In the non-relativistic limit, with $V_\mathrm{s} \ll c$ and $\gamma_\mathrm{s} \simeq 1$ the unstable branch has $|\omega^2| \ll K^2c^2$ and the solution for the growth rate $\tilde{\sigma}$ ($\omega = i\tilde{\sigma}$) is (cf. Akhiezer et al. [6], equation 6.1.5.10)

$$\tilde{\sigma}^2 \approx \frac{K^2}{K^2c^2 + \sum_\mathrm{s} \tilde{\omega}_\mathrm{ps}^2} \left\{ \sum_\mathrm{s} \omega_\mathrm{ps}^2 V_\mathrm{s}^2 - \frac{\left(\sum_\mathrm{s} \tilde{\omega}_\mathrm{ps}^2 V_\mathrm{s} \right)^2}{\sum_\mathrm{s} \tilde{\omega}_\mathrm{ps}^2} \right\} . \tag{6.24}$$

This non-relativistic dispersion relation remains correct even if one assumes that the magnitude of the velocity of the two beams is not equal. In the symmetric case, where $n_+ = n_- = n_\mathrm{b}/2$ and $V_\pm = \pm V_\mathrm{b}$, the term $\sum_\mathrm{s} \tilde{\omega}_\mathrm{ps}^2 V_\mathrm{s}$ vanishes identically and one has:

$$\tilde{\sigma}^2 = \frac{\tilde{\omega}_\mathrm{pb}^2 K^2 V_\mathrm{b}^2}{K^2c^2 + \tilde{\omega}_\mathrm{bg}^2 + \tilde{\omega}_\mathrm{pb}^2} < \tilde{\omega}_\mathrm{pb}^2 \left(\frac{V_\mathrm{b}}{c} \right)^2 , \tag{6.25}$$

where the maximum growth rate, $\tilde{\sigma}_\mathrm{max} \approx \tilde{\omega}_\mathrm{pb}(V_\mathrm{b}/c)$, occurs when $K^2c^2 \gg \tilde{\omega}_\mathrm{bg}^2 + \tilde{\omega}_\mathrm{pb}^2$. Here $\tilde{\omega}_\mathrm{bg}^2 \equiv \sum_{\mathrm{s}\in\mathrm{bg}} 4\pi q_\mathrm{s}^2 n_\mathrm{s}/m_\mathrm{s}$ is the plasma frequency associated

with the background plasma, and $\tilde{\omega}_{pb}^2 = 4\pi q_b^2 n_b / m_b$ is the plasma frequency associated with the beams. Equation (6.25) corresponds to the well-known expression for the non-relativistic Weibel instability, which Weibel [98] derived for an unstable plasma without a background plasma ($\tilde{\omega}_{bg} = 0$).

It should be emphasized that the net current in the plasma should vanish,

$$\mathbf{J} = \sum_s n_s q_s V_s \, \hat{\mathbf{z}} = 0 \tag{6.26}$$

for a cold plasma. Since $\tilde{\omega}_{ps}^2 \propto q_s^2 n_s / m_s$ this implies that the growth rate reducing term $\propto (\sum_s \tilde{\omega}_{ps}^2 V_s)^2$ in relation (6.24) will vanish if the currents in the plasma are carried by a single species, for instance: by the electrons.

6.5 Weibel instability driven by two symmetric beams

We now consider two counterstreaming beams with equal density and equal temperature that are propagating through a thermal background plasma at rest. In that case one can use dispersion relation (6.21).

In the fluid approximation, the expression for $\mathcal{D}_{33}$ in the set of relations (6.138) for the components of $\mathcal{D}_{ij}$ leads to dispersion relation

$$\omega^2 = K^2 + \tilde{\omega}_{bg}^2 + \tilde{\omega}_{pb}^2 \left(1 - \frac{(\omega^2 - K^2)\, \tilde{V}_b^2}{\omega^2 - K^2 \tilde{C}_b^2} \right) . \tag{6.27}$$

Here we define the two velocities

$$\tilde{C}_b = \frac{C_b}{\gamma_b \sqrt{1 - C_b^2 V_b^2}} \;\; , \;\; \tilde{V}_b = \frac{V_b}{\gamma_{C_b} \sqrt{1 - C_b^2 V_b^2}} \tag{6.28}$$

with $\gamma_{C_b} \equiv 1/\sqrt{1 - C_b^2}$. The background and beam plasma frequencies are given respectively by

$$\tilde{\omega}_{bg}^2 \equiv \sum_{s \in bg} \tilde{\omega}_{ps}^2 \;\; , \;\; \tilde{\omega}_{pb}^2 \equiv \frac{4\pi q_b^2 n_b}{m_b h_b} \, , \tag{6.29}$$

with $h_b \equiv 1 + (e + P)_\pm / n_\pm m_b$ the beam enthalpy per unit mass, which is identical for the two beams in view of our assumption of equal beam temperatures.

For the kinetic description of the beams we use a mathematically convenient momentum distribution function for the kinetic version of the Weibel instability: the *waterbag distribution* as employed by Yoon and Davidson [105] and by Silva et al. [89]. This distribution takes the form

$$\begin{aligned} f_{0\mathrm{b}}(\mathbf{p}) &= \frac{\Theta(p_x + p_{x0}) - \Theta(p_x - p_{x0})}{2\,p_{x0}}\,\delta(p_y)\,\times \\ &\times \left[\frac{1+\Delta}{2}\,\delta(p_z - p_{z0}) + \frac{1-\Delta}{2}\,\delta(p_z + p_{z0})\right]. \end{aligned} \tag{6.30}$$

Here $\Theta(x) = \frac{1}{2}(1 + x/|x|)$ is the Heaviside step function.

The waterbag distribution describes two beams, counterstreaming along the z-axis with a lab-frame density $\overline{n}_{\pm} = (1 \pm \Delta)\,\overline{n}_{\mathrm{b}}/2$, and with a momentum dispersion along the x-axis that is described by a 'top hat' distribution in the range $-p_{x0} \leq p_x \leq p_{x0}$. The y-component of the momentum vanishes identically. Note that the 'beam temperature', as defined by the spread in the momentum component p_x, is the same for both beams. The waterbag distribution allows an analytical calculation of the plasma response, while preserving the two essential features of more realistic distributions: the bulk drift of beam particles in the beam direction and the beam velocity dispersion along the wave vector due to thermal motions in the beams. As we show below, the final results for a waterbag distribution are close to those obtained with the fluid model, strengthening the validity of this approach.

It has been shown by Milosavljević et al. [68] that the dispersion relation for a momentum distribution that is isotropic in the plane perpendicular to the beam (so that $p_y \neq 0$, but the distribution only depends on $\sqrt{p_x^2 + p_y^2}$ and p_z) gives very similar, but algebraically more complicated, results.

For the response of the background plasma we will (for the moment) continue to use the results from the fluid approximation, even though strictly speaking one should use kinetic theory in order to take the large velocity dispersion in the background into account. As discussed in section 6.7 below, this leads to the *anomalous skin effect*, cf. Lyubarsky and Eichler [55]. There we will show that the difference between the two approaches is small. Alternatively, one can use the dispersion functions derived recently by Schlickeiser [86] for a relativistic Maxwellian distribution.

Using the equation (6.148) of Appendix 6.13 one finds that the Weibel dispersion relation (6.21) for a symmetric waterbag distribution with $\Delta = 0$ be-

comes

$$\omega^2 = K^2 + \tilde{\omega}_{\rm bg}^2 + \hat{\omega}_{\rm pb}^2 \left(\mathcal{G}_{\rm b} + \frac{K^2 V_{z0}^2}{\omega^2 - K^2 V_{x0}^2} \right) . \tag{6.31}$$

Here we define the following characteristic beam parameters: the beam plasma frequency $\hat{\omega}_{\rm pb}$, the characteristic Lorentz factor γ_0 and the two velocities V_{x0} and V_{z0}:

$$\begin{aligned} \hat{\omega}_{\rm pb}^2 &= \frac{\bar{\omega}_{\rm pb}^2}{\gamma_0} = \frac{4\pi q_{\rm b}^2 \overline{n}_{\rm b}}{\gamma_0 m_{\rm b}} \ , \ \gamma_0 = \sqrt{1 + \frac{p_{x0}^2}{m_{\rm b}^2 c^2} + \frac{p_{z0}^2}{m_{\rm b}^2 c^2}} \ , \\ V_{x0} &= \frac{p_{x0}}{\gamma_0 m_{\rm b}} \ , \ V_{z0} = \frac{p_{z0}}{\gamma_0 m_{\rm b}} . \end{aligned} \tag{6.32}$$

The function $\mathcal{G}_{\rm b}(p_{x0}\,,\,p_{z0})$ is given by:

$$\mathcal{G}_{\rm b}(p_{x0}\,,\,p_{z0}) = \frac{1}{2V_{x0}} \ln\left(\frac{1+V_{x0}}{1-V_{x0}}\right) - \frac{p_{z0}^2}{p_{z0}^2 + m_{\rm b}^2} . \tag{6.33}$$

When $V_{x0} \ll 1$ (so that $\gamma_0 \simeq \gamma_{\rm b}$) the frequency $\hat{\omega}_{\rm pb}$ reduces to the beam plasma frequency $\tilde{\omega}_{\rm pb}$ based on the proper density $n_{\rm b} \approx \overline{n}_{\rm b}/\gamma_{\rm b}$ of the beam particles. The beam contribution to $\mathcal{D}_{33}$ (the last term on the right-hand side of equation 6.31) has been derived before by Silva et al. [89].

The two dispersion relations (6.27) and (6.31) can both be written as a bi-quadratic equation for ω of the form

$$\omega^4 - \mathcal{B}(K)\,\omega^2 + \mathcal{C}(K) = 0 \,, \tag{6.34}$$

Such a bi-quadratic equation for ω occurs often in the theory of the Weibel instability [98, 84]. The two coefficients $\mathcal{B}(K)$ and $\mathcal{C}(K)$ are:

$$\mathcal{B}(K) = \begin{cases} \tilde{\omega}_{\rm bg}^2 + \tilde{\omega}_{\rm pb}^2 \left(1 - \tilde{V}_{\rm b}^2\right) + K^2 \left(1 + \tilde{C}_{\rm b}^2\right) & \text{(fluid model)} \\ \tilde{\omega}_{\rm bg}^2 + \hat{\omega}_{\rm pb}^2\, \mathcal{G}_{\rm b} + K^2 \left(1 + V_{x0}^2\right) & \text{(waterbag model)} \end{cases} \tag{6.35}$$

and

$$\mathcal{C}(K) = \begin{cases} \left(\tilde{\omega}_{\rm bg}^2 + K^2\right) K^2 \tilde{C}_{\rm b}^2 - \tilde{\omega}_{\rm pb}^2 K^2 \left(\tilde{V}_{\rm b}^2 - \tilde{C}_{\rm b}^2\right) & \text{(fluid model)} \\ \left(\tilde{\omega}_{\rm bg}^2 + K^2\right) K^2 V_{x0}^2 - \hat{\omega}_{\rm pb}^2 K^2 \left(V_{z0}^2 - \mathcal{G}_{\rm b}\, V_{x0}^2\right) & \text{(waterbag model)} \end{cases} \tag{6.36}$$

The analogy between these two sets of expressions is clear. The solution for ω,

$$\omega_{\pm}^2 = \tfrac{1}{2}\mathcal{B} \pm \tfrac{1}{2}\sqrt{\mathcal{B}^2 - 4\mathcal{C}}\,, \tag{6.37}$$

has an unstable branch with $\omega_{-}^2 < 0$, i.e. $\omega_{-} = i\tilde{\sigma}$ with $\tilde{\sigma} > 0$, provided $\mathcal{C}(K) < 0$. This condition defines a maximum unstable wavenumber $K_{\max}$ so that perturbations with

$$K^2 < K_{\max}^2 = \begin{cases} \tilde{\omega}_{\mathrm{pb}}^2 \left(\mathcal{M}^2 - 1\right) - \tilde{\omega}_{\mathrm{bg}}^2 & \text{(fluid model)} \\ \\ \hat{\omega}_{\mathrm{pb}}^2 \left(\mathcal{M}^2 - \mathcal{G}_{\mathrm{b}}\right) - \tilde{\omega}_{\mathrm{bg}}^2 & \text{(waterbag model)} \end{cases} \tag{6.38}$$

are unstable and will grow. Here we define an effective 'Mach number' for the beams by

$$\mathcal{M} \equiv \begin{cases} \dfrac{\tilde{V}_{\mathrm{b}}}{\tilde{C}_{\mathrm{b}}} = \dfrac{\gamma_{\mathrm{b}} V_{\mathrm{b}}}{\gamma_{C_{\mathrm{b}}} C_{\mathrm{b}}} & \text{(fluid model)} \\ \\ \dfrac{V_{z0}}{V_{x0}} = \dfrac{p_{z0}}{p_{x0}} & \text{(waterbag model)} \end{cases} \tag{6.39}$$

for the fluid and waterbag model respectively. This shows the stabilizing influence of the thermal motion of beam particles in the direction of the wave vector $\mathbf{k} = K\hat{\mathbf{x}}$, suppressing the instability at sufficiently large values of $|K|$.

6.6 The case of ultra-relativistic beams

We now concentrate on the ultra-relativistic case, of importance for the Weibel instability in the shock transition layer of shocks with bulk velocity V_{sh} such that $\gamma_{\mathrm{sh}} = 1/(1 - V_{\mathrm{sh}}^2)^{1/2} \gg 1$. In the frame of the hot (shocked) plasma, the unshocked material forms a relativistic beam. This implies $\gamma_{\mathrm{b}} \sim \gamma_{\mathrm{sh}} \gg 1$ and $\tilde{V}_{\mathrm{b}} \gg \tilde{C}_{\mathrm{b}}$ in the fluid case and $p_{z0} \gg m_{\mathrm{b}}$, $p_{z0} \gg p_{x0}$ in the waterbag case. It is then possible to describe the properties of the symmetric Weibel instability using two parameters. The first is the 'Mach number' $\mathcal{M}$ defined in equation (6.39) that now satisfies[1] $\mathcal{M}^2 \sim (\gamma_{\mathrm{b}}/\gamma_{\mathrm{Cb}} C_{\mathrm{b}})^2 \gg 1$. The second parameter is a measure of the strength of the two beams, defined by

$$\eta \equiv \begin{cases} \tilde{\omega}_{\mathrm{pb}}^2/\tilde{\omega}_{\mathrm{bg}}^2 & \text{(fluid model)} \\ \\ \hat{\omega}_{\mathrm{pb}}^2/\tilde{\omega}_{\mathrm{bg}}^2 & \text{(waterbag model)} \end{cases} \tag{6.40}$$

[1] For an ideal gas one has $C_{\mathrm{b}} < 1/\sqrt{3}$ and $\gamma_{\mathrm{Cb}} C_{\mathrm{b}} < 1/\sqrt{2}$

The ultra-relativistic limit of the fluid model has $\tilde{C}_b \simeq 1/\mathcal{M} \ll 1$, $\tilde{V}_b \simeq V_b \simeq 1$, and in the waterbag model one has $\mathcal{G}_b \ll 1$ and $V_{x0} \simeq 1/\mathcal{M} \ll V_{z0} \approx V_b \simeq 1$. To leading order, the expressions (6.35) and (6.36) become identical in both models. In terms of η and $\mathcal{M}$ one can write:

$$\begin{aligned} \mathcal{B}(K) &\simeq \tilde{\omega}_{bg}^2 + K^2 \,, \\ \mathcal{C}(K) &\simeq K^2 \left(\frac{\tilde{\omega}_{bg}^2 + K^2}{\mathcal{M}^2} - \eta\, \tilde{\omega}_{bg}^2 \right) . \end{aligned} \tag{6.41}$$

Terms of order $1/\gamma_b^2$, $\tilde{C}_b^2$ or V_{x0}^2 have been consistently neglected with respect to unity.

If we define a dimensionless growth rate σ and a dimensionless wavenumber κ by

$$\sigma^2 = -\omega^2/\tilde{\omega}_{bg}^2 \;\;,\;\; \kappa = K/\tilde{\omega}_{bg} \,, \tag{6.42}$$

dispersion relation (6.34) can be written as

$$\sigma^4 + \left(1+\kappa^2\right)\sigma^2 - \frac{\kappa^2\,\left(\kappa_{max}^2 - \kappa^2\right)}{\mathcal{M}^2} = 0 \,. \tag{6.43}$$

Here we use that ω is either real (stable modes) or purely imaginary with $\omega^2 < 0$. The dimensionless maximum wavenumber κ_{max} (see equation 6.38) of the unstable modes equals in the ultra-relativistic limit:

$$\kappa_{max} \approx \sqrt{\eta\,\mathcal{M}^2 - 1} \,. \tag{6.44}$$

The Weibel instability occurs only if $\eta\mathcal{M}^2 > 1$ for $0 \le |\kappa| < \kappa_{max}$. The unstable branch has a growth rate

$$\sigma^2 = \sqrt{\left(\frac{1+\kappa^2}{2}\right)^2 + \frac{\kappa^2\,\left(\kappa_{max}^2 - \kappa^2\right)}{\mathcal{M}^2}} - \frac{1+\kappa^2}{2} \,. \tag{6.45}$$

In many cases expression (6.45) can be simplified further. Provided that $(1+\kappa^2)^2 \gg 4\kappa^2\,\left(\kappa_{max}^2 - \kappa^2\right)/\mathcal{M}^2$ one can expand the root in (6.45). This yields:

$$\sigma^2 \simeq \frac{\kappa^2\,\left(\kappa_{max}^2 - \kappa^2\right)}{\mathcal{M}^2\left(1+\kappa^2\right)} \,. \tag{6.46}$$

This approximation corresponds to the neglect of the σ^4 term in dispersion relation (6.43), and is valid for all unstable wavelengths if the beams are weak in the sense that $\eta \ll 1$. In that case one has $\sigma^2 < \eta \ll 1$. For η of order unity ($\tilde{\omega}_{\rm pb}$, $\tilde{\omega}_{\rm pb} \sim \tilde{\omega}_{\rm bg}$) the approximated solution (6.46) is valid everywhere except in the vicinity of $|\kappa| = 1$ where $\sigma \approx 1$. For very strong beams with $\eta \gg 1$ one has to use the full solution (6.45) except when $\sqrt{\eta} \ll |\kappa| \leq \kappa_{\rm max} \sim \sqrt{\eta}\mathcal{M}$.

Figure 6.1 gives the growth rate of the Weibel instability in units of the background plasma frequency as a function of the dimensionless wavenumber κ ($= Kc/\tilde{\omega}_{\rm bg}$ if one uses units with $c \neq 1$). The curves are labeled by the pair of parameters (η, $\mathcal{M}$). This figure shows that the dimensionless growth rate $\sigma = {\rm Im}(\omega)/\tilde{\omega}_{\rm bg}$ has the following properties:

- For $\kappa = K/\tilde{\omega}_{\rm bg} \ll 1$ it grows as $\sigma \propto \kappa$. If the approximated solution (6.46) applies one has
$$\sigma \approx \frac{\kappa\kappa_{\rm max}}{\mathcal{M}} \approx \sqrt{\eta}\,\kappa\ . \tag{6.47}$$
The last approximation is valid if $\eta < 1$.

- Around $\kappa \sim 1$ the growth rate saturates. If $\kappa_{\rm max} \gg 1$ the growth rate has a nearly constant value for $1 \ll \kappa \ll \kappa_{\rm max}$ which, in the approximation (6.46), equals:
$$\sigma \approx \frac{\kappa_{\rm max}}{\mathcal{M}} \approx \sqrt{\eta}\ . \tag{6.48}$$

- The growth rate rapidly decreases to zero at $\kappa \approx \kappa_{\rm max} \approx \sqrt{\eta}\,\mathcal{M}$.

Comparing the ultra-relativistic result (6.46) to the classic non-relativistic result for a cold plasma (6.25) we can identify the following differences:

- The cold plasma result does not have a cut-off wave number $\kappa_{\rm max}$.

- The denominator of the non-relativistic expression contains an extra $\tilde{\omega}_{\rm pb}^2$ term because one can not apply the limit $\eta \leq 1$, $\gamma_{\rm b} \gg 1$ in that case. The corresponding term in the ultra-relativistic case is $\tilde{\omega}_{\rm pb}^2/\gamma_{\rm b}^2$, which has been neglected with respect to $\tilde{\omega}_{\rm bg}^2$. That is allowed whenever $\eta \ll \gamma_{\rm b}^2$.

- In the relativistic case it is important to use the appropriate relativistic expressions for the plasma frequencies.

Note, however, that the peak value of the growth rate $\sigma \approx \sqrt{\eta}$ for the ultra-relativistic case is the relativistic equivalent for $V_{\rm b} \simeq c$ of the maximum growth rate for the non-relativistic case.

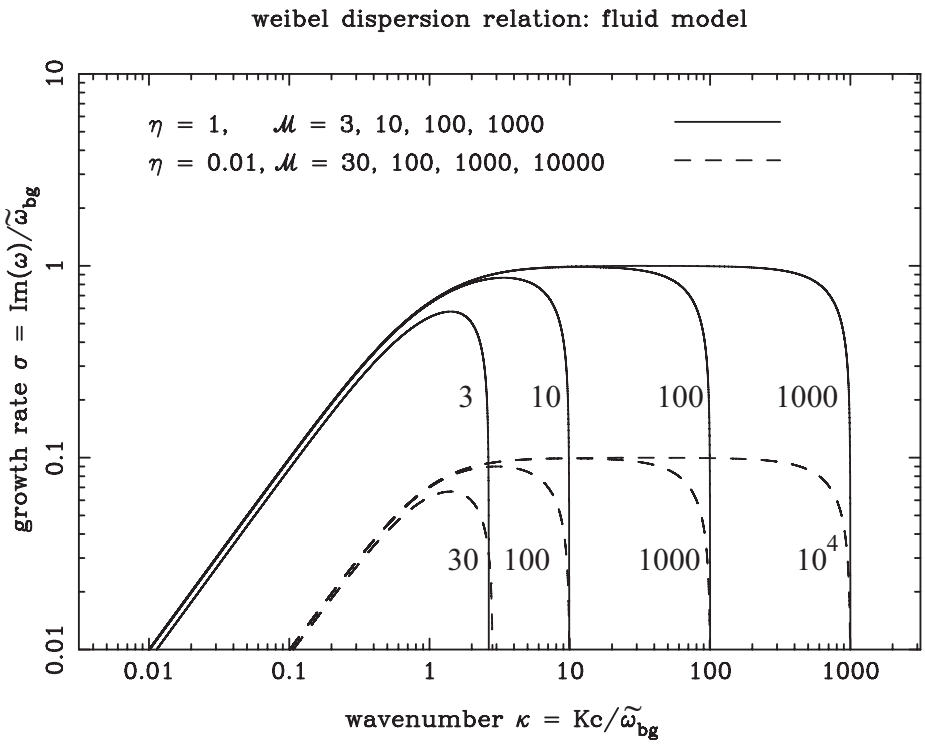

Figure 6.1: The dimensionless growth rate of the ultra-relativistic Weibel instability in the fluid model for the background response. Shown is $\sigma = \mathrm{Im}(\omega)/\tilde{\omega}_{\mathrm{bg}}$, as a function of the dimensionless wavenumber, $\kappa = Kc/\tilde{\omega}_{\mathrm{bg}}$, for an instability driven by two beams of equal strength (the symmetric case). Growth rates are shown for two different values of η, $\eta = 0.01$ and $\eta = 1$, and for a range of values of the 'Mach number' $\mathcal{M}$. The different curves are labeled by the value of $\mathcal{M}$.

6.7 Ultra-relativistic background gas

Next we consider the case where the background plasma is described as an isotropic, ultra-relativistic gas. We approximate the distribution function of the background electrons by the ultra-relativistic limit (thermal energy $k_\mathrm{b}T \gg m_\mathrm{e}c^2$) of the well-known Juttner distribution with temperature T:

$$f_0(\mathbf{p}) = \frac{1}{8\pi}\left(\frac{c}{k_\mathrm{b}T}\right)^3 \exp(-c|\mathbf{p}|/k_\mathrm{b}T)\,, \tag{6.49}$$

Substituting this into equation 6.143 of the Appendix (with $(f_{0\mathrm{b}}(\mathbf{p}) \rightarrow f_0(\mathbf{p}))$ one finds [cf. 7, 61]

$$\alpha_{33}^{\mathrm{bg}} = \frac{\tilde{\omega}_{\mathrm{bg}}^2\omega}{4Kc}\left[\frac{2\omega}{Kc} + \left(1-\frac{\omega^2}{K^2c^2}\right)\ln\left(\frac{\omega+Kc}{\omega-Kc}\right)\right]\,. \tag{6.50}$$

Here the background plasma frequency is defined as

$$\tilde{\omega}_{\mathrm{bg}}^2 \equiv \frac{4\pi e^2 n c^2}{k_\mathrm{b}T}\,. \tag{6.51}$$

The contribution of the ions is neglected, assuming that the ions have not thermalized yet in the shock transition.

If the frequency is purely imaginary, $\omega = i\tilde{\sigma}$ as is the case here for the unstable mode, one can write $\alpha_{33}^{\mathrm{bg}}$ as:

$$\begin{aligned}\alpha_{33}^{\mathrm{bg}} \;=\; & \frac{\tilde{\omega}_{\mathrm{bg}}^2}{2}\left[\frac{\pi}{2}\left(\frac{\tilde{\sigma}}{Kc}\right)\left(1+\frac{\tilde{\sigma}^2}{K^2c^2}\right) - \left(\frac{\tilde{\sigma}}{Kc}\right)^2 - \right.\\ & \left. - \left(\frac{\tilde{\sigma}}{Kc}\right)\left(1+\frac{\tilde{\sigma}^2}{K^2c^2}\right)\tan^{-1}\left(\frac{\tilde{\sigma}}{Kc}\right)\right]\,.\end{aligned} \tag{6.52}$$

This follows from the representation $\tan^{-1}(x) = (i/2)\ln[(i+x)/(i-x)]$ together with $\tan^{-1}(x) = \pi/2 - \tan^{-1}(1/x)$, cf. [1]. The dispersion relation for the Weibel instability due to symmetric counterstreaming beams, $\mathcal{D}_{33} = 0$, now reads:

$$\begin{aligned}&\sigma^2 + \kappa^2 + \eta\mathcal{G}_\mathrm{b} + \frac{\sigma}{2\kappa}\left[\frac{\pi}{2}\left(1+\frac{\sigma^2}{\kappa^2}\right) - \frac{\sigma}{\kappa} - \right.\\ &\left. - \left(1+\frac{\sigma^2}{\kappa^2}\right)\tan^{-1}\left(\frac{\sigma}{\kappa}\right)\right] - \frac{\eta\kappa^2 V_{z0}^2}{\sigma^2+\kappa^2V_{x0}^2} = 0\,.\end{aligned} \tag{6.53}$$

Here we employ the dimensionless quantities introduced in the previous section. In the limit $\mathcal{M}^2 = V_{z0}^2/V_{x0}^2 \to \infty$ (cold beams) and $\sigma^2 \ll \kappa^2$, this corresponds to the dispersion relation considered recently by Lyubarsky and Eichler [55].

The unstable modes extend from $0 < \kappa < \kappa_{\max}$, where the value of $\kappa_{\max}$ follows from the condition $\sigma(\kappa_{\max}) = 0$. It is easily seen that $\kappa_{\max}$ equals

$$\kappa_{\max} = \sqrt{\eta \, \left(\mathcal{M}^2 - \mathcal{G}_{\rm b}\right)} \, , \tag{6.54}$$

essentially the same value as obtained in the waterbag beam/fluid background model for $\eta \mathcal{M}^2 \gg 1$, the ultra-relativistic limit.

Figure 6.2 shows the unstable Weibel-branch solutions of dispersion relation (6.53). When one compares the dispersion curves in this figure with the corresponding fluid results of figure 6.1, one finds that the curves are very similar. The *physical* reason is that -in both the fluid and the kinetic model- the presence of the hot background leads to a screening current, which slows the instability at small κ. In the fluid model, which can never fully capture the effect of the large velocity dispersion of the background electrons, the classical screening current leads to a diminished growth rate at wavelengths larger than the skin depth $\lambda_{\rm sk} = c/\tilde{\omega}_{\rm bg}$. In the kinetic model of this section, which takes proper account of the velocity dispersion, it is the anomalous screening current due to the velocity dispersion of the particles along $\mathbf{k}$ that leads to a similar effect.

We will consider the low frequency limit, $|\tilde{\sigma}| \ll Kc$. In that case one has

$$\alpha_{33}^{\rm bg} = \frac{\pi \tilde{\omega}_{\rm bg}^2 \tilde{\sigma}}{4Kc} = \frac{\pi \tilde{\omega}_{\rm bg}^2}{4} \left(\frac{\sigma}{\kappa}\right) \, . \tag{6.55}$$

This result corresponds to the *anomalous skin effect* in an isotropic ultra-relativistic thermal plasma. Taking the ultra-relativistic limit for the beams, in effect putting $\mathcal{G}_{\rm b} \approx 0$, $V_{z0} \approx 1 \gg V_{x0}$ and $\eta \, \mathcal{M}^2 \gg 1$, one can replace the full dispersion relation (6.53) by the simpler relation

$$\kappa^2 \left(\sigma^2 + \frac{\kappa^2}{\mathcal{M}^2} - \eta\right) + \frac{\pi}{4} \frac{\sigma}{\kappa} \left(\sigma^2 + \frac{\kappa^2}{\mathcal{M}^2}\right) = 0 \, . \tag{6.56}$$

It is possible to write down a rather complicated expression for the analytical solution of the cubic equation (6.56) for the dimensionless growth rate σ. However, the close similarity (see figure 6.2) with the results for the growth rate

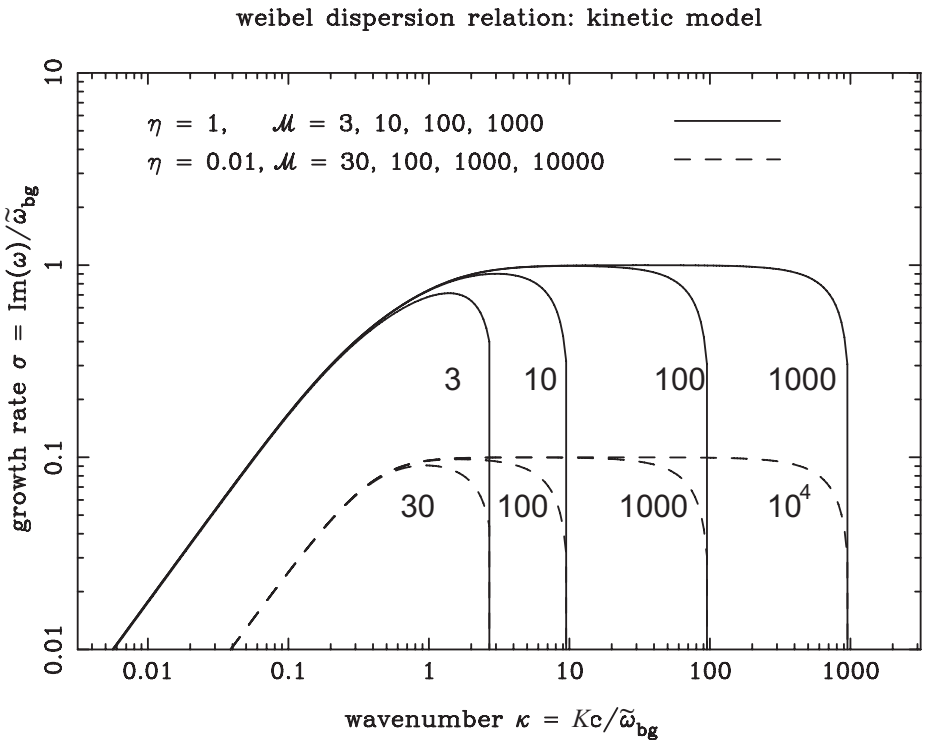

Figure 6.2: The dimensionless growth rate of the ultra-relativistic Weibel instability that follows from dispersion relation (6.53), which employs a kinetic model for the background response. Shown is $\sigma = \tilde{\sigma}/\tilde{\omega}_{\rm bg}$ as a function of the dimensionless wavenumber, $\kappa = Kc/\tilde{\omega}_{\rm bg}$, for an instability driven by two beams of equal strength (the symmetric case). Growth rates are shown for two different values of η and for a range of values of the 'Mach number' $\mathcal{M}$. The different curves are labeled by the value of $\mathcal{M}$. The reduction of the growth rate for $\kappa \ll 1$ corresponds to the effect of anomalous screening by the hot background plasma.

obtained with a fluid treatment of the background plasma suggests that the following interpolation formula applies, asymptotically exact for both $\kappa^2 \ll 1$ and $\kappa^2 \gg 1$ when $\eta \leq 1$:

$$\sigma^2 \simeq \frac{\kappa^2 \left(\kappa_{\rm max}^2 - \kappa^2\right)}{\mathcal{M}^2 \left(\kappa_{\rm s}^2 + \kappa^2\right)} \,. \tag{6.57}$$

The screening wavenumber $\kappa_{\rm s}$, which in this case quantifies the anomalous skin effect, follows from a consideration of the solution of dispersion relation (6.56) in the limit $\kappa^2 \ll 1$, $\sigma^2 \ll 1$ and $\kappa_{\rm max}^2 \approx \eta \mathcal{M}^2 \gg 1$:

$$\sigma^2 \approx \left(\frac{4\eta}{\pi}\right)^{2/3} \kappa^2 \,. \tag{6.58}$$

Comparing this with (6.57) in this limit,

$$\sigma^2 \approx \frac{\kappa^2 \kappa_{\rm max}^2}{\kappa_{\rm s}^2 \mathcal{M}^2} = \frac{\eta\, \kappa^2}{\kappa_{\rm s}^2} \tag{6.59}$$

one finds that one must have

$$\kappa_{\rm s} = \left(\frac{\pi}{4}\right)^{1/3} \eta^{1/6} \,. \tag{6.60}$$

This defines the dimensionless screening wave number $\kappa_{\rm s}$ for the kinetic model for the background plasma. The fluid approximation for the background corresponds to putting $\kappa_{\rm s} = 1$. Anomalous screening is important when $\kappa \leq \kappa_{\rm s}$. Note that the value of $\kappa_{\rm s}$ depends only weakly on the strength of the beams, and will be of order unity unless η is very small or very large. Figure 6.3 compares the growth rate as calculated from the various dispersion relations for the Weibel instability, both exact and approximate. The comparison is shown for two cases with an identical value of $\kappa_{\rm max} \approx 33$: for a relatively dense beam ($\eta = 1$), and for an underdense beam with $\eta = 0.01$. For $\kappa \gg 1$ there is little difference as the screening currents of the hot background are relatively unimportant. In the case $\eta = 1$ the largest differences occur between the various approaches, but the difference between the growth rate as calculated from the fluid model and the kinetic model for the background is no more than a factor 2. In the case $\eta = 0.01$ the difference between the two models is somewhat more pronounced as the screening wavenumber squared, $\kappa_{\rm s}^2 \approx 0.18$, becomes significantly smaller than unity. The growth rates as obtained numerically from

the exact dispersion relations, and the approximate growth rates obtained from the approximate relations (6.46) and (6.57), agree fairly well for $\eta = 1$, and give an excellent approximation in the case $\eta = 0.01$. This is to be expected in view of the approximation $\sigma^2 \ll \kappa^2$ employed in the derivation of the approximate growth rates, as the maximum growth rate in all cases is $\sigma_{\max} \sim \sqrt{\eta}$.

6.8 Magnetized Weibel instability

The previous calculations have been for an unmagnetized plasma. In this section we briefly consider the magnetized case, in order to compare the results obtained using our formalism with those of Tautz and Schlickeiser [91] and to show that, for typical parameters, the unmagnetized case applies to the Weibel instability near ultra-relativistic shocks propagating into the interstellar (or circumstellar) medium.

We can only consider the case where the Lorentz force on all species in the unperturbed plasma vanishes: $F^{\mu\nu}U_{s\nu} = 0$. This implies that there is no ambient electric field in the laboratory frame, and that we are dealing with two equal counterstreaming beams, $\Delta = 0$, with the beam velocity aligned with the magnetic field. These conditions are rather restrictive. A calculation of the response of the plasma in the fluid approximation (see Appendix 6.14) leads to an instability of the *ordinary electromagnetic mode* in a plasma, cf. Tautz and Schlickeiser [91]. In the ordinary mode the wave electric field is along the beam direction/ambient magnetic field in the lab frame so that $\tilde{\mathbf{E}} = \tilde{E}\hat{\mathbf{z}}$. As before, we choose a wave vector in the laboratory frame perpendicular to the beam direction: $\mathbf{k} = K\hat{\mathbf{x}}$. The presence of the magnetic field modifies dispersion relation (6.27) to (see equation (6.157) of Appendix 6.14):

$$\omega^2 = K^2 + \tilde{\omega}_{\mathrm{bg}}^2 + \tilde{\omega}_{\mathrm{pb}}^2 \left(1 - \frac{(\omega^2 - K^2)\,\tilde{V}_{\mathrm{b}}^2}{\omega^2 - K^2\tilde{C}_{\mathrm{b}}^2 - \tilde{\Omega}_{\mathrm{b}}^2}\right) . \tag{6.61}$$

Here

$$\tilde{\Omega}_{\mathrm{b}} = \frac{q_{\mathrm{b}}B}{\gamma_{\mathrm{b}}m_{\mathrm{b}}h_{\mathrm{b}}\sqrt{1 - V_{\mathrm{b}}^2C_{\mathrm{b}}^2}} \equiv \frac{\Omega_{\mathrm{b}}}{\gamma_{\mathrm{b}}\sqrt{1 - V_{\mathrm{b}}^2C_{\mathrm{b}}^2}} , \tag{6.62}$$

is an effective gyration frequency of the beam plasma, with B the magnetic field strength and $\Omega_{\mathrm{b}} \equiv q_{\mathrm{b}}B/m_{\mathrm{b}}h_{\mathrm{b}}$. For field-aligned beams the magnetic field is the same in the lab frame and in the two respective rest frames of the forward and backward beam. In the limit of a vanishing beam temperature ($\mathcal{C}_{\mathrm{b}} = 0$, $h_{\mathrm{b}} = 1$), of low frequency ($|\omega^2| \ll K^2$) perturbations and for a non-relativistic beam

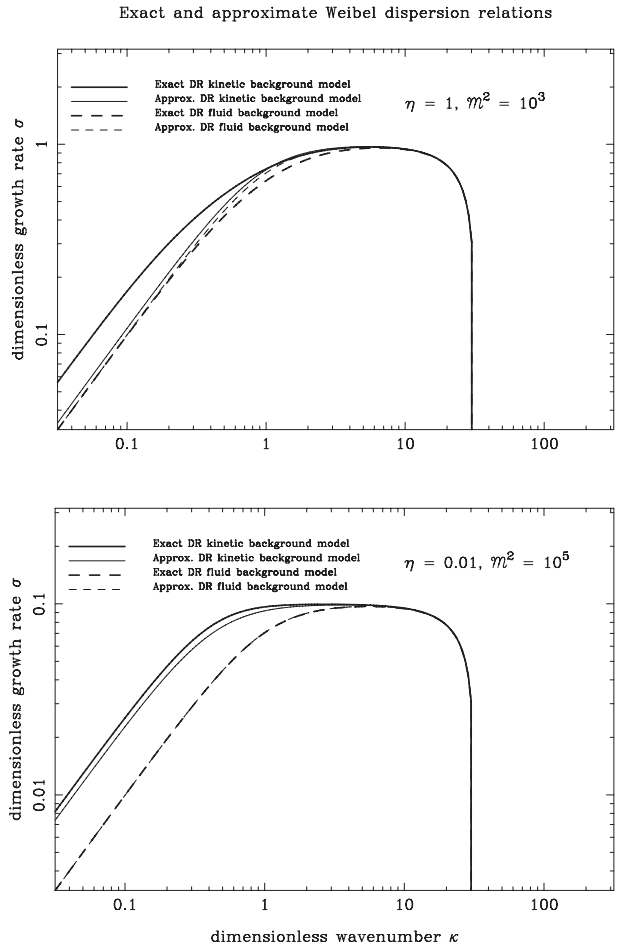

Figure 6.3: A comparison of the growth rates calculated from the fluid and the kinetic model for the background response, and from the approximate dispersion relations in both these models: equation (6.46) and (6.57). Dispersion curves are shown in two cases: $\eta = 1$ (top figure) and $\eta = 0.01$ (bottom figure), with $\mathcal{M}^2 = 10^3$ and $\mathcal{M}^2 = 10^5$ respectively, so that the value of the maximum unstable wavenumber, $\kappa_{\max} \approx \sqrt{\eta}\,\mathcal{M}$, is identical in both cases.

velocity (so that $V_\mathrm{b} \ll 1$, $\gamma_\mathrm{b} \simeq 1$ and $\tilde{\Omega}_\mathrm{b} \simeq q_\mathrm{b} B / m_\mathrm{b}$) dispersion relation (6.61) reduces to the dispersion relation derived by Tautz and Schlickeiser [91], their equation 6.19, in the corresponding case.

The dispersion relation for the magnetized Weibel instability again takes the form of equation (6.34): $\omega^4 - \mathcal{B}(K)\,\omega^2 + \mathcal{C}(K) = 0$. The relevant coefficients $\mathcal{B}(K)$ and $\mathcal{C}(K)$ are listed in equations (6.159) and (6.160) of Appendix 6.14.

The most important effect of the magnetic field is a modification of the range of unstable wavenumbers that follows from the instability condition $\mathcal{C}(K) < 0$. It introduces a wavenumber K_-, below which the magnetic field stabilizes the Weibel instability. Unstable modes occur for $K_- < |K| < K_+$, where K_- (K_+) are the smaller (larger) real roots of $\mathcal{C}(K) = 0$. From expression (6.160) for $\mathcal{C}(K)$ one finds that the two limiting wavenumbers $K_\pm$ are given by:

$$K_\pm^2 = \frac{K_\mathrm{max}^2 - K_\mathrm{B}^2}{2} \pm \sqrt{\left(\frac{K_\mathrm{max}^2 - K_\mathrm{B}^2}{2}\right)^2 - \left(\tilde{\omega}_\mathrm{pb}^2 + \tilde{\omega}_\mathrm{bg}^2\right) K_\mathrm{B}^2}\,. \tag{6.63}$$

The wavenumber K_B is defined by

$$K_\mathrm{B} \equiv \frac{|\tilde{\Omega}_\mathrm{b}|}{\tilde{C}_\mathrm{b}} = \frac{|q_\mathrm{b}| B}{m_\mathrm{b} h_\mathrm{b} C_\mathrm{b}}\,, \tag{6.64}$$

and K_max is the maximum unstable wavenumber in the field-free case as defined in equation (6.38). The Weibel instability disappears in the magnetized case when the unstable wavenumber range shrinks to zero. This happens when the argument of the square root in expression (6.63) vanishes or becomes negative for

$$K_\mathrm{B} > \sqrt{K_\mathrm{max}^2 + 4\left(\tilde{\omega}_\mathrm{pb}^2 + \tilde{\omega}_\mathrm{bg}^2\right)} - 2\sqrt{\tilde{\omega}_\mathrm{pb}^2 + \tilde{\omega}_\mathrm{bg}^2}\,. \tag{6.65}$$

The presence of a magnetic field also raises the threshold velocity: there is only an instability at a given wavenumber K if

$$\left(\frac{V_\mathrm{b}}{C_\mathrm{b}}\right)^2 = \mathcal{M}^2 > \frac{\left(K^2 + K_\mathrm{B}^2\right)\left(K^2 + \tilde{\omega}_\mathrm{pb}^2 + \tilde{\omega}_\mathrm{bg}^2\right)}{K^2 \tilde{\omega}_\mathrm{pb}^2}\,. \tag{6.66}$$

This last condition is analogous to condition (20b) of Tautz and Schlickeiser [91] (after correcting a misprint), who only consider the non-relativistic case.

For the remainder of this section we consider the ultra-relativistic limit with $\mathcal{M}^2 \gg 1$, $V_\mathrm{b} \simeq 1 \gg C_\mathrm{b} \simeq 1/\mathcal{M}$. Defining the dimensionless limiting wavenumbers $\kappa_\pm = K_\pm / \tilde{\omega}_\mathrm{bg}$ and a dimensionless gyration frequency

$\sigma_B = \tilde{\Omega}_b/\tilde{\omega}_{bg}$, the growth rate of the unstable solution can be represented by the analogue for the magnetized case of relation (6.45):

$$\sigma^2 = \sqrt{\left(\frac{1+\kappa^2+\sigma_B^2}{2}\right)^2 + \frac{\left(\kappa^2-\kappa_-^2\right)\,\left(\kappa_+^2-\kappa^2\right)}{\mathcal{M}^2}} - \frac{1+\kappa^2+\sigma_B^2}{2}\,. \tag{6.67}$$

The magnetized equivalent of approximate relation (6.46), valid when $(1+\kappa^2+\sigma_B^2)^2 \gg 4(\kappa^2-\kappa_-^2)\,\left(\kappa_+^2-\kappa^2\right)/\mathcal{M}^2$, reads:

$$\sigma^2 \approx \frac{\left(\kappa^2-\kappa_-^2\right)\,\left(\kappa_+^2-\kappa^2\right)}{\mathcal{M}^2\,\left(1+\kappa^2+\sigma_B^2\right)}\,. \tag{6.68}$$

In the ultra-relativistic limit with $C_b \ll 1$ and $\mathcal{M}^2 \gg 1$ one has $K_B \simeq \mathcal{M}\,(\Omega_b/\gamma_B)$ and $K_{max} \simeq \mathcal{M}\,\tilde{\omega}_{pb}$. If $K_{max}^2 \gg \tilde{\omega}_{pb}^2 + \tilde{\omega}_{bg}^2$ ($\eta\mathcal{M}^2 \gg 1+\eta$) the Weibel instability vanishes according to (6.65) if the magnetic field gets so large that $K_B \approx K_{max}$, or equivalently

$$\frac{|\Omega_b|}{\gamma_b} \simeq \frac{|q_b|B}{\gamma_b m_b} \approx \tilde{\omega}_{pb}\,. \tag{6.69}$$

In figure 6.4 we show the solution for the dimensionless growth rate $\sigma(\kappa)$ of the unstable Weibel mode (ordinary mode) in the magnetized case.

6.8.1 When can non-magnetic results be used?

We are mostly interested in the application of the Weibel instability to the ultra-relativistic shocks associated with Gamma Ray Bursts. The influence of the magnetic field on the Weibel instability will be small if $K_- \ll \tilde{\omega}_{bg}$ ($\kappa_- \ll 1$), so that both the maximum growth rate and the range of unstable wavenumbers are comparable with their values in the field-free case, see figure 6.4. From the discussion above, and in particular from equation (6.63), it is clear that this situation occurs if $K_B \ll K_{max}$. In the ultra-relativistic regime, the growth rate of the instability, $\tilde{\sigma} = \mathrm{Im}(\omega)$, is then roughly constant over a wide wavelength range, with

$$\tilde{\sigma} \approx \tilde{\omega}_{pb} V_b \;\text{ for }\; \tilde{\omega}_{bg} < K < \tilde{\omega}_{pb}\,\mathcal{M}\,, \tag{6.70}$$

assuming $\eta\mathcal{M}^2 \gg 1$. This should be compared with the gyration frequency of beam particles, which for a relativistic cold beam with $C_b \ll 1$ is

$$|q_b|B/\gamma_b m_b \approx |\Omega_b|/\gamma_b\,, \tag{6.71}$$

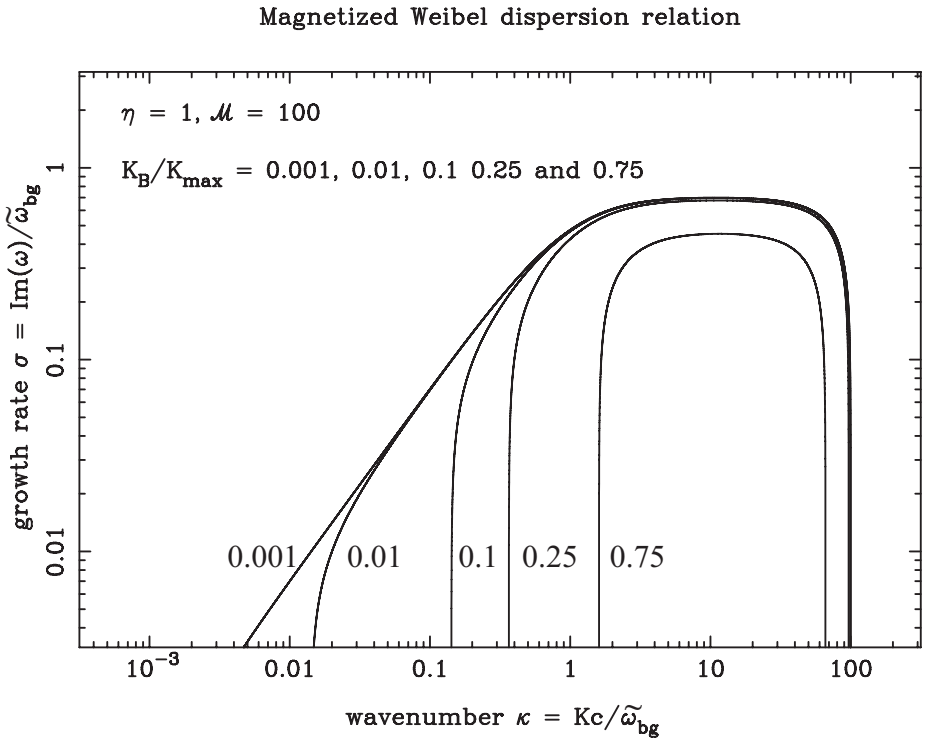

Figure 6.4: The dimensionless growth rate σ for the magnetized Weibel instability for field-aligned beams as a function of dimensionless wavenumber κ as calculated from the fluid model, for $\eta = 1$, $\mathcal{M} = 100$ and $K_B/K_{max} = 0.001$, 0.01, 0.1, 0.25 and 0.75, corresponding to an increasing magnetic field. The different curves are labeled by the value of K_B/K_{max}. The modification with respect to the field-free case becomes important for $K_B \sim K_{max}$.

The ratio of the gyration frequency and typical Weibel growth rate is therefore

$$\frac{|\Omega_{\rm b}|}{\gamma_{\rm b}\tilde{\sigma}} \approx \frac{|\Omega_{\rm b}|}{\gamma_{\rm b}\tilde{\omega}_{\rm pb}V_{\rm b}} \approx \frac{K_{\rm B}}{K_{\rm max}} \,. \tag{6.72}$$

This shows that the condition $K_{\rm B} \ll K_{\rm max}$ *also* ensures that the growth rate of the instability is much larger than the gyration frequency of the beam particles.

Taking the beam material to be the unshocked (cold) hydrogen plasma interpenetrating the (hot) shocked plasma, the ratio of the beam gyration frequency and growth rate of the Weibel instability equals:

$$\frac{|\Omega_{\rm b}|}{\gamma_{\rm b}\tilde{\omega}_{\rm pb}} \approx \begin{cases} 3\times 10^{-4}\,\dfrac{B_{\mu\rm G}}{\gamma_{\rm b}\sqrt{n_{\rm e}}} & \text{(electrons)} \\ \\ 7\times 10^{-5}\,\dfrac{B_{\mu\rm G}}{\gamma_{\rm b}\sqrt{n_{\rm p}}} & \text{(protons)} \end{cases} \tag{6.73}$$

Here $B_{\mu\rm G}$ is the strength of the pre-existing magnetic field in the shock transition layer in units of micro-Gauss, and $n_{\rm e}$ ($n_{\rm p}$) is the *proper* density of the electron (proton) beam. This proper density is always of the same order as the density of the particles in the pre-shock medium. The magnetic field strength in the transition layer depends on the orientation of the pre-shock magnetic field. For a magnetic field parallel to the shock normal (the case for which the magnetized Weibel dispersion relation was derived) there is no field amplification due to shock compression, and the ambient magnetic field in the transition layer equals the upstream field, even after a Lorentz transformation to the rest frame of the hot post-shock material. In that case, the ratio $|\Omega_{\rm b}|/\gamma_{\rm b}\tilde{\omega}_{\rm pb}$ is always much smaller than unity for typical parameters: $B_{\mu\rm G} \sim 1-100$, $\gamma_{\rm b} \sim \gamma_{\rm sh}/\sqrt{2} \sim 100$ and $n_{\rm e,p} \sim 1-100$ cm^{-3}. That implies that in this case the effect of the magnetic field can be neglected altogether: the growth of the Weibel instability is so rapid that particles do not get a chance to start gyrating around the ambient (pre-existing) magnetic field. Their dynamics can be described as being unmagnetized, and the range of unstable wavenumbers and instability growth rate are hardly affected in this case.

If there is a component $B_{\rm t}$ of the magnetic field along the shock surface, it could be amplified considerably, with $B_{\rm t2} \approx 2\sqrt{2}\,\gamma_{\rm sh}B_{\rm t1}$ upon completion of the shock transition according to the relativistic MHD shock jump conditions (see section 6.1). But even then one has $B_{\rm t2}/\gamma_{\rm b} \approx \sqrt{2}B_{\rm t2}/\gamma_{\rm sh} \sim 4B_{\rm t1}$. Here we have used that $\gamma_{\rm b} \approx \gamma_{\rm rel} \approx \gamma_{\rm sh}/\sqrt{2}$, where $\gamma_{\rm rel}$ is the Lorentz factor associated with

the relative motion between the up- and downstream flow. We may speculate that -at least for the light electrons- the growth rate of a Weibel-like instability in this case is still much larger than the gyrofrequency for typical parameters and the unmagnetized treatment of the instability is still a good approximation, while at the same time the growth of the electron-driven Weibel instability is rapid enough that the large-scale electric fields due to ion/electron charge separation in the shockfront play only a minor role in the local electron dynamics. We reiterate however that this case, where the beams are not (anti)parallel with the magnetic field, has **not** been treated here. In fact, the plasma dynamics near a perpendicular relativistic shock may very well involve quite different plasma instabilities, in particular for the thermalization of the heavier ions, such as the ion-driven gyroresonant instability discussed by Spitkovsky and Arons [90] in the context of the relativistic shocks in the pulsar wind that creates the Crab Nebula.

Some support for the relative unimportance of the magnetic field in the relativistic case when $K_B \ll K_{max}$ comes from the simulations of Hededal and Nishikawa [36]. Because of numerical limitations they can only follow the electron-driven Weibel instability. In the case of field-aligned beams they find that the Weibel instability develops unhindered if $\tilde{\omega}_{pb} \gg \Omega_b/\gamma_b$, and that the instability is totally suppressed if the beam plasma frequency and the beam gyrofrequency become of equal: $\tilde{\omega}_{pb} \sim \Omega_b/\gamma_b$ in our notation. In the case of a magnetic field that is perpendicular to the beam they find a significant modification of the plasma behavior when $\Omega_b/\gamma_b > 0.05\,\tilde{\omega}_{pb}$.

It should be pointed out that a similar conclusion does *not* necessarily hold for the non-relativistic version of the Weibel instability. If the beam velocity satisfies $V_b \ll c$, the maximum growth rate (for a cold beam) is (see equation 6.25):

$$\tilde{\sigma} = \tilde{\omega}_{pb} \left(\frac{V_b}{c} \right) . \tag{6.74}$$

The ratio of this growth rate and the typical gyration frequency $\Omega_b = q_b B/m_b c$ of the beam particles is now

$$\frac{\tilde{\sigma}}{\Omega_b} \approx \frac{V_b}{V_{Ab}} , \tag{6.75}$$

where $V_{Ab} \equiv B/\sqrt{4\pi n_b m_b}$ is an Alfvén velocity associated with the beams. In this case one needs $V_b \gg V_{Ab}$ in order for the unmagnetized result to apply. This is not guaranteed, especially for light particles such as electrons. Also, the

long-wavelength cutoff of the unstable wavelength range can be important in this case.

6.9 The asymmetric case

With the exception of our discussion of the cold beam/cold background case in section 6.4, we have so far treated the symmetric case of the Weibel instability driven by two identical but counterstreaming beams. In that case the beams carry no net current and the Weibel instability is purely transverse in the rest frame of the background plasma. In this section we briefly consider the asymmetric case with $\Delta \neq 0$, using the waterbag approximation for the beams.

We neglect the drift in the background plasma which occurs in the asymmetric case if the beams carry only one sign of charge. This drift supplies the return current to the beam current which is needed in the steady state. The effect of the drift will be small if the beam density is small compared to the density of the background plasma. If the beams themselves are electrically neutral, containing an equal amount of positively and negatively charged particles, our results apply after a straightforward generalization to a multi-species beam.

We will first transform dispersion relation (6.20) into a more convenient form. The longitudinal dielectric response of both background plasma and beams is contained in $\mathcal{D}_{11}(\omega, K)$, which is (see equation 6.148 of Appendix 6.13)

$$\mathcal{D}_{11}(\omega, K) = -\,|k \cdot k| \left(1 - \sum_{s \in \mathrm{bg}} \frac{\tilde{\omega}_{\mathrm{ps}}^2}{\omega^2 - K^2 C_{\mathrm{s}}^2} - \frac{\hat{\omega}_{\mathrm{pb}}^2}{\omega^2 - K^2 V_{x0}^2} \right). \quad (6.76)$$

The off-diagonal term $\mathcal{D}_{31}$ gives the coupling between the electrostatic and transverse fields. We now assume that the background plasma is relativistically hot, with $C_{\mathrm{s}} \approx 1/\sqrt{3}$ for all species, and that the beam is ultra-relativistic so that $V_{x0} \ll V_{z0} \approx 1$. In the low-frequency limit ($\omega \ll K$) one has

$$\begin{aligned} \mathcal{D}_{11}(\omega\,,\,K) &\approx -K^2 \left(1 + \frac{3\tilde{\omega}_{\mathrm{bg}}^2}{K^2} - \frac{\hat{\omega}_{\mathrm{pb}}^2}{\omega^2 - K^2 V_{x0}^2} \right), \\ \mathcal{D}_{33}(\omega\,,K) &\approx K^2 + \tilde{\omega}_{\mathrm{bg}}^2 + \frac{\hat{\omega}_{\mathrm{pb}}^2\, K^2}{\omega^2 - K^2 V_{x0}^2}, \\ \mathcal{D}_{31}(\omega\,,K) &\approx \Delta \left(\frac{\hat{\omega}_{\mathrm{pb}}^2\, K^2}{\omega^2 - K^2 V_{x0}^2} \right), \end{aligned} \quad (6.77)$$

where we have put $V_{z0} = 1$ everywhere.

We define a new dimensionless variable to parameterize the solution of the dispersion relation (6.20),

$$\mathcal{Z}(\omega\,,\,K) \equiv \frac{\omega^2 - K^2 V_{x0}^2}{\hat{\omega}_{\rm pb}^2}\,, \tag{6.78}$$

and introduce the two quantities

$$\begin{aligned} \mathcal{Z}_1(K) &= \left(1 + \frac{3\tilde{\omega}_{\rm bg}^2}{K^2}\right)^{-1} = \frac{\kappa^2}{3+\kappa^2}\,; \\ \mathcal{Z}_2(K) &= \frac{K^2}{\tilde{\omega}_{\rm bg}^2 + K^2} = \frac{\kappa^2}{1+\kappa^2}\,. \end{aligned} \tag{6.79}$$

The dispersion relation (6.20) can be written in the form

$$(\mathcal{Z}(\omega\,,\,K) - \mathcal{Z}_1)\;(\mathcal{Z}(\omega\,,\,K) + \mathcal{Z}_2) + \Delta^2\,\mathcal{Z}_1\mathcal{Z}_2 = 0\,. \tag{6.80}$$

The general solution for $\mathcal{Z}(\omega\,,\,K)$ in the asymmetric case reads

$$\mathcal{Z}_\pm(\omega\,,\,K) = \frac{\mathcal{Z}_1 - \mathcal{Z}_2}{2} \pm \sqrt{\left(\frac{\mathcal{Z}_1 + \mathcal{Z}_2}{2}\right)^2 - \Delta^2\,\mathcal{Z}_1\mathcal{Z}_2}\,, \tag{6.81}$$

which implicitly determines the wave frequency.

For the choice of parameters considered here one has $\mathcal{Z}_2 > \mathcal{Z}_1$ and therefore $\mathcal{Z}_+ > 0$ and $\mathcal{Z}_- \leq 0$. As the frequency of the two solutions satisfies

$$\omega_\pm^2 = \hat{\omega}_{\rm pb}^2\,\mathcal{Z}_\pm + K^2 V_{x0}^2\,, \tag{6.82}$$

the potentially unstable Weibel branch corresponds with the solution branch $\mathcal{Z}_-$, with a corresponding frequency ω_-. The solution corresponding with $\mathcal{Z}_+$ is stable. It corresponds to the stable transverse mode with $\tilde{\mathbf{E}} \perp \mathbf{V}_{\rm b}$ mentioned in section 6.3.

The Weibel branch has a dimensionless growth rate $\sigma^2 \equiv -\omega_-^2/\tilde{\omega}_{\rm bg}^2 = -\eta\,\mathcal{Z}_- - \kappa^2 V_{x0}^2$, which is :

$$\sigma^2 = \frac{\eta}{2}\left\{\sqrt{(\mathcal{Z}_1 + \mathcal{Z}_2)^2 - 4\Delta^2\,\mathcal{Z}_1\mathcal{Z}_2} - (\mathcal{Z}_1 - \mathcal{Z}_2)\right\} - \kappa^2 V_{x0}^2\,. \tag{6.83}$$

This solution is represented graphically in figure 6.5.

We now consider a number of specific cases. In the symmetric case ($\Delta = 0$) the transverse Weibel mode corresponds to the solution $\mathcal{Z}_- = -\mathcal{Z}_2$, with a frequency that satisfies $\omega_-^2 = -\hat{\omega}_{\rm pb}^2 \mathcal{Z}_2 + K^2 V_{x0}^2$. This is the case treated in section 6.7, which leads to an instability if $\mathcal{Z}_2 > K^2 V_{x0}^2/\hat{\omega}_{\rm pb}^2$. In the case of a single beam ($\Delta = 1$) in a relativistically hot background one has $\mathcal{Z}_- = \mathcal{Z}_1 - \mathcal{Z}_2$ and the dimensionless growth rate becomes

$$\sigma^2 = \kappa^2 \left(\frac{2\eta}{(1+\kappa^2)(3+\kappa^2)} - V_{x0}^2 \right) . \tag{6.84}$$

This case is unstable for wavenumbers satisfying

$$\kappa < \kappa_{\rm max}(\Delta = 1) \equiv \left(\sqrt{1 + 2\eta\, \mathcal{M}^2} - 2 \right)^{1/2} . \tag{6.85}$$

One can find a general expression for the maximum unstable wavenumber by putting $\sigma = 0$. We give the result in the limit of a beam velocity close to light speed ($1 - V_{z0} \ll 1$) so that $V_{x0} \approx 1/\mathcal{M} \ll 1$:

$$\kappa_{\rm max}(\Delta) = \left(\sqrt{\left(\eta \mathcal{M}^2 + 1\right)^2 - \eta^2 \Delta^2 \mathcal{M}^4} - 2 \right)^{1/2} . \tag{6.86}$$

The asymmetry has the effect of shrinking the range of unstable wavenumbers with respect to the symmetric case of $\Delta = 0$. The condition $\kappa_{\rm max}^2 > 0$ shows that the Weibel instability only occurs if

$$\eta \mathcal{M}^2 > \frac{\sqrt{4 - 3\Delta^2} - 1}{1 - \Delta^2} . \tag{6.87}$$

For the symmetric case ($\Delta = 0$) one finds $\eta \mathcal{M}^2 > 1$, while for the case of a single beam ($\Delta = 1$) equation (6.85) gives $\eta \mathcal{M}^2 > 3/2$.

If the beams are sufficiently strong, so that $\eta \mathcal{M}^2 \gg 1$ and $\kappa_{\rm max}(\Delta) \gg 1$, one can approximate dispersion relation (6.83) in the range $\kappa^2 \gg 1$ by using $\mathcal{Z}_1 \approx \mathcal{Z}_2 \approx 1$:

$$\sigma^2 \approx \eta \sqrt{1 - \Delta^2} - \frac{\kappa^2}{\mathcal{M}^2} . \tag{6.88}$$

This clearly shows that the main effect of the asymmetry is to suppress the maximum growthrate and maximum wave number (Figure 6.5). However, the effects are small unless Δ is very close to 1.

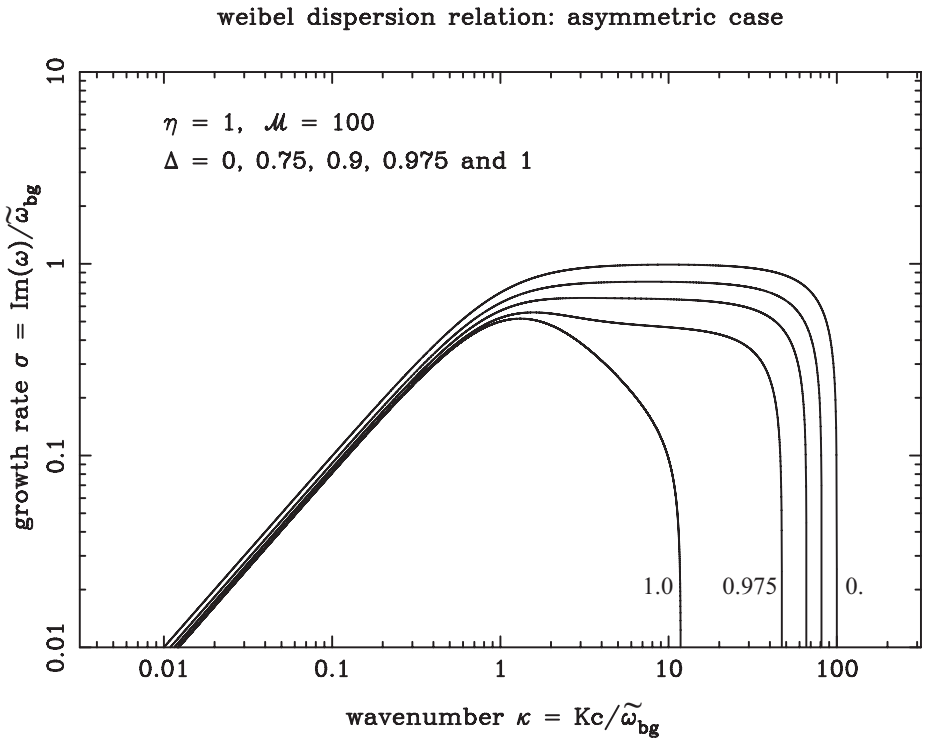

Figure 6.5: The dimensionless growth rate of the Weibel instability, $\sigma = \mathrm{Im}(\omega)/\tilde{\omega}_{\mathrm{bg}}$, as a function of the dimensionless wavenumber, $\kappa = Kc/\tilde{\omega}_{\mathrm{bg}}$, in the case of unequal beam densities. Growth rates are shown for $\eta = 1$ and $\mathcal{M} = 100$, and for a range of values of the asymmetry parameter Δ as defined in equation (6.19). The different curves are labeled by the corresponding value of Δ.

6.10 Conclusions

We have discussed the Weibel instability of relativistic beams in a relativistically hot background plasma. We have based our calculations on the first principles of the fluid and the Vlasov description of the plasma. Our calculations generalize and extend the results existing in the literature by presenting a detailed analysis of the dispersion relation in tensor form. Our aims have been, in particular:

- to obtain accurate expressions to use in further non-linear calculations which we present in chapter 9;
- to determine the basic parameters that characterize the dispersion in the plasma;
- and to estimate whether background magnetic fields or asymmetry play an important role.

We have shown that the linear growth rate in the relativistic limit is characterized by only two parameters in the symmetric case of identical but counterstreaming beams: the ratio $\eta = \tilde{\omega}_{\rm pb}^2/\tilde{\omega}_{\rm bg}^2$ of the effective plasma frequencies of beams and background plasma, and an effective Mach-number $\mathcal{M}$, which is a measure for the ratio of the momentum of beam particles in the beam direction and the typical momentum of the thermal motion (velocity dispersion) in the direction along the wave vector. The latter component is a measure for the pressure in the beam plasma. These conclusions are independent of the precise model, fluid or kinetic, that is used to describe the beam-plasma system.

For ultra-relativistic beams ($\gamma_{\rm b} \gg 1$) the maximum growth rate is of order $\mathrm{Im}(\omega) \approx \sqrt{\eta}\,\tilde{\omega}_{\rm bg}$, and the maximum unstable wavenumber is $K_{\rm max} \approx \sqrt{\eta}\,\mathcal{M}^2\,(\tilde{\omega}_{\rm bg}/c)$.

The presence of an ambient magnetic field does not change the behavior of the Weibel instability unless the field is so strong that the beam plasma frequency and the gyration frequency of the beam particles become comparable in magnitude: $\tilde{\omega}_{\rm pb} \simeq |q_{\rm b}|B/\gamma_{\rm b}m_{\rm b}$. A similar conclusion was reached by Hededal and Nishikawa [36] on the basis of numerical simulations. For the typical parameters associated with the ultra-relativistic shocks of Gamma Ray Bursts (external shocks) that propagate into the interstellar or circumstellar medium the unmagnetized treatment of the Weibel instability is a good approximation.

In the asymmetric case, characterized by the additional parameter $\Delta = (n_+ - n_-)/(n_+ + n_-)$ where $n_\pm$ are the densities of the two counterstreaming beams, the main effect of the asymmetry is that the range of unstable

wavenumbers shrinks, with the maximum unstable wavenumber and maximum growth rate scaling as $\mathrm{Im}(\omega)_{\max}$, $K_{\max} \propto (1-\Delta^2)^{1/4}$ (cf. equation 6.88) in the ultra-relativistic limit with $Kc/\tilde{\omega}_{\mathrm{bg}} \gg 1$.

The beam-driven Weibel instability will lead to the generation of magnetic fields over a wide range of wavelengths, as also discussed by references [32], [31], [58], [24] and [68]. In this respect it behaves not unlike the original version of the instability, driven by temperature anisotropies [98]. The next step is a detailed study of the stabilization mechanisms that terminate the phase of exponential growth of the instability discussed here. A first discussion of these stabilization mechanisms can be found in chapter 8. Chapter 9 discusses them in more detail.

6.11 Appendix: Covariant formulation of plasma response

The usual procedure for determining the response of a plasma to small-amplitude electromagnetic field, which is found in any book on plasma physics [e.g. 40, 63] relates the electric field **E** and the current density **J** it induces in the plasma by solving the linearized plasma equations. This determines the conductivity tensor σ. In the Fourier domain the amplitudes of the current density and the electric field are related by $\tilde{J}_i(\omega\,,\,\mathbf{k}) = \sigma_{ij}(\omega\,,\,\mathbf{k})\,\tilde{E}_j(\omega\,,\,\mathbf{k})$, where (i,j) enumerate the spatial components and a tilde ($\sim$) is used to denote Fourier amplitudes. One then calculates the susceptibility tensor, $\chi_{ij}(\omega\,,\,\mathbf{k}) = \frac{4\pi i}{\omega}\,\sigma_{ij}(\omega\,,\,\mathbf{k})$, and the dielectric tensor $\epsilon_{ij}(\omega\,,\,\mathbf{k}) = \delta_{ij} + \chi_{ij}$ in the Fourier domain. The dispersion relation of the various linear wave modes that the plasma supports follows from Maxwell's equations as

$$\det\{(c^2/\omega^2)(k_i k_j - k^2\,\delta_{ij}) + \epsilon_{ij}(\omega,\,\mathbf{k})\} = 0. \tag{6.89}$$

The electromagnetic response of a plasma can also be formulated covariantly [62, 61, 18]. This has the advantage of immediately yielding results that are valid for an arbitrary choice of reference frame. The starting point for such a formulation is the covariant set of Maxwell's equations,

$$\partial_\mu F^{\mu\nu} = 4\pi J^\nu \quad , \quad \partial_\mu \left(\epsilon^{\mu\nu\alpha\beta}\,F_{\alpha\beta}\right) = 0\,, \tag{6.90}$$

with $F^{\mu\nu}$ the Faraday tensor defined in terms of the electromagnetic four-potential $A^\mu \equiv (\Phi\,,\,\mathbf{A})$ as [e.g. 41]

$$F^{\mu\nu} = \partial^\mu A^\nu - \partial^\nu A^\mu\,, \tag{6.91}$$

and where $\epsilon^{\mu\nu\alpha\beta}$ is the totally antisymmetric (Levi-Cevita) tensor. For linear wave phenomena, this set of equations will be completed by a linear relation between the four-current J^μ and the electromagnetic fields.

It is convenient to formulate the linear response in terms of the four-potential perturbation $\delta A^\mu(x)$ and the associated four-current perturbation $\delta J^\mu(x)$. Assuming plane waves, one can represent these perturbed quantities in terms of a Fourier integral with the Fourier amplitudes $\tilde{A}^\mu(k)$ and $\tilde{J}^\mu(k)$:

$$\begin{pmatrix} \delta A^\mu(x) \\ \\ \delta J^\mu(x) \end{pmatrix} = \int \frac{\mathrm{d}^4 k}{(2\pi)^4} \begin{pmatrix} \tilde{A}^\mu(k) \\ \\ \tilde{J}^\mu(x) \end{pmatrix} \exp(-ik\cdot x) \; . \tag{6.92}$$

Here (and in what follows) a tilde $\sim$ is used to denote Fourier amplitudes of the wave-like perturbations in the various physical fields.

The Fourier-amplitude of the linearized four-current perturbation carried by some species s in a multi-species plasma can be related to the Fourier amplitude of the four-potential through

$$4\pi \tilde{J}^\mu_{\mathrm{s}}(k) = \left(\alpha^\mu_{\ \nu}\right)_{\mathrm{s}}(k)\, \tilde{A}^\nu(k) \; . \tag{6.93}$$

The quantity $\alpha^{\mu\nu}_{\mathrm{s}}(k)$ is the *polarization tensor*. The Faraday tensor associated with the waves, $\delta F^{\mu\nu} = \partial^\mu \delta A^\nu - \partial^\nu \delta A^\mu$, has the Fourier amplitude

$$\tilde{F}^{\mu\nu}(k) = i\left(k^\nu \tilde{A}^\mu - k^\mu \tilde{A}^\nu\right) \; , \tag{6.94}$$

which follows from the replacement $\partial^\mu \longrightarrow -ik^\mu$ when going from configuration space to Fourier space. As a result, the first set of Maxwell's equations (6.90) reads in the Fourier domain

$$(k\cdot\tilde{A})k^\mu - (k\cdot k)\tilde{A}^\mu = 4\pi \sum_{\mathrm{s}} \tilde{J}^\mu_{\mathrm{s}} = \sum_{\mathrm{s}} \left(\alpha^\mu_{\ \nu}\right)_{\mathrm{s}} \tilde{A}^\nu \; . \tag{6.95}$$

The polarization tensor has a number of simple properties, which are related to charge conservation and to the gauge freedom of the electromagnetic field. Charge conservation of each species s reads $\partial\cdot\, \delta J^\mu_{\mathrm{s}} = 0$, which in the Fourier domain becomes

$$k_\mu \tilde{J}^\mu_{\mathrm{s}}(k) = 0 \; . \tag{6.96}$$

Also, the four-current of each individual species should be invariant under a general gauge transformation of the form

$$\delta A_\mu \implies \delta A_\mu + \partial_\mu \chi \iff \tilde{A}_\mu \implies \tilde{A}_\mu - ik_\mu \tilde{\chi} \; . \tag{6.97}$$

equations (6.96) and (6.97) together imply that the polarization tensor must satisfy the relations

$$k_\mu \alpha_{\rm s}^{\mu\nu}(k) = \alpha_{\rm s}^{\mu\nu}(k) k_\nu = 0 \,. \tag{6.98}$$

6.11.1 Plasma response in the fluid approach

If one calculates the plasma response in the fluid approximation the two conditions (6.98) imply that the linear polarization tensor of species s can always be written in the form [cf. 18, 61, Ch. 4]

$$\left(\alpha^\mu{}_\nu\right)_{\rm s} = \mathcal{P}^\mu_{{\rm s}\alpha} \left(\Pi^\alpha{}_\beta\right)_{\rm s} \mathcal{P}^{\dagger\beta}_{{\rm s}\nu} \,, \tag{6.99}$$

with

$$\mathcal{P}^\mu_{{\rm s}\nu} \equiv \delta^\mu_\nu - \frac{U^\mu_{\rm s} k_\nu}{k\cdot U_{\rm s}} \quad , \quad \mathcal{P}^{\dagger\mu}_{{\rm s}\nu} \equiv \delta^\mu_\nu - \frac{k^\mu U_{{\rm s}\nu}}{k\cdot U_{\rm s}} \,. \tag{6.100}$$

Here $U^\mu_{\rm s}$ is the four-velocity of the frame where species s is at rest, apart from the thermal motions, so that the unperturbed mass current of species s is $\Sigma^\mu = n_{\rm s0} m_{\rm s} U^\mu_{\rm s}$, with $n_{\rm s0}$ the proper density and $m_{\rm s}$ the rest mass of the species. The projection tensor $\mathcal{P}^\mu_{{\rm s}\nu}$ and its transpose $\mathcal{P}^{\dagger\mu}_{{\rm s}\nu}$ project to the hyperplane perpendicular to k, and satisfy

$$k_\mu \, \mathcal{P}^\mu_{{\rm s}\nu} = \mathcal{P}^{\dagger\mu}_{{\rm s}\nu} k^\nu = 0 \quad , \quad \mathcal{P}^\mu_{{\rm s}\nu} U^\nu_{\rm s} = U_{{\rm s}\mu} \mathcal{P}^{\dagger\mu}_{{\rm s}\nu} = 0 \,. \tag{6.101}$$

The determination of $\alpha^{\mu\nu}_{\rm s}$ in the fluid approach can then be reduced to the calculation of $(\Pi^\alpha_\beta)_{\rm s}$.

Linearizing the covariant fluid equation (equation 6.7 of the main paper) to first order in perturbed quantities, assuming that there is no electromagnetic field in the unperturbed state and that the unperturbed state is uniform and time-independent, yields:

$$(\rho + e + P)_{\rm s} \, (U_{\rm s}\cdot\partial) \, \delta U^\mu_{\rm s} = h^{\mu\nu}_{\rm s} \, \partial_\nu \, \delta P_{\rm s} + n_{\rm s} q_{\rm s} \, (\delta F^{\mu\nu}) \, U_{{\rm s}\nu} \,. \tag{6.102}$$

Here (and in what follows) $\rho_{\rm s}$, $e_{\rm s}$, $P_{\rm s}$ and $U^\mu_{\rm s}$ are the *unperturbed* (equilibrium) values of the proper density, internal energy density, pressure and four-velocity of species s, and $h^{\mu\nu}_{\rm s} = \eta^{\mu\nu} - U^\mu_{\rm s} U^\nu_{\rm s}$ is the projection tensor based on the unperturbed four-velocity. In the Fourier domain, using $\partial_\mu \longrightarrow -ik_\mu$, this linearized equation of motion becomes:

$$i(k\cdot U_{\rm s}) \, (\rho + e + P)_{\rm s} \, \tilde{U}^\mu_{\rm s} = ik^\mu_\perp \tilde{P}_{\rm s} - n_{\rm s} q_{\rm s} U_{{\rm s}\nu} \, \tilde{F}^{\mu\nu} \,. \tag{6.103}$$

Here

$$k^{\mu}_{\mathrm{s}\perp} \equiv h^{\mu\nu}\, k_{\nu} = k^{\mu} - (k \cdot U_{\mathrm{s}})\, U^{\mu}_{\mathrm{s}} \ . \tag{6.104}$$

Note that

$$k \cdot U_{\mathrm{s}} = \gamma_{\mathrm{s}}\, (\omega - \mathbf{k} \cdot \mathbf{v}_{\mathrm{s}}) \tag{6.105}$$

is a Doppler-shifted frequency that corresponds to the wave frequency in the rest frame of species s.

The continuity equation (see equation 6.8 of the main paper) upon linearization becomes

$$(U_{\mathrm{s}} \cdot \partial)\, \delta n_{\mathrm{s}} = -n_{\mathrm{s}}\ (\partial \cdot \delta U_{\mathrm{s}}) \ , \tag{6.106}$$

and the equation of state yields

$$\delta P_{\mathrm{s}} = \Gamma_{\mathrm{s}} P_{\mathrm{s}} \left(\frac{\delta n_{\mathrm{s}}}{n_{\mathrm{s}}} \right) \ . \tag{6.107}$$

These two relations yield expressions for the density perturbation $\tilde{n}_{\mathrm{s}}$ and pressure perturbation $\tilde{P}_{\mathrm{s}}$ in the Fourier domain:

$$\begin{aligned} \tilde{n}_{\mathrm{s}} &= -n_{\mathrm{s}} \left(\frac{k \cdot \tilde{U}_{\mathrm{s}}}{k \cdot U_{\mathrm{s}}} \right) \ . \\ \tilde{P}_{\mathrm{s}} &= -\Gamma_{\mathrm{s}} P_{\mathrm{s}} \left(\frac{k \cdot \tilde{U}_{\mathrm{s}}}{k \cdot U_{\mathrm{s}}} \right) \ . \end{aligned} \tag{6.108}$$

If one substitutes these two relations into equation (6.103), and substitutes relation (6.94) for the Fourier amplitude $\tilde{F}^{\mu\nu}$ of the Faraday tensor, one obtains a set of four linear relations between the components of the two four vectors $\tilde{U}^{\mu}_{\mathrm{s}}$ and $\tilde{A}^{\nu}$:

$$\begin{aligned} &(\rho + e + P)_{\mathrm{s}}\, (k \cdot U_{\mathrm{s}}) \tilde{U}^{\mu}_{\mathrm{s}} + \Gamma_{\mathrm{s}} P_{\mathrm{s}} \left(\frac{k \cdot \tilde{U}_{\mathrm{s}}}{k \cdot U_{\mathrm{s}}} \right) k^{\mu}_{\mathrm{s}\perp} \\ &= n_{\mathrm{s}} q_{\mathrm{s}}\ \left\{ (U_{\mathrm{s}} \cdot \tilde{A})\, k^{\mu} - (k \cdot U_{\mathrm{s}})\, \tilde{A}^{\mu} \right\} \ . \end{aligned} \tag{6.109}$$

However, one of these relations is redundant as the unit normalization of the *total* four-velocity implies that $\tilde{U}^{\mu}_{\mathrm{s}} \cdot U_{\mathrm{s}\mu} = 0$, as is easily checked by contracting equation (6.109) with $U_{\mathrm{s}\mu}$.

The contribution of species s to the linear current four-vector is:

$$\tilde{J}^{\mu}_{\mathrm{s}} = q_{\mathrm{s}} \tilde{n}_{\mathrm{s}}\, U^{\mu}_{\mathrm{s}} + q_{\mathrm{s}} n_{\mathrm{s}}\, \tilde{U}^{\mu}_{\mathrm{s}} \ . \tag{6.110}$$

The first term in this expression is the *advection current* due to charge density perturbations advected by the unperturbed flow. This contribution to the current density is responsible for the occurrence of the Weibel instability. The second term is the *conduction current* due to the velocity perturbations induced by the electromagnetic fields. Using the first relation of equation (6.108), one can write the Fourier amplitude of the four-current density as

$$\tilde{J}^{\mu}_{\rm s}(k) = \frac{q_{\rm s} n_{\rm s}}{k \cdot U_{\rm s}} \left\{ (k \cdot U_{\rm s})\, \tilde{U}^{\mu}_{\rm s} - (k \cdot \tilde{U}_{\rm s})\, U^{\mu}_{\rm s} \right\} . \tag{6.111}$$

Solving equation (6.109), in effect expressing the components of $\tilde{U}^{\mu}_{\rm s}$ in terms of the components of $\tilde{A}^{\mu}$, and substituting the resulting expressions into equation (6.111), one can calculate the linearized current density $\tilde{J}_{\rm s}$ in terms of $\tilde{A}$, and from that read off the components of the corresponding polarization tensor $(\alpha^{\mu}_{\nu})_{\rm s}$. We just give the final result in terms of the tensor $(\Pi^{\alpha}{}_{\beta})_{\rm s}$:

$$\left(\Pi^{\alpha}{}_{\beta}\right)_{\rm s} = -\tilde{\omega}^2_{\rm ps} \left(\delta^{\alpha}{}_{\beta} - \frac{C_{\rm s}^2\, k^{\alpha} k_{\beta}}{(k \cdot U_{\rm s})^2 - K^2_{\rm s\perp} C_{\rm s}^2} \right) . \tag{6.112}$$

For a cold plasma one has $C_{\rm s}^2 = 0$, so that $(\Pi^{\alpha}{}_{\beta})_{\rm s} = -\tilde{\omega}^2_{\rm ps}\, \delta^{\alpha}_{\beta}$ with $\tilde{\omega}^2_{\rm ps} = 4\pi q_{\rm s}^2 n_{\rm s}/m_{\rm s}$. The cold plasma result has been derived previously by Dewar [18], his equations 95 and 114.

6.11.2 Plasma response in the kinetic approach

In the kinetic approach one must solve the covariant Vlasov equation. Let $\mathcal{F}_{\rm s}(x^{\mu}\,,\, p^{\mu})\ {\rm d}^4x\ {\rm d}^4p$ be the number of particles of species s in the infinitesimal volume ${\rm d}^4x$ in space-time and four-momentum interval ${\rm d}^4p$. The covariant Vlasov equation is

$$\frac{{\rm d}\mathcal{F}_{\rm s}}{{\rm d}\tau} \equiv \frac{{\rm d}x^{\mu}}{{\rm d}\tau} \frac{\partial \mathcal{F}_{\rm s}}{\partial x^{\mu}} + \frac{{\rm d}p^{\mu}}{{\rm d}\tau} \frac{\partial \mathcal{F}_{\rm s}}{\partial p^{\mu}} = 0 . \tag{6.113}$$

Here τ is the proper time, and

$$\frac{{\rm d}x^{\mu}}{{\rm d}\tau} = u^{\mu} = \frac{p^{\mu}}{m_{\rm s}} \quad , \quad \frac{{\rm d}p^{\mu}}{{\rm d}\tau} = q_{\rm s} F^{\mu}_{\nu} u^{\nu} \tag{6.114}$$

are the four-velocity and the Lorentz force acting on a particle with mass $m_{\rm s}$ and charge $q_{\rm s}$. We assume a plane-wave perturbation of the distribution function and all electromagnetic fields with the perturbations represented by a

Fourier integral. The total Vlasov distribution can be written as

$$\mathcal{F}(x\,,\,p) = \mathcal{F}_0(p) + \int \frac{\mathrm{d}^4k}{(2\pi)^4}\,\tilde{\mathcal{F}}(k\,,\,p)\,\exp(-ik\cdot x)\,, \tag{6.115}$$

and the linearized Vlasov equation yields:

$$-i(k\cdot u)\,\tilde{\mathcal{F}}_{\mathrm{s}}(k\,,\,p) = -\frac{q_{\mathrm{s}}}{m_{\mathrm{s}}}\tilde{F}^{\mu}_{\ \nu}\,p^{\nu}\,\frac{\partial\mathcal{F}_{0\mathrm{s}}(p)}{\partial p^{\mu}}\,. \tag{6.116}$$

Here we have assumed that the unperturbed distribution $\mathcal{F}_0(p)$ is uniform in space-time and that there is no unperturbed electromagnetic field. The linear current density associated with this perturbation has an amplitude

$$\tilde{J}^{\mu}_{\mathrm{s}}(k) = \frac{q_{\mathrm{s}}}{m_{\mathrm{s}}}\int \mathrm{d}^4p\,p^{\mu}\tilde{\mathcal{F}}_{\mathrm{s}}(k\,,\,p) \tag{6.117}$$

for particle species s. Using equation (6.94) for the Faraday tensor $\tilde{F}^{\mu}_{\ \nu}$ and solving (6.116) for $\tilde{\mathcal{F}}(k,p)$ and substituting the resulting expression one finds:

$$4\pi\tilde{J}^{\mu}_{\mathrm{s}} = \frac{4\pi q_{\mathrm{s}}^2}{m_{\mathrm{s}}}\int \mathrm{d}^4p\,p^{\mu}\left(\tilde{A}^{\nu} - \frac{(\tilde{A}\cdot p)}{(k\cdot p)}\,k^{\nu}\right)\frac{\partial\mathcal{F}_{0\mathrm{s}}(p)}{\partial p^{\nu}}\,. \tag{6.118}$$

After a partial integration one can write (6.118) in the form $4\pi\tilde{J}^{\mu}_{\mathrm{s}} = (\alpha^{\mu}_{\ \nu})_{\mathrm{s}}\,\tilde{A}^{\nu}$, which defines the polarization tensor of species s in the kinetic approach:

$$\left(\alpha^{\mu}_{\ \nu}\right)_{\mathrm{s}} \equiv -\frac{4\pi q_{\mathrm{s}}^2}{m_{\mathrm{s}}}\int \mathrm{d}^4p\,\mathcal{F}_{0\mathrm{s}}(p)\,M^{\mu}_{\ \nu}(k\,,\,p)\,, \tag{6.119}$$

with

$$M^{\mu}_{\ \nu}(k\,,\,p) = \delta^{\mu}_{\nu} - \frac{k^{\mu}p_{\nu} + p^{\mu}k_{\nu}}{(k\cdot p)} + \frac{(k\cdot k)\,p^{\mu}p_{\nu}}{(k\cdot p)^2}\,. \tag{6.120}$$

This result is in fact closely related to the fluid results (6.99) and (6.100). This can be seen by writing (6.119) in the form

$$\left(\alpha^{\mu}_{\ \nu}\right)_{\mathrm{s}}(k) = \int \mathrm{d}^4p\,\mathcal{F}_{0\mathrm{s}}(p)\,\left[\mathcal{P}^{\mu}_{\ \alpha}(k\,,\,p)\,\left(\Pi^{\alpha}_{\ \beta}\right)_{\mathrm{s}}\mathcal{P}^{\dagger\beta}_{\ \ \nu}(k\,,\,p)\right]\,, \tag{6.121}$$

with

$$\begin{aligned}\mathcal{P}^{\mu}_{\ \alpha}(k\,,\,p) &= \delta^{\mu}_{\alpha} - \frac{p^{\mu}k_{\alpha}}{(k\cdot p)}\\ \mathcal{P}^{\dagger\beta}_{\ \ \nu}(k\,,\,p) &= \delta^{\beta}_{\nu} - \frac{k^{\beta}p_{\nu}}{(k\cdot p)}\end{aligned} \tag{6.122}$$

and

$$\left(\Pi^{\alpha}_{\ \beta}\right)_{\rm s} = -\frac{4\pi q_{\rm s}^2}{m_{\rm s}}\,\delta^{\alpha}_{\ \beta}\ . \tag{6.123}$$

In the case of cold beams the fluid and kinetic results are completely equivalent.

Result (6.119) was derived in a different context by Achterberg [2], and also corresponds to expression 227 of Dewar [18] and the corresponding expression in Melrose [61], Ch. 4.1, for the response tensor of an unmagnetized plasma. These relations show explicitly that both charge conservation, and the invariance of the current density under gauge transformations of the vector potential, are once again ensured.

6.12 Appendix: Covariant dispersion relation

The linear dispersion relation for modes supported by the plasma follows from equation (6.95), which can be written as

$$D^{\mu\nu}(k)\,\tilde{A}_{\nu}(k) = 0\ . \tag{6.124}$$

Here we define

$$D^{\mu\nu}(k) \equiv (k\cdot k)\,\eta^{\mu\nu} - k^{\mu}k^{\nu} + \alpha^{\mu\nu}(k) \tag{6.125}$$

with $\alpha^{\mu\nu}(k) \equiv \sum_{\rm s}(\alpha^{\mu\nu})_{\rm s}(k)$. However, this set of equations is not linearly independent. The tensor $D^{\mu\nu}$ satisfies (see equation 6.98): $k_{\mu}\,D^{\mu\nu} = D^{\mu\nu}\,k_{\nu} = 0$. This means that the determinant of the 4×4 matrix $D^{\mu\nu}$ vanishes identically: $\det[D^{\mu\nu}\,] = 0$.

The dispersion relation for linear waves can be obtained by noting that one can factor equation (6.124) as:

$$\left(\delta^{\mu}_{\alpha} - \frac{k^{\mu}k_{\alpha}}{(k\cdot k)}\right)\,[(k\cdot k)\,\eta^{\alpha\nu} + \alpha^{\alpha\nu}\,]\,\tilde{A}_{\nu} = 0\ , \tag{6.126}$$

since $k_{\alpha}\,\alpha^{\alpha\nu} = 0$. The first factor leads to the vanishing determinant of $D^{\mu\nu}$. Therefore, the dispersion relation for the waves in the plasma follows from the requirement that the determinant of the *second* factor vanishes identically:

$$\det\left[(k\cdot k)\,\eta^{\mu\nu} + \sum_{\rm s}\alpha^{\mu\nu}_{\rm s}(k)\right] = 0\ . \tag{6.127}$$

The problem of determining the wave properties therefore corresponds to determining the polarization tensor $\alpha^{\mu\nu}$ and solving dispersion relation (6.127)

In this paper we take a different (but equivalent) approach, which avoids dealing with the problem $\det[D^{\mu\nu}] = 0$ altogether. First of all, we impose the invariant Lorentz-gauge on the wave electromagnetic fields,

$$k^\mu \tilde{A}_\mu(k) = 0 \, . \tag{6.128}$$

This choice is convenient, but it should be stressed that the correct dispersion relation can be derived in *any* gauge. The one longitudinal and two transverse degrees of freedom in a plasma can be described by three 'unit' *polarization vectors* e^μ_ℓ, $e^\mu_{\rm tr1}$ and $e^\mu_{\rm tr2}$. In addition, one has the gauge degree of freedom (equation 6.97) which defines a fourth *gauge vector*: $e^\mu_{\rm G} \equiv k^\mu / \sqrt{|k \cdot k|}$. We will not need to consider the degenerate case where $k \cdot k = 0$.

These four vectors define an orthonormal tetrad e_i with $e^\mu_0 = e^\mu_{\rm G}$, $e^\mu_1 = e^\mu_\ell$, $e^\mu_2 = e^\mu_{\rm tr1}$ and $e^\mu_3 = e^\mu_{\rm tr2}$. This tetrad can be used to describe all electromagnetic wave-like phenomena in a plasma. Assuming that the ordinary wave vector $\mathbf{k}$ is along the x-axis so that $k^\mu = (\omega \, , \, K \, , \, 0 \, , \, 0)$, we can choose these four vectors as[2]

$$\begin{aligned} e^\mu_{\rm G} &= \frac{(\omega \, , \, K \, , \, 0 \, , \, 0)}{\sqrt{|k \cdot k|}} \quad , \quad e^\mu_\ell = \frac{(K \, , \, \omega \, , \, 0 \, , \, 0)}{\sqrt{|k \cdot k|}} \, , \\ e^\mu_{\rm tr1} &= (0 \, , \, 0 \, , \, 1 \, , \, 0) \quad , \quad e^\mu_{\rm tr2} = (0 \, , \, 0 \, , \, 0 \, , \, 1) \, . \end{aligned} \tag{6.129}$$

The three polarization vectors satisfy

$$k \cdot e_\ell = k \cdot e_{\rm tr1} = k \cdot e_{\rm tr2} = 0 \, . \tag{6.130}$$

Using these definitions one has

$$e_i \cdot e_j \equiv g_{ij} = \mathrm{diag}(\pm 1 \, , \, \mp 1 \, , \, -1 \, , \, -1), \tag{6.131}$$

where the upper sign applies in the superluminal case, $\omega^2 - K^2 > 0$, and the lower sign in the subluminal case, $\omega^2 - K^2 < 0$. This choice of polarization vectors is convenient for the problem at hand, but depends on our adoption of the Lorentz gauge.

The Lorentz gauge implies that one can expand the four-potential in terms of the three polarization vectors as

$$\tilde{A}^\mu(k) = \sum_{j=1}^{3} \tilde{\mathcal{A}}^j(k) \, e^\mu_j \, . \tag{6.132}$$

[2]We limit the discussion to the case where $k \cdot k = \omega^2 - K^2$ is a real quantity, which includes the case of a purely imaginary frequency where $\omega^2 < 0$.

This defines three independent four-potential components[3]. Contracting the wave equation (6.124) from the left with e_i^μ one finds, using relation (6.130) and definition (6.131), that the wave equation can be written as

$$\mathcal{D}_{ij}(k)\,\tilde{\mathcal{A}}^j(k) = 0\ , \tag{6.133}$$

Here we employ the summation convention for $i, j = 1\ ,\ 2\ ,\ 3$ and define the 3×3 dispersion matrix $\mathcal{D}_{ij}$ by

$$\mathcal{D}_{ij}(k) \equiv e_i^\mu\ D_{\mu\nu}\ e_j^\nu = (k \cdot k)\, g_{ij} + \alpha_{ij}\ , \tag{6.134}$$

where

$$\alpha_{ij}(k) \equiv \sum_s e_i^\mu\ \left(\alpha_{\mu\nu}\right)_s e_j^\nu \equiv \sum_s \left(\alpha_{ij}\right)_s (k)\ . \tag{6.135}$$

The gauge vector $e_{\rm G}$ does not figure in these equations. Since $k_\mu D^{\mu\nu} = D^{\mu\nu} k_\nu = 0$ the component $\mathcal{D}_{00}$ vanishes identically, as does $\mathcal{D}_{0i}$ and $\mathcal{D}_{i0}$, where $i = 1\ ,\ 2\ ,\ 3$.

This procedure correctly isolates the physical wave modes involving the three vectors e_ℓ and $e_{\rm tr1,2}$, and removes the apparent singularity in the calculation of the determinant of $D^{\mu\nu}$. The dispersion relation for electromagnetic waves in a plasma therefore follows from the solution condition for (6.133):

$$\det\left[\mathcal{D}_{ij}(k)\right] = 0\ . \tag{6.136}$$

Another choice of gauge corresponds to another choice of the polarization vectors e_i, and of the components of $\mathcal{D}_{ij}$. However, the resulting dispersion relation, again formally given by (6.136), will yield the same modes.

6.13 Appendix: The components of the dispersion tensor

For the sake of completeness we give all the non-zero components of the dispersion tensor used in this paper, assuming a wave vector $\mathbf{k} = K\hat{\mathbf{x}}$ and wave frequency ω in the lab frame, where the background plasma is at rest.

6.13.1 Fluid approximation

In addition to the background plasma with sound speed $C_{\rm s} = \Gamma P_{\rm s}/(\rho + e + P)_{\rm s}$ for species s, there are two beams with bulk four-velocity $U_{\rm b}^\mu = \gamma_{\rm b}(1, 0, 0, \pm V_{\rm b})$, and a proper density

$$n_\pm = \frac{1 \pm \Delta}{2}\, n_{\rm b}\ . \tag{6.137}$$

[3]The Lorentz-gauge implies $\mathcal{A}_0 = e_0 \cdot A = 0$.

Here $n_{\rm b}$ is the total proper density of the two beams. For simplicity we assume that the two beams have equal temperature so that their internal sound speed satisfies $C_+ = C_- = C_{\rm b}$.

For waves propagating in the direction perpendicular to the beam so that $k^\mu = (\omega\,,\,K\,,\,0\,,\,0)$ the components of the dispersion tensor are:

$$\begin{aligned}
\mathcal{D}_{11} &= -|k\cdot k|\left(1-\sum_{s\in{\rm bg}}\frac{\tilde\omega_{\rm ps}^2}{\omega^2-K^2C_{\rm s}^2}-\frac{\tilde\omega_{\rm pb}^2}{\omega^2-K^2\tilde C_{\rm b}^2}\right)\,,\\
\mathcal{D}_{22} &= K^2+\sum_{s\in{\rm bg}}\tilde\omega_{\rm ps}^2+\tilde\omega_{\rm pb}^2-\omega^2\,,\\
\mathcal{D}_{33} &= K^2+\sum_{s\in{\rm bg}}\tilde\omega_{\rm ps}^2+\tilde\omega_{\rm pb}^2\left(1-\frac{(\omega^2-K^2)\,\tilde V_{\rm b}^2}{\omega^2-K^2\tilde C_{\rm b}^2}\right)-\omega^2\,,\\
\mathcal{D}_{31} &= \Delta\left(\sqrt{|k\cdot k|}\right)\left[\frac{\tilde\omega_{\rm pb}^2}{\gamma_{C_{\rm b}}\sqrt{1-C_{\rm b}^2V_{\rm b}^2}}\left(\frac{K\tilde V_{\rm b}}{\omega^2-K^2\tilde C_{\rm b}^2}\right)\right]\,.
\end{aligned}\tag{6.138}$$

Here we have defined

$$\tilde C_{\rm b}=\frac{C_{\rm b}}{\gamma_{\rm b}\sqrt{1-C_{\rm b}^2V_{\rm b}^2}}\quad,\quad\tilde V_{\rm b}=\frac{V_{\rm b}}{\gamma_{C_{\rm b}}\sqrt{1-C_{\rm b}^2V_{\rm b}^2}}\tag{6.139}$$

with $\gamma_{C_{\rm b}}\equiv 1/\sqrt{1-C_{\rm b}^2}$, and

$$\tilde\omega_{\rm ps}^2\equiv\frac{4\pi n_{\rm s}^2q_{\rm s}^2}{(\rho+e+P)_{\rm s}}\quad,\quad\tilde\omega_{\rm pb}^2=\frac{4\pi q_{\rm b}^2n_{\rm b}}{m_{\rm b}h_{\rm b}}\,.\tag{6.140}$$

The beam enthalpy per unit mass that appears in the expression for $\tilde\omega_{\rm pb}$ equals $h_{\rm b}=1+(e+P)_\pm/n_\pm m_{\rm b}$, and is identical for the two beams.

6.13.2 Kinetic theory

We express the covariant distribution $\mathcal{F}_0$ in terms of the more familiar phase-space density $f_{0{\rm s}}(\mathbf{x}\,,t\,,\,\mathbf{p})$, which is defined in terms of the ordinary momentum $\mathbf{p}$ and particle density $\overline{n}_{\rm s}$ in the lab frame. Particles must lie on the mass shell: $(p^0)^2-|\mathbf{p}|^2=E^2-|\mathbf{p}|^2=m_{\rm s}^2$ for $c=1$. If one assumes that the unperturbed distribution is spatially uniform and time-independent, the relation

between $\mathcal{F}_{0\mathrm{s}}$ and $f_{0\mathrm{s}}$ reads

$$\mathcal{F}_{0\mathrm{s}}(x^\mu\,,\,p^\mu) = \overline{n}_\mathrm{s}\, f_{0\mathrm{s}}(\mathbf{p})\,\frac{\delta(p^0-\gamma(\mathbf{p})\,m_\mathrm{s})}{\gamma(\mathbf{p})}\;. \tag{6.141}$$

Here $\gamma(\mathbf{p}) = \sqrt{1+|\mathbf{p}|^2/m_\mathrm{s}^2}$. The momentum distribution $f_{0\mathrm{s}}(\mathbf{p})$ has been normalized so that

$$\int \mathrm{d}^3\mathbf{p}\, f_{0\mathrm{s}}(\mathbf{p}) = 1\;. \tag{6.142}$$

The quantity $\overline{n}_\mathrm{s}$ is the lab frame density of species s. The momentum integration then formally changes according to $\mathrm{d}^4p\, F_{0\mathrm{s}}(p^\mu) \implies \overline{n}_\mathrm{s}\,\mathrm{d}^3\mathbf{p}\, f_{0\mathrm{s}}(\mathbf{p})/\gamma(\mathbf{p})$, which remains Lorentz-invariant as both $\mathrm{d}^3\mathbf{p}/\gamma(\mathbf{p})$ and $\overline{n}_\mathrm{s}\, f_{0\mathrm{s}}$ are Lorentz-invariants [e.g. 50].

As in the fluid treatment, we can use the set of polarization vectors and their properties to derive the kinetic equivalent of the fluid results. General expression (6.119) for the covariant polarization tensor $(\alpha^\mu_\nu)_\mathrm{s}$, together with the choice (6.129) for the polarization vectors, leads to the following components of the corresponding polarization tensor $(\alpha_{ij})_\mathrm{s}$ of particle species s in the Lorentz-gauge $k_\mu \tilde{A}^\mu = 0$:

$$\big(\alpha_{ij}\big)_\mathrm{s} = -\frac{4\pi q_\mathrm{s}^2 \overline{n}_\mathrm{s}}{m_\mathrm{s}}\int \frac{\mathrm{d}^3\mathbf{p}}{\gamma(\mathbf{p})}\, f_{0\mathrm{s}}(\mathbf{p})\,\mathcal{M}_{ij}(k\,,\,p)\;. \tag{6.143}$$

Here $\mathcal{M}_{ij}(k\,,\,p)$ is defined as

$$\mathcal{M}_{ij} \equiv e_i^\mu\, M_{\mu\nu}\, e_j^\nu = g_{ij} + \frac{(k\cdot k)\, p_i p_j}{(k\cdot p)^2}\;, \tag{6.144}$$

with $p_i \equiv p\cdot e_i$, where $p^\mu = (\gamma(\mathbf{p})\, m_\mathrm{s}\,,\,\mathbf{p})$.

The components of the polarization tensor with $k^\mu = (\omega\,,\, K\,, 0\,,\, 0)$ follow as

$$\begin{aligned}
\alpha^{\rm b}_{11} &= |k\cdot k|\ \frac{4\pi q_{\rm b}^2 \overline{n}_{\rm b}}{m_{\rm b}}\ \int \frac{{\rm d}^3\mathbf{p}}{\gamma(\mathbf{p})}\, f_{0{\rm b}}(\mathbf{p})\ \left\{\frac{1-v_x^2}{(\omega - Kv_x)^2}\right\}\,,\\
\alpha^{\rm b}_{22} &= \frac{4\pi q_{\rm b}^2 \overline{n}_{\rm b}}{m_{\rm b}}\ \int \frac{{\rm d}^3\mathbf{p}}{\gamma(\mathbf{p})}\, f_{0{\rm b}}(\mathbf{p})\,,\\
\alpha^{\rm b}_{33} &= \frac{4\pi q_{\rm b}^2 \overline{n}_{\rm b}}{m_{\rm b}}\ \int \frac{{\rm d}^3\mathbf{p}}{\gamma(\mathbf{p})}\, f_{0{\rm b}}(\mathbf{p})\ \left\{1-\frac{v_z^2\,(\omega^2-K^2)}{(\omega - Kv_x)^2}\right\}\,,\\
\alpha^{\rm b}_{31} &= \alpha^{\rm b*}_{13}\\
&= -\sqrt{|k\cdot k|}\,\frac{4\pi q_{\rm b}^2 \overline{n}_{\rm b}}{m_{\rm b}}\ \int \frac{{\rm d}^3\mathbf{p}}{\gamma(\mathbf{p})}\, f_{0{\rm b}}(\mathbf{p})\ \left\{\frac{v_z\ (K-\omega v_x)}{(\omega - Kv_x)^2}\right\}\,.
\end{aligned} \tag{6.145}$$

Here $\mathbf{v} = \mathbf{p}/\gamma m_{\rm b}$ is the velocity of beam particles with momentum $\mathbf{p}$.

It can be shown by partial integration that this is equivalent with

$$\begin{aligned}
\alpha^{\rm b}_{11} &= -\frac{4\pi q_{\rm b}^2 \overline{n}_{\rm b}|k\cdot k|}{K^2}\ \int {\rm d}^3\mathbf{p}\ \left\{\frac{K\,\dfrac{\partial f_{0{\rm b}}(\mathbf{p})}{\partial p_x}}{\omega - Kv_x}\right\}\,,\\
\alpha^{\rm b}_{33} &= \frac{4\pi q_{\rm b}^2 \overline{n}_{\rm b}}{m_{\rm b}}\ \int \frac{{\rm d}^3\mathbf{p}}{\gamma(\mathbf{p})}\, f_{0{\rm b}}(\mathbf{p})\ \left(1-v_z^2\right)\\
&\quad -4\pi q_{\rm b}^2 \overline{n}_{\rm b}\ \int {\rm d}^3\mathbf{p}\ \left\{\frac{v_z^2}{\omega - Kv_x}\ \left(K\,\frac{\partial f_{0{\rm b}}(\mathbf{p})}{\partial p_x}\right)\right\}\,,\\
\alpha^{\rm b}_{31} &= \frac{\sqrt{|k\cdot k|}}{\omega}\ \left[\frac{4\pi q_{\rm b}^2 \overline{n}_{\rm b}}{m_{\rm b}}\ \int \frac{{\rm d}^3\mathbf{p}}{\gamma(\mathbf{p})}\, f_{0{\rm b}}(\mathbf{p})\, v_x v_z\right.\\
&\quad \left. + 4\pi q_{\rm b}^2 \overline{n}_{\rm b}\ \int {\rm d}^3\mathbf{p}\ \left\{\frac{v_x v_z}{\omega - Kv_x}\ \left(K\,\frac{\partial f_{0{\rm b}}(\mathbf{p})}{\partial p_x}\right)\right\}\right]\,.
\end{aligned} \tag{6.146}$$

This particular form is convenient in the waterbag approximation discussed below.

6.13.3 Waterbag approximation

We use a momentum distribution for the beams of the form

$$\begin{aligned} f_{0\mathrm{b}}(\mathbf{p}) &= \frac{\Theta(p_x + p_{x0}) - \Theta(p_x - p_{x0})}{2\,p_{x0}}\,\delta(p_y)\,\times \\ &\times \left[\frac{1+\Delta}{2}\,\delta(p_z - p_{z0}) + \frac{1-\Delta}{2}\,\delta(p_z + p_{z0})\right]. \end{aligned} \tag{6.147}$$

For the background we continue to use the fluid approximation.

Substituting (6.147) into (6.146) the evaluation of the α_{ij}^{b} is straightforward as the p_x-derivatives in these expressions convert the Heaviside step functions in (6.147) into Dirac delta functions. The resulting components of the dispersion tensor are:

$$\begin{aligned} \mathcal{D}_{11} &= -|k\cdot k|\left(1 - \sum_{s\in\mathrm{bg}} \frac{\tilde{\omega}_{\mathrm{ps}}^2}{\omega^2 - K^2 C_{\mathrm{s}}^2} - \frac{\hat{\omega}_{\mathrm{pb}}^2}{\omega^2 - K^2 V_{x0}^2}\right), \\ \mathcal{D}_{22} &= K^2 + \sum_{s\in\mathrm{bg}} \tilde{\omega}_{\mathrm{ps}}^2 + \hat{\omega}_{\mathrm{pb}}^2\,\tilde{\mathcal{G}}_{\mathrm{b}} - \omega^2, \\ \mathcal{D}_{33} &= K^2 + \sum_{s\in\mathrm{bg}} \tilde{\omega}_{\mathrm{ps}}^2 + \hat{\omega}_{\mathrm{pb}}^2\left(\mathcal{G}_{\mathrm{b}} + \frac{K^2 V_{z0}^2}{\omega^2 - K^2 V_{x0}^2}\right) - \omega^2, \\ \mathcal{D}_{31} &= \Delta\left(\sqrt{|k\cdot k|}\right)\left[\frac{\hat{\omega}_{\mathrm{pb}}^2\,K V_{z0}}{\omega^2 - K^2 V_{x0}^2}\right]. \end{aligned} \tag{6.148}$$

Here we define the beam plasma frequency by

$$\hat{\omega}_{\mathrm{pb}}^2 = \frac{4\pi q_{\mathrm{b}}^2 \overline{n}_{\mathrm{b}}}{\gamma_0 m_{\mathrm{b}}}, \tag{6.149}$$

define a characteristic Lorentz-factor and velocity components

$$\begin{aligned} \gamma_0 &= \sqrt{1 + \frac{p_{x0}^2}{m_{\mathrm{b}}^2 c^2} + \frac{p_{z0}^2}{m_{\mathrm{b}}^2 c^2}}, \\ V_{x0} &= \frac{p_{x0}}{\gamma_0 m_{\mathrm{b}}}\ ,\ V_{z0} = \frac{p_{z0}}{\gamma_0 m_{\mathrm{b}}}, \end{aligned} \tag{6.150}$$

and introduce the two functions

$$\begin{aligned} \tilde{\mathcal{G}}_\mathrm{b} &= \gamma_0 \int \frac{\mathrm{d}^3\mathbf{p}}{\gamma(\mathbf{p})}\, f_{0\mathrm{b}}(\mathbf{p}) = \frac{1}{2V_{x0}} \ln\left[\frac{1+V_{x0}}{1-V_{x0}}\right] \\ \mathcal{G}_\mathrm{b} &= \gamma_0 \int \frac{\mathrm{d}^3\mathbf{p}}{\gamma(\mathbf{p})}\, f_{0\mathrm{b}}(\mathbf{p})\, \left(1 - v_z^2\right) \\ &= \tilde{\mathcal{G}}_\mathrm{b} - \frac{p_{z0}^2}{p_{z0}^2 + m_\mathrm{b}^2 c^2}\ . \end{aligned} \tag{6.151}$$

The result for the beam contribution to the polarization tensor, α_{ij}^b, has been derived by Silva et al. [89], using a somewhat different notation.

6.14 Appendix: Magnetized Weibel instability

We briefly consider the magnetized case, in order to compare the results obtained with the present formalism with those of Tautz and Schlickeiser [91]. We limit the discussion to the case where the electric field vanishes in the laboratory frame (the rest frame of the background plasma), and where the beam velocity is along the magnetic field in the z-direction. The beam trajectory then remains straight, and we do not have to deal with the much more difficult case of oscillator beams that gyrate around the ambient magnetic field. This means that the Lorentz force on all components vanishes in the unperturbed state: in a covariant notation

$$F^{\mu\nu} U_{\mathrm{s}\nu} = 0\ . \tag{6.152}$$

In both the laboratory frame and the rest frame of the beams, moving with velocity $\pm V_\mathrm{b}$ along the z-axis, the only non-vanishing components of the Faraday tensor are $F^{21} = -F^{12} = B$, with B the strength of the magnetic field $\mathbf{B} = B\hat{\mathbf{z}}$ in the laboratory frame.

In the fluid approximation the linearized equation of motion for small perturbations in the four-velocity of species s now reads, when transformed to the Fourier domain:

$$\begin{aligned} &(\rho + e + P)_\mathrm{s}\, (k\cdot U_\mathrm{s})\tilde{U}_\mathrm{s}^\mu + \Gamma_\mathrm{s} P_\mathrm{s} \left(\frac{k\cdot\tilde{U}_\mathrm{s}}{k\cdot U_\mathrm{s}}\right) k_{\mathrm{s}\perp}^\mu - i n_\mathrm{s} q_\mathrm{s} F^{\mu\nu}\tilde{U}_{\mathrm{s}\mu} \\ &= n_\mathrm{s} q_\mathrm{s}\, \left\{(U_\mathrm{s}\cdot\tilde{A})\, k^\mu - (k\cdot U_\mathrm{s})\, \tilde{A}^\mu\right\}\ . \end{aligned} \tag{6.153}$$

The last term on the left-hand side gives the first-order Lorentz force. Solving this equation, expressing the four-velocity perturbation in terms of the vector potential $\tilde{A}^\mu$, and calculating the associated four-current density, one finds the polarization tensor α^μ_ν. As before, we express the final result in terms of the tensor $(\Pi^\alpha_\beta)_\mathrm{s}$ for each species in the plasma:

$$\begin{aligned}\left(\Pi^\alpha_\beta\right)_\mathrm{s} \;=\; & -\frac{\tilde{\omega}^2_\mathrm{ps}}{N(k)}\,\Big\{(k\cdot U_\mathrm{s})^2\,\left[(k\cdot U_\mathrm{s})^2 - K^2_{\mathrm{s}\perp}C^2_\mathrm{s}\right]\,\delta^\alpha_\beta \\ & -i\,(k\cdot U_\mathrm{s})\,\Omega_\mathrm{s}\,\left[(k\cdot U_\mathrm{s})^2 - (k\cdot b)^2 C^2_\mathrm{s}\right]\,\epsilon^\alpha_{\beta\mu\nu}U^\mu_\mathrm{s}b^\nu \\ & +i\,(k\cdot U_\mathrm{s})\,\Omega_\mathrm{s}(k\cdot b)C^2_\mathrm{s}\,\left[\epsilon^\alpha_{\nu\mu\lambda}k^\nu U^\mu_\mathrm{s}b^\lambda b_\beta - b^\alpha\epsilon_{\beta\nu\mu\lambda}k^\nu U^\mu_\mathrm{s}b^\lambda\right] \\ & -(k\cdot U_\mathrm{s})^2\,C^2_\mathrm{s}\,k^\alpha k_\beta + (k\cdot U_\mathrm{s})^2\,\Omega^2_\mathrm{s}\,b^\alpha b_\beta\Big\}\end{aligned} \tag{6.154}$$

In this expression we define

$$N(k) \equiv (k\cdot U_\mathrm{s})^2\,\left[(k\cdot U_\mathrm{s})^2 - K^2_{\mathrm{s}\perp}C^2_\mathrm{s}\right] - \Omega^2_\mathrm{s}\,\left[(k\cdot U_\mathrm{s})^2 - (k\cdot b)^2C^2_\mathrm{s}\right] \tag{6.155}$$

and

$$\Omega_\mathrm{s} \equiv \frac{n_\mathrm{s}q_\mathrm{s}B}{(\rho+e+P)_\mathrm{s}}\,, \tag{6.156}$$

which is an effective gyrofrequency with B the magnetic field strength in the lab frame. In this particular case it is also the strength of the magnetic field in the rest frame of the beams, as follows from the Lorentz-transformations of the electromagnetic field, e.g. Jackson [41], Ch. 11. The quantity $K^2_{\mathrm{s}\perp}$ is defined in equation (6.11) of the main paper. The quantity $\epsilon^{\alpha\beta\gamma\delta}$ is the totally antisymmetric Levi-Cevita tensor, and the four-vector $b^\mu = (0\,,\,\mathbf{B}/B)$ corresponds to a space-like vector whose spatial component is along the magnetic field in the lab frame, where it takes the form $b^\mu = (0\,,\,0\,,\,0\,,\,1)$. It is easily checked that we recover the earlier result (A.23) for the unmagnetized case by putting $\Omega_\mathrm{s} = 0$.

We limit the discussion to the case where the wavevector $\mathbf{k} = K\hat{\mathbf{x}}$ in the laboratory frame is perpendicular to the magnetic field $\mathbf{B} = B\hat{\mathbf{z}}$ (and the beam velocity) so that $(k\cdot b) = 0$. We assume two symmetric counterstreaming beams. The Weibel instability then corresponds to the instability of the *ordinary mode*,

cf. Tautz and Schlickeiser [91], with the wave electric field $\delta\mathbf{E}$ along the unperturbed magnetic field in the laboratory frame where the background plasma is at rest. A straightforward calculation then shows that the relevant component of the dispersion tensor, $\mathcal{D}_{33}$, becomes:

$$\mathcal{D}_{33} \equiv K^2 - \omega^2 + \sum_{s\in \mathrm{bg}} \tilde{\omega}_{\mathrm{ps}}^2 + \tilde{\omega}_{\mathrm{pb}}^2 \left(1 - \frac{(\omega^2 - K^2)\,\tilde{V}_{\mathrm{b}}^2}{\omega^2 - K^2\tilde{C}_{\mathrm{b}}^2 - \tilde{\Omega}_{\mathrm{b}}^2}\right) . \tag{6.157}$$

Here we define

$$\tilde{\Omega}_{\mathrm{b}} = \frac{\Omega_{\mathrm{b}}}{\gamma_{\mathrm{b}}\sqrt{1 - V_{\mathrm{b}}^2 C_{\mathrm{b}}^2}} , \tag{6.158}$$

and all other quantities have been defined in Appendix 6.13, equations (6.139) and (6.140).

The Weibel dispersion relation, $\mathcal{D}_{33} = 0$, again takes the form of a biquadratic equation for the lab-frame wave frequency ω, see equation (6.34) of the main paper, but now with the coefficients

$$\mathcal{B}(K) = \tilde{\omega}_{\mathrm{bg}}^2 + \tilde{\Omega}_{\mathrm{b}}^2 + \tilde{\omega}_{\mathrm{pb}}^2 \left(1 - \tilde{V}_{\mathrm{b}}^2\right) + K^2 \left(1 + \tilde{C}_{\mathrm{b}}^2\right) , \tag{6.159}$$

and

$$\mathcal{C}(K) = \left(\tilde{\omega}_{\mathrm{bg}}^2 + \tilde{\omega}_{\mathrm{pb}}^2 + K^2\right) \left(K^2\tilde{C}_{\mathrm{b}}^2 + \tilde{\Omega}_{\mathrm{b}}^2\right) - \tilde{\omega}_{\mathrm{pb}}^2\, K^2 \tilde{V}_{\mathrm{b}}^2 . \tag{6.160}$$

This corresponds to the replacement $K^2\tilde{C}_{\mathrm{b}}^2 \longrightarrow K^2\tilde{C}_{\mathrm{b}}^2 + \tilde{\Omega}_{\mathrm{b}}^2$ with respect to the field-free case. As before, the instability condition reads $\mathcal{C}(K) < 0$.

Chapter 7

Variations on the Weibel instability

In the previous chapter we saw how, in a relativistic shock front, the Weibel instability will cause the magnetic field strength to grow in time. However, seen from the point of view of the shock wave one might expect a stationary situation instead, with the magnetic field becoming stronger as you go deeper into the shock front.

In this chapter we briefly show that the two points of view yield equivalent results. We also show that the Weibel instability preferentially produces electrical currents oriented perpendicularly to the shock front, which justifies the one-dimensional assumption that we make in much of the rest of this thesis.

7.1 Introduction

One can model plasma instabilities, like the Weibel instability, with solutions that grow in time (the usual approach) but also with solutions that grow in space, the relevant approach being dictated by the initial situation and boundary conditions that are used. The normal approach of looking for (exponentially) growing solutions of the equations that describe the plasma determines whether a certain situation is unstable at all, and determines such basic quantities as the typical length scale of the unstable perturbations and the growth rate. In recent theoretical research of relativistic collisionless shock waves, the instability analysis is taken a step further: the rapid growth of instabilities is used to model the shock ramp, the initial sudden increase in internal energy density and especially in magnetic energy density at the shock front [104, 58]. To model the (quasi-stationary) situation in the shock rest frame one would be interested in a spatially growing solution for the instability rather than one growing in time. In particular, depending on the boundary conditions, one would expect such a quasi-stationary state to form (after a certain time) in numerical simulations that use a constant inflow of particles (*e.g.*, as in Frederiksen et al. [24]; see also Hededal [35, chapter 4]).

The Weibel or filament instability is one of a few known mechanisms that are capable of increasing the magnetic field strength in collisionless shocks. Enhancement of the magnetic energy density is necessary, for example, to explain Gamma-ray Burst afterglows with the synchrotron (or jitter) radiation mechanism [*e.g.* 32].

To see if a Weibel-like instability might also produce a region of spatially growing magnetic field we will derive a dispersion relation for a plasma whose properties are allowed to vary in two spatial directions. In Sect. 7.3.5 we will show that the spatially growing solution for two counterstreaming beams of plasma is almost the same as the normal Weibel instability.

This analysis also yields equations describing a temporally growing Weibel-like instability with a wave vector that is not strictly perpendicular to the beam direction, *i.e.*, a mixed transverse/longitudinal mode, and we will show that this mixed instability only occurs for wave vectors that fall outside a certain cone around the shock normal (Sect. 7.3.6).

7.2 Counterstreaming beam model

7.2.1 Initial condition

We consider the stability of a system consisting of two counterstreaming beams of charged particles. Such a situation is similar to what we believe to exist in

shock fronts, where the unshocked material flows into the shock front and part of the incoming particles gets reflected to form a counterstream [*e.g.* 24]. To simplify the situation we will assume that the two beams are symmetrical even though this is probably only an approximation to the real situation. We expect that any asymmetry modifies the results only slightly (see section 6.9).

We also assume that the plasma beams are cold (negligible thermal kinetic energy density) in the region of interest so that the pressure term can be left out of their equations of motion. We ignore the dynamical influence of ions in the plasma and assume that they are present only to provide global charge neutrality. The electrons can be described by a fluid obeying the equations of motion

$$\begin{aligned} &\frac{\partial n}{\partial t} + \operatorname{div}(n\mathbf{v}) = 0, \\ &\frac{\partial \mathbf{p}}{\partial t} + \mathbf{v} \cdot \operatorname{grad} \mathbf{p} = q\left(\mathbf{E} + \frac{\mathbf{v}}{c} \times \mathbf{B}\right), \end{aligned} \tag{7.1}$$

where n is the electron density, $\mathbf{v}$ is their bulk velocity, $\mathbf{p} = \gamma m \mathbf{v}$ is their bulk momentum with $\gamma = (1 - |\mathbf{v}|^2)^{-1/2}$ the Lorentz factor of the bulk flow and $\mathbf{E}$ and $\mathbf{B}$ are the electric and magnetic field.

We indicate the quantities describing the forward and backward beam with subscripts plus and minus respectively. The beams start with initial velocity

$$\mathbf{v}_{0,\pm} = (0, 0, \pm v_0). \tag{7.2}$$

We take the total density of beam particles n_0 such that

$$n_{0,+} = n_{0,-} = \tfrac{1}{2} n_0. \tag{7.3}$$

We assume that no electromagnetic fields are present in the equilibrium situation.

7.2.2 Background plasma

The instability will take place in a region where there is also a population of already-shocked particles. We assume that the background plasma is stationary (no initial bulk velocity) so that the linear response is non-relativistic: $\mathbf{v} \simeq \mathbf{p}/m$. However, we allow the background plasma to be relativistically hot, so we do need to include the (relativistic) pressure terms:

$$\frac{\partial \mathbf{v}}{\partial t} + \mathbf{v} \cdot \operatorname{grad} \mathbf{v} = -\frac{1}{nhm} \operatorname{grad} P + \frac{q}{hm}\left(\mathbf{E} + \frac{\mathbf{v}}{c} \times \mathbf{B}\right), \tag{7.4}$$

where P is the pressure and the quantity h is the enthalpy per unit mass given by

$$h = 1 + \frac{e + P}{nmc^2}, \tag{7.5}$$

where e is the internal energy density of the plasma.

The equation given above is formally only valid when the plasma is well described with a fluid model. For a relativistically hot plasma a kinetic model would actually be more appropriate: see section 6.7. However, in chapter 6 we showed that the differences between results for the two approaches are small, so in this chapter we will favor the fluid description because it keeps the mathematics simpler.

7.2.3 Maxwell's equations

We describe the electromagnetic fields through a scalar potential ϕ and a vector potential $\mathbf{A}$ in the Lorentz gauge:

$$\mathbf{E} = -\operatorname{grad}\phi - \frac{1}{c}\frac{\partial \mathbf{A}}{\partial t}, \qquad \mathbf{B} = \operatorname{curl}\mathbf{A}. \tag{7.6}$$

Maxwell's equations reduce to (*e.g.*, Jackson [41, equations 6.37,38])

$$\begin{aligned} \nabla^2\phi - \frac{1}{c^2}\frac{\partial^2\phi}{\partial t^2} &= -4\pi q(n - n_0), \\ \nabla^2\mathbf{A} - \frac{1}{c^2}\frac{\partial^2\mathbf{A}}{\partial t^2} &= -\frac{4\pi}{c}\mathbf{J}, \end{aligned} \tag{7.7}$$

where n_0 is the equilibrium density and $\mathbf{J}$ is the total current density in the plasma.

7.3 Instability analysis

7.3.1 Linear response of the beams

Assume that the instability is a small-amplitude, plane wave perturbation on top of the equilibrium situation. We substitute $n \to n_0 + n\exp(ik_x x + ik_z z - i\omega t)$ and similarly for all the other quantities. We assume that there are no initial electromagnetic fields ($E_0 = B_0 = 0$). We neglect the electrostatic potential ($\phi = 0$), and concentrate on the electromagnetic response of the plasma instead.

For small perturbations the response of the plasma to the electromagnetic field can be expressed as a linear relation between the current density $\mathbf{J}$ and

the vector potential $\mathbf{A}$. The derivation of this expression from the equations of motion (7.1) can be found, for example in Melrose [60], Sect. 2.1 (see also exercise 1.2). The current density for each beam becomes:

$$\mathbf{J}_{\pm} = -\frac{q^2 n_{0,\pm}}{\gamma_0 mc}\left\{\mathbf{I} \pm \frac{\mathbf{k}\,\mathbf{v}_0 + \mathbf{v}_0\,\mathbf{k}}{\omega \mp \mathbf{k}\cdot\mathbf{v}_0} + \frac{(k^2-\omega^2)\mathbf{v}_0\,\mathbf{v}_0/c^2}{(\omega \mp \mathbf{k}\cdot\mathbf{v}_0)^2}\right\}\cdot\mathbf{A}, \tag{7.8}$$

where $\mathbf{I}$ is the identity tensor, $k^2 = |\mathbf{k}|^2$ and we have indicated the expressions for the forward and backward beam with the $\pm$ signs. The total contribution of both beams is $\mathbf{J}_\mathrm{b} = \mathbf{J}_+ + \mathbf{J}_-$:

$$\begin{aligned}\mathbf{J}_\mathrm{b} = -\frac{q^2 n_0}{\gamma_0 mc}\Bigg\{&\mathbf{I} + \frac{(\mathbf{k}\cdot\mathbf{v}_0)(\mathbf{k}\,\mathbf{v}_0 + \mathbf{v}_0\,\mathbf{k})}{\omega^2 - (\mathbf{k}\cdot\mathbf{v}_0)^2} \\ &+ \frac{(k^2 - \omega^2/c^2)(\omega^2 + (\mathbf{k}\cdot\mathbf{v}_0)^2)\mathbf{v}_0\,\mathbf{v}_0}{(\omega^2 - (\mathbf{k}\cdot\mathbf{v}_0)^2)^2}\Bigg\}\cdot\mathbf{A}.\end{aligned} \tag{7.9}$$

7.3.2 Linear response of the background plasma

The background plasma will also contribute to the current density. Linearizing the equation of motion (7.4) for the background plasma yields an expression for the velocity perturbation of the background plasma:

$$-i\omega\mathbf{v} = -i\mathbf{k}\frac{P}{n_0 h_0 m} + i\omega\frac{q}{h_0 mc}\mathbf{A}. \tag{7.10}$$

To eliminate the pressure perturbation P we make use of a polytropic equation of state $P_0 + P = P_0\,(n/n_0)^\Gamma$, where Γ is the adiabatic index of the background plasma. Linearizing this equation of state gives

$$P = \Gamma P_0 \frac{n}{n_0}. \tag{7.11}$$

The density perturbation is given by the continuity equation (remember that $\mathbf{v}_0 = 0$ for the background plasma):

$$n = n_0 \frac{\mathbf{k}\cdot\mathbf{v}}{\omega}. \tag{7.12}$$

Substituting equations (7.11) and (7.12) into the equation of motion (7.10) yields

$$\mathbf{v} - C_\mathrm{s}^2 \frac{(\mathbf{k}\cdot\mathbf{v})\mathbf{k}}{\omega^2} = -\frac{q}{h_0 mc}\mathbf{A}, \tag{7.13}$$

where $C_s^2 = \Gamma P_0/(n_0 h_0 m)$ is the relativistic sound speed. To solve (7.13) for $\mathbf{v}$ we need to eliminate the $\mathbf{k}\cdot\mathbf{v}$ term and we can do that by first taking the dot-product with $\mathbf{k}$ to get an expression for $\mathbf{k}\cdot\mathbf{v}$:

$$\mathbf{k}\cdot\mathbf{v} = -\frac{q}{h_0 mc}\frac{\omega^2}{\omega^2 - k^2 C_s^2}\mathbf{k}\cdot\mathbf{A}. \tag{7.14}$$

Eliminating $\mathbf{k}\cdot\mathbf{v}$ from equation (7.13) now gives an expression for $\mathbf{v}$ which we can use to find the contribution of the background plasma to the current density:

$$\mathbf{J}_{\rm bg} = qn_0\mathbf{v} = -\frac{q^2 n_0}{h_0 mc}\left\{\mathbf{I} + \frac{C_s^2\mathbf{k}\,\mathbf{k}}{\omega^2 - k^2 C_s^2}\right\}\cdot\mathbf{A}. \tag{7.15}$$

7.3.3 Dispersion relation

The electromagnetic field must satisfy Maxwell's equations (7.7) with both the background and beam contributions as sources:

$$\left(\frac{\omega^2}{c^2} - k^2\right)\mathbf{A} = -\frac{4\pi}{c}(\mathbf{J}_{\rm b} + \mathbf{J}_{\rm bg}). \tag{7.16}$$

To get Weibel-like modes we will take $\mathbf{k} = (k_x, 0, k_z)$ and $\mathbf{v}_0 = (0, 0, v_0)$. Note that we leave $k_z \neq 0$ to allow for the possibility of solutions growing in the z-direction. We can then write the dispersion equation (7.16) as $\mathbf{M}\cdot\mathbf{A} = 0$ involving the vector $\mathbf{A} = (A_x, A_z)$ and the 2×2 matrix $\mathbf{M}$ with components:

$$\begin{aligned}
M_{xx} &= k^2c^2 - \omega^2 + \tilde{\omega}_{\rm pbg}^2 + \hat{\omega}_{\rm pb}^2 + \tilde{\omega}_{\rm pbg}^2\frac{C_s^2 k_x^2}{\omega^2 - k^2 C_s^2}\\
M_{xz} = M_{zx} &= \tilde{\omega}_{\rm pbg}^2\frac{C_s^2 k_x k_z}{\omega^2 - k^2 C_s^2} + \hat{\omega}_{\rm pb}^2\frac{v_0^2 k_x k_z}{\omega^2 - k_z^2 v_0^2},\\
M_{zz} &= k^2c^2 - \omega^2 + \tilde{\omega}_{\rm pbg}^2 + \hat{\omega}_{\rm pb}^2 + \tilde{\omega}_{\rm pbg}^2\frac{C_s^2 k_z^2}{\omega^2 - k^2 C_s^2}\\
&\quad + \hat{\omega}_{\rm pb}^2\left[\frac{2v_0^2 k_z^2}{\omega^2 - k_z^2 v_0^2} + \frac{(\omega^2 + k_z^2 v_0^2)(k^2 - \omega^2/c^2)v_0^2}{(\omega^2 - k_z^2 v_0^2)^2}\right],
\end{aligned} \tag{7.17}$$

where

$$\hat{\omega}_{\rm pb}^2 \equiv \frac{4\pi n_{\rm b} q^2}{\gamma_0 m}, \qquad \tilde{\omega}_{\rm pbg}^2 \equiv \frac{4\pi n_{\rm bg} q^2}{h_0 m}. \tag{7.18}$$

7.3.4 The "Normal" Weibel instability

The "normal" transverse Weibel instability growing in time follows from the dispersion equation of the previous section by taking $k_z = 0$. In that case $M_{xz} = M_{zx} = 0$ so the dispersion equation $\det \mathbf{M} = 0$ factors into

$$M_{xx}\, M_{zz} = 0. \tag{7.19}$$

The longitudinal mode with $M_{xx} = 0$ is always stable and the transverse mode with $M_{zz} = 0$ contains the Weibel instability. It obeys the dispersion equation

$$M_{zz} = k_x^2 c^2 - \omega^2 + \tilde{\omega}_{\mathrm{pbg}}^2 + \hat{\omega}_{\mathrm{pb}}^2 + \hat{\omega}_{\mathrm{pb}}^2 \frac{(k_x^2 - \omega^2/c^2) v_0^2}{\omega^2} = 0. \tag{7.20}$$

We can write this as

$$\omega^4 + B\omega^2 + C = 0, \tag{7.21}$$

with

$$\begin{aligned} B &= -\left(k_x^2 c^2 + \tilde{\omega}_{\mathrm{pbg}}^2 + \hat{\omega}_{\mathrm{pb}}^2 (1 - v_0^2/c^2)\right), \\ C &= -\hat{\omega}_{\mathrm{pb}}^2 k_x^2 v_0^2. \end{aligned} \tag{7.22}$$

The solution is

$$\omega^2 = \frac{-B \pm \sqrt{B^2 - 4C}}{2}. \tag{7.23}$$

Note that both B and C are negative, so the unstable solution $\omega^2 < 0$ is the solution with the minus sign. For $\omega \ll k_x^2 c^2$ we can neglect the ω^4 term in equation (7.21) and the solution is approximated by

$$\omega^2 = -\frac{C}{B} = -\frac{\hat{\omega}_{\mathrm{pb}}^2 k_x^2 v_0^2}{k_x^2 c^2 + \tilde{\omega}_{\mathrm{pbg}}^2 + \hat{\omega}_{\mathrm{pb}}^2 (1 - v_0^2)}. \tag{7.24}$$

7.3.5 Dispersion relation for spatial modes

In this section we will calculate the allowed growth length of stationary perturbations. If we take $\omega = 0$ the components of $\mathbf{M}$ in equation (7.17) simplify to

$$\begin{aligned} M_{xx} &= k^2 c^2 + \hat{\omega}_{\mathrm{pb}}^2 + \tilde{\omega}_{\mathrm{pbg}}^2 - \tilde{\omega}_{\mathrm{pbg}}^2 \frac{k_x^2}{k^2}, \\ M_{xz} &= -\left(\frac{\tilde{\omega}_{\mathrm{pbg}}^2}{k^2} + \frac{\hat{\omega}_{\mathrm{pb}}^2}{k_z^2} \right) k_x k_z, \\ M_{zz} &= k^2 c^2 + \hat{\omega}_{\mathrm{pb}}^2 + \tilde{\omega}_{\mathrm{pbg}}^2 - \left(\frac{\tilde{\omega}_{\mathrm{pbg}}^2}{k^2} + \frac{\hat{\omega}_{\mathrm{pb}}^2}{k_z^2} \right) k_z^2 + \hat{\omega}_{\mathrm{pb}}^2 \frac{k_x^2}{k_z^2}. \end{aligned} \tag{7.25}$$

We can conveniently represent the matrix with

$$\mathbf{M} = \begin{pmatrix} D + Fk_x^2 & Fk_xk_z \\ Fk_xk_z & D + Fk_z^2 \end{pmatrix} \tag{7.26}$$

where

$$\begin{aligned} D &= k^2c^2 + \hat{\omega}_{\mathrm{pb}}^2 + \tilde{\omega}_{\mathrm{pbg}}^2 + \hat{\omega}_{\mathrm{pb}}^2 \frac{k_x^2}{k_z^2}, \\ F &= -\left(\frac{\tilde{\omega}_{\mathrm{pbg}}^2}{k^2} + \frac{\hat{\omega}_{\mathrm{pb}}^2}{k_z^2} \right). \end{aligned} \tag{7.27}$$

There is only a nontrivial solution for $\mathbf{A}$ when $\det \mathbf{M} = 0$:

$$\det \mathbf{M} = D^2 + DFk^2 = Dk^2c^2 = 0, \tag{7.28}$$

where we have used $D + Fk^2 = k^2c^2$. For $k^2 \neq 0$ we obtain

$$k_z^4 + B'k_z^2 + C' = 0. \tag{7.29}$$

where

$$\begin{aligned} B' &= k_x^2 + \frac{\hat{\omega}_{\mathrm{pb}}^2 + \tilde{\omega}_{\mathrm{pbg}}^2}{c^2}, \\ C' &= \frac{\hat{\omega}_{\mathrm{pb}}^2}{c^2} k_x^2. \end{aligned} \tag{7.30}$$

The solution is

$$k_z^2 = \frac{-B' \pm \sqrt{B'^2 - 4C'}}{2}. \tag{7.31}$$

The solution with the minus sign corresponds to a plasma skin effect as we can see by considering the case without beams ($\hat{\omega}_{\mathrm{pb}} = 0$). The solution with the plus sign contains a spatially growing solution with purely imaginary k_z that resembles the Weibel instability:

$$k_z^2 \simeq -C'/B' = -\frac{\hat{\omega}_{\mathrm{pb}}^2 k_x^2}{k_x^2c^2 + \tilde{\omega}_{\mathrm{pbg}}^2} \qquad \text{for } k_z^2 \ll k_x^2. \tag{7.32}$$

The imaginary part of k_z has a simple dependence on k_x (Fig. 7.1): for small k_x it grows linearly with k_x, for large k_x it reaches a plateau. In more realistic models the instability will be cut off at large k_x due to a thermal spread in the momentum (*cf.* chapter 6 and reference [105]). Section 7.4 discusses the differences and similarities with the temporally growing solution (7.24).

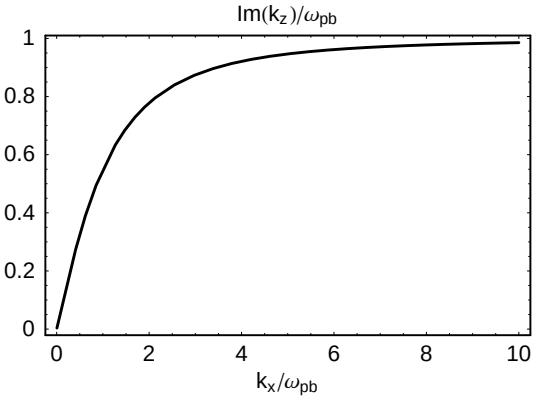

Figure 7.1: The imaginary part of k_z for the solution in equation (7.31). Both $\Im(k_z)$ and k_x are measured in units of $\hat{\omega}_{\rm pb}$ with $v_0 \sim c = 1$ and $\tilde{\omega}_{\rm pbg} = \hat{\omega}_{\rm pb}$.

7.3.6 Weibel instability for oblique propagation

Temporally growing modes with a wave vector that is oblique to the shock normal ($k_z \neq 0$) instead of perpendicular correspond to an instability that is no longer purely transverse, but partly longitudinal ($\mathbf{k} \cdot \mathbf{E} \neq 0$). To find the allowed growth rate for such modes we must consider the full matrix $\mathbf{M}$ in equation (7.17). We reorder the terms to get:

$$\mathbf{M} = \begin{pmatrix} D_{xx} + Fk_x^2 & Fk_xk_z \\ Fk_xk_z & D_{zz} + Fk_z^2 \end{pmatrix}, \tag{7.33}$$

where

$$\begin{aligned} F &= \frac{\tilde{\omega}_{\rm pbg}^2 C_{\rm s}^2}{\omega^2 - k^2 C_{\rm s}^2} + \frac{\hat{\omega}_{\rm pb}^2 v_0^2}{\omega^2 - k_z^2 v_0^2}, \\ D_{xx} &= k^2c^2 - \omega^2 + \hat{\omega}_{\rm pb}^2 \left(1 - \frac{k_x^2 v_0^2}{\omega^2 - k_z^2 v_0^2}\right), \\ D_{zz} &= k^2c^2 - \omega^2 \\ &\quad + \hat{\omega}_{\rm pb}^2 \left(1 + \frac{k_z^2 v_0^2}{\omega^2 - k_z^2 v_0^2} + \frac{(\omega^2 + k_z^2 v_0^2)(k^2 - \omega^2/c^2) v_0^2}{(\omega^2 - k_z^2 v_0^2)^2}\right). \end{aligned} \tag{7.34}$$

A non-trivial solution for $\mathbf{A}$ requires $\det \mathbf{M} = 0$:

$$D_{xx}D_{zz} + F(D_{xx}k_z^2 + D_{zz}k_x^2) = 0. \tag{7.35}$$

Dividing this equation by $D_{xx} + Fk_x^2$ we can write it as

$$D_{zz} + G = 0, \tag{7.36}$$

where

$$G(\omega, \mathbf{k}) \equiv \frac{D_{xx}Fk_z^2}{D_{xx} + Fk_x^2}. \tag{7.37}$$

Because the "normal" Weibel instability is a transverse instability we expect that a large k_z will disable the instability so we will assume $k_z \ll k_x$. When $k_z = 0$ the instability obeys the dispersion equation $D_{zz} = 0$ and we will assume that the same equation forms a good approximation for small k_z. This neglects G in the full dispersion equation (7.36). We will discuss the circumstances in which this term can be neglected at the end of this section.

We also take the limit $\omega \ll k_x c$. We will discuss the justification of this limit at the end of this section as well. In this limit we can write the equation $D_{zz} = 0$ (through some algebraic manipulation) as

$$\omega^4 + B''\omega^2 + C'' = 0, \tag{7.38}$$

where

$$\begin{aligned} B'' &= \alpha k_x^2 v_0^2 - (2+\alpha)k_z^2 v_0^2, \\ C'' &= k_z^2 v_0^4 \{k_z^2(1+\alpha) + \alpha k_x^2\}, \\ \alpha &= \frac{\hat{\omega}_{\mathrm{pb}}^2}{\tilde{\omega}_{\mathrm{pbg}}^2 + k^2 c^2}. \end{aligned} \tag{7.39}$$

Note that the dimensionless quantity α is *not* a constant, but a function of k_x and k_z (through $k^2 = k_x^2 + k_z^2$). In the limit $k_z \ll k_x$ it can be considered to be a function of k_x only. As we will see below, α determines the scaling of all the different terms. We will show that the approximations that we made so far are justified if $\alpha \ll 1$: this means that $kc \gg \hat{\omega}_{\mathrm{pb}}$ (large k limit) or $\tilde{\omega}_{\mathrm{pbg}} \gg \hat{\omega}_{\mathrm{pb}}$ (weak beam limit).

The solution of the dispersion equation (7.38) is

$$\omega^2 = -\tfrac{1}{2}B'' \pm \tfrac{1}{2}\sqrt{B''^2 - 4C''}. \tag{7.40}$$

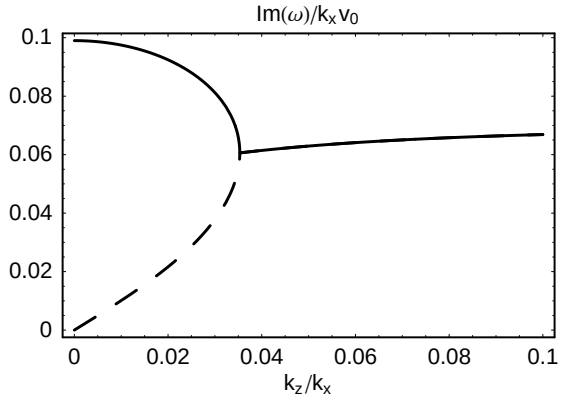

Figure 7.2: The imaginary part of the frequency for the two modes in equation (7.40) as a function of k_z (solid: mode with the minus sign, dashed: mode with plus sign). Both $\Im(\omega)$ and k_z are measured in units of k_x with $v_0 \sim c = 1$ and $\alpha = 0.01$. The bifurcation occurs at $k_z^2 = \alpha k_x^2/8$.

For $k_z = 0$ we have $C'' = 0$ and the root with the minus sign (solid line in Fig. 7.2) yields $\omega^2 = -B'' = -\alpha k_x^2 v_0^2$ which corresponds to the purely transverse Weibel instability (7.24). As k_z grows B'' becomes smaller and C'' becomes larger so that the growth rate drops. The solution with the plus sign (dashed line in Fig. 7.2) has a much smaller growth rate.

At the point where $B''^2 = 4C''$ a larger k_z will mean that ω^2 becomes complex, which means that ω will also become complex instead of purely imaginary. The condition $B''^2 = 4C''$ yields a biquadratic equation for k_z. The root that we are interested in (the one with $k_z < k_x$) is

$$k_z^2 = \frac{4 + \alpha - \sqrt{(4+\alpha)^2 - \alpha^2}}{\alpha} k_x^2 \simeq \tfrac{1}{8}\alpha k_x^2. \tag{7.41}$$

The corresponding frequency is

$$\omega^2 = -\tfrac{1}{2}B'' = -\frac{(2+\alpha)\sqrt{16+8\alpha} - 8 - 6\alpha}{\alpha} k_x^2 v_0^2 \simeq -\tfrac{3}{8}\alpha k_x^2 v_0^2. \tag{7.42}$$

The approximate equalities apply for $\alpha \ll 1$. When $k_z^2 > \alpha k_x^2/8$ we get $B''^2 < 4C''$ and the roots of (7.40) become complex, which means that the waves become overstable.

Now we will justify the approximations that we used in the preceding calculations. We use α as the ordering parameter. As mentioned above $\alpha \ll 1$ means that the results are valid in the limit of large $\mathbf{k}$ or weak beams. The non-oscillating mode that corresponds to the Weibel instability at $k_z = 0$ only exists for $k_z^2 < \alpha k_x^2/8$ and in this parameter range we always have

$$\frac{\omega^2}{k_x^2 v_0^2} = O(\alpha), \quad \text{and} \quad \frac{k_z^2}{k_x^2} = O(\alpha). \tag{7.43}$$

This justifies the assumption that $\omega \ll kc$.

We can make the dispersion equation (7.36) dimensionless by dividing it by $k^2c^2 + \tilde{\omega}_{\mathrm{pbg}}^2$ to give:

$$\frac{D_{zz}}{k^2c^2 + \tilde{\omega}_{\mathrm{pbg}}^2} + \frac{G}{k^2c^2 + \tilde{\omega}_{\mathrm{pbg}}^2} = 0. \tag{7.44}$$

If the second term in this equation can be neglected with respect to the dominant terms in the first then $D_{zz} = 0$ is a good approximation to the full dispersion relation.

We can write:

$$\frac{G}{k^2c^2 + \tilde{\omega}_{\mathrm{pbg}}^2} = \frac{D_{xx}}{k^2c^2 + \tilde{\omega}_{\mathrm{pbg}}^2} \frac{Fk_x^2}{D_{xx} + Fk_x^2} \frac{k_z^2}{k_x^2}. \tag{7.45}$$

The first and second factors on the right-hand-side are $O(1)$ and the last one is $O(\alpha)$. Here, we made use of $k^2c^2 + \tilde{\omega}_{\mathrm{pbg}}^2 > k_x^2 v_0^2$ and $(\omega^2 - k_z^2 v_0^2)/(k_x^2 v_0^2) = O(\alpha)$. Inspection of $D_{zz}/(k^2c^2 + \tilde{\omega}_{\mathrm{pbg}}^2)$ shows that the dominant terms, which were used to derive equation (7.40), are $O(1)$. Because the right hand side of equation (7.45) is $O(\alpha)$ we can safely neglect G in the dispersion equation (7.36).

7.4 Discussion

Based on the model presented in Sect. 7.2 we have derived theoretical estimates for the linear growth rate for spatially growing Weibel-like instabilities (Sect. 7.3.5) and for temporally growing solutions with a wave vector oblique to the shock normal (Sect. 7.3.6).

Comparing the growth rate (7.24) for the normal (transverse, temporally growing) Weibel instability and (7.32) for the spatially growing solution we

see that they resemble each other closely. In particular, in the case of an ultra-relativistic streaming velocity the term containing $(1 - v_0^2)$ drops out of the denominator of equation (7.24) and the only remaining difference is the factor v_0^2 in the numerator. This proportionality of the growth rate with the streaming velocity is one of the main properties of the Weibel instability. The co-moving growth rate $ik_z v_0$ with k_z given by equation (7.32) has the same proportionality.

That the spatial Weibel instability so closely resembles the "normal" Weibel instability may be an expected result, but there are some subtleties. For one, whereas the normal Weibel instability is an instability with wave vector $\mathbf{k}$ perpendicular to the streaming velocity $\mathbf{v}_0$, this is not strictly true for the spatial case because it has an imaginary component of $\mathbf{k}$ along $\mathbf{v}_0$. This is reflected by the matrix $\mathbf{M}$ having non-zero off-diagonal components in the spatial case; see equation (7.25). The eigenvectors of the normal Weibel instability result in a vector potential with only a z-component producing a transverse electric field $\mathbf{E} = i\omega\mathbf{A}/c$ and magnetic field $\mathbf{B} = i\mathbf{k} \times \mathbf{A}$, whereas the spatial instability involves a vector potential $\mathbf{A} = (A_x, 0, A_z)$ and no electric field since $\omega = 0$. Nevertheless, the dispersion relations (7.21) and (7.29) for the pertinent modes turn out almost identical, but only through a fortuitous cancellation of terms.

The calculations in this chapter do not include temperature effects. For a numerical solution of the oblique dispersion equation including temperature effects see the work of Bret et al. [10].

The presence of counterstreaming beams in a plasma modifies the skin effect (the root in equation (7.31) with the minus sign) and creates the possibility of a spatially growing mode that closely resembles the Weibel instability (the root with the plus sign). We expect that this Weibel-like mode can model the quasi-stationary start of the shock ramp in collisionless shocks. With a suitable model for the saturation level, our results might also help in numerical simulations of the collisionless shock ramp as a starting point to speed the convergence to a quasi-stationary state.

In Sect. 7.3.6 we have also presented results for the temporally growing Weibel-like mode with a wave vector that is not strictly perpendicular to the beam direction ($k_z \neq 0$). The growth rate of the instability decreases slightly with increasing k_z (Fig. 7.2) up to $k_z/k_x = (\alpha/8)^{1/2}$, where α is defined in equation (7.39). At this value of k_z the growth rate drops sharply and instead of a purely growing instability, the modes change to overstable (growing oscillating) waves. In most applications of the Weibel instability one either has weak beams or large wave vectors (because the fast-growing modes typically have small wave lengths) so that α is small. This implies that the dominant instability only allows small k_z. This shows that the linear theory predicts that

the initial Weibel instability is mostly transverse and produces steadily growing currents parallel to the beam direction, which agrees with the results of numerical simulations [24, for example].

Chapter 8

Proton Weibel instability

In the previous two chapters we considered how the Weibel instability can produce exponentially growing magnetic fields. What we are interested in now is when the growth of the magnetic field will stop. In this chapter I present an estimate for the attainable magnetic field for the specific case of protons in a background of electrons. This case is interesting because we expect that the kinetic energy of the electrons can get thermalized much more quickly than the kinetic energy of the protons because electrons are so much lighter in mass. However, most of the kinetic energy is carried by the protons because of their large mass so we might expect the instability to continue for the protons when the instability of the electrons has already ended.

In this chapter I show how magnetic trapping of the protons predicts that the proton currents cannot grow much stronger than the electron currents so that surprisingly little of the kinetic energy of the protons can be used by the Weibel instability to produce magnetic fields. In chapter 9 we present more general results regarding the end of the Weibel instability and a more in-depth look at the mechanisms responsible for this chapter's result.

This chapter was published in Astronomy & Astrophysics [100].

8.1 Introduction

Magnetic field generation in relativistic shocks in a hydrogen (electron-proton) plasma is important for the fireball model for Gamma-ray Bursts [79, for example]. This model proposes that the non-thermal radiation we observe in the prompt and afterglow emission from the Gamma-ray Burst is synchrotron radiation from collisionless relativistic shocks. To explain the observed intensity of the afterglows as synchrotron emission, the models need a magnetic field strength B of at least ten per cent of the equipartition field strength [32, 72]. This means that the magnetic energy density must contribute about one to ten per cent to the total energy density of the plasma behind the shock: $B^2/8\pi \sim (0.01 - 1) \times e$, with e the post-shock thermal energy density. In electron-proton plasmas this implies a much stronger magnetic field than in pair plasmas because the energy density in an ultra-relativistic shock propagating into a cold medium (where $nmc^2 \gg P$, with n the number density, m the rest mass and P the thermal pressure) is roughly proportional to the rest mass m of the particles. In this chapter, we look at what happens in a plasma consisting of particles of widely different mass.

In collisionless shocks, plasma instabilities can generate magnetic fields. Within the shock transition layer the relative motion of the mixing pre- and post-shock plasma produces very anisotropic velocity distributions for all particle species concerned. Fluctuating electromagnetic fields deflect the incoming charged particles and act as the effective collisional process needed to complete the shock transition [*e.g.*, 38]. These fluctuating fields occur naturally because anisotropic velocity distributions are unstable against several plasma instabilities, such as the electrostatic two-stream instability and the electromagnetic Weibel instability. The first is an instability of (quasi-)longitudinal charge density perturbations and leads to fluctuating electric fields satisfying $|\mathbf{E}| \gg |\mathbf{B}|$ where $\mathbf{E}$ and $\mathbf{B}$ are the fluctuating electric and magnetic fields. The second is an instability of the advection currents (proportional to the beam velocity) that result from charge bunching in the beams, and leads to spontaneously growing transverse waves [98] with $|\mathbf{B}| \geq |\mathbf{E}|$. In a relativistic shock, where the relative velocity of the pre- and post-shock plasma approaches the velocity of light, the Weibel instability dominates because it has the largest growth rate [12].

As both analytical estimates and numerical simulations show, the Weibel instability in pair plasmas can produce a magnetic field of near-equipartition strength [21, 33, 45, 58, 104]. In numerical simulations, the magnetic field generation always undergoes an exponentially growing phase that agrees with the estimates from linear analytical theory, and enters a nonlinear phase after that.

Yang et al. [104] have shown that in pair plasmas, the magnetic field strength reaches its maximum value at the end of the linear phase of the instability. The question arises whether the same holds true for the Weibel instability operating in an electron-proton plasma [58]. Numerical simulations [24] show that the nonlinear phase may be more important in electron-ion plasmas.

In this chapter we present an analytical estimate that shows that the linear phase of the instability ends much earlier for proton beams in a hydrogen plasma than for electron(-positron) beams in a pair plasma. We do not present a full self-consistent shock model: rather we consider the plasma processes that could generate a magnetic field in a plasma with properties such as one expects near the front of a collisionless relativistic shock. The chapter is organized as follows. In section 8.2 we define a model for the shock situation in terms of the momentum distributions of the particles. We calculate the conditions for the instability in section 8.3.1 and the magnetic field strength at the end of the linear phase of the instability in section 8.3.2. In section 8.3.3, we compare the energy density associated with this magnetic field strength with the total available energy density associated with the beams. Section 8.4 contains the discussion and section 8.5 the conclusions.

8.2 A simple model for a relativistic shock transition

In an electron-proton plasma, the protons dominate the shock energetics because they have a much larger rest mass than the electrons. Therefore, we will study the proton-driven Weibel instability. In this section we present a simple model for the plasma in the transition layer at the front of the shock.

The plasma in an astrophysical relativistic shock does not necessarily behave as a *single* fluid. Coulomb collisions between electrons and protons are not sufficiently fast to create thermal equilibrium between the protons and electrons. This problem of the non-equilibration of the electron and ion energies already exists in the much slower ($\sim$ 1000 km/s) shocks associated with Supernova Remnants [19, 95].

We assume that scattering by plasma waves is far more efficient for the light electrons than for the heavy ions so that when the trajectories of the incoming protons start to become significantly perturbed, the electrons have already undergone the fast-growing electron Weibel instability [24, 58], which has converted the kinetic energy of their bulk motion into the thermal energy of a relativistically hot electron plasma with an (almost) isotropic thermal velocity distribution. The incoming protons form, seen from the rest frame of the hot electrons, a relativistic beam. We also assume that part of the protons are

reflected further downstream although that assumption is not critical for our final conclusions (see section 8.6).

The electron-driven Weibel instability produces a weak fluctuating magnetic field with $B^2/8\pi \sim e_\mathrm{e}$, with e_e the energy density of the shocked electrons. We ignore this magnetic field in the calculations for proton beams, but it could serve as a seed perturbation for the proton-driven Weibel instability.

8.2.1 The proton velocity distribution

A simple model for the anisotropic proton velocity distribution within the shock transition layer is a *waterbag distribution* [89, 105]. We consider a similar situation as in Fig. 6 of Frederiksen et al. [24]: we take two counter-streaming proton beams moving along the z-direction, with a small velocity spread in the x-direction to model thermal motions:

$$\begin{aligned} F(\mathbf{p}) = \frac{n_\mathrm{p}}{4p_{x0}}\, &[\Theta(p_x + p_{x0}) - \Theta(p_x - p_{x0})] \\ &\times \delta(p_y)\,[\delta(p_z - p_{z0}) + \delta(p_z + p_{z0})]\,. \end{aligned} \tag{8.1}$$

Here n_p is the total proton density, p_{z0} is the bulk momentum of the proton beams, p_{x0} is the maximum momentum in thermal motions and $\Theta(x) = (1 + x/|x|)/2$ is the Heaviside step function. The assumption of two beams of equal strength is mathematically convenient, but not essential (see section 8.6).

This is a simple model that mimics the properties of non-relativistic collisionless shocks [see the *Microstructure* section in 93] in which (partial) reflection of the ions occurs as a result of deflection by an electrostatic potential jump in the shock transition, or by 'overshoots' in the strong magnetic field in the wake of the shock. In addition, the waterbag model accounts for partial ion heating by including a velocity dispersion in the direction perpendicular to both the beam direction and the wave magnetic field. This direction lies along the wave vector of the unstable modes (the x-direction in our configuration).

8.2.2 The shock conditions for the electrons

We assume that the electrons have (almost) completed the shock transition so that their properties obey the relativistic shock conditions [8], which follow from the generally valid conservation laws for particle number, energy and momentum (see chapter 5).

Here and below, we will label properties of the post-shock electron plasma with subscript 2, and those of the pre-shock plasma with subscript 1. We will assume that the pre-shock plasma is cold in the sense that $e_{\mathrm{e},1} \ll n_{\mathrm{e},1} m_\mathrm{e} c^2$. Then

the shock conditions for the proper density $n_{\rm e}$ and the proper energy density $e_{\rm e}$ for the electrons are:

$$\begin{aligned} n_{\rm e,2} &= (4\gamma_{\rm rel}+3)n_{\rm e,1}, \\ e_{\rm e,2} &= (4\gamma_{\rm rel}+3)\gamma_{\rm rel}n_{\rm e,1}m_{\rm e}c^2, \end{aligned} \tag{8.2}$$

where $\gamma_{\rm rel}^2 = 1+u_{\rm z0}^2$ is the Lorentz factor of the relative velocity between the pre- and post-shock plasma (with $u_{\rm z0} = p_{\rm z0}/m_{\rm p}c$).

We neglect the dynamical influence of a pre-shock magnetic field on the electron-fluid jump conditions. This influence will be small if $V_{\rm Ae,1} \ll c$ where $V_{\rm Ae,1} \equiv B_1/\sqrt{4\pi n_{e,1}m_{\rm e}}$ is the Alfvén speed based on the electron mass (instead of the proton mass). We also neglect any large-scale electrostatic field in the shock that might accelerate the electrons to higher energies while decelerating the incoming protons.

8.3 The Weibel instability

8.3.1 The dispersion relation

We consider the instability of a purely transverse electromagnetic wave with wave vector $\mathbf{k} = k\mathbf{e}_x$ and frequency ω. The instability will grow with a rate equal to the imaginary part of the wave frequency: $\sigma = \Im(\omega)$.

The Weibel instability for the model of the previous section obeys a dispersion relation of the form [*e.g.*, 89]

$$k^2c^2 - \omega^2\left[\,1+\chi_{zz}(\omega,k)\,\right] = 0, \tag{8.3}$$

where $\chi_{zz}(\omega,k) \equiv \chi_{zz,\rm e}(\omega,k) + \chi_{zz,\rm p}(\omega,k)$ is the zz-component[1] of the plasma susceptibility tensor, which contains contributions of both the electrons and the protons.

Since the electrons have a relativistically hot thermal velocity distribution their contribution is

$$\chi_{zz,\rm e}(\omega,k) = -\frac{\tilde{\omega}_{\rm pe}^2}{\omega^2}\,, \tag{8.4}$$

where $\tilde{\omega}_{\rm pe}$ is the electron plasma frequency (in Gaussian units):

$$\tilde{\omega}_{\rm pe}^2 = \frac{4\pi q^2 n_{\rm e,2}}{m_{\rm e}h}, \tag{8.5}$$

[1]Note that we have changed the notation ($x \leftrightarrow z$) from the published article to be consistent with the rest of this thesis.

with n_e the electron proper density, q the electron charge, m_e the electron mass and $h = (e_\mathrm{e} + P_\mathrm{e})/(n_\mathrm{e} m_\mathrm{e} c^2) \simeq 4e_\mathrm{e}/(3n_\mathrm{e} m_\mathrm{e} c^2)$ the electron enthalpy per unit rest energy for the relativistically hot electrons with $e_\mathrm{e} \simeq 3P_\mathrm{e} \gg n_\mathrm{e} m_\mathrm{e} c^2$. If we assume that the electrons are fully shocked, the shock conditions (8.2) enable us to express $\tilde{\omega}_\mathrm{pe}$ in terms of the pre-shock electron number density:

$$\tilde{\omega}_\mathrm{pe}^2 = \frac{12\pi q^2 n_{\mathrm{e},1}}{m_\mathrm{e}} \left(\frac{4\gamma_\mathrm{rel} + 3}{4\gamma_\mathrm{rel}} \right). \tag{8.6}$$

The factor between brackets approaches unity in ultra-relativistic shocks with $\gamma_\mathrm{rel} \gg 1$.

The proton contribution to dispersion relation (8.3) is [see 89]

$$\chi_{zz,\mathrm{p}}(\omega, k) = -\frac{\omega_\mathrm{pp}^2}{\gamma_\mathrm{b0}\,\omega^2} \left(\mathcal{F} + \frac{k^2 v_{z0}^2}{\omega^2 - k^2 v_{x0}^2} \right), \tag{8.7}$$

with

$$\mathcal{F} = \frac{c}{2v_{x0}} \ln\left(\frac{c + v_{x0}}{c - v_{x0}} \right) - \frac{u_{z0}^2}{1 + u_{z0}^2}. \tag{8.8}$$

(see also chapter 6). Here $\omega_\mathrm{pp} = \sqrt{4\pi q^2 n_\mathrm{p}/m_\mathrm{p}}$ is the (non-relativistic) proton plasma frequency based on the density in the lab frame, m_p is the proton rest mass, $u_i = p_i/(m_\mathrm{p} c)$, $\gamma_\mathrm{b0} = (1 + u_{x0}^2 + u_{z0}^2)^{1/2}$ and $v_i = u_i c/\gamma_\mathrm{b0}$. To ensure quasi-neutrality of the plasma we must have

$$n_\mathrm{p} \approx n_{\mathrm{e},2}, \tag{8.9}$$

and the associated plasma frequency is

$$\omega_\mathrm{pp}^2 = (4\gamma_\mathrm{rel} + 3)\, \frac{4\pi q^2 n_{\mathrm{e},1}}{m_\mathrm{p}}. \tag{8.10}$$

For what follows it is convenient to introduce the frequency $\hat{\omega}_\mathrm{pp}$ defined by

$$\hat{\omega}_\mathrm{pp}^2 = \frac{\omega_\mathrm{pp}^2}{\gamma_\mathrm{b0}}. \tag{8.11}$$

If the velocity dispersion in the beam is small, which is always true for a Weibel-unstable proton distribution (see the end of this section), we have $\gamma_\mathrm{b0} \simeq \gamma_\mathrm{rel}$ so that

$$\frac{\hat{\omega}_\mathrm{pp}^2}{\tilde{\omega}_\mathrm{pe}^2} \simeq \frac{4m_\mathrm{e}}{3m_\mathrm{p}}. \tag{8.12}$$

Note that one can get the equations for an electron-positron beam in an electron-positron plasma [see also 89, 104] by replacing $n_{\rm p}$ and $m_{\rm p}$ with the beam density and electron mass respectively. We will use this in what follows to compare results for electron-proton plasmas with those for electron-positron plasmas. In those cases we assume that the density of the electron-positron beams is comparable to the density of the background electron-positron plasma.

Substituting the contributions (8.4) and (8.7) in (8.3) we can write the dispersion relation as a biquadratic equation for ω:

$$\omega^4 - \mathcal{B}\omega^2 + \mathcal{C} = 0, \tag{8.13}$$

with

$$\mathcal{B} = k^2(c^2 + v_{x0}^2) + \Omega^2, \tag{8.14}$$

$$\mathcal{C} = k^2\{v_{x0}^2(k^2c^2 + \Omega^2) - \hat{\omega}_{\rm pp}^2 v_{z0}^2\}, \tag{8.15}$$

where

$$\Omega^2 \equiv \tilde{\omega}_{\rm pe}^2 + \hat{\omega}_{\rm pp}^2\,\mathcal{F}. \tag{8.16}$$

Since $\mathcal{B} > 0$ the wave is unstable for $\mathcal{C} < 0$ with $\omega^2 \equiv -\sigma^2 < 0$ where the growth rate σ follows from

$$\sigma^2 = \frac{\sqrt{\mathcal{B}^2 - 4\mathcal{C}} - \mathcal{B}}{2}. \tag{8.17}$$

For a given set of shock parameters ($\gamma_{\rm b0}$, v_{x0}, n_0), the growth rate is a function of the wave number (Fig. 8.1).

Anticipating our results for a proton beam in a background of (relativistically) hot electrons, we will assume that the growth rate of the unstable modes satisfies

$$\sigma \ll kc \quad \text{and} \quad \sigma \ll \tilde{\omega}_{\rm pe}, \tag{8.18}$$

and that the characteristic plasma frequencies satisfy

$$\hat{\omega}_{\rm pp}^2 \ll \Omega^2, \tag{8.19}$$

see equation (8.27) below.

Under these assumptions we can approximate the solution of the dispersion relation with $\sigma^2 \simeq -\mathcal{C}/\mathcal{B}$, which leaves the instability criterion ($\mathcal{C} < 0$)

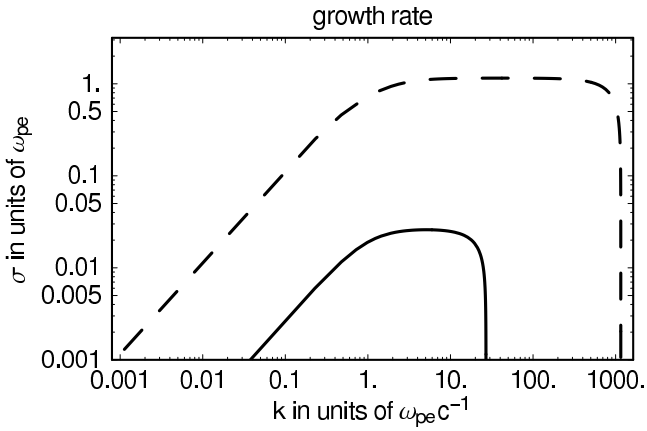

Figure 8.1: Growth rate as a function of wave number for a shock with $\gamma_{b0} = 1000$ and $v_{x0} = 0.001c$. The solid line is for proton beams in a background of hot electrons; the dashed line is for electron-positron beams in an electron-positron plasma.

unchanged. We will also make the approximation of a small beam velocity dispersion: $v_{x0}^2 \ll c^2$. Then the dispersion relation reduces to

$$\sigma^2 = \frac{k^2(\hat{\omega}_{pp}^2\, v_{z0}^2 - \Omega^2\, v_{x0}^2 - k^2 c^2\, v_{x0}^2)}{k^2 c^2 + \Omega^2}. \tag{8.20}$$

For further analysis we introduce the following dimensionless quantities:

$$\kappa = \frac{kc}{\Omega}, \quad \nu = \frac{\sigma}{\Omega}, \quad \alpha = \frac{\hat{\omega}_{pp}}{\Omega}\left(\frac{v_{z0}}{v_{x0}}\right), \tag{8.21}$$

Expressed in these quantities the dispersion relation (8.20) reads

$$\begin{aligned} \nu^2 &= \left(\frac{v_{x0}}{c}\right)^2 \frac{\kappa^2\left(\kappa_{max}^2 - \kappa^2\right)}{1+\kappa^2} \\ &= \left(\frac{\hat{\omega}_{pp}}{\Omega}\right)^2 \left(\frac{v_{z0}}{c}\right)^2 \frac{\kappa^2(\kappa_{max}^2 - \kappa^2)}{(1+\kappa^2)(1+\kappa_{max}^2)}, \end{aligned} \tag{8.22}$$

where we have eliminated v_{x0} using the definition of α and we define

$$\kappa_{\max} \equiv \sqrt{\alpha^2 - 1}, \tag{8.23}$$

which is the limiting wavenumber of the Weibel instability: the instability condition is satisfied for $\kappa < \kappa_{\max}$. The parameter α is a measure for the range of unstable wave numbers. The Weibel instability occurs only if $\alpha > 1$. This condition poses a restriction on the velocity spread v_{x0}:

$$\frac{v_{x0}}{v_{z0}} < \frac{\hat{\omega}_{\rm pp}}{\Omega}\,. \tag{8.24}$$

The quantity Ω depends on v_{x0} through equations (8.16) and (8.8), but a quick inspection shows that $\mathcal{F}$ and Ω are increasing functions of v_{x0} so if condition (8.24) holds, then we also have

$$\frac{v_{x0}}{v_{z0}} < \frac{\hat{\omega}_{\rm pp}}{\Omega|_{v_{x0}=0}} = \frac{\hat{\omega}_{\rm pp}}{(\tilde{\omega}_{\rm pe}^2 + \hat{\omega}_{\rm pp}^2/\gamma_{\rm rel}^2)^{1/2}}\,. \tag{8.25}$$

It follows that for relativistic shocks with $v_{z0} \to c$ the proton-driven instability requires $v_{x0} \ll c$ so that

$$\mathcal{F} \simeq \frac{1}{\gamma_{\rm b0}^2} + \frac{v_{x0}^2}{3c^2} \ll 1, \tag{8.26}$$

and

$$\Omega \simeq \tilde{\omega}_{\rm pe} \gg \hat{\omega}_{\rm pp} \tag{8.27}$$

(see equation 8.12).

The largest growth rate occurs for a mode with wave number k_*, which follows from $(\mathrm{d}\sigma/\mathrm{d}k)_{k=k_*} = 0$. Using the approximated dispersion relation (8.22) we find that this wavenumber equals

$$\frac{k_* c}{\Omega} \equiv \kappa_*(\alpha) = \sqrt{\alpha - 1}\,, \tag{8.28}$$

with the corresponding growth rate

$$\begin{aligned} \frac{\sigma(k_*)}{\Omega} \equiv \nu_* &= (\alpha - 1)\,\frac{v_{x0}}{c} \\ &= \frac{\alpha - 1}{\alpha}\,\left(\frac{\hat{\omega}_{\rm pp}}{\Omega}\right)\,\frac{v_{z0}}{c}\,. \end{aligned} \tag{8.29}$$

In the last equality we have used the definition of α. For a strong, relativistic shock we find $\sigma(k_*) \simeq \hat{\omega}_{\rm pp}$.

In view of this fact and equation (8.27), conditions (8.18) and (8.19) automatically hold for the proton-driven Weibel instability.

8.3.2 Stabilization of the Weibel instability

The linear phase of the Weibel instability (during which perturbations grow exponentially with time) ends when the generated electromagnetic fields significantly perturb the trajectories of the particles taking part in the instability. Because the magnetic fields generated by the instability are inhomogeneous, the particles will quiver under the influence of the Lorentz force. When the amplitude of these quiver motions exceeds the wavelength of the instability, the linear theory breaks down. Yang et al. [104] give a full treatment of these quiver motions and show that this criterion agrees with the magnetic trapping argument, which says that the instability will stop when the wave magnetic field becomes so strong that it traps the beam particles (see also chapter 9).

The linearized equation describing the quiver motions in the x-direction for a beam particle in a magnetic field $B(x,t)\,\mathbf{e}_y$ reads:

$$\frac{{\rm d}^2\xi_x}{{\rm d}t^2} = \frac{q v_{z0}\, B(x,t)}{\gamma_{\rm b0} m_{\rm p} c}\,, \tag{8.30}$$

where ξ_x is the displacement. In the linear stage of the instability the wave magnetic field varies as $B(x,t) = |\mathbf{B}|\exp(\sigma t)\sin(kx)$ for a wave with wave number k and growth rate σ, so the amplitude of the quiver motion is

$$|\xi_x| \sim \frac{q|\mathbf{B}|v_{z0}}{\gamma_{\rm b0} m_{\rm p} c \sigma^2}\,. \tag{8.31}$$

The trapping criterion $k|\xi_x| < 1$ corresponds to $|\mathbf{B}| < B_{\rm trap}$ with

$$B_{\rm trap} = \frac{\gamma_{\rm b0} m_{\rm p} c \sigma^2(k)}{k v_{z0} q}\,. \tag{8.32}$$

This corresponds to equation (18) of Yang et al. [104]. Assuming that trapping saturates the Weibel instability at *all* wavelengths we get the typical field amplitude as a function of wavenumber (Fig. 8.2).

The maximum field amplitude is reached at those wave numbers where σ^2/k has the maximum value. For dispersion relation (8.22) this maximum is

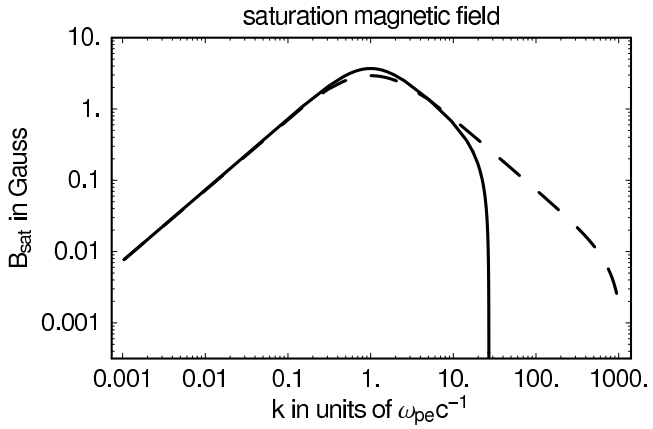

Figure 8.2: Saturation magnetic field as a function of wave number for a proton-driven instability and for an instability in an electron-positron plasma, using the same parameters as in Fig. 8.1 with $n_{e,1} = 1\,\mathrm{cm}^{-3}$.

reached at a wavenumber $k^{\dagger}$ that follows from

$$\frac{k^{\dagger}c}{\Omega} \equiv \kappa^{\dagger}(\alpha) = \left\{ \frac{\alpha}{2}\sqrt{8+\alpha^2} - 1 - \frac{\alpha^2}{2} \right\}^{1/2}. \tag{8.33}$$

If the instability is strong, so that $\alpha \gg 1$, we find that this wavenumber and the associated growth rate are

$$\frac{k^{\dagger}c}{\Omega} \simeq 1\,, \quad \frac{\sigma(k^{\dagger})}{\Omega} \simeq \frac{\alpha}{\sqrt{2}}\,\frac{v_{x0}}{c} = \left(\frac{\hat{\omega}_{\mathrm{pp}}}{\sqrt{2}\,\Omega}\right)\,\frac{v_{z0}}{c}\,. \tag{8.34}$$

Note that the trapping criterion predicts the largest field amplitude at a wavenumber $k^{\dagger}$, which is not equal to the wavenumber k_* of the fastest growing mode (equation 8.28): $k^{\dagger} \simeq \Omega/c \ll k_* \simeq \sqrt{\alpha}\Omega/c$ for $\alpha \gg 1$. Eventually, this slower growing long-wavelength mode reaches a higher magnetic field than the faster growing mode [see also the discussion in 104]. If $\alpha \gg 1$ the saturation field strength due to trapping at $k^{\dagger} \simeq \Omega/c$ is

$$\begin{aligned} B_{\mathrm{trap}} &\simeq \frac{\gamma_{\mathrm{b}0} m_{\mathrm{p}} v_{z0}}{q}\,\frac{\hat{\omega}_{\mathrm{pp}}^2}{2\Omega} \\ &\simeq \frac{2\gamma_{\mathrm{b}0} m_{\mathrm{e}} \tilde{\omega}_{\mathrm{pe}} c}{3q}, \end{aligned} \tag{8.35}$$

where we have used equations (8.12) and (8.27) to eliminate $\hat{\omega}_{\rm pp}$ and Ω.

For parameters typical for the external shock associated with Gamma-ray Bursts we have

$$B_{\rm trap} \simeq 3.7\sqrt{n_1}\,\gamma_{1000}\,{\rm Gauss}, \tag{8.36}$$

with $n_1 = n_0/(1\,{\rm cm}^{-3})$ and $\gamma_{1000} = \gamma_{\rm b0}/1000$.

We should note that Medvedev and Loeb [58] use a different method for estimating B: they propose that the instability saturates when the beam ions become magnetized. This happens when the Larmor radius $r_{\rm L} = \gamma v mc^2/qB$ of the beam particles in the generated magnetic field becomes smaller than the wavelength of the fastest growing mode of the instability. This criterion $k_* r_{\rm L} < 1$ corresponds to $|\mathbf{B}| < B_{\rm magn}$ with

$$B_{\rm magn} = \frac{\gamma_{\rm b0} v_{z0} m_{\rm p} c k_*}{q}, \tag{8.37}$$

with k_* given by equation (8.28). However, the trapping argument predicts the smallest saturation amplitude $|\mathbf{B}|$. In particular, we have

$$\frac{B_{\rm trap}}{B_{\rm magn}} = \frac{\sigma^2(k^\dagger)}{k^\dagger k_* v_{z0}^2} = \left(\frac{\hat{\omega}_{\rm pp}}{\Omega}\right)^2 \Phi(\alpha), \tag{8.38}$$

where

$$\Phi(\alpha) \equiv \frac{\kappa^\dagger(\alpha)}{\alpha^2\sqrt{\alpha-1}}\left(\frac{3\alpha - \sqrt{8+\alpha^2}}{\sqrt{8+\alpha^2}-\alpha}\right). \tag{8.39}$$

To derive this relation we have used definition (8.21) to write

$$v_{x0}/v_{z0} = \hat{\omega}_{\rm pp}/(\alpha\Omega).$$

For a proton beam in a hot electron background we have $\hat{\omega}_{\rm pp}^2/\Omega^2 \ll 1$ and $\Phi(\alpha) < 0.3$ for all $\alpha \geq 1$. For a strong instability with $\alpha \gg 1$ we have $\Phi(\alpha) \simeq (4\alpha)^{-1/2} \ll 1$. Therefore, trapping occurs well before the field can totally magnetize a proton beam with a density comparable to the density of the hot background electrons. In view of this we will use $B_{\rm trap}$ as an estimate of the saturation magnetic field strength (see also section 9.2).

The criteria (8.32) and (8.37) predict the typical amplitude of the magnetic field as one particular wave mode k saturates. In a realistic situation the instability will involve a superposition of wave modes and one should interpret B as the amplitude that follows from the power spectrum $\mathcal{I}_{\rm B}(k)$ of the field

fluctuations: $B^2/8\pi \sim k\mathcal{I}_{\rm B}(k)$ with $k \approx k_*$ for magnetization and $k \approx k^\dagger$ for trapping. The total magnetic energy in the unstable modes is

$$U_{\rm B} = \frac{B^2}{8\pi} = \int_0^{k_{\rm max}} {\rm d}k\, \mathcal{I}_{\rm B}(k). \tag{8.40}$$

8.3.3 The equipartition parameter

A measure of the strength of the magnetic field is the equipartition parameter, which compares the energy density in the magnetic field with the total energy density.

The protons dominate the energy budget, and the total available energy density is

$$e_{\rm p} = \int {\rm d}\mathbf{p}\, F(\mathbf{p})\gamma(\mathbf{p}) m_{\rm p} c^2 \simeq \gamma_{\rm b0} n_{\rm p} m_{\rm p} c^2, \tag{8.41}$$

where the approximation is valid for $v_{x0} \ll v_{z0}$.

We define the proton equipartition parameter as

$$\varepsilon_{\rm B} = \frac{B^2_{\rm trap}}{8\pi e_{\rm p}}\,. \tag{8.42}$$

Using equation (8.35) for the magnetic field, with the definition (8.11) for $\hat{\omega}_{\rm pp}$ and the approximation $v_{z0} \simeq c$ for relativistic shocks we get

$$\varepsilon_{\rm B} = \frac{\hat{\omega}^2_{\rm pp}}{8\Omega^2}\,. \tag{8.43}$$

Then from equations (8.12) and (8.27) we have

$$\varepsilon_{\rm B} \simeq \frac{m_{\rm e}}{6m_{\rm p}} \sim 10^{-4}\,. \tag{8.44}$$

8.4 Discussion

The small value of the equipartition parameter (8.44) implies that the proton-driven Weibel instability in a background of relativistically hot electrons saturates long before the magnetic field reaches equipartition with the available proton free energy. Equation (8.25) demonstrates that the proton-driven Weibel instability in a hydrogen plasma is not a suitable candidate for the mechanism responsible for 'thermalization' of the incoming protons in the shock layer. In

electron(-positron) beams in a hot pair background the instability condition, $a > 1$, allows a large beam velocity dispersion: $v_{x0}/v_{z0} \leq 1$ if the number densities in the beam and in the hot background are of similar magnitude [see also 105]. Therefore, the Weibel instability is in principle capable of randomizing a significant fraction of the beam momentum of an electron(-positron) beam, as asserted in section 8.2, whereas this is not true for a proton beam in a hydrogen plasma.

In the limit of a cold, relativistic proton beam the properties of the electrons and not those of the protons determine many of the results. The electron plasma frequency determines the wave number (8.33) of the mode with the maximum magnetic field so that the electron skin depth $c/\tilde{\omega}_{\rm pe}$ sets the length scale of the dominant mode. This happens because the low inertia of the electrons makes them very responsive to the perturbations of the protons. The dispersion relation for the Weibel modes (Fig. 8.1), also supports this view: the plateau around the maximum growth rate starts roughly at a wave number $k \sim \tilde{\omega}_{\rm pe}/c$. Studies that do not include the response of the background electrons (by treating the protons as an isolated system) miss this point. The peak magnetic field (8.35) does not contain any parameters connected with the protons. Therefore, proton beams in a hydrogen plasma generate nearly the same magnetic field strength as electron(-positron) beams in an electron-positron plasma (Fig. 8.2) *despite* the larger kinetic energy of the protons.

Gruzinov [31] anticipated this when he excluded the case where a small parameter in the theory might be important in his analysis of the Weibel instability: our analysis shows that the relevant small parameter is $\hat{\omega}_{\rm pp}^2/\Omega^2 \sim 4m_{\rm e}/3m_{\rm p}$. The result is a small equipartition parameter (8.44). In this respect our result is similar to the one found by Sagdeev [82, p. 88], who argued for the Weibel instability in a non-relativistic plasma that the electrons have a quenching effect on the ion instability.

In our analysis we have excluded electrostatic waves, which could also play an important role in the shock transition zone [88]. In that case electrostatic Bremsstrahlung could be an alternative explanation for the Gamma-ray Burst afterglow emission [85], relaxing the need in synchrotron models for a high magnetic field strength.

8.5 Conclusions

We have presented an analytical estimate of the magnetic field produced at the end of the linear phase of the Weibel instability at the front of an ultra-relativistic shock propagating into a cold hydrogen plasma, a situation that

applies to the external shocks that produce gamma-ray burst afterglows in the fireball model [79]. The magnetic field strength that we find is too weak to explain the observed synchrotron radiation [32]: the equipartition parameter (equation 8.44) is at least two orders of magnitude too small. This is radically different from the results for the Weibel instability in pair plasmas. The reason is that the contribution of the electrons to the electromagnetic response of the plasma inhibits the instability of the protons.

The saturation magnetic field (8.35) which this low equipartition parameter corresponds to is the magnetic field at the point where the linear approximation breaks down and where non-linear trapping effects start to limit the growth of the unstable Weibel mode. After this happens, it is likely that the instability enters a nonlinear phase or that another type of instability takes over: numerical simulations [24] of similar plasmas show near-equipartition magnetic fields behind the Weibel-unstable region in the shock transition. The nonlinear phase would then be the dominant phase in electron-ion plasmas and deserves further study to determine the physical mechanism and the properties of the resulting magnetic field.

8.6 Appendix: Asymmetric beams

We consider asymmetric proton beams and show that we can neglect the effect of the asymmetry for typical parameters. We replace the proton distribution (8.1) by

$$F(\mathbf{p}) = \frac{n_\mathrm{p}}{2p_{x0}} \left[\frac{1+\Delta}{2}\,\delta(p_z - p_{z0}) + \frac{1-\Delta}{2}\,\delta(p_z + p_{z0}) \right] \times \delta(p_y)\,[\Theta(p_x + p_{x0}) - \Theta(p_x - p_{x0})]\,, \tag{8.45}$$

with $0 \leq \Delta \leq 1$ the parameter measuring the asymmetry between the two beams. This asymmetry changes the dispersion relation of the waves to [6]:

$$k^2c^2 - \omega^2 \left[1 + \chi_{zz}(\omega,\, k) - \frac{\chi_{zx}^2(\omega,\, k)}{1 + \chi_{xx}(\omega,\, k)} \right] = 0. \tag{8.46}$$

The extra term $\propto \chi_{zx}^2$ appears in relation (8.46) because the waves are no longer transverse: the charge bunching of asymmetric beams produces a net charge density, leading to a component of the wave electric field along the wave vector.

We will give the extra components of the susceptibility tensor and publish a derivation elsewhere (see chapter 6). The proton contribution to $\chi_{zz}(\omega,\, k)$ is

the same as in the symmetric case. For a thermal electron background with an isotropic momentum distribution, only the two proton beams contribute to the off-diagonal components of the susceptibility tensor so that

$$\chi_{zx}(\omega,k) = \chi_{zx,\mathrm{p}}(\omega,k) = \frac{\Delta\,\hat{\omega}_{\mathrm{pp}}^2}{\omega^2 - k^2 v_{x0}^2}\,\frac{k v_{z0}}{\omega}\,. \tag{8.47}$$

This off-diagonal component vanishes in the symmetric case ($\Delta = 0$). The longitudinal response of the beam-plasma system is contained in

$$1 + \chi_{xx}(\omega,\,k) = 1 - \frac{\tilde{\omega}_{\mathrm{pe}}^2}{\omega^2 - k^2 C_{\mathrm{e}}^2} - \frac{\hat{\omega}_{\mathrm{pp}}^2}{\omega^2 - k^2 v_{x0}^2}\,. \tag{8.48}$$

Here $C_{\mathrm{e}}^2 = 4P_{\mathrm{e}}/3n_{\mathrm{e}}m_{\mathrm{e}}h$ is the effective sound speed in the hot electron gas. In the ultra-relativistic case one has $C_{\mathrm{e}} \simeq c/\sqrt{3}$. For proton beams in a hot electron background one has $\tilde{\omega}_{\mathrm{pe}}^2 \gg \hat{\omega}_{\mathrm{pp}}^2$ and $|\omega| \leq \hat{\omega}_{\mathrm{pp}} \ll kC_{\mathrm{e}}$ for the Weibel instability (see section 8.3.1). This implies that

$$1 + \chi_{xx} \simeq 1 + \frac{\tilde{\omega}_{\mathrm{pe}}^2}{k^2 C_{\mathrm{e}}^2} - \frac{\hat{\omega}_{\mathrm{pp}}^2}{\omega^2 - k^2 v_{x0}^2}. \tag{8.49}$$

The resulting dispersion relation can be written in terms of the dimensionless variable

$$\mathcal{Z}(\omega,\,k) \equiv \frac{\omega^2 - k^2 v_{x0}^2}{\hat{\omega}_{\mathrm{pp}}^2}. \tag{8.50}$$

One finds

$$(\mathcal{Z} - \mathcal{Z}_1)\,(\mathcal{Z} + \mathcal{Z}_2) - \Delta^2\,\mathcal{Z}_1\mathcal{Z}_2 = 0. \tag{8.51}$$

Here $\mathcal{Z}_{1,2}$ are defined by

$$\mathcal{Z}_1 = \frac{k^2 C_{\mathrm{e}}^2}{k^2 C_{\mathrm{e}}^2 + \tilde{\omega}_{\mathrm{pe}}^2}\,,\quad \mathcal{Z}_2 = \frac{k^2 v_{z0}^2}{k^2 c^2 + \Omega^2} \tag{8.52}$$

with $\mathcal{Z}_2 > \mathcal{Z}_1$ for the parameters considered here. The solution of this quadratic equation,

$$\mathcal{Z}_{\pm} = \frac{\mathcal{Z}_1 - \mathcal{Z}_2}{2} \pm \sqrt{\left(\frac{\mathcal{Z}_1 + \mathcal{Z}_2}{2}\right)^2 - \Delta^2\,\mathcal{Z}_1\mathcal{Z}_2}, \tag{8.53}$$

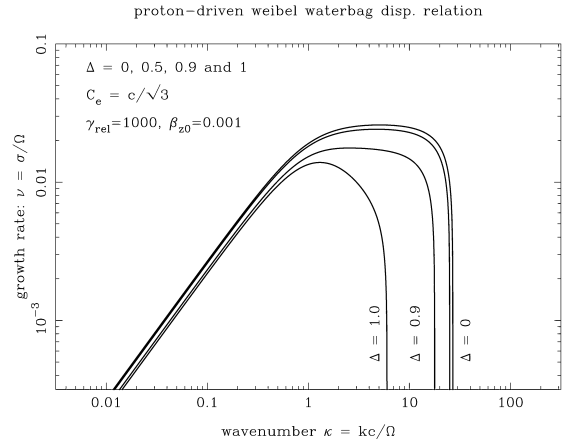

Figure 8.3: The growth rate as a function of wavenumber for asymmetric proton beams in a relativistically hot electron background with sound speed $C_e = c/\sqrt{3}$. Different lines correspond to different values of the parameter Δ, which measures the asymmetry between the beams.

determines the frequency through

$$\omega_{\pm}^2 = \hat{\omega}_{pp}^2 \, \mathcal{Z}_{\pm} + k^2 v_{x0}^2. \tag{8.54}$$

The Weibel-unstable branch corresponds to the solution branch ω_- as $\mathcal{Z}_- < 0$. In the symmetric case ($\Delta = 0$) one has $\mathcal{Z}_- = -\mathcal{Z}_2$ which follows from (8.51), and one recovers dispersion relation (8.20). The stable branch ω_+ is a modified (largely electrostatic) ion-acoustic wave.

Although the asymmetry decreases the range of unstable wave numbers (Fig. 8.3) and lowers the growth rate with respect to the symmetric case $\Delta = 0$, the change is small unless $\Delta \approx 1$: the case where there is almost no reflection. For a single beam, $\Delta = 1$, one has $\mathcal{Z}_- = \mathcal{Z}_1 - \mathcal{Z}_2$, which gives the following dispersion relation for $\nu^2 = -\omega_-^2/\Omega^2$ in the ultra-relativistic limit with $C_e = c/\sqrt{3}$ and $\Omega^2 \approx \tilde{\omega}_{pe}^2$:

$$\nu^2 = \frac{\hat{\omega}_{pp}^2}{\Omega^2} \, \frac{\kappa^2 \left\{ \left(\frac{3v_{z0}^2}{c^2} - 1 \right) - \kappa^2 \left(1 - \frac{v_{z0}^2}{c^2} \right) \right\}}{(3+\kappa^2)(1+\kappa^2)} - \kappa^2 \frac{v_{x0}^2}{c^2} \, . \tag{8.55}$$

Chapter 9

The end of the Weibel instability

When the particles inside a shock front undergo the Weibel instability they will, at some point, start to feel the influence of the magnetic field that they generated themselves. This chapter considers some of the resulting effects: how the particles become trapped in the magnetic field, and how the sloshing motion of the particles in the magnetic field diffuses the velocity distribution. These processes signal the end of the Weibel instability.

The electrical currents that the instability produces can keep growing if they merge into larger currents, but we also show that this process will not provide much additional gain because the plasma has the tendency to shield the interaction of the electrical currents when they become too large.

This shows that the order of magnitude of the magnetic field strength produced by the Weibel instability is of the order of the well-known magnetic trapping estimate, confirming the estimate in the previous chapter.

In the last sections of this chapter we discuss what this means for the role of the Weibel instability in relativistic shock fronts. In particular, we discuss how the Weibel instability can cause the electrons in the shock front to convert their energy into heat. The free energy of the heavier particles in the shock front (protons and ions) cannot be converted into heat by the Weibel instability. Instead, these particles will heat up more slowly through their interaction with the magnetic field that the Weibel instability leaves behind. The thermalization length scale of these heavy particles will determine the thickness of the shock front.

This chapter has been submitted to Astronomy & Astrophysics [5].

9.1 Introduction

The Weibel instability is a plasma instability that arises in plasmas with an anisotropic velocity distribution. This chapter discusses the nonlinear dynamics of the plasma in the late stages of this instability in the relativistic shock fronts that are produced by Gamma Ray Burst sources.

The prompt and afterglow emission from Gamma Ray Bursts (GRBs) is often interpreted as synchrotron emission or as jitter radiation [56] from relativistic electrons in a magnetic field. In order to explain the observed intensity, the magnetic field in the emission region must have a strength of 1 to 10% of the equipartition field strength B_e, e.g. [102], which is defined in terms of the internal (thermal) energy e of the plasma as

$$B_e = \sqrt{8\pi e}\,. \tag{9.1}$$

This holds true for both the emission from internal shocks [see 80], which are believed to be responsible for the prompt emission, and for the emission from external shocks [e.g. 79] which are believed to be the source of the afterglow emission. A full account of the observations and theory of GRBs can be found in the reviews of Piran [74, 75] and of Mészáros [65, 66].

The strong magnetic fields associated with GRBs must somehow be self-generated by the strong (relativistic) shocks invoked in GRB models. In particular for the external shocks the compression of interstellar/circumstellar magnetic fields in a relativistic shock leads to $B \ll B_e$ in the post-shock plasma (see section 6.1).

It has been proposed (see [58] and [31]) that a plasma instability, the *Weibel instability*, leads to the generation of the necessary magnetic fields. The basic picture is that this instability operates in the shock transition layer, where the unshocked incoming plasma mixes with the (relativistically) hot shocked plasma. The mixture is unstable against the generation of low-frequency electromagnetic waves with $|\omega| \ll kc$, where ω is the wave frequency and $k = 2\pi/\lambda$ is the wave number. This instability is due to the anisotropy of the momentum distribution of the incoming plasma, which looks like a beam in the reference frame of the shocked plasma. Since Maxwell's equations imply that the Fourier amplitudes $\tilde{\mathbf{E}}$ and $\tilde{\mathbf{B}}$ of the electric and magnetic fields associated with the instability satisfy the relation $|\tilde{\mathbf{E}}| \sim (|\omega|/kc)\,|\tilde{\mathbf{B}}| \ll |\tilde{\mathbf{B}}|$, the resulting turbulent electromagnetic field is almost purely magnetic.

Although it is now long known that the Weibel instability can generate magnetic fields in relativistic shock fronts, estimates of the attainable magnetic field strength have been mostly restricted to ad hoc arguments. In this chapter

we present an in-depth look into the nonlinear dynamics of a Weibel-unstable plasma to obtain a reliable foundation for our estimates of the attainable magnetic field strength. In addition, we discuss the mechanisms that contribute to the stabilization of the Weibel instability and the subsequent thermalization of the plasma.

Our calculations concentrate on the case of ultra-relativistic shocks (with Lorentz factor $\gamma \gg 1$). We will assume that we can model the plasma in the shock front with two symmetric counterstreaming plasmas because the effect of asymmetries is small (see section 6.9). We also take the beams to be cold, as one would expect in a shock front encountering the cold interstellar medium. At various points, we will take into account the presence of a relativistically hot stationary background plasma that corresponds to the already thermalized post-shock plasma. We discuss kinetic and fluid processes that take place on time and length scales of the order of the plasma frequency and the plasma skin depth respectively.

In the companion paper [3, chapter 6 in this thesis] we have considered the linear phase of the Weibel instability, where the magnetic field grows exponentially in time. The main conclusions of chapter 6 can be summarized as follows:

The growth rate of the instability due to two equal but counterstreaming beams in the presence of a (hot) background plasma is mostly determined by two parameters: η and $\mathcal{M}$. The first parameter is defined as

$$\eta = \left(\hat{\omega}_{\mathrm{pb}}/\tilde{\omega}_{\mathrm{bg}}\right)^2 , \tag{9.2}$$

the square of the ratio of the effective plasma frequency $\hat{\omega}_{\mathrm{pb}}$ of the beam particles and the the plasma frequency $\tilde{\omega}_{\mathrm{bg}}$ of thermal background. In a hydrogen plasma, the background plasma frequency is almost entirely determined by the contribution of the hot electrons and one has

$$\tilde{\omega}_{\mathrm{bg}}^2 \simeq \frac{4\pi e^2 n_{\mathrm{e}}}{m_{\mathrm{e}} h_{\mathrm{e}}} . \tag{9.3}$$

Here h_{e} is the enthalpy per unit rest energy of the electron gas, with $h_{\mathrm{e}} \approx 1$ if the electron gas is cold so that $k_{\mathrm{b}} T_{\mathrm{e}} \ll m_{\mathrm{e}} c^2$, and $h_{\mathrm{e}} \simeq k_{\mathrm{b}} T_{\mathrm{e}}/m_{\mathrm{e}} c^2 \gg 1$ for a relativistically hot electron gas. The beam plasma frequency is

$$\hat{\omega}_{\mathrm{pb}}^2 = \frac{4\pi q_{\mathrm{b}}^2 n_{\mathrm{b}}}{m_{\mathrm{b}} h_{\mathrm{b}}} , \tag{9.4}$$

in terms of the charge q_b and mass m_b of the beam particles, their proper density n_b and the enthalpy per unit rest energy h_b. When the beams are cold we have $h_b \simeq 1$.

The parameter $\mathcal{M}$ can be thought of as an effective 'beam Mach Number': it is a measure for the importance of the velocity dispersion in the beam plasma in the direction perpendicular to the beam direction, which we will take along the z-axis. If the momentum of the directed motion of the beam particles is p_{z0} and if the typical momentum associated with the velocity dispersion perpendicular to the beam direction is p_{x0}, one has:

$$\mathcal{M} \sim p_{z0}/p_{x0} \; . \tag{9.5}$$

A full set of definitions can be found in section 6.5, where both a fluid model and a waterbag model employing kinetic theory are employed to describe the beams. If the beams are cold one has $\mathcal{M} \to \infty$. As we will see below, the value of $\mathcal{M}$ together with η determines the range of unstable wavenumbers, and η determines the maximum growth rate.

In the symmetric case the beam particles are distributed over two counter-streaming but otherwise identical beams, each with proper density $n_b/2$. In this case there is a simple approximation for the growth rate of the instability in the limit of perturbations with the wavevector perpendicular to the beam direction: $\mathbf{k} \cdot \mathbf{V}_b = 0$. This approximation is almost universally valid for ultra-relativistic beams (with $p_{z0} \gg m_b c$) if $\mathcal{M} \gg 1$, $\eta \leq 1$ and $\eta \mathcal{M}^2 \gg 1$, and still gives a rather good approximation for $\eta \sim \mathcal{M} \sim 1$. In terms of a dimensionless growth rate and wavenumber, defined as[1]

$$\sigma \equiv \mathrm{Im}(\omega)/\tilde{\omega}_{bg} \;\; , \;\; \kappa \equiv kc/\tilde{\omega}_{bg} \; , \tag{9.6}$$

one finds (chapter 6, equation 6.57):

$$\sigma^2(\kappa) \approx \frac{\kappa^2}{\kappa_s^2 + \kappa^2} \left(\frac{\kappa_{max}^2 - \kappa^2}{\mathcal{M}^2} \right) \; . \tag{9.7}$$

Here κ_s is the (dimensionless) wavenumber below which screening currents in the background plasma slow the growth of the instability, see section 6.6, equation (6.46) and section 6.7, equations (6.57) and (6.60). In our application to ultra-relativistic beams one has $\kappa_s \sim 0.1 - 1$.

[1] Note that in this chapter we write k (rather than K as in chapter 6) for the wave number in the laboratory frame, which coincides with the rest frame of the thermal plasma.

The wavenumber $\kappa_{\rm max}$ is the maximum unstable wavenumber that, in the limit $\eta\mathcal{M}^2 \gg 1$ that concerns us here, equals

$$\kappa_{\rm max} \equiv \sqrt{\eta\mathcal{M}^2 - 1} \approx \sqrt{\eta}\,\mathcal{M}\,. \tag{9.8}$$

The maximum growth rate, which follows from $\mathrm{d}\sigma/\mathrm{d}\kappa = 0$, occurs at a wavenumber κ_*, which for dispersion relation (9.7) is given by

$$\kappa_* = \left(\kappa_{\rm s}\sqrt{\kappa_{\rm max}^2 + \kappa_{\rm s}^2} - \kappa_{\rm s}^2\right)^{1/2} \approx \sqrt{\kappa_{\rm s}\kappa_{\rm max}}\,. \tag{9.9}$$

It equals $\sigma(\kappa_*) \equiv \sigma_*$, which is:

$$\sigma_* = \frac{\sqrt{\kappa_{\rm s}^2 + \kappa_{\rm max}^2} - \kappa_{\rm s}}{\mathcal{M}} \approx \frac{\kappa_{\rm max}}{\mathcal{M}} = \sqrt{\eta}\,. \tag{9.10}$$

In these two expressions the last approximate terms on the right-hand side are valid in the limit $\eta\mathcal{M}^2 \gg 1$, when $\kappa_{\rm max} \gg \kappa_{\rm s}$.

This implies that the Weibel instability is most vigorous at wavelengths shorter than the effective skin depth $\lambda_{\rm sk} \sim c/\tilde{\omega}_{\rm bg}\kappa_{\rm s}$ of the hot background plasma. The linear growth rate is almost independent of wavenumber, and close to σ_*, on a broad 'plateau' in the wavenumber range corresponding to $\kappa_{\rm s} < \kappa < \kappa_{\rm max}$, see figures 6.1 and 6.2 in chapter 6. The maximum unstable wavelength is determined by the 'temperature' of the beam plasma, which determines the value of $\mathcal{M}$ through the velocity dispersion of beam particles along the wave vector.

In the rest of this chapter we will discuss the stabilization of the Weibel instability and the subsequent evolution of the plasma. In section 9.2 we start off with an overview of stabilization mechanisms that have already been discussed in the literature. In section 9.3 we present a fluid model for the nonlinear wave breaking of a single wave mode of the Weibel instability. In section 9.4 we briefly consider a kinetic model for the nonlinear dynamics of the Weibel-unstable plasma once a broad-band spectrum of unstable modes has been excited. In section 9.5 we estimate whether and for how long the electrical currents can keep growing stronger after the instability itself has stabilized. Section 9.6 discusses the implications of our results for the plasma in an ultra-relativistic shock front, considering thermalization of the electrons and the ions in the plasma separately. For the ions we estimate the thermalization length scale due to scattering in the turbulent magnetic fields produced by the Weibel instability. In section 9.7 we summarize the conclusions that we draw from our results.

9.2 Stabilization mechanisms: an overview

A number of stabilization mechanisms have been proposed for the beam-driven Weibel instability in an astrophysical context. In this section we compare two mechanisms employed in recent literature to estimate the attainable magnetic field strength of the Weibel instability: magnetization of the plasma and magnetic trapping of particles in the plasma wave fields. We will show that the latter gives the most stringent limit on the attainable magnetic field for the parameter regime that we are interested in.

Medvedev and Loeb [58] have proposed that the deflection of beam particles in the self-generated magnetic field stabilizes the instability if the Larmor radius in this field becomes of the order of the wavelength of the most unstable mode. This essentially means that the beam particles become magnetized. For simplicity we consider the case of a cold beam.

The gyration radius $r_{\rm g}$ of beam particles of mass $m_{\rm b}$, beam velocity $V_{\rm b}$, bulk (beam) Lorentz factor $\gamma_{\rm b} = 1/\sqrt{1 - V_{\rm b}^2/c^2}$ and charge $q_{\rm b}$ is of order:

$$r_{\rm g} = \frac{\gamma_{\rm b} m_{\rm b} c V_{\rm b}}{q_{\rm b} B} = \frac{V_{\rm b}}{\Omega_{\rm g}} \,. \tag{9.11}$$

Here $\Omega_{\rm g} = q_{\rm b} B / \gamma_{\rm b} m_{\rm b} c$ is the gyration frequency of the beam particles in a magnetic field of strength B. The corresponding stabilization criterion according to Medvedev and Loeb [58] reads:

$$k_* r_{\rm g} = \frac{k_* V_{\rm b}}{\Omega_{\rm g}} \sim 1 \,, \tag{9.12}$$

with k_* the wavenumber of the fastest growing mode. We will refer to this as the *magnetization criterion*.

Alternatively, Yang et al. [104] have proposed that magnetic trapping of particles in the waves stabilizes the Weibel instability. This stabilization mechanism was already considered by Davidson et al. [16] for the non-relativistic Weibel instability in a plasma with a temperature anisotropy. The same stabilization mechanism was briefly discussed by Gruzinov [31] in the context of magnetic field generation in GRB shocks.

The electromagnetic field of the waves produced by the instability will cause the beam particles to 'quiver'. Trapping occurs when the amplitude of the quiver motion in the direction of the wave vector reaches an amplitude comparable to the wavelength of the unstable mode. This quiver motion is induced by the Lorentz force on the beam particles due to the wave magnetic

field $\mathbf{B} = B(x\,,\,t)\,\hat{\mathbf{y}}$. The equation of motion to first order in the wave amplitude reads (see also the more complete treatment below)

$$\frac{\mathrm{d}^2\xi_x}{\mathrm{d}t^2} = -\frac{q_\mathrm{b} V_\mathrm{b} B}{\gamma_\mathrm{b} m_\mathrm{b} c}\,, \tag{9.13}$$

with ξ_x the displacement of a beam particle in the x-direction. For a magnetic field varying as $B(x\,,\,t) = B_0 \exp(\tilde{\sigma} t)\,\sin(kx)$, with $\tilde{\sigma} = \mathrm{Im}(\omega) > 0$ the growth rate of the instability, one finds that the typical amplitude of the quiver motion is

$$|\xi_x| \approx \left| \frac{q_\mathrm{b} V_\mathrm{b} B}{\gamma_\mathrm{b} m_\mathrm{b} c \tilde{\sigma}^2} \right| \,. \tag{9.14}$$

The stabilization condition reads [e.g. 17]

$$|k\,\xi_x| = \left| k\,\frac{q_\mathrm{b} V_\mathrm{b} B}{\gamma_\mathrm{b} m_\mathrm{b} c \tilde{\sigma}^2} \right| \sim 1\,. \tag{9.15}$$

which we will refer to as the *trapping criterion*.

As we pointed out in chapter 8, the trapping criterion (9.15) is the most stringent criterion of the two for external GRB shocks, which have $\eta \leq 1$, $V_\mathrm{b} \simeq c$ and $\mathcal{M} \gg 1$. This is easily checked for dispersion relation (9.7). From (9.12) and (9.15) one finds that the field amplitudes B^m and B^tr predicted respectively by these two criteria are:

$$B^\mathrm{m} \sim \frac{\gamma_\mathrm{b} m_\mathrm{b} c\, k_* V_\mathrm{b}}{q_\mathrm{b}} \;\;,\;\; B^\mathrm{tr} \sim \frac{\gamma_\mathrm{b} m_\mathrm{b} c\, \tilde{\sigma}^2(k_\dagger)}{q_\mathrm{b} k_\dagger V_\mathrm{b}}\,. \tag{9.16}$$

Here $k_\dagger$ is the wavenumber where $\tilde{\sigma}^2(k)/k$ reaches its maximum value. We define a third characteristic dimensionless parameter,

$$\alpha \equiv \sqrt{1 + \frac{\kappa_\mathrm{max}^2}{\kappa_\mathrm{s}^2}}\,, \tag{9.17}$$

with the beam-driven Weibel instability occurring for $\alpha > 1$. The characteristic dimensionless wavenumbers $\kappa_* = k_* c/\tilde{\omega}_\mathrm{bg}$, $\kappa_\dagger = k_\dagger c/\tilde{\omega}_\mathrm{bg}$ and $\kappa_\mathrm{max} = k_\mathrm{max} c/\tilde{\omega}_\mathrm{bg}$ can be written in terms of α as

$$\kappa_\mathrm{max} = \kappa_\mathrm{s}\,\sqrt{\alpha^2 - 1} \;\;,\;\; \kappa_* = \kappa_\mathrm{s}\,\sqrt{\alpha - 1} \;\;,\;\; \kappa_\dagger = \kappa_\mathrm{s}\,S(\alpha)\,, \tag{9.18}$$

with $S(\alpha)$ for dispersion relation (9.7) given by:

$$S(\alpha) \equiv \left\{ \frac{\alpha}{2} \sqrt{8+\alpha^2} - 1 - \frac{\alpha^2}{2} \right\}^{1/2} . \tag{9.19}$$

The ratio of the field amplitudes $B^{\rm tr}$ and $B^{\rm m}$ can be written for $V_{\rm b} \simeq c$ as

$$\frac{B^{\rm tr}}{B^{\rm m}} = \frac{\sigma_+^2}{\kappa_+ \kappa_*} = \frac{S(\alpha)}{\sqrt{\alpha - 1}\, \mathcal{M}^2} \left(\frac{3\alpha - \sqrt{8+\alpha^2}}{\sqrt{8+\alpha^2} - \alpha} \right) , \tag{9.20}$$

where $\sigma_+ = \tilde{\sigma}(k_+)/\tilde{\omega}_{\rm bg}$. For $\alpha \gg 1$ ($\eta \mathcal{M}^2 \gg 1$) one has $\kappa_{\rm max} \simeq \alpha\, \kappa_{\rm s} = \sqrt{\eta}\mathcal{M}$, $\kappa_* \simeq \sqrt{\alpha}\, \kappa_{\rm s}$, $\kappa_+ \simeq \kappa_{\rm s}$ and $\sigma_+ \simeq \kappa^{\rm max}/\sqrt{2}\mathcal{M} = \sqrt{\eta/2}$. In that case (9.20) reduces to

$$\frac{B^{\rm tr}}{B^{\rm m}} \simeq \frac{\eta}{2\sqrt{\alpha}\kappa_{\rm s}^2} = \frac{\eta^{3/4}}{2\kappa_{\rm s}^{3/2}\mathcal{M}^{1/2}} . \tag{9.21}$$

For GRB external shocks, with $\eta \leq 1$, $\alpha \gg 1$, $\mathcal{M} \gg 1$ and $\kappa_{\rm s} \leq 1$ one has $B^{\rm tr} \ll B^{\rm m}$, and trapping rather than magnetization stabilizes the beam-driven Weibel instability.

For the Weibel instability operating in the transition layer of an ultra-relativistic shock one expects $\eta \approx 1$ for an electron(-positron) beam, and

$$\eta \approx 4m_{\rm e}/3m_{\rm p} \simeq 7 \times 10^{-4}$$

for a proton beam in a hot electron background, see chapter 8 for more details. Since one must have $\mathcal{M} > 1 + 1/\eta$ for an instability to occur this implies that trapping will occur long before the beam particles are fully magnetized so that the exponential growth of the magnetic field saturates at $|B| \simeq B^{\rm tr}$.

Figure 9.1 shows the characteristic wavenumbers κ_* and κ_+ and $\kappa_{\rm max}$, and the ratio of the field amplitudes at trapping and magnetization, $B^{\rm tr}/B^{\rm m} = \sigma_+^2/\kappa_+\kappa_*$, all as a function of the parameter α for $\mathcal{M} = 100$.

9.3 Nonlinear effects: fluid model for the beam response

We now present calculations that justify the order-of-magnitude estimates of the previous section for two different situations. In this section we consider the nonlinear effects due to the Weibel instability using a fluid model. This allows us to investigate the effect of nonlinear coupling, and in particular of *wave breaking* of the Weibel mode when only a single dominant mode is present. In the next section we will consider the kinetic theory, which is appropriate

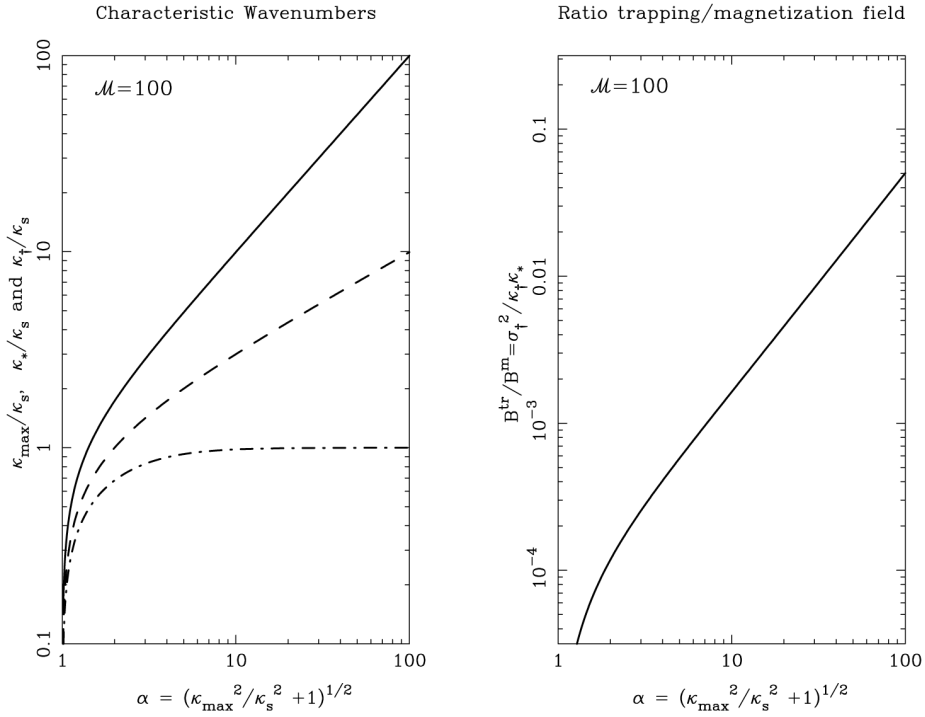

Figure 9.1: The left-hand panel shows, as a function of α and for a beam Mach number $\mathcal{M} = 100$, the behavior of the maximum unstable wavenumber $\kappa_{\max}$ (solid curve), the wavenumber κ_* of the maximum linear growth rate (dashed curve), and the wavenumber $\kappa_\dagger$ associated with the largest wave amplitude in the case of stabilization by trapping (dash-dot curve). The right-hand panel shows, again as a function of α, the ratio of the magnetic field strength predicted by the trapping argument and the magnetization argument, $B^{\rm tr}/B^{\rm m}$.

for a broad-band spectrum of unstable modes, and where *phase mixing* of the quiver motion in the collection of waves is the dominant stabilization process.

We will show that the wave breaking considered in this section will slow down the exponential growth of individual wave modes and could even reverse the growth. This wave breaking will, however, inevitably excite higher wave modes, leading to a broad-band spectrum of wave modes. When that happens the stabilization mechanisms considered in the next section will describe the plasma dynamics more accurately.

Note that for stable plasma modes (with a real frequency ω) a fluid calculation such as presented below would yield the well-known equations for *mode coupling*, see for instance [28]. This leads to resonant interactions between different waves (normal modes) of the form $\mathbf{k}_1 \pm \mathbf{k}_2 = \mathbf{k}_3$, $\omega_1 \pm \omega_2 = \omega_3$, where the indices enumerate the different wave modes. However, in the case of the unstable Weibel modes considered here such resonances do not occur as ω is purely imaginary, and the interactions are qualitatively different. In particular, we will show below that the dominant effect is through the nonlinear distortion of the wave profile, not unlike what happens to large-amplitude electron plasma oscillations in a cold plasma, see Davidson [17], Ch. 3. This is a non-resonant process.

In order to keep the mathematics tractable we make a number of simplifying assumptions:

1. We treat the symmetric case with two oppositely directed beams of equal strength propagating along the z-axis with velocity $\mathbf{V}_\pm = \pm V_\mathrm{b}\,\hat{\mathbf{z}}$. In that case the *linear* Weibel mode is purely electromagnetic. We also assume that all electromagnetic fields vary as plane waves in the x-direction ($\mathbf{k} = k\,\hat{\mathbf{x}}$), so that $E(x\,,\,t)$, $B(x\,,\,t) \propto \exp(ikx - i\omega t)$. The Fourier amplitudes $\tilde{\mathbf{B}}$ and $\tilde{\mathbf{E}}_\perp$ of the electromagnetic field then satisfy

$$\tilde{\mathbf{B}} = \tilde{B}(k\,,\,\omega)\,\hat{\mathbf{y}} \quad , \quad \tilde{\mathbf{E}}_\perp = \tilde{E}_\perp(k\,,\,\omega)\,\hat{\mathbf{z}} = -\frac{\omega}{kc}\,\tilde{B}(k\,,\,\omega)\,\hat{\mathbf{z}}\,. \tag{9.22}$$

   The last relation follows from Faraday's law: $c(\mathrm{curl}\,\mathbf{E}) + \partial\mathbf{B}/\partial t = 0$. Here we use the subscript $\perp$ to distinguish the transverse electric field (with $\mathbf{k}\cdot\tilde{\mathbf{E}}_\perp = 0$) from the longitudinal electric field $\tilde{E}_\parallel$ that is introduced below.

2. We consider the wavelength range where $|\omega|/kc \ll 1$. For the low-frequency electromagnetic Weibel mode this implies that the magnetic

field amplitude is much larger than the amplitude of the transverse electric field:

$$\left|\tilde{B}(k,\omega)\right| = \left|\frac{kc}{\omega}\right| \left|\tilde{E}_\perp(k,\omega)\right| \gg \left|\tilde{E}_\perp(k,\omega)\right| \ .$$

3. For the moment we will neglect pressure effects in the beam dynamics, putting the kinetic temperature of the beam particles equal to zero.

In this case, the equation of motion for the fluid of beam particles is formally the same as that for a *single* particle of mass m_b and charge q_b:

$$\frac{\mathrm{d}\mathbf{p}}{\mathrm{d}t} = q_\mathrm{b}\left(\mathbf{E} + \frac{\mathbf{V}\times\mathbf{B}}{c}\right) \ . \tag{9.23}$$

Here $\mathbf{p}(\mathbf{x}\,,\ t)$ is the momentum of the fluid, defined as usual in terms of the fluid velocity $\mathbf{V}(\mathbf{x}\,,\ t)$ as

$$\mathbf{p} = \gamma m_\mathrm{b}\mathbf{V} = \frac{m_\mathrm{b}\mathbf{V}}{\sqrt{1-V^2/c^2}} \ . \tag{9.24}$$

The time-derivative in equation (9.23) should be interpreted as the convective (Lagrangian) time derivative,

$$\frac{\mathrm{d}}{\mathrm{d}t} \equiv \frac{\partial}{\partial t} + \mathbf{V}\cdot\mathrm{grad} \ . \tag{9.25}$$

We consider the symmetric case with two counterstreaming but otherwise identical beams, directed along the z-axis. Each beam has an unperturbed laboratory frame density $n_+ = n_- = \overline{n}_\mathrm{b}/2$. Here, and in what follows, we use a subscript $\pm$ to distinguish quantities associated with the forward beam (with unperturbed velocity $\mathbf{V} = +V_\mathrm{b}\,\hat{\mathbf{z}}$) and the backward beam (with unperturbed velocity $\mathbf{V} = -V_\mathrm{b}\,\hat{\mathbf{z}}$) . The density satisfies the continuity equation,

$$\frac{\partial n_\pm}{\partial t} + \mathrm{div}\,(n_\pm\mathbf{V}_\pm) = 0 \ . \tag{9.26}$$

Note that the *proper* density of each of the two beams is $n_{0\pm} = n_\pm/\gamma_\pm$. Finally, the charge density and current density associated with the two beams is

$$\rho_\pm = q_\mathrm{b}n_\pm \ \ , \ \ \mathbf{J}_\pm = q_\mathrm{b}n_\pm\,\mathbf{V}_\pm \ . \tag{9.27}$$

9.3.1 Dynamics of the beam particles

The equation of motion in the x and z direction reads respectively:

$$\left(\frac{\partial}{\partial t} + V_x \frac{\partial}{\partial x}\right) p_x = q_\mathrm{b} \left(E_\parallel - \frac{V_z}{c} B\right) ; \tag{9.28}$$

$$\left(\frac{\partial}{\partial t} + V_x \frac{\partial}{\partial x}\right) p_z = q_\mathrm{b} \left(E_\perp + \frac{V_x}{c} B\right) . \tag{9.29}$$

The y-component reads $\mathrm{d}p_y/\mathrm{d}t = 0$, and we can put $p_y = 0$.

The transverse electromagnetic fields are associated with the Weibel mode, and can be written in terms of a vector potential $\mathbf{A} = A(x\,,\,t)\,\hat{\mathbf{z}}$:

$$E_\perp = -\frac{1}{c}\frac{\partial A}{\partial t} \;\;,\;\; B = -\frac{\partial A}{\partial x} . \tag{9.30}$$

The longitudinal electric field can be derived from a scalar potential $\Phi(x\,,\,t)$:

$$E_\parallel = -\frac{\partial \Phi}{\partial x} . \tag{9.31}$$

In the Weibel instability of two counterstreaming beams of equal density ($n_+ = n_-$) this longitudinal field is absent in the linear approximation, and can only be nonlinearly excited by the beams (see section 6.3).

If one substitutes these definitions into the z-component of the equation of motion (equation 9.29) one finds that it can be written as

$$\left(\frac{\partial}{\partial t} + V_x \frac{\partial}{\partial x}\right) \left(p_z + \frac{q_\mathrm{b}}{c} A\right) = \frac{\mathrm{d}P_z}{\mathrm{d}t} = 0 , \tag{9.32}$$

with $P_z \equiv p_z + \frac{q_\mathrm{b}}{c} A$ the z-component of the canonical momentum. This can immediately be integrated to

$$P_z = p_z + \frac{q_\mathrm{b}}{c} A = \text{constant} , \tag{9.33}$$

the conservation of the canonical momentum in the z-direction, which arises as z is an ignorable coordinate. If one turns on the waves adiabatically, it follows that one must have

$$(P_z)_\pm = \pm m_\mathrm{b} \gamma_\mathrm{b} V_\mathrm{b} , \tag{9.34}$$

i.e. the canonical momentum in the z-direction equals the unperturbed beam momentum.

We expand all fields as plane waves by defining the Fourier amplitudes for the vector and scalar potentials:

$$\begin{pmatrix} A(x\,,\,t) \\ \\ \Phi(x\,,\,t) \end{pmatrix} = \int \frac{\mathrm{d}k\,\mathrm{d}\omega}{(2\pi)^2} \begin{pmatrix} \tilde{A}(k,\omega) \\ \\ \tilde{\Phi}(k,\omega) \end{pmatrix} \exp(ikx - i\omega t)\,. \tag{9.35}$$

Maxwell's equations imply that the Fourier components of the electric and magnetic field are

$$\tilde{E}_\perp = \frac{i\omega}{c}\,\tilde{A} \;\;,\;\; \tilde{B} = -ik\,\tilde{A} \;\;,\;\; \tilde{E}_\parallel = -ik\,\tilde{\Phi}\,. \tag{9.36}$$

In addition, we will assume that the beams are ultra-relativistic, with $\gamma_\mathrm{b} \gg 1$.

It is easily checked that the motion induced by the low-frequency Weibel mode in an ultra-relativistic beam is almost one-dimensional with the perturbed velocity directed along the x-axis. One can use a standard perturbation expansion [e.g. 60, Ch. 2] in terms of the field amplitudes, by writing the momentum of beam particles as

$$\mathbf{p} = \pm\gamma_\mathrm{b} m_\mathrm{b}\, V_\mathrm{b}\,\hat{\mathbf{z}} + \mathbf{p}_{(1)} + \mathbf{p}_{(2)} + \cdots \tag{9.37}$$

and solving the equation of motion order-by-order. Here $|\mathbf{p}_{(n)}| \propto |\tilde{A}|^n$ is the n-th order momentum perturbation. A similar expansion can be written down for the velocity: $\mathbf{V} = \pm V_\mathrm{b}\,\hat{\mathbf{z}} + \mathbf{V}_{(1)} + \mathbf{V}_{(2)} + \cdots$, where one must use $\mathbf{V} = c\mathbf{p}/\sqrt{p^2 + m_\mathrm{b}^2 c^2}$ to relate the terms in the momentum and velocity expansions.

The first-order terms in this expansion can be found written out explicitly in Melrose [60], p. 18. In our application of the theory we will exploit the fact that there are (by assumption) two small parameters: $1/\gamma_\mathrm{b} \ll 1$ and $|\omega/kc| \ll 1$. Using this, one finds from the general perturbation expansion that the first-order velocity perturbations in the beam satisfy

$$\left|\frac{\tilde{V}_{(1)\,z}(k\,,\,\omega)}{\tilde{V}_{(1)\,x}(k\,,\,\omega)}\right| = \frac{1}{\gamma_\mathrm{b}^2}\,\left|\frac{\omega}{kV_\mathrm{b}}\right| \approx \frac{1}{\gamma_\mathrm{b}^2}\,\left|\frac{\omega}{kc}\right| \ll 1. \tag{9.38}$$

Here $\tilde{\mathbf{V}}_{(1)}(k,\omega)$ is the Fourier component of the linear velocity perturbation, defined in a manner analogous to equation (9.35). This implies that one can

neglect the wave-induced motion along the beam direction (along the z-axis) to first order. It can be shown that a similar conclusion holds for the higher-order velocity perturbations $\tilde{\mathbf{V}}_{(2)}(k,\omega)$, $\tilde{\mathbf{V}}_{(3)}(k,\omega)\cdots$. This allows one to approximate the equation of motion (9.28) by

$$\left(\frac{\partial}{\partial t} + V_\pm \frac{\partial}{\partial x}\right) V_\pm(x\,,\,t) = \frac{q_\mathrm{b}\mathcal{E}_\pm(x\,,\,t)}{\gamma_\mathrm{b} m_\mathrm{b}}\ . \tag{9.39}$$

Here we have written $V_\pm(x\,,\,t)$ for the x-component $V_x(x\,,\,t)$ of the velocity for the forward and backward beam. Note that this velocity component vanishes for the unperturbed beam, so that $V_\pm = V_{\pm(1)} + V_{\pm(2)} + \cdots$ in a perturbation expansion. We also define

$$\mathcal{E}_\pm(x\,,\,t) = E_\parallel \mp \frac{V_\mathrm{b}}{c} B \approx E_\parallel \mp B\ . \tag{9.40}$$

The last approximation follows from our assumption $\gamma_\mathrm{b} \gg 1$.

The approximate equation of motion (9.39) neglects the relatively small nonlinear contributions to the Lorentz force due to variations in V_z, and also the equally small nonlinear variations in γ, keeping only the dominant nonlinearity due to ponderomotive effects, which is associated with the advective term, $V_\pm\,(\partial V_\pm/\partial x)$, in the equation of motion (9.39).

In the same limit, the current density carried by the beams is almost entirely due to the *advection current* that is associated with the charge density perturbations in the beams:

$$\mathbf{J}_\mathrm{b} \approx q_\mathrm{b}\ (n_+ - n_-)\, V_\mathrm{b}\, \hat{\mathbf{e}}_z\ . \tag{9.41}$$

The *conduction current*, which is induced by the perturbations in the z-component of the beam velocity, is a factor $\sim |\omega/\gamma_\mathrm{b} kc|^2 \ll 1$ smaller, and will be neglected in what follows.

9.3.2 Reduced set of Maxwell's equations

In the low-frequency limit $|\omega| \ll kc$ one can employ a set of reduced Maxwell equations to describe the plasma response: Ampère's Law neglecting the displacement current, $\mathrm{curl}\,\mathbf{B} = (4\pi/c)\,\mathbf{J}$, and Poisson's equation $\mathrm{div}\,\mathbf{E} = 4\pi\rho$ for the longitudinal electric field. Here ρ and $\mathbf{J}$ are the charge and current densities. For the moment we will neglect the effect of the background plasma, except as an infinitely massive neutralizing agent that compensates the charge of the

beam particles in the unperturbed state, carrying a charge density $\rho_{\rm bg} = -q_{\rm b}\overline{n}_{\rm b}$ in the laboratory frame. In this case Maxwell's equations reduce to

$$\begin{aligned} \frac{\partial E_{\parallel}}{\partial x} &= 4\pi q_{\rm b}\ (n_+ + n_- - \overline{n}_{\rm b}) \\ \frac{\partial B}{\partial x} &= 4\pi q_{\rm b}\,\frac{V_{\rm b}}{c}\ (n_+ - n_-) \simeq 4\pi q_{\rm b}\,(n_+ - n_-)\ . \end{aligned} \tag{9.42}$$

Using the definition (9.40) for $\mathcal{E}_{\pm}$ one finds that the reduced set of Maxwell's equations is equivalent to

$$\frac{\partial \mathcal{E}_{\pm}}{\partial x} = 8\pi q_{\rm b}\ \left(n_{\mp} - \tfrac{1}{2}\overline{n}_{\rm b}\right)\ . \tag{9.43}$$

The density of the two beams satisfies the continuity equation:

$$\frac{\partial n_{\pm}}{\partial t} + \frac{\partial}{\partial x}\,(n_{\pm}V_{\pm}) = 0\ . \tag{9.44}$$

Together with relation (9.43) this implies:

$$\frac{\partial^2 \mathcal{E}_{\pm}}{\partial x \partial t} = -8\pi q_{\rm b}\,\frac{\partial}{\partial x}\,(n_{\mp}V_{\mp})\ . \tag{9.45}$$

This last relation can be integrated to

$$\frac{\partial \mathcal{E}_{\pm}}{\partial t} = C_{\pm}(t) - 8\pi q_{\rm b} n_{\mp} V_{\mp}\ . \tag{9.46}$$

Here the $C_{\pm}(t)$ are arbitrary functions of time, but do not depend on the position x. For waves periodic in x it is easily checked by averaging over one wavelength that these two integration constants must vanish: $C_+ = C_- = 0$. In that case one can combine equations (9.43) and (9.46) to show that $\mathcal{E}_+$ and $\mathcal{E}_-$ satisfy:

$$\mathcal{D}_-\mathcal{E}_+ = -4\pi q_{\rm b}\overline{n}_{\rm b}\,V_-\ \ ,\ \ \mathcal{D}_+\mathcal{E}_- = -4\pi q_{\rm b}\overline{n}_{\rm b}\,V_+\ . \tag{9.47}$$

Here we use the following notation for the convective derivatives associated with the two beams:

$$\mathcal{D}_{\pm} \equiv \frac{\partial}{\partial t} + V_{\pm}\,\frac{\partial}{\partial x}\ . \tag{9.48}$$

In this notation the equations of motion (9.39) read:

$$\mathcal{D}_+ V_+ = \frac{q_\mathrm{b}\mathcal{E}_+}{\gamma_\mathrm{b} m_\mathrm{b}} \ , \ \mathcal{D}_- V_- = \frac{q_\mathrm{b}\mathcal{E}_-}{\gamma_\mathrm{b} m_\mathrm{b}} \ . \tag{9.49}$$

The coupled set of nonlinear equations (9.47) and (9.49) describes oscillations in the beam plasma. Note that *all* the nonlinear effects are in the left-hand sides of these four coupled equations: the right-hand sides are all linear! The nonlinearities are associated with the $V_\pm(\partial V_\pm/\partial x)$ terms in the convective derivatives $\mathcal{D}_\pm$. Also, these equations exhibit a remarkable symmetry that we will employ below.

By operating with $\mathcal{D}_-$ on the first equation of (9.49) and with $\mathcal{D}_+$ on the second equation one can reduce the system further: one finds two coupled equations for $V_\pm$:

$$\mathcal{D}_-\mathcal{D}_+ V_+ = -\hat{\omega}_\mathrm{pb}^2 \, V_- \ , \ \mathcal{D}_+\mathcal{D}_- V_- = -\hat{\omega}_\mathrm{pb}^2 \, V_+ \ . \tag{9.50}$$

Here the *constant* beam plasma frequency is defined as

$$\hat{\omega}_\mathrm{pb}^2 = \frac{4\pi q_\mathrm{b}^2 \overline{n}_\mathrm{b}}{\gamma_\mathrm{b} m_\mathrm{b}} \ . \tag{9.51}$$

9.3.3 Linear response of the beam plasma

If one neglects nonlinear effects one can put $\mathcal{D}_+ = \mathcal{D}_- = \partial/\partial t$. The set of two equations (9.50) is then equivalent with the single equation

$$\frac{\partial^4 V_\pm}{\partial t^4} = \hat{\omega}_\mathrm{pb}^4 \, V_\pm \ , \tag{9.52}$$

Assuming $V_\pm \propto \exp(i\omega t)$ one finds that $\omega^4 = \hat{\omega}_\mathrm{pb}^4$, and the solutions are

$$\omega = \pm\hat{\omega}_\mathrm{pb} \ , \ \omega = \pm i\hat{\omega}_\mathrm{pb} \ . \tag{9.53}$$

The first two solutions are symmetric in the sense that $V_+ = V_-$, as is easily seen by substituting the solution back into the original set of equations. In the linear case this implies $\mathcal{E}_+ = \mathcal{E}_-$, so that one must have $E_\parallel \neq 0$ and $B = 0$. These are stable electrostatic (longitudinal) plasma waves in the beam plasma. The second set of solutions for ω correspond to an exponentially growing and an exponentially decaying mode. Both these solutions are antisymmetric in the sense that $V_+ = -V_-$. The Weibel instability in the short-wavelength limit

corresponds to the growing mode. In this case $\mathcal{E}_+ = -\mathcal{E}_-$, so that one must have $E_\parallel = 0$ and $B \neq 0$, and the waves are transverse. In this limit, where we have assumed that terms of order $|\omega/kc|$ and $1/\gamma_\mathrm{b}$ can be neglected with respect to unity, these two transverse modes are purely magnetic.

9.3.4 The nonlinear response for single modes: the effect of wave breaking

As argued above, the dominant nonlinearity for $|\omega| \ll kc$ and $\gamma_\mathrm{b} \gg 1$ is associated with the $V_\pm\,(\partial V_\pm/\partial x)$ terms in the convective derivatives $\mathcal{D}_\pm$. These terms describe the distortion of the waves from the initial sinusoidal shape by the process of *wave breaking*. One usually defines the displacement of beam particles in the x-direction by

$$\xi_\pm(r_\pm\,,\,t) = x_\pm(t) - r_\pm \;\text{ with }\; r_\pm \equiv x_\pm(t=0)\;. \tag{9.54}$$

The $r_\pm$ are Lagrangian labels that are carried along by the particles. The convective derivative and the velocity in the x-direction can be reinterpreted in terms of these labels as [cf. 81, Ch. 1.7]

$$\mathcal{D}_\pm = \left(\frac{\partial}{\partial t}\right)_{r_\pm}\;,\;\; V_\pm = \mathcal{D}_\pm \xi_\pm = \left(\frac{\partial \xi_\pm}{\partial t}\right)_{r_\pm}\;. \tag{9.55}$$

Using these definitions it follows that the formal solution of the two equations (9.47) for $\mathcal{E}_\pm$ reads:

$$\begin{aligned} \mathcal{E}_+(r_- + \xi_-\,,\,t) &= -4\pi q_\mathrm{b}\overline{n}_\mathrm{b}\,\xi_-(r_-\,,\,t)\;, \\ \mathcal{E}_-(r_+ + \xi_+\,,\,t) &= -4\pi q_\mathrm{b}\overline{n}_\mathrm{b}\,\xi_+(r_+\,,\,t)\;. \end{aligned} \tag{9.56}$$

This shows that (in this limit) the $\mathcal{E}_+$-field is determined by the motion of the particles in the $-$-beam, and *vice versa*. This result is important for the rest of the discussion.

Consider now the motion of particles in one of the two beams, say the forward (+) beam. The equation of motion can be written as

$$\left(\frac{\partial^2 \xi_+}{\partial t^2}\right)_{r_+} = \frac{q_\mathrm{b}}{\gamma_\mathrm{b} m_\mathrm{b}}\,\mathcal{E}_+(r_+ + \xi_+\,,\,t)\;. \tag{9.57}$$

In the linear approximation one puts $r_+ + \xi_+ \approx r_+ \approx r_-$, neglecting the difference between the orbits followed by the particles in the forward and backward

beam. Consider now the case of the initial condition $r_+ = r_- \equiv r$. In the linear stage of the Weibel instability one can put

$$\xi_+(r\,,\,t) = -\xi_-(r\,,t) = a(t)\ \sin(kr)\ , \tag{9.58}$$

which describes a plane wave in the Lagrangian coordinate r with wavelength $2\pi/k$. The amplitude $a(t)$ grows initially as $a(t) \propto \exp(\hat{\omega}_{\rm pb}t)$.

As the beam particles move in x, the wave is distorted from its initial sinusoidal shape. From (9.56) and (9.58) one has:

$$\begin{aligned}
\mathcal{E}_+(r+\xi_+\,,\,t) &\approx \mathcal{E}_+(r+\xi_- + 2\xi_+\,,\,t) \\
&= -4\pi q_{\rm b}\overline{n}_{\rm b}\ \xi_-(r+2\xi_+\,,\,t) \\
&\approx 4\pi q_{\rm b}\overline{n}_{\rm b}\ a(t)\sin\left(kr + 2ka(t)\ \sin(kr)\right)\ .
\end{aligned} \tag{9.59}$$

With the help of an expansion in terms of the Bessel functions of integer order[2],

$$\sin(kr + 2ka\ \sin(kr)) = \sum_{m=-\infty}^{\infty} J_m(2ka)\ \sin([m+1]kr)\ , \tag{9.60}$$

one sees that 1. higher spatial harmonics are generated by the nonlinearity through the $m \neq 0$ terms and 2. that there is a phase shift due to wave breaking, which ultimately slows the instability.

Some insight into the nonlinear development can be gained by considering the initially dominant $m = 0$ term. The motion of the beam particles is approximately described by:

$$\frac{\partial^2 a}{\partial t^2} \approx \hat{\omega}_{\rm pb}^2 a(t)\ J_0(2ka(t))\ , \tag{9.61}$$

neglecting the higher spatial harmonics (i.e. the terms with $m \neq 0$). Using the property

$$x\ J_0(x) = \frac{\rm d}{{\rm d}x}\left(x\ J_1(x)\right) \tag{9.62}$$

[2]This result follows from the better-known expansion $e^{ib\,\sin\theta} = \sum_m J_m(b)\,\exp(im\theta)$, together with $\sin z = (e^{iz} - e^{-iz})/2i$ and $J_m(-b) = (-1)^m\,J_m(b) = J_{-m}(b)$.

of the zero-order Bessel function $J_0(x)$, it is easily checked that equation (9.61) corresponds to motion in a potential, with an energy integral that can be expressed as

$$\frac{1}{2}\left(\frac{\mathrm{d}\tilde{a}}{\mathrm{d}\tilde{t}}\right)^2 + V(\tilde{a}) = \text{constant} , \tag{9.63}$$

where $\tilde{a} = 2ka$ and $\tilde{t} = \hat{\omega}_{\mathrm{pb}}t$, and the potential is

$$V(\tilde{a}) = -\tilde{a}\, J_1(\tilde{a}) . \tag{9.64}$$

The form of the potential (see figure 9.2) is such that, after the initially almost exponential growth of $a(t)$, a *stable* nonlinear oscillation results whenever the amplitude of the initial perturbation is small. If the instability starts with $|\tilde{a}| \ll 1$ and $|\mathrm{d}\tilde{a}/\mathrm{d}\tilde{t}| \ll 1$, the integration constant in (9.63) will be close to zero as $V(0) = 0$. In that case the two turning points of the motion of $\tilde{a}$ will be located close to the first zeroes of $J_1(\tilde{a})$, which are at

$$|\tilde{a}_{\max}| = 2k\,|a_{\max}| \approx 3.83 . \tag{9.65}$$

This simplified analysis predicts that the distortion of the wave profile, together with the relative shift $\Delta\xi = \xi_+ - \xi_- \approx 2\xi_+$ between the orbits of the particles in the two beams, stabilizes the instability, and leads to oscillations with an amplitude

$$|a| \approx \frac{3.83}{2k} \approx 0.3\,\lambda , \tag{9.66}$$

where $\lambda = 2\pi/k$ is the wavelength of the original perturbation.

This result shows that wave breaking will limit the amplitude of the displacement $\xi_\pm$ of the beam particles, see equation (9.58). Because this displacement is directly related to the electromagnetic fields through equation (9.56), this also yields a limit on the electromagnetic field strength. However, to get an accurate estimate of the resulting magnetic field strength we have to take the influence of the background plasma into account, which we will do in the next section.

9.3.5 Influence of the background plasma

So far we have neglected the response of the background plasma, treating it in effect as an infinitely massive neutralizing background. We will now relax this assumption. The main effect of the background is to introduce screening currents and charges that slow the growth of the Weibel instability. We will

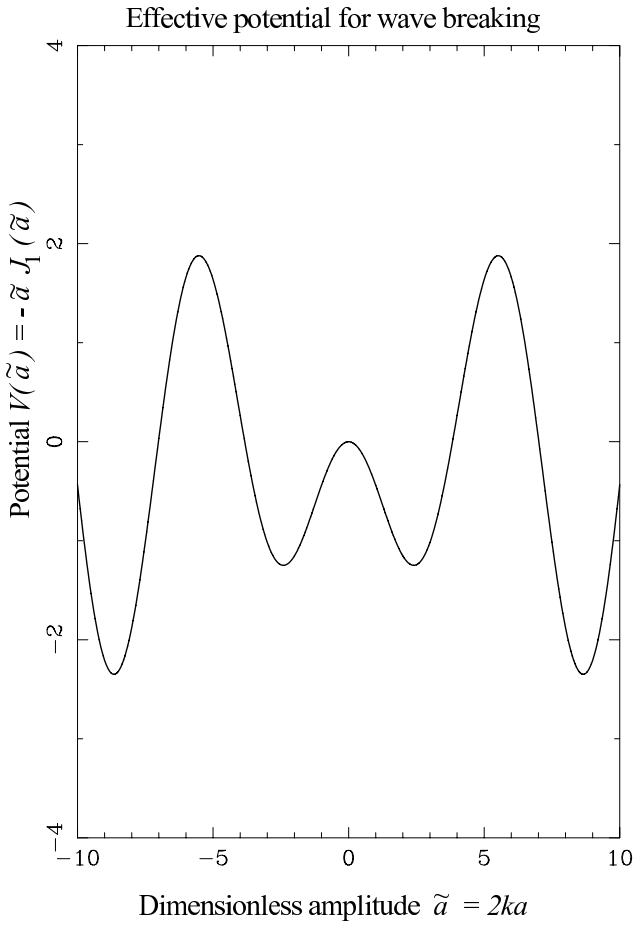

Figure 9.2: The potential $V(\tilde{a})$ as function of the dimensionless amplitude $\tilde{a} = 2ka$.

describe the background as an isotropic plasma. Since the Weibel instability is mainly magnetic, we will only need the transverse response of the plasma. The Fourier-transformed reduced Maxwell equations that include the background response replace the equation for the Fourier-amplitude of the magnetic field, $ik\,\tilde{B} \simeq 4\pi q_{\rm b}\,(\tilde{n}_+ - \tilde{n}_-)$, by

$$ik\epsilon_\perp(k\,,\,\omega)\tilde{B} = 4\pi q_{\rm b}\,\,(\tilde{n}_+ - \tilde{n}_-)\,\,. \tag{9.67}$$

Here $\epsilon_\perp(k,\omega)$ is the transverse response (dielectric) function of the background plasma. We have again assumed a relativistic beam with $V_{\rm b} \simeq c$. In terms of the components α_{ij} of the polarization tensor defined in chapter 6 (equation 6.5) one has:

$$\epsilon_\perp(k\,,\,\omega) = 1 + \frac{\alpha_{33}^{\rm bg}(k\,,\,\omega)}{k^2c^2}\,. \tag{9.68}$$

It gives the effect of screening currents carried by the background plasma. In the linear approximation, where $\mathcal{E}_+ \approx -\mathcal{E}_- = -B$, equation (9.67) together with the equation of motion and the continuity equation of the beam particles imply that the electromagnetic fields in the Fourier domain that are associated with the unstable Weibel mode now satisfy:

$$\tilde{\mathcal{E}}_\pm(k,\omega) \approx -\frac{4\pi q_{\rm b}\overline{n}_{\rm b}}{\epsilon_\perp(k\,,\,\omega)}\,\tilde{\xi}_\mp(k,\omega)\,. \tag{9.69}$$

As shown in chapter 6, the effect of screening currents can be described in a good approximation by putting

$$\epsilon_\perp(k\,,\,\omega) \approx \frac{\kappa^2+\kappa_{\rm s}^2}{\kappa^2}\,, \tag{9.70}$$

with $\kappa = kc/\tilde{\omega}_{\rm bg}$ with $\tilde{\omega}_{\rm bg}$ the plasma frequency of the background plasma, and where $\kappa_{\rm s}$ is the dimensionless screening wavenumber. The equation for the Weibel mode with a given wavelength $\lambda = 2\pi/k$ is then equivalent with

$$\frac{\partial^2\tilde{\xi}_\pm(k\,,\,t)}{\partial t^2} = \frac{\hat{\omega}_{\rm pb}^2}{\epsilon_\perp(k)}\,\tilde{\xi}_\pm(k\,,\,t)\,. \tag{9.71}$$

Again this leads to an exponentially growing amplitude, $\tilde{\xi}_\pm(t) \propto \exp(\tilde{\sigma}_{\rm W}t)$, where

$$\tilde{\sigma}_{\rm W}(k) = \frac{\hat{\omega}_{\rm pb}}{\sqrt{\epsilon_\perp(k)}} = \frac{\kappa}{\sqrt{\kappa^2+\kappa_{\rm s}^2}}\,\hat{\omega}_{\rm pb}\,. \tag{9.72}$$

The factor $1/\sqrt{\epsilon_\perp(k)}$ shows that the background response lowers the growth rate of the linear instability. Expression (9.72) is exactly the growth rate that follows from equation (9.7) in the case of cold beams ($\mathcal{M} \to \infty$) as considered here. For $\kappa \gg \kappa_s$ the effect of the background plasma is very small.

The presence of screening currents does not influence the stabilization argument of the previous section. The analysis presented there (e.g. equation 9.65) predicts that the Weibel instability saturates at a level where

$$k \left|\tilde{\xi}_\pm\right| \simeq 1.9 \; . \tag{9.73}$$

From (9.69) one has

$$\left|\tilde{\mathcal{E}}_\pm\right| \approx \left|\tilde{B}\right| \approx \frac{4\pi q_b \overline{n}_b}{\epsilon_\perp(k)} \; \left|\tilde{\xi}_\pm\right| \approx \frac{8\pi q_b \overline{n}_b}{k\,\epsilon_\perp(k)} \; . \tag{9.74}$$

It is easily checked that this estimate is equivalent to the standard trapping argument (see, for example, chapter 8).

9.4 Kinetic theory: stabilization due to quiver motion

We now consider the stabilization of the Weibel instability from the point-of-view of kinetic theory. We assume a *broad-band spectrum* of unstable modes with a bandwidth $\Delta k \sim k$, in contrast to the calculation of the previous section which assumed a single (dominant) mode.

Such a broad-band spectrum leads to *phase mixing* of the particle motion (the so-called quiver motion) in the collection of waves. This ultimately results in a broadening of the momentum distribution function $f_b(\mathbf{p})$ of the beam particles in phase space. Traditionally this process is described as 'fake diffusion' [e.g. 17], where the term 'fake' refers to the fact that this process, unlike true diffusion, is in principle *reversible*! In more modern incarnations of the theory of wave-particle interactions one uses *oscillation center theory* to define the average distribution function in the presence of waves, see for instance Cary and Kaufman [13]. Since the linear Weibel instability has $\mathrm{Re}(\omega) = 0$, there are no resonant non-linear effects, such as resonant wave-wave coupling as already discussed above, or such typical *kinetic* nonlinear resonant processes as nonlinear Landau damping. These processes usually dominate the non-linear dynamics of plasma waves with $|\mathrm{Re}(\omega)| \gg |\mathrm{Im}(\omega)|$.

This broadening of the momentum distribution effectively heats the plasma and it is well known that heating of the plasma will stabilize the Weibel instability. In this section we will first estimate the broadening of the velocity

distribution in terms of the amplitude of the magnetic field generated by the instability. Using this estimate we will calculate the effect on the response of the beam particles and derive the magnetic field strength at the point where the broadening slows down the instability appreciably.

9.4.1 Broadening of the momentum distribution

Once again we consider the case of two counterstreaming and ultra-relativistic beams that propagate along the z-axis. The dispersion relation for the Weibel instability as derived in chapter 6 reads, in the limit $|\omega^2| \ll k^2c^2$:

$$c^2k^2 + \alpha_{33}^{\rm bg}(\omega\,,\,k) + \alpha_{33}^{\rm b}(\omega\,,\,k) = 0\,, \tag{9.75}$$

where the polarization tensor component α_{33} has a contribution $\alpha_{33}^{\rm bg}(\omega\,,\,k)$ due to the background plasma, and $\alpha_{33}^{\rm b}(k\,,\,\omega)$ due to the beams. This last contribution is (chapter 6, appendix, equation 6.145):

$$\begin{aligned}\alpha_{33}^{\rm b}(\omega\,,\,k) = {} & \frac{4\pi q_{\rm b}^2 \overline{n}_{\rm b}}{m_{\rm b}} \int \frac{{\rm d}^3\mathbf{p}}{\gamma(\mathbf{p})}\, f_{0{\rm b}}(\mathbf{p}) \left(1 - \frac{v_z^2}{c^2}\right) \\ & -4\pi q_{\rm b}^2 \overline{n}_{\rm b} \int {\rm d}^3\mathbf{p} \left\{ \frac{v_z^2}{\omega - kv_x} \left(k\, \frac{\partial f_{0{\rm b}}(\mathbf{p})}{\partial p_x} \right) \right\}\,.\end{aligned} \tag{9.76}$$

Here $f_{0{\rm b}}(\mathbf{p})$ is the average phase-space density of the beam particles, normalized to

$$\int {\rm d}^3\mathbf{p}\, f_{0{\rm b}}(\mathbf{p}) = 1\,, \tag{9.77}$$

and $\gamma(\mathbf{p}) = \sqrt{1 + |\mathbf{p}|^2/m_{\rm b}^2c^2}$.

The effect of the quiver motion is a broadening of the mean distribution function. We will denote the spatially averaged distribution function of the beam particles by $f_{0{\rm b}}$, to be distinguished from the exact distribution $f_{\rm b}$, which includes a fluctuating part. In the limit $|\omega| \ll kc$ and for $\mathbf{k} = k\hat{\mathbf{x}}$ and $\mathbf{B} = B\,\hat{\mathbf{y}}$ the Vlasov equation for the exact distribution $f_{\rm b}(\mathbf{x}\,,\,t\,,\,\mathbf{p})$ can be approximated by

$$\frac{\partial f_{\rm b}}{\partial t} + v_x\, \frac{\partial f_{\rm b}}{\partial x} - \left(\frac{q_{\rm b}\, v_z B}{c} \right) \frac{\partial f_{\rm b}}{\partial p_x} = 0\,. \tag{9.78}$$

Here $f_{\rm b}(x\,,\,t\,,\,p_x\,,p_y\,,\,P_z)$ is taken to be a function of the x-coordinate and time, of the momentum components p_x and p_y perpendicular to the beam direction

(which equal the canonical momentum components P_x and P_y because $A_x = A_y = 0$) and the (conserved) canonical momentum $P_z = p_z + q_\mathrm{b} A/c$. Using standard techniques of weak plasma turbulence [e.g. 17, Ch. 8], one can show that the mean distribution function $f_{0\mathrm{b}}$ satisfies a diffusion equation of the form

$$\frac{\partial f_{0\mathrm{b}}}{\partial t} = \frac{\partial}{\partial p_x} \left\{ \left(\frac{q_\mathrm{b} v_z}{c} \right)^2 \int \frac{\mathrm{d}k \, \mathrm{d}\omega}{(2\pi)^2} \frac{\tilde{\sigma} \, \langle |\tilde{B}(k,\omega)|^2 \rangle}{(\omega_\mathrm{r} - k v_x)^2 + \tilde{\sigma}^2} \frac{\partial f_{0\mathrm{b}}}{\partial p_x} \right\} . \tag{9.79}$$

This equation gives the effect of the quiver motion on the mean distribution function. Here the wave frequency is written in terms of its real and imaginary part as $\omega(k) = \omega_\mathrm{r} + i\tilde{\sigma}$. For a broad-band spectrum of normal modes the ensemble average satisfies

$$\left\langle |\tilde{B}(k,\omega)|^2 \right\rangle = \tilde{B}^2(k) \, 2\pi\delta(\omega - \omega(k)) , \tag{9.80}$$

with $\omega(k)$ the wave frequency as determined by the solution of the dispersion relation (9.75).

We now make the assumption of beams that are initially cold in the direction perpendicular to the beam direction so that $|k v_x| \ll |\omega|$. In the linear stage of the Weibel instability the amplitude of the magnetic perturbations grows as

$$\frac{\partial \tilde{B}^2(k)}{\partial t} = 2\tilde{\sigma}(k) \, \tilde{B}^2(k) , \tag{9.81}$$

and $\omega_\mathrm{r} = \mathrm{Re}(\omega) = 0$. In this limit, equation (9.79) can be approximated by

$$\frac{\partial f_{0\mathrm{b}}}{\partial t} = \int \frac{\mathrm{d}k}{2\pi} \frac{\partial \tilde{B}^2(k)}{\partial t} \frac{\partial}{\partial p_x} \left\{ \frac{q_\mathrm{b}^2 v_z^2}{2\tilde{\sigma}^2 c^2} \frac{\partial f_{0\mathrm{b}}}{\partial p_x} \right\} . \tag{9.82}$$

In the linear stage of the Weibel instability, the growth rate $\tilde{\sigma}$ for $kc/\tilde{\omega}_\mathrm{bg} > 1$ is almost independent of wavenumber. In addition we have $f_{0\mathrm{b}} \propto \delta(P_z + \gamma_\mathrm{b} m_\mathrm{b} V_\mathrm{b}) + \delta(P_z - \gamma_\mathrm{b} m_\mathrm{b} V_\mathrm{b})$ (see equation 9.34) and $p_z \approx P_z$, so we can put $v_z = \pm V_\mathrm{b}$. We define the typical magnetic field strength B by the relation

$$B^2 = \int \frac{\mathrm{d}k}{2\pi} \, \tilde{B}^2(k) . \tag{9.83}$$

Together, equations (9.81), (9.82) and (9.83) imply that $f_{0\mathrm{b}}$ satisfies a diffusion equation of the form:

$$\frac{\partial f_{0\mathrm{b}}}{\partial (B^2)} = \frac{\partial f_{0\mathrm{b}}/\partial t}{\partial (B^2)/\partial t} = \frac{\partial}{\partial p_x} \left\{ \frac{q_\mathrm{b}^2 V_\mathrm{b}^2}{2\tilde{\sigma}^2 c^2} \frac{\partial f_{0\mathrm{b}}}{\partial p_x} \right\} . \tag{9.84}$$

If the beams are ultra-relativistic and cold at $t = 0$, the momentum distribution is given by:

$$\begin{aligned} f_{0\mathrm{b}}(t=0) &= \delta(p_x)\,\delta(p_y)\times \\ &\times \tfrac{1}{2}\left[\delta(P_z+\gamma_\mathrm{b} m_\mathrm{b} V_\mathrm{b})+\delta(P_z-\gamma_\mathrm{b} m_\mathrm{b} V_\mathrm{b})\right]\,. \end{aligned} \tag{9.85}$$

Using $\gamma_\mathrm{b} \gg 1$ the solution to equation (9.84) can then be written as a quasi-Maxwellian distribution in $v_x = p_x/\gamma_\mathrm{b} m_\mathrm{b}$:

$$\begin{aligned} f_{0\mathrm{b}}(t) &= \frac{1}{\sqrt{2\pi}\,\gamma_\mathrm{b} m_\mathrm{b} v_\mathrm{q}}\, e^{-(v_x^2/2v_\mathrm{q}^2)}\;\delta(p_y)\times \\ &\times \tfrac{1}{2}\left[\delta(P_z+\gamma_\mathrm{b} m_\mathrm{b} V_\mathrm{b})+\delta(P_z-\gamma_\mathrm{b} m_\mathrm{b} V_\mathrm{b})\right]\,. \end{aligned} \tag{9.86}$$

Here the quiver velocity v_q is defined by:

$$v_\mathrm{q}^2 \approx \frac{q_\mathrm{b}^2 V_\mathrm{b}^2 B^2}{2\gamma_\mathrm{b}^2 m_\mathrm{b}^2 \tilde{\sigma}^2 c^2}\,. \tag{9.87}$$

This explicitly shows how the mean distribution in v_x (with associated momentum $p_x \approx \gamma_\mathrm{b} m_\mathrm{b} v_x$) broadens due to phase mixing of the quiver motion as the rms magnetic field grows. The above procedure generalizes a similar result derived by [43], p. 25, for electrostatic waves.

If we relax the assumption that the wave vector $\mathbf{k}$ is in the x-direction, and allow for $k_y \neq 0$, $B_x \neq 0$ while keeping $k_z = 0$, a similar broadening occurs in the distribution of the y-component of momentum. If the situation is cylindrically symmetric around the beam direction, with

$$\tilde{B}_x^2(k) = \tilde{B}_y^2(k) \equiv \tilde{B}^2(k)\,, \tag{9.88}$$

expression (9.86) is replaced by

$$\begin{aligned} f_{0\mathrm{b}}(t) &= \frac{1}{2\pi\,(\gamma_\mathrm{b} m_\mathrm{b}\, v_\mathrm{q})^2}\, e^{-(v_x^2+v_y^2)/2v_\mathrm{q}^2}\;\times \\ &\times \tfrac{1}{2}\left[\delta(P_z+\gamma_\mathrm{b} m_\mathrm{b} V_\mathrm{b})+\delta(P_z-\gamma_\mathrm{b} m_\mathrm{b} V_\mathrm{b})\right]\,. \end{aligned} \tag{9.89}$$

In conclusion: the effect of the phase mixing of the quiver motion is to heat the beam plasma, in particular by creating a quasi-Maxwellian distribution of the components of the particle momentum in the xy-plane, the plane perpendicular to the beam direction.

9.4.2 Effect on the beam response

The change in the beam momentum distribution also changes the contribution of the beam to the polarization tensor component $\alpha_{33}(\omega\,,\,k)$ that figures in the dispersion relation for the Weibel instability. Using distribution function (9.89) in definition (9.76) gives the beam contribution to α_{33} in the limit $v_{\rm q} \ll c$ so that $p_x \approx \gamma_{\rm b} m_{\rm b} v_x$:

$$\alpha_{33}^{\rm b} = \hat{\omega}_{\rm pb}^2 \left(\frac{1}{\gamma_{\rm b}^2} + \frac{4 v_{\rm q}^2}{c^2} \right) - \hat{\omega}_{\rm pb}^2 \, \frac{k^2 V_{\rm b}^2}{\omega^2} \, Z^2 \, W(Z) \; . \tag{9.90}$$

Here $Z \equiv \omega / k v_{\rm q}$ and $W(Z)$ is the plasma dispersion function defined by Ichimaru [40],

$$W(Z) \equiv \frac{1}{\sqrt{2\pi}} \int_{-\infty}^{+\infty} {\rm d}x \, \frac{x \exp\left(-x^2/2\right)}{x - Z} \; , \tag{9.91}$$

and $\hat{\omega}_{\rm pb}^2 = 4\pi q_{\rm b}^2 \overline{n}_{\rm b} / \gamma_{\rm b} m_{\rm b}$ is the effective plasma frequency associated with the beams. To obtain result (9.90) we have used

$$1 - \frac{v_z^2}{c^2} = \frac{1}{\gamma^2} + \frac{v_x^2}{c^2} + \frac{v_y^2}{c^2} \; . \tag{9.92}$$

Initially $v_{\rm q} \ll |\omega/k| \ll c$ and $|Z| \gg 1$, and we can use the expansion (valid for $\tilde{\sigma} = {\rm Im}(\omega) > 0$):

$$W(Z) \approx -\frac{1}{Z^2} - \frac{3}{Z^4} \tag{9.93}$$

For $k V_{\rm b} \sim kc \gg |\omega|$, $\gamma_{\rm b} \gg 1$ and $v_{\rm q} \ll c$ we can neglect the first term in (9.90), and the dispersion relation (9.75) can be approximated by:

$$k^2 c^2 + \alpha_{33}^{\rm bg}(i\tilde{\sigma}\,,\,k) - \hat{\omega}_{\rm pb}^2 \, \frac{k^2 V_{\rm b}^2}{\tilde{\sigma}^2} \left(1 - \frac{3 k^2 v_{\rm q}^2}{\tilde{\sigma}^2} \right) = 0 \; . \tag{9.94}$$

Here we put $\omega = i\tilde{\sigma}$. This approximate dispersion relation shows that the instability slows down appreciably if $k v_{\rm q} \sim \tilde{\sigma}$, or equivalently when

$$\frac{k v_{\rm q}}{\tilde{\sigma}} \approx \frac{k q_{\rm b} V_{\rm b} B}{\gamma_{\rm b} m_{\rm b} c \tilde{\sigma}^2} \approx 1. \tag{9.95}$$

This is essentially the trapping criterion (9.15), with the quiver amplitude $\xi_{\rm q} = v_{\rm q}/\tilde{\sigma}$ as the typical amplitude. A similar argument for the stabilization of the

Weibel instability has been proposed previously by Gruzinov [31]. A more precise evaluation of the dispersion relation using expression (9.90) for α_{33}^{b} needs an evaluation of $W(Z) = W(\omega/kv_{\mathrm{q}})$ in the complex plane, and is beyond the scope of this paper.

9.5 Further field growth through current channel coalescence

In the previous two sections we have calculated how the exponential phase of the Weibel instability is terminated when the amplitude of the magnetic field becomes comparable with the trapping field $B \sim B^{\mathrm{tr}}$, see equation (9.16). If a single (dominant) wave mode of given wavenumber k is present, the stabilization can be understood as the effect of wave breaking. In a broad-band spectrum of unstable modes the broadening of the average distribution function essentially gives the beam plasma a finite temperature in the plane perpendicular to the beam direction. Since wave breaking generates higher harmonics, the single-mode case will evolve naturally into a broad-band spectrum.

Once trapping finishes the quasi-exponential growth of the magnetic field, further field amplification is still possible. The numerical simulations of Lee and Lampe [52], and more recently by Frederiksen et al. [24] show how the filamentary currents generated by the Weibel instability merge into larger current channels. Physically, this coalescence is the result of the attractive force between parallel currents. Medvedev et al. [59] have considered a simple model of this coalescence phase, assuming that the process can be approximated by treating the current channels as thin current wires with a magnetic field at a distance r from the wire axis equal to $B(r) = 2I/cr$. Their calculation neglects the screening currents of a background plasma which, at least in the exponential stage of the instability, play an important role in determining the wavenumber $k_{\dagger}$ at which the trapping field reaches the maximum value (see equation 9.18).

In this section we will include the effect of screening currents. In particular, we investigate how the presence of the hot background plasma influences the coalescence process. We will show that the screening currents supported by this background slow the coalescence process once the typical transverse size of the current channels becomes comparable with the skin depth, $c/\tilde{\omega}_{\mathrm{bg}}$, of the hot background.

9.5.1 Maximum current for a cylindrical channel: the Alfvén current

Following Kato [44] we define typical currents and the associated magnetic fields for a cylindrical current filament of a given radius r_0. A single beam of

charged particles with lab frame density $\overline{n}_{\rm b}$, with charge $q_{\rm b}$ per particle and with a bulk velocity $V_{\rm b}$ can carry a maximum current equal to

$$\mathcal{I}_{\rm b} = \pi r_0^2 q_{\rm b} \overline{n}_{\rm b} V_{\rm b} \ . \tag{9.96}$$

If the current channels result from the Weibel instability, the typical size of the channels will be $r_0 \leq c/\tilde{\omega}_{\rm bg}$. If one neglects screening currents, the typical magnetic field at the outer edge of the filament is

$$B_{\rm b} = \frac{2\mathcal{I}_{\rm b}}{c r_0} = \frac{2\pi q_{\rm b} \overline{n}_{\rm b} c}{\tilde{\omega}_{\rm bg}} \left(\frac{V_{\rm b}}{c}\right) \left(\frac{r_0}{(c/\tilde{\omega}_{\rm bg})}\right) \ . \tag{9.97}$$

The Alfvén current follows (up to factors of order unity) from the requirement that the gyration radius of the beam particles, with an energy $E = \gamma_{\rm b} m_{\rm b} c^2$, in the self-generated magnetic field becomes equal to the radius of the current channel:

$$r_{\rm g} = \frac{\gamma_{\rm b} m_{\rm b} c V_{\rm b}}{q_{\rm b} B} \sim r_0 \ . \tag{9.98}$$

Using $B \approx 2\mathcal{I}/c r_0$ this gives the critical Alfvén current,

$$\mathcal{I}_{\rm A} = \frac{\gamma_{\rm b} m_{\rm b} c^2 V_{\rm b}}{2 q_{\rm b}} \ . \tag{9.99}$$

The associated magnetic field is equal to

$$\begin{aligned} B_{\rm A} &= \frac{\gamma_{\rm b} m_{\rm b} c V_{\rm b}}{q_{\rm b} r_0} \\ &= \frac{4\pi q_{\rm b} \overline{n}_{\rm b} c}{\tilde{\omega}_{\rm bg}} \left(\frac{\tilde{\omega}_{\rm bg}^2}{\hat{\omega}_{\rm pb}^2}\right) \left(\frac{V_{\rm b}}{c}\right) \left(\frac{r_0}{(c/\tilde{\omega}_{\rm bg})}\right)^{-1} \ . \end{aligned} \tag{9.100}$$

One has $B_{\rm b}(r_0) < B_{\rm A}(r_0)$ for $r_0 < \sqrt{2}\,(c/\hat{\omega}_{\rm pb})$.

The trapping condition (9.15) implies that the magnetic field amplitude for a wave mode with a wavenumber $k = 2\pi/\lambda$ at the end of the phase of exponential growth is

$$B^{\rm tr}(k) = \frac{\gamma_{\rm b} m_{\rm b} c}{q_{\rm b}} \left(\frac{\tilde{\sigma}^2}{k V_{\rm b}}\right) \ . \tag{9.101}$$

This trapping field serves as an initial condition for the coalescence phase of magnetic field growth. Using the expression for the growth rate of the Weibel

instability in the ultra-relativistic limit [3] , equation (9.7), one has for $k \ll k_{\rm max}$, $h_{\rm b} \approx 1$ (cold beam) and $V_{\rm b} \approx c$:

$$B^{\rm tr}(k) \approx \frac{4\pi q_{\rm b}\gamma_{\rm b} n_{\rm b}}{k} \left(\frac{k^2}{k^2+k_{\rm s}^2}\right) . \tag{9.102}$$

The maximum field amplitude occurs at a wavenumber close to the screening wavenumber: $k \sim k_{+} \sim k_{\rm s} = \tilde{\omega}_{\rm bg}\kappa_{\rm s}/c$. For typical parameters (see below) one has $\kappa_{\rm s} \approx 0.25 - 1$. For the order-of-magnitude estimates we will use the fluid result: $\kappa_{\rm s} = 1$. Note that the field amplitude $B^{\rm tr}$ is *independent* of the mass of the beam particles for $k \gg k_{\rm s}$.

For relativistic beams with $V_{\rm b} \approx c$ and for a wavenumber $k \geq \tilde{\omega}_{\rm bg}/c$ the trapping field is comparable to the field of a cylindrical current with a radius equal to $r_0 = 1/k = \lambda/2\pi$:

$$B_{\rm b}(r_0) \sim B^{\rm tr}(k = 1/r_0) . \tag{9.103}$$

The magnetic field associated with the critical Alfvén current equals

$$B_{\rm A}(r_0) \sim \frac{B^{\rm tr}(k=1/r_0)}{\eta\,(\tilde{\omega}_{\rm bg} r_0/c)^2} = \frac{B^{\rm tr}(k=1/r_0)}{(\hat{\omega}_{\rm pb} r_0/c)^2} . \tag{9.104}$$

Here we have used definition (9.2) for η. The current channels created by the Weibel instability typically have $r_0 \sim 1/k_{+} \leq c/\tilde{\omega}_{\rm bg}$.

The estimates (9.103) and (9.104) have immediate consequences for the coalescence of the current filaments created by the Weibel instability that we will explore in section 9.6.

9.5.2 Simple model for field growth

The growth of the small-scale field can be estimated using the toy model for current merging of Medvedev et al. [59]. This model considers the merging of identical and cylindrical current channels with radius r_m and cross section $\pi r_{\rm m}^2$ after the m-th merger. After m mergers of currents with the same initial scale r_0 and current $\mathcal{I}_0$, the resulting current filament carries a current $\mathcal{I}_m$, has a radius r_m and a magnetic field $B_m = 2\mathcal{I}_m/cr_m$ at its outer edge, which are given by [59]

$$\mathcal{I}_m = 2^m\,\mathcal{I}_0 \;\;,\;\; r_m = 2^{m/2}\,r_0 \;\;,\;\; B_m = 2^{m/2}\,B_0 . \tag{9.105}$$

[3] Although formally expression (9.7) for the growth rate $\tilde{\sigma}$ has been derived under the assumption $\tilde{\sigma} \ll kc$, it turns out that it gives a good approximation even if $\tilde{\sigma} \sim kc$.

This calculation neglects screening currents, which is a reasonable approximation for $r_m \ll c/\tilde{\omega}_{\rm bg}$, and uses mass conservation and current conservation. Combining the last two relations of (9.105) one has

$$B_m = \left(\frac{r_m}{r_0}\right) B_0 \ . \tag{9.106}$$

We first consider the merging of electron current filaments. At this stage of the development of the instability, the electrons are already (partially) thermalized, and $\eta \approx 1$, see also the discussion in Section 9.6 below. Using as an initial condition for the merger process the trapping field generated at the end of the exponential phase of the Weibel instability, $B_0 = B_{\rm tr}(k = 1/r_0) \approx B_{\rm b}(r_0)$, this yields for $r_m \leq c/\tilde{\omega}_{\rm bg}$:

$$B_m = \frac{2\pi q_{\rm b} \overline{n}_{\rm b} c}{\tilde{\omega}_{\rm bg}} \, \frac{\tilde{\omega}_{\rm bg} r_m}{c} \approx B_{\rm b}(r_m) \approx B^{\rm tr}(k \sim 1/r_m) \ . \tag{9.107}$$

This simple merging model gives a magnetic field of the merged current filaments of size $r_{\rm m}$ that is comparable with the trapping field at the same scale, which equals the field created by the exponential Weibel instability at that scale. When, after multiple mergers, the radius of the resulting filament becomes comparable with the skin depth, $r_m \sim c/\tilde{\omega}_{\rm bg}$, the Alfvén limit $B^{\rm tr}(r = c/\tilde{\omega}_{\rm bg}) \sim B_{\rm A}$ is reached as $\tilde{\omega}_{\rm bg} \sim \hat{\omega}_{\rm pb}$ for the electrons. The electron current can not grow beyond the (radius-independent) Alfvén limit (9.99), and the associated magnetic field (9.100) will decay as r_m^{-1} if merging continues.

We will argue below that further merging to filaments of a transverse size larger than the skin depth is slowed down considerably by the screening currents generated in the background plasma. This means that for all intents and purposes the merging almost stops when $r_m \sim c/\tilde{\omega}_{\rm bg}$ when the magnetic field has a magnitude $B_{\rm b} \sim B_{\rm A} \sim B^{\rm tr}$. The decay of the field due to further merging, $B_m \propto r_m^{-1}$ for $B_m > B_{\rm A}$, is present, but proceeds at a much slower rate than the growth of the field in the Weibel instability.

Protons have $\eta = \eta_{\rm p} \sim m_{\rm e}/m_{\rm p} \ll 1$. This means that the Alfvén field satisfies $B_{\rm A} \sim B^{\rm tr}/\eta \gg B^{\rm tr}$ at $r \simeq c/\tilde{\omega}_{\rm bg}$. Merging of proton current filaments could therefore in principle lead to continuing magnetic field growth. However, the screening currents act here also, slowing down the merging rate. Therefore, the additional field growth will be limited.

9.5.3 The effect of screening currents

The hot background plasma that one expects to be present in shock transition layers will influence the coalescence process because it supports screening currents, which diminish both the total current of a filament and the resulting magnetic field outside the filament. The latter determines the strength of the force between adjacent current filaments. In this section we calculate the influence of the screening currents on the merger rate, and how they modify the results of the simple merger model employed above for $r_m > c/\tilde{\omega}_{\rm bg}$.

The magnitude of the screening current in the z-direction (along the beams) that is carried by the background can be readily calculated from the z-component of the equation of motion for species s in the hot background. This equation is formally identical to the corresponding equation (9.29) for the beam particles. The only difference is that the effective inertia of a hot plasma is $m_{\rm s}h_{\rm s}$ with $h_{\rm s}$ the enthalpy per unit rest energy, cf. [49]. One has:

$$m_{\rm s}h_{\rm s}\,\frac{{\rm d}\,(\gamma_{\rm s}V_{\rm sz})}{{\rm d}t} = q_{\rm s}\,\left(\mathbf{E}+\frac{\mathbf{V}\times\mathbf{B}}{c}\right)_z\,. \tag{9.108}$$

In a cylindrically symmetric situation around a filament aligned with the z-axis, with $\mathbf{B} = B(r)\,\hat{\mathbf{e}}_\phi$ and $\partial/\partial\phi = 0$, one has $B(r) = -\partial A/\partial r$, $(\mathbf{V}\times\mathbf{B})_z = V_r B(r)$, $E_z = -(1/c)(\partial A/\partial t)$ and ${\rm d}/{\rm d}t = \partial/\partial t + V_r\,(\partial/\partial r)$. Here $\mathbf{A} = A(r)\,\hat{\mathbf{z}}$ is the vector potential, r is the cylindrical radius centered on the filament axis and ϕ is the azimuthal angle around the filament. In that case equation (9.108) can be integrated to

$$m_{\rm s}h_{\rm s}\gamma_{\rm s}V_{\rm sz} + \frac{q_{\rm s}A}{c} = \text{constant} \equiv \mathcal{P}_{\rm sz}\,, \tag{9.109}$$

which is the equivalent of relation (9.33) for a species belonging to the background plasma. For a growing field the integration constant $\mathcal{P}_{\rm sz}$ can be neglected. Solving for $V_{\rm sz}$ with $\mathcal{P}_{\rm sz} = 0$ one finds the screening current due to the background:

$$\begin{aligned}\mathbf{J}_{\rm bg} &= \sum_s q_{\rm s}n_{\rm s}V_{\rm sz}\,\hat{\mathbf{z}}\\ &= -\sum_{\rm s}\frac{q_{\rm s}^2 n_{\rm s}}{m_{\rm s}h_{\rm s}c}\,\frac{\mathbf{A}}{\sqrt{1+\left(\dfrac{q_{\rm s}A}{m_{\rm s}h_{\rm s}c^2}\right)^2}}\,.\end{aligned} \tag{9.110}$$

In what follows we will neglect the non-linearity in this relation due to the relativistic mass correction, replacing (9.110) by its non-relativistic equivalent

$$\mathbf{J}_{\rm bg} \approx -\sum_{\rm s} \frac{q_{\rm s}^2 n_{\rm s}}{m_{\rm s} h_{\rm s} c}\,\mathbf{A} = -\frac{\tilde{\omega}_{\rm bg}^2}{4\pi c}\,\mathbf{A}\,. \tag{9.111}$$

This is allowed if $J_{\rm s} \ll n_{\rm s} q_{\rm s} c$, which is formally satisfied if the beam density satisfies $\overline{n}_{\rm b} \ll n_{\rm s}$, or if the beam-current filaments have a size $r_0 \ll c/\tilde{\omega}_{\rm bg}$ so that the screening currents remain small. For the fields created by the Weibel instability this last condition is (marginally) satisfied. Nevertheless, our results should remain *qualitatively* valid even when $J_{\rm s} \approx n_{\rm s} q_{\rm s} c$.

We note in passing that relation (9.110) implies that $J_{\rm s} < n_{\rm s} q_{\rm s} c$, a limit which is physically obvious. Therefore, in a situation where the beam density is much larger than the density of the species in the background plasma so that $\overline{n}_{\rm b} \gg n_{\rm s}$ for all species, screening currents are always much smaller than the maximum current density that can be carried by the beam, $J_{\rm b} = \overline{n}_{\rm b} q_{\rm b} c$. In that case screening can be much less effective. In what follows we will assume that (at most) $\overline{n}_{\rm b} \approx n_{\rm s}$, and that this particular situation does not occur.

In a quasi-steady state, where the fields only depend on the distance r from the filament axis and $\mathbf{A} = A(r)\,\hat{\mathbf{z}}$, Maxwell's equation for the vector potential $\mathrm{curl}(\mathrm{curl}\,\mathbf{A}) = (4\pi/c)\,\mathbf{J}$ [e.g. 41, Ch. 6.4] reads, with approximation (9.111),

$$\frac{1}{r}\frac{\partial}{\partial r}\left(r\,\frac{\partial A}{\partial r}\right) - \frac{\tilde{\omega}_{\rm bg}^2}{c^2}\,A = -\frac{4\pi}{c}\,J_{\rm b}\,. \tag{9.112}$$

Here $J_{\rm b}$ is the current density due to the beam particles in a current filament. The screening current of the background plasma corresponds to the second term on the left-hand side of the equation.

Let us calculate the magnetic field due to a single cylindrical current filament embedded in a background plasma with a uniform background density $n_{\rm s}$ and pressure $P_{\rm s}$. This last assumption is a reasonable approximation as long as the radial gradients in pressure and density induced by the radial magnetic pinching force remain small. This will be the case if $B^2/8\pi \ll P_{\rm s}$. In the relativistic case this condition is met when the field amplitude is much less than the equipartition field: $B \ll B_{\rm e}$. As a first approximation, the current density carried by the beam is taken to be constant over the cross section of the filament of radius r_0, $J_{\rm b} = J_0$ for $r \le r_0$, and vanishes outside the filament: $J_{\rm b} = 0$ for $r > r_0$.

Equation (9.112) is readily solved for constant $\tilde{\omega}_{\rm bg}$ in terms of the modified Bessel functions of integer order $I_{\rm n}$ and $K_{\rm n}$:

$$A(r) = \frac{4\pi J_0}{ck_{\rm s}^2} \times \begin{cases} 1 - k_{\rm s}r_0\, K_1(k_{\rm s}r_0) I_0(k_{\rm s}r) & \text{for } r \le r_0; \\ \\ k_{\rm s}r_0\, I_1(k_{\rm s}r_0) K_0(k_{\rm s}r) & \text{for } r > r_0 \end{cases} \tag{9.113}$$

Here $k_{\rm s} \equiv \tilde{\omega}_{\rm bg}/c$ is the inverse skin depth. The magnetic field as a function of cylindrical radius r follows from $B(r) = -\partial A/\partial r$:

$$B(r) = 2B_0 \times \begin{cases} K_1(k_{\rm s}r_0) I_1(k_{\rm s}r) & \text{for } r \le r_0; \\ \\ I_1(k_{\rm s}r_0) K_1(k_{\rm s}r) & \text{for } r > r_0 \end{cases} \tag{9.114}$$

Here $B_0 = 2\mathcal{I}_0/cr_0 = 2\pi r_0 J_0/c$ is the field at the outer radius r_0 of an unscreened current filament with a total beam current $\mathcal{I}_0 = \pi r_0^2 J_0$. The *total* current contained within a cylindrical radius r_0 equals

$$\mathcal{I}_{\rm tot} = \frac{cr_0\, B(r_0)}{2} = 2\mathcal{I}_0\, I_1(k_{\rm s}r_0) K_1(k_{\rm s}r_0)\ . \tag{9.115}$$

For a large current filament, with a radius such that $k_{\rm s}r_0 \gg 1$, $\mathcal{I}_{\rm tot}$ decays with increasing filament radius as

$$\mathcal{I}_{\rm tot} \approx \mathcal{I}_0/k_{\rm s}r_0\ , \tag{9.116}$$

while the magnetic field for $r > r_0$ falls off rapidly:

$$B(r) \approx B_0\, \frac{e^{-k_{\rm s}(r-r_0)}}{k_{\rm s}\sqrt{rr_0}}\ . \tag{9.117}$$

9.5.4 Equation of motion for two attracting screened filaments

Now consider two identical and parallel current filaments of radius r_0, with their axes at a distance $d > 2r_0$. As an admittedly crude model let us assume that we can describe the interaction between the two current filaments as the interaction between two current wires, with a total current equal to the partially screened current $\mathcal{I}_{\rm tot}$ of equation (9.115), and with a magnetic field outside the filament given by equation (9.114). The attractive interaction force per unit length between the current wires equals ${\rm d}F/{\rm d}\ell = -\mathcal{I}_{\rm tot}B(d)/c$, which is

$$\frac{{\rm d}F}{{\rm d}\ell} = -\frac{8\mathcal{I}_0^2}{c^2 r_0}\, I_1^2(k_{\rm s}r_0) K_1(k_{\rm s}r_0) K_1(k_{\rm s}d)\ . \tag{9.118}$$

For $k_s r_0 \ll 1$ and $k_s d \ll 1$ we can use the expansion of the modified Bessel functions for a small argument: $I_1(\xi) \approx \xi/2$ and $K_1(\xi) \approx 1/\xi$. In that case equation (9.118) reduces to the well-known result $\mathrm{d}F/\mathrm{d}\ell = -2\mathcal{I}_0^2/c^2 d$.

The mass per unit length of a current filament is approximately equal to

$$\mu \equiv \frac{\mathrm{d}m}{\mathrm{d}\ell} \approx \pi r_0^2 \ (n_e m_e h_e + \gamma_b m_b \overline{n}_b) \ . \tag{9.119}$$

Here we have used that the effective mass of the hot electron background equals $m_{\mathrm{eff}} \approx m_e h_e$, and that the effective mass of the beam particles for motions perpendicular to the beam direction is $\gamma_b m_b$. This assumes that the beam currents and the hot electron background, which provides the screening current, move together inside the filament.

The equation of motion for a filament is

$$\mu \, \frac{\mathrm{d}^2 d}{\mathrm{d}t^2} = -\frac{8\mathcal{I}_0^2}{c^2 r_0} \, I_1^2(k_s r_0) K_1(k_s r_0) K_1(k_s d) \ . \tag{9.120}$$

The modified Bessel function K_0 satisfies $\mathrm{d}K_0(\xi)/\mathrm{d}\xi = -K_1(\xi)$. This means that the force on the right-hand side of equation (9.120) can be written in the form $-\partial V_{\mathrm{int}}/\partial d$, where the interaction potential $V_{\mathrm{int}}(d)$ is given by:

$$V_{\mathrm{int}}(d) = -\frac{8\mathcal{I}_0^2}{k_s c^2 r_0} \, I_1^2(k_s r_0) K_1(k_s r_0) K_0(k_s d) \ . \tag{9.121}$$

9.5.5 The coalescence time scale

If the filaments start from rest at an initial distance d_i, the equation of motion has an energy integral:

$$\frac{\mu}{2} \left(\frac{\mathrm{d}d}{\mathrm{d}t} \right)^2 + V_{\mathrm{int}}(d) = V_{\mathrm{int}}(d_i) \ . \tag{9.122}$$

The coalescence time now follows as

$$t_{\mathrm{coal}}(d_i) = \int_{2r_0}^{d_i} \frac{\mathrm{d}r}{\sqrt{\dfrac{2}{\mu} \, [V_{\mathrm{int}}(d_i) - V_{\mathrm{int}}(r)\,]}} \ . \tag{9.123}$$

Here we end the coalescence phase when the filaments touch so that $d = 2r_0$. Defining dimensionless variables

$$\varrho \equiv k_s d \ \ , \ \ \varrho_0 \equiv k_s r_0 \ , \tag{9.124}$$

one finds

$$t_{\rm coal}(\varrho_{\rm i}) = T_0 \int_{2\varrho_0}^{\varrho_{\rm i}} \frac{{\rm d}\varrho}{\sqrt{K_0(\varrho) - K_0(\varrho_{\rm i})}} \,, \tag{9.125}$$

with a characteristic time T_0 given by

$$\begin{aligned} T_0 &\equiv \left(\frac{16\mathcal{I}_0^2 k_{\rm s}}{\mu c^2\, r_0}\right)^{-1/2} \Big(I_1^2(\varrho_0)K_1(\varrho_0)\Big)^{1/2} \\ &= \frac{1}{2\hat{\omega}_{\rm pb}} \left(\frac{c}{V_{\rm b}}\right) \left(1 + \frac{n_{\rm e} m_{\rm e} h_{\rm e}}{\overline{n}_{\rm b} m_{\rm b} \gamma_{\rm b}}\right)^{1/2} \left(\frac{B_0}{B_{\rm b}}\right)^{-1} \psi(\varrho_0) \,. \end{aligned} \tag{9.126}$$

Here we define

$$\psi(\varrho_0) \equiv 1/\sqrt{\varrho_0\, I_1^2(\varrho_0) K_1(\varrho_0)} \,, \tag{9.127}$$

normalize the beam current with the maximum current (9.96) and use $\mathcal{I}_0/\mathcal{I}_{\rm b} = B_0/B_{\rm b}$. Note that for current filaments left by the Weibel instability the trapping argument predicts that $B_0 \approx B_{\rm b}$ and that $V_{\rm b} \simeq c$ for the relativistic beams we are considering. In that case (for typical values of the parameters) one has $T_0 \simeq 1/\hat{\omega}_{\rm pb}$ for $r_0 \sim c/\tilde{\omega}_{\rm bg}$, and the time scale of the merging process and the growth time of the preceding Weibel instability, $t_{\rm W} \sim 1/\tilde{\sigma} \simeq 1/\hat{\omega}_{\rm pb}$, are of the same order.

In what follows we will neglect the factor $\sqrt{1 + n_{\rm e} m_{\rm e} h_{\rm e}/\overline{n}_{\rm b}\gamma_{\rm b} m_{\rm b}}$, which is always of order unity in our applications. Assuming $\varrho_0 \gg 1$ and $\varrho_i \gg 1$ we can use the asymptotic expansion of the modified Bessel functions for large arguments, $I_{\rm n}(\varrho) \approx e^{\varrho}/\sqrt{2\pi\varrho}$ and $K_{\rm n}(\varrho) \approx \sqrt{\pi/2\varrho}\, e^{-\varrho}$. In that case

$$\psi(\varrho_0) \approx (8\pi\varrho_0)^{1/4}\, e^{-\varrho_0/2} \,, \tag{9.128}$$

and the integral appearing in (9.125) can be approximated by

$$\left(\frac{2}{\pi}\right)^{1/4} \int_{2\varrho_0}^{\varrho_{\rm i}} \frac{{\rm d}\varrho\, \varrho^{1/4}\, e^{\varrho/2}}{\sqrt{1 - (\varrho/\varrho_{\rm i})^{1/2}\, e^{\varrho - \varrho_{\rm i}}}} \equiv \mathcal{K} \,. \tag{9.129}$$

In its present form the integral can not be evaluated analytically. However, for $2\varrho_0 \gg 1$ an excellent approximation can be derived. To that end we define a new variable,

$$\zeta \equiv \left(\frac{\varrho}{\varrho_{\rm i}}\right)^{1/4} e^{(\varrho - \varrho_{\rm i})/2} \,. \tag{9.130}$$

With a little algebra it is easy to show that the integral (9.129) can be rewritten as

$$\mathcal{K} = 2\left(\frac{2\varrho_{\rm i}}{\pi}\right)^{1/4} e^{\varrho_i/2} \int_{\zeta_0}^{1} \frac{{\rm d}\zeta}{\sqrt{1-\zeta^2}\,(1+1/2\varrho(\zeta))} \,. \tag{9.131}$$

For $\varrho \gg 1$ we can safely neglect $1/2\varrho$ in the factor $(1+1/2\varrho)$, and the integral becomes

$$\mathcal{K} \approx 2\left(\frac{2\varrho_{\rm i}}{\pi}\right)^{1/4} e^{\varrho_i/2} \left(\frac{\pi}{2} - \sin^{-1}(\zeta_0)\right) \,. \tag{9.132}$$

Together with (9.125), (9.126) and (9.128) this gives the coalescence time for $\zeta_0 = (2\varrho_0/\varrho_{\rm i})^{1/4} \exp[(2\varrho_0 - \varrho_{\rm i})/2\,] \ll 1$:

$$t_{\rm coal} \approx \frac{2\pi}{\hat{\omega}_{\rm pb}} \left(\frac{B_0}{B_{\rm b}}\right)^{-1} \left(\frac{c}{V_{\rm b}}\right) (\varrho_0\varrho_{\rm i})^{1/4}\, e^{(\varrho_{\rm i}-2\varrho_0)/2} \,. \tag{9.133}$$

For $\varrho_{\rm i} - \varrho_0 \geq \varrho_0 \gg 1$ the coalescence time grows exponentially with increasing distance between the two filaments. This behavior is illustrated in figure 9.3, which was obtained through direct numerical integration of the equation of motion (9.120) for $B_0 = B_{\rm b}$, $V_{\rm b} \approx c$ and $\overline{n}_{\rm b} m_{\rm b} \gamma_{\rm b} \gg n_{\rm e} m_{\rm e} h_{\rm e}$.

These calculations imply that the coalescence slows down appreciably as soon as the distance between current filaments exceeds the skin depth of the hot background, $k_{\rm s} d_{\rm i} > 1$. Note that in the simple model of Medvedev et al. [59] the distance between pairwise merging current wires increases as $d_m = 2^m d_0$ after the m-th merger, if the process starts with an initial collection of wires that are separated by a distance d_0. The ratio of the distance between the wires and their radius scales therefore as $d_m/r_m \propto 2^{m/2}$. This means that, as soon as screening currents become important when $k_{\rm s} r_m \sim 1$, the coalescence rate slows rapidly in the following steps of the merger process, and the coalescence of current filaments effectively 'stalls' after a few additional steps.

9.6 Implications for ultra-relativistic shocks

We now consider the implications of the results of the previous sections for the generation of magnetic fields near ultra-relativistic shocks. In particular we discuss the shock transition layer, where the kinetic energy of the incoming ions (with mass $m_{\rm i}$) and electrons (and possibly positrons, both with mass $m_{\rm e}$) is thermalized, creating a relativistically hot plasma. Since we are dealing with a collisionless plasma, the behavior of the ions and electrons must be considered separately.

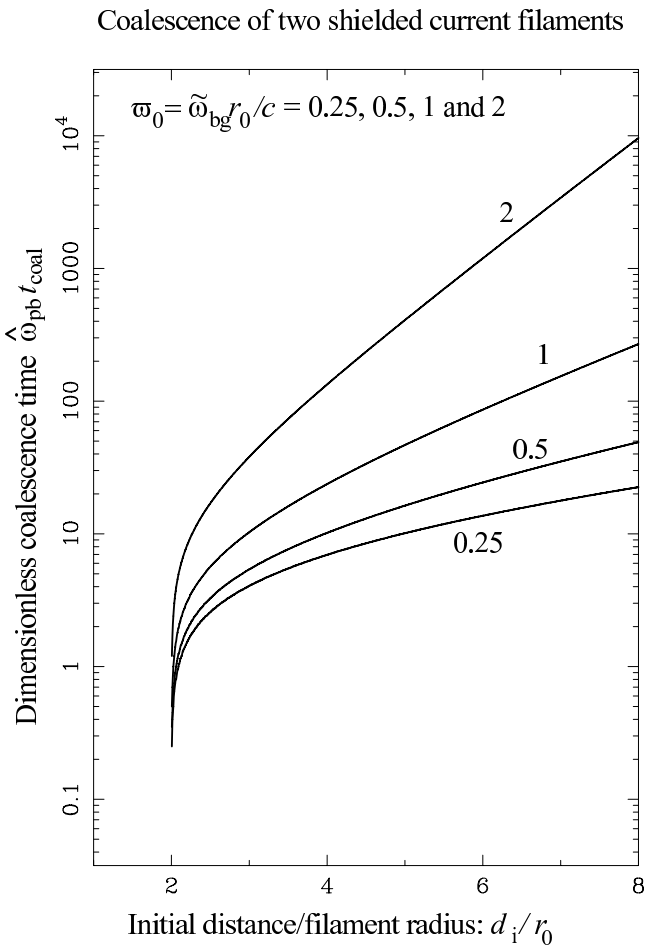

Figure 9.3: The coalescence time, plotted as $\hat{\omega}_{\rm pb}\, t_{\rm coal}$, as a function of the distance between the current wires in units of their radius: $d_{\rm i}/r_0 = \varrho_{\rm i}/\varrho_0$. It is assumed that the beam consists of heavy ions with a current equal to $I_{\rm b}$, so that $B_0 \approx B_{\rm b} \approx B_{\rm tr}$, and that $V_{\rm b} \approx c$. Note that for large distances the coalescence time increases exponentially, in agreement with the asymptotic result of equation (9.133). The figure uses the symbol ϖ_0 for ϱ_0.

9.6.1 Thermalization through the Weibel instability

We first consider the effect of the electron-driven Weibel instability. Simulations (e.g., [24]) show that the electron-driven Weibel instability develops rapidly in a shock transition. The ion-driven instability also occurs, but has a maximum growth rate that is a factor $(\hat{\omega}_{\rm pb})_{\rm e}/(\hat{\omega}_{\rm pb})_{\rm p} \approx \sqrt{m_{\rm p}/m_{\rm e}} \sim 43$ slower than the electron-driven instability. Here we assume a hydrogen plasma with the ion mass equal to the proton mass: $m_{\rm i} = m_{\rm p}$. Incidentally: simulations often use (for computational reasons) a much smaller ion-electron mass ratio, of the order $m_{\rm i}/m_{\rm e} \sim 16$ corresponding to $\sqrt{m_{\rm i}/m_{\rm e}} \sim 4$. Therefore, the difference in the growth rates of the electron- and ion-driven instabilities is not nearly as pronounced in these simulations as in reality.

If the electrons form their own 'subshock', then the shock jump conditions should apply to the electron fluid. For ultra-relativistic shocks, where the incoming flow in the shock frame has a Lorentz factor $\gamma_{\rm sh} \gg 1$ and the incoming electron gas is cold in the sense that $k_{\rm b}T_1 \ll m_{\rm e}c^2$, the relation for the velocity difference $v_{\rm rel} = (v_1 - v_2)(1 - v_1 v_2/c^2)$ between the up- and downstream flow is purely kinematic, cf. Blandford and McKee [8]. The corresponding Lorentz-factor is $\gamma_{\rm rel} \simeq \gamma_{\rm sh}/\sqrt{2}$ with $\gamma_{\rm sh} = 1/\sqrt{1 - v_1^2/c^2}$, independent of the mass of the particles that make up the plasma. It is natural to associate $\gamma_{\rm rel}$ with the beam Lorentz factor $\gamma_{\rm b}$ in the rest of the discussion. For $\gamma_{\rm sh} \gg 1$ proper densities on both sides of the shock are related by $n_2/n_1 \simeq 4\,\gamma_{\rm rel}$, and the downstream temperature T_2 follows from $e_2 \simeq 3P_2 = 3n_2 k_{\rm b} T_2 \simeq \gamma_{\rm rel} n_2 mc^2$, with m the rest mass of the particles involved. For electrons or positrons this implies $k_{\rm b}T_2 \approx \gamma_{\rm rel} m_{\rm e}c^2/3$. Here we have used a subscript 1 (2) to denote the pre-shock (post-shock) state. Below we will take these post-shock values as indicative values for the thermal electron background.

Initially, the electron-driven Weibel instability will proceed almost as in the case of no background, the limit $\eta \gg 1$, or equivalently $(\hat{\omega}_{\rm pb})_{\rm e}^2 \gg \tilde{\omega}_{\rm bg}^2$. This implies that the instability grows over a wide range of wavelengths, with a growth rate $\tilde{\sigma} \simeq (\hat{\omega}_{\rm pb})_{\rm e}$. As the beam(s) get further and further behind the shock front, the quiver motion in the self-generated magnetic field will grow in amplitude, and the electron-driven instability starts to stabilize, starting at the longer wavelengths. The typical amplitude of the magnetic field (equation 9.102) for perturbations with wavelength $\lambda = 2\pi/k$ equals, with $V_{\rm b} \simeq c$

$$B \sim B^{\rm tr} \approx \frac{4\pi e \gamma_{\rm b} n_{\rm e}}{k}\ . \tag{9.134}$$

where $n_{\rm e} \approx n_1$ is the proper density of the electron beams and where we have

put $h_e = 1$ as the electrons are initially cold. The amplitude of the quiver velocity that corresponds with this field amplitude is quite large. From the approximate expression (9.87) with $\tilde{\sigma} = (\hat{\omega}_{pb})_e$ and $V_b \simeq c$ one finds

$$\left(\frac{v_q}{c}\right)_e \sim \frac{(\hat{\omega}_{pb})_e}{\sqrt{2}\,kc} \ , \tag{9.135}$$

which is of order unity for $k \sim (\hat{\omega}_{pb})_e/c$, implying that waves with $k < (\hat{\omega}_{pb})_e/c$ stabilize first. The electron-driven Weibel instability should be capable of completely thermalizing the electrons. The perturbations with $k > (\hat{\omega}_{pb})_e/c$ will continue to grow even when the electron plasma is partially thermalized, with a typical value of the parameter $\eta_e \sim 1$.

The electron beam plasma frequency, and the downstream electron plasma frequency once the electrons are fully thermalized, are similar in magnitude (see also the discussion in chapter 8). We express them in terms of the plasma frequency $\omega_{pe} = \sqrt{4\pi e^2 n_e/m_e}$ of the cold *upstream* electron gas with density $n_1 = n_e$. Using the above shock relations one finds:

$$\left(\hat{\omega}_{pb}\right)_e^2 \simeq \frac{4\pi e^2 n_e}{m_e} = \omega_{pe}^2 \ , \ \left(\tilde{\omega}_{bg}\right)_e^2 = \frac{4\pi e^2 n_2 c^2}{k_b T_2} \simeq 12\,\omega_{pe}^2 \ . \tag{9.136}$$

In view of our discussion in section 9.5.1, these estimates imply that the trapping magnetic field and the Alfvén critical field for electrons are of the same order at a scale comparable to the effective skin depth: $c/(\tilde{\omega}_{bg})_e \sim c/(\hat{\omega}_{pb})_e$. As a result further magnetic field growth due to coalescence of the current filaments created by the electron-driven Weibel instability at a scale $r_0 \simeq c/(\tilde{\omega}_{bg})_e$ will stall after a few mergers because of the exponential increase of the coalescence time, as calculated in section 9.5.5. Filaments created at $r_0 \sim 1/k \ll c/(\tilde{\omega}_{bg})_e$ will merge almost unimpeded, but the scaling laws (9.106) and (9.107) imply that the resulting magnetic field strength at some scale $r > r_0$ is comparable to the magnetic field that was created initially at that scale by the quasi-exponential phase of the Weibel instability. However, the filling factor of the current filaments decreases as merging proceeds further and further.

The ion-driven Weibel instability develops more slowly, and takes place mostly in the hot background of the already thermalized (shocked) electrons. A complication is the fact that there will possibly be strong effects in the transition layer due to electrostatic potentials generated by electron-ion charge separation, and due to a strong overshoot of the compressed magnetic field. We can not treat these effects, but point out that, for typical parameters, magnetic

effects on the Weibel instability are estimated to be small, as discussed in section 6.8.

The ion-driven instability is weak in the sense that $\eta \ll 1$: for a hydrogen plasma one has

$$\eta_{\rm p} = \frac{(\hat{\omega}_{\rm pb})_{\rm p}^2}{(\tilde{\omega}_{\rm bg})_{\rm e}^2} \simeq \frac{m_{\rm e}}{m_{\rm p}} \ll 1 \,. \tag{9.137}$$

The precise numerical constant in front of the electron-proton mass ratio in relation (9.137) is difficult to predict without a complete shock model, but will be of order unity. If one assumes charge neutrality it equals $4/3$. The presence of screening currents in the hot electron background impedes the ion-driven Weibel instability for wavelengths larger than the effective electron skin depth. The screening wavenumber is $k_s = [(\tilde{\omega}_{\rm bg})_{\rm e}/c]\,\kappa_{\rm s}$, where (see chapter 6)

$$\kappa_{\rm s} = \begin{cases} 1 & \text{fluid background model,} \\ \\ \left(\dfrac{\pi}{4}\right)^{1/3} \eta_{\rm p}^{1/6} \approx 0.26 & \text{kinetic background model.} \end{cases} \,. \tag{9.138}$$

In that case relation (9.102) applies, the maximum trapping field in the ion-driven instability occurs at $k \sim k_{\rm s}$, and the typical field amplitude for $k > k_{\rm s}$ (up to factors of order unity) is again given by (equation 9.134), assuming $n_{\rm p} \approx n_{\rm e} \simeq n_1$. This also implies that for protons

$$\left(\frac{v_{\rm q}}{c}\right)_{\rm p} \sim \frac{(\hat{\omega}_{\rm pb})_{\rm p}}{\sqrt{2}\,kc} \leq \frac{\eta_{\rm p}}{\sqrt{2}} \ll 1 \,. \tag{9.139}$$

Unlike what happens with the electrons, the Weibel instability is therefore not capable of *immediately* thermalizing the incoming protons on a scale of a few times $c/(\hat{\omega}_{\rm pb})_{\rm p}$.

A second important difference with the electron-driven case is that the trapping field is smaller than the critical Alfvén field $B_{\rm A}$ for the ions at the same scale, a consequence of the larger ion mass, which makes them more difficult to deflect. One has $B_{\rm A} \sim B^{\rm tr}/\eta_{\rm p}$ at $r_0 \sim c/(\tilde{\omega}_{\rm bg})_{\rm e}$ with $\eta_{\rm p} \ll 1$. This means that merging of ion current filaments, and the associated growth of the magnetic field, is possible in principle. However, the calculations in the preceding section show that, analogous to what happens with the linear ion-driven Weibel instability at wavelengths exceeding the skin depth, further merging is impeded by the screening currents in the (now thermalized) electron background plasma. The merging rate slows down strongly once the radius of the filaments

becomes larger than a few times the plasma skin depth $c/(\tilde{\omega}_{\rm bg})_{\rm e} \simeq c/(\hat{\omega}_{\rm pb})_{\rm e}$. The overall conclusion therefore is that the ion-driven Weibel instability does not generate magnetic fields that are much stronger than the ones already created by the faster electron-driven instability.

9.6.2 Thermalization of protons

Because the ions will thermalize well after the electrons do, the overall width of the shock transition is now determined by the ion thermalization length. To a large extent, the implications of this have already been investigated by Lyubarsky and Eichler [55]. Here we refine their calculation.

Ion thermalization takes place due to scattering in the magnetic fields that have been generated by the electron-driven Weibel instability. This process can be described as diffusion of the direction of flight unit vector $\hat{\mathbf{n}} = \mathbf{p}/p = (n_x\,,\, n_y\,,\, n_z)$, where $\mathbf{p}$ is the proton momentum. The equation of motion for an ultra-relativistic proton with energy E can be written as

$$\frac{{\rm d}\hat{\mathbf{n}}}{{\rm d}s} = \frac{e}{E}\,\left(\hat{\mathbf{n}} \times \mathbf{B}\right)\,. \tag{9.140}$$

Here s is the path length along the orbit of the proton. We neglect the influence of the shock-compressed background magnetic field as the amplitude of the Weibel-generated field is much larger: from relation (9.134) with $k_{\rm s} \sim (\tilde{\omega}_{\rm bg})_{\rm e}/c$ and (9.136) one finds:

$$\frac{B^{\rm tr}}{B_2} \approx \frac{1}{4\sqrt{3}}\,\left(\frac{\omega_{\rm pe}}{\omega_{\rm ce}}\right) = 4.6\times 10^2\,\sqrt{n_{\rm e1}}\,B_1^{-1}(\mu G)\,. \tag{9.141}$$

Here $\omega_{\rm ce} = eB_1/m_{\rm e}c$ is the upstream value of the electron gyrofrequency, where we have used $B_2 = 4\gamma_{\rm rel}B_{\rm t1} \approx 2\gamma_{\rm rel}B_1$ for the strength of the shock-compressed magnetic field.

The vector $\hat{\mathbf{n}}$ will diffuse with a diffusion coefficient $\mathcal{D}_{ij} \equiv \left\langle \Delta n_i \Delta n_j \right\rangle /2\Delta s$, where the angular brackets denote an ensemble average. A standard quasi-linear calculation, which uses the unperturbed (ballistic) particle orbits, leads to a diffusion coefficient of the form

$$D_{ij} = \frac{\pi e^2}{E^2}\,\int \frac{{\rm d}^3\mathbf{k}}{(2\pi)^3}\,\left(\hat{\mathbf{n}}\hat{\mathbf{n}} : \left\langle \tilde{\mathbf{A}}\tilde{\mathbf{A}}^* \right\rangle (\mathbf{k})\right)\,k_i k_j\,\delta(\mathbf{k}\cdot\hat{\mathbf{n}})\,. \tag{9.142}$$

The dyadic correlation tensor $\left\langle \tilde{\mathbf{A}}\tilde{\mathbf{A}}^* \right\rangle$ in this expression is the correlation tensor of the Fourier components of the vector potential $\tilde{\mathbf{A}}$. The Fourier components

of the vector potential and of the turbulent magnetic field are related in the usual manner: $\tilde{\mathbf{B}} = i\mathbf{k} \times \tilde{\mathbf{A}}$. The correlation tensor follows from the random phase approximation [e.g. 17, p. 135] for the ensemble average of the turbulent fields:

$$\left\langle \tilde{\mathbf{A}}(\mathbf{k}) \tilde{\mathbf{A}}^*(\mathbf{k}') \right\rangle = \left\langle \tilde{\mathbf{A}} \tilde{\mathbf{A}}^* \right\rangle (\mathbf{k}) (2\pi)^3 \, \delta^3(\mathbf{k} + \mathbf{k}') \; . \tag{9.143}$$

Beam protons initially have $\hat{\mathbf{n}} \approx \hat{\mathbf{z}}$. In that case the only non-vanishing components of the diffusion tensor D_{ij} are $D_{xx} = D_{yy} = D_0$, if we assume that the magnetic turbulence is axisymmetric around the beam direction. The scalar diffusion coefficient D_0 equals

$$D_0 = \frac{\pi e^2}{2E^2} \int_0^\infty \frac{\mathrm{d}k_\perp k_\perp}{(2\pi)^2} \left\langle \tilde{\mathbf{A}} \tilde{\mathbf{A}}^* \right\rangle_{zz} (k_\perp \, , \, k_\parallel = 0) \, k_\perp^2 \; . \tag{9.144}$$

Here $k_\perp = \sqrt{k_x^2 + k_y^2}$ is the wave vector component perpendicular to the beam direction, and $k_\parallel = k_z$ the component along the beam direction. The trivial integration over $k_\parallel$ has been performed, using $\delta(\mathbf{k} \cdot \hat{\mathbf{n}}) = \delta(k_\parallel)$.

So far, we have considered the Weibel instability in the limit $k_\parallel = 0$. In that case the quasilinear diffusion approximation for the direction of flight $\hat{\mathbf{n}}$ does *not* apply, as the unperturbed orbit never leaves a single current filament. Fortunately, the assumption $k_\parallel = 0$ can be relaxed, as the Weibel instability persists for $k_\parallel \neq 0$. The theory in this case is rather complicated, see for instance the discussion in [10]. An approximate calculation (not reproduced here) shows that the dispersion relation for $|k_\parallel| \ll k_\perp$ leads to a dimensionless growth rate for $\kappa \ll \kappa_{\max}$ (compare equation 9.7):

$$\sigma^2 \approx \frac{\eta \kappa^2 \sin^2 \theta}{\kappa_\mathrm{s}^2 + \kappa^2} - 3\kappa^2 \cos^2 \theta \; . \tag{9.145}$$

Here $\sin\theta = k_\perp / k$, $\cos\theta = k_\parallel / k$. The growth rate will be reduced well below the value for $\theta = \pi/2$, $\sin\theta = 1$ when $\tan^2\theta \simeq 3\,(\kappa^2 + \kappa_\mathrm{s}^2)/\eta \sim 6/\eta$, where the last equality is for $\kappa \approx \kappa_\mathrm{s} \simeq 1$. For the electron-driven instability one has (at least initially) $\eta_\mathrm{e} \approx 1$, and the instability will act with a growth rate close to the maximum value for wavevectors inclined at an angle $\theta > 68$ degrees with the beam direction. This corresponds with $|\cos\theta| \leq 0.37 \equiv \cos\theta_\mathrm{c}$.

A simple model for the turbulent power spectrum of the Weibel-generated magnetic field is

$$\left\langle |\tilde{\mathbf{B}}|^2 \right\rangle (\mathbf{k}) = k_\perp^2 \, \left\langle \tilde{\mathbf{A}} \tilde{\mathbf{A}}^* \right\rangle_{zz} (k_\perp \, , \, k_\parallel) = (2\pi)^2 \, \mathcal{B}(k_\perp) \, \frac{L_\parallel \, e^{-k_\parallel^2 L_\parallel^2 / 2}}{\sqrt{2\pi} k_\perp} \; . \tag{9.146}$$

Here $L_\parallel$ is the correlation length of the magnetic turbulence in the beam direction, corresponding to a bandwidth $\Delta|k_\parallel| = 1/L_\parallel$. The case $k_\parallel = 0$ corresponds with the limit $L_\parallel \longrightarrow \infty$. With this definition the rms amplitude of the turbulent magnetic field follows from:

$$B^2_{\rm rms} = \int \frac{{\rm d}k_\parallel {\rm d}k_\perp k_\perp}{(2\pi)^2} \left\langle |\tilde{\mathbf{B}}|^2 \right\rangle (k_\perp\,,\, k_\parallel) = \int_0^\infty {\rm d}k_\perp \mathcal{B}(k_\perp)\,. \tag{9.147}$$

The power spectrum $\mathcal{B}(k_\perp)$ can be calculated by noting that the trapping field $B^{\rm tr}(k)$ (see equation 9.102) at some wavenumber $k_\perp$ is related to the magnetic power spectrum $\mathcal{B}(k_\perp)$ by $(B^{\rm tr}(k \simeq k_\perp))^2 \approx k_\perp\, \mathcal{B}(k_\perp)$. This yields for $k_\perp \ll k_{\rm max}$:

$$\mathcal{B}(k_\perp) = \frac{B_0^2}{k_{\rm s}} \frac{k_\perp/k_{\rm s}}{\left(1+(k_\perp/k_{\rm s})^2\right)^2}\,. \tag{9.148}$$

Here we define

$$B_0 = \frac{4\pi e \gamma_{\rm b} n_{\rm e}}{k_{\rm s}} \tag{9.149}$$

with $n_{\rm e}$ the density of the electron beam and $k_{\rm s} = \kappa_{\rm s}(\tilde{\omega}_{\rm bg})_{\rm e}/c$ the screening wave number. It is easy to show that this spectrum has $B^2_{\rm rms} = B_0^2/2$. This spectrum falls of as $\mathcal{B}(k_\perp) \propto k_\perp^{-3}$ for $k_\perp \gg k_{\rm s}$, so the restriction $k_\perp < k_{\rm max}$ is not very important for the evaluation of integrals over the power spectrum as long as $k_{\rm s} \ll k_{\rm max}$.

Using this magnetic power spectrum in expression (9.144) for the scalar diffusion coefficient one finds:

$$D_0 = \frac{\sqrt{\pi} L_\parallel}{2\sqrt{2}} \int_0^\infty {\rm d}k_\perp\, \mathcal{B}(k_\perp) = \frac{\sqrt{\pi}}{4\sqrt{2}} \left(\frac{eB_0}{E}\right)^2 L_\parallel\,. \tag{9.150}$$

One sees from this expression that $L_\parallel = 1/\Delta|k_\parallel|$ plays the role of a correlation length. It also shows, as argued above, that the limit $k_\parallel = 0$, $L_\parallel = \infty$ is formally ill-defined.

If we define a gyroradius $r_{\rm g} = E/eB_0$ one has:

$$D_0 = \frac{\sqrt{\pi}}{4\sqrt{2}} \frac{L_\parallel}{r_{\rm g}^2}\,. \tag{9.151}$$

Lyubarsky and Eichler [55] arrive at a similar expression, in effect putting $L_\parallel \sim 1/k_{\rm s}$ and neglecting the numerical constant. In view of our discussion above

of the behavior of the Weibel instability for $\theta < \pi/2$ the obvious choice for $L_\parallel$ is

$$L_\parallel \sim \frac{1}{k_\mathrm{s} \cos\theta_\mathrm{c}} \approx \frac{2.65}{k_\mathrm{s}} \,. \tag{9.152}$$

Here we use the fact that the largest contribution to the integral over the power spectrum comes from the region $k_\perp \simeq k_\mathrm{s}$. This gives

$$D_0 = 0.83 \left(\frac{r_\mathrm{sk}}{r_\mathrm{g}^2} \right) \,, \tag{9.153}$$

with $r_\mathrm{sk} = 1/k_\mathrm{s}$ the effective skin depth of the hot electron background, which according to (9.136) equals

$$r_\mathrm{sk} \simeq \frac{c}{(\tilde{\omega}_\mathrm{bg})_\mathrm{e}} = \frac{1}{2\sqrt{3}} \frac{c}{\omega_\mathrm{pe}} \,. \tag{9.154}$$

As protons are scattered by the random fields the components of the direction of flight satisfy [cf. 4]

$$\left\langle n_x^2 \right\rangle = \left\langle n_y^2 \right\rangle \approx 2\mathcal{D}_0 s \;\;,\;\; \left\langle n_z^2 \right\rangle \approx 1 - 4\mathcal{D}_0 s \,, \tag{9.155}$$

where the brackets indicate an average over the distribution. This shows that the thermalization length is

$$\ell_\mathrm{th} = \frac{1}{6\mathcal{D}_0} \simeq 0.2 \left(\frac{r_\mathrm{g}^2(E)}{r_\mathrm{sk}} \right) \,, \tag{9.156}$$

the distance where according to (9.155) one has $\langle n_x^2 \rangle = \left\langle n_y^2 \right\rangle = \langle n_z^2 \rangle = 1/3$, corresponding to an isotropic distribution of momenta. The more precise theory in Achterberg et al. [4] shows that ℓ_th is indeed the relevant length scale: the initial correlation of the momentum direction of the beam particles decays with distance s due to scattering as $\exp(-6D_0 s)$.

Using (9.149) with $k_\mathrm{s} \simeq (\tilde{\omega}_\mathrm{bg})_\mathrm{e}/c \simeq 2\sqrt{3}\,\omega_\mathrm{pe}/c$ (as $\kappa_\mathrm{s} \simeq 1$ in the electron-driven instability) one has for beam protons with energy $E \simeq \gamma_\mathrm{b} m_\mathrm{p} c^2$:

$$r_\mathrm{g} \simeq \frac{m_\mathrm{p} c^2 k_\mathrm{s}}{4\pi e^2 n_\mathrm{p}} = \frac{c\,(\tilde{\omega}_\mathrm{bg})_\mathrm{e}}{(\hat{\omega}_\mathrm{pb})_\mathrm{p}^2} \simeq 2\sqrt{3} \left(\frac{m_\mathrm{p}}{m_\mathrm{e}} \right) \frac{c}{\omega_\mathrm{pe}} \,. \tag{9.157}$$

Here $n_{\rm p}$ is the density of beam protons, which equals $n_{\rm e}$ because of quasi-neutrality in the upstream flow, and we have used relation (9.136). This gives the proton thermalization length in terms of the upstream electron skin depth:

$$\ell_{\rm th}^{\rm p} = 8.3 \left(\frac{m_{\rm p}}{m_{\rm e}}\right)^2 \frac{c}{\omega_{\rm pe}} \simeq 1.5 \times 10^{13} n_{\rm e}^{-1/2} \text{ cm}. \tag{9.158}$$

Apart from the numerical factor ~ 8, this is the same result as derived by Lyubarsky and Eichler [55].

9.7 Conclusions

In this chapter we have presented two detailed non-linear calculations of the Weibel instability in the ultra-relativistic limit. The first uses a relativistic fluid approximation to calculate the response of the beam particles, while the second uses kinetic plasma theory for the beam plasma. Although the physics of the two calculations is subtly different, pertaining respectively to the case of a single dominant mode where wave breaking occurs and to fake diffusion in a broad-band collection of waves due to the quiver motion that 'heats' the beam plasma in the plane perpendicular to the beam direction, these calculations both confirm that the Weibel instability due to relativistic beams will end the phase of exponential growth when particle trapping occurs, i.e. when the amplitude of the quiver motion, driven by the Lorentz force of the wave-generated magnetic field, becomes comparable with the wavelength of the unstable modes. A similar conclusion was reached by Davidson et al. [16] for the Weibel instability in a non-relativistic plasma with a temperature anisotropy, by Yang et al. [104] for the Weibel instability in a magnetized electron-positron plasma, and our results also confirm the estimate of Gruzinov [31] (see also chapter 8) for this particular case. This means that the typical field strength at the end of the quasi-exponential phase of the instability is independent of the mass of the beam particles in a hydrogen plasma. The fast electron-driven Weibel instability creates a field that is approximately two orders of magnitude larger than the shock-compressed magnetic field, see equation (9.141). Its value is set by the skin depth (inertial length) $c/\omega_{\rm pe}$ and density of the upstream electron plasma, $B \sim \pi e n_{\rm e}(c/\omega_{\rm pe})$, *independent* of the shock Lorentz factor. The slower proton-driven instability is impeded by the presence of the now thermalized post-shock electron gas. The trapping argument shows that the typical field strength associated with this instability is of the same order as the field generated by the electron-driven instability: the electron screening

currents result in a the trapping field that is independent of the mass of the beam particles driving the instability.

We have also considered the subsequent evolution of the magnetic fields generated by the Weibel instability. We point out that the merging of current filaments [as proposed by 59] and the associated algebraic growth of the magnetic field associated with these filaments, is slowed down drastically by the effects of screening currents once the the transverse size of the filaments and the filament-filament separation distance becomes comparable with, or larger than with the electron skin depth. The coalescence time increases exponentially as the merged filaments are further and further apart. This limits any further field amplification (or decay) at scales larger than the skin depth. At smaller scales, the merging is essentially unimpeded, but the resulting magnetic field at some scale r has an amplitude comparable to the trapping field left behind by the Weibel instability at that scale. Therefore, the magnetic field strength never grows much beyond the trapping field.

We have used our results to calculate the effect of the magnetic turbulence on the ion beams that, in contrast to what happens to the electrons, are not *directly* thermalized by the Weibel instability. This happens indirectly, not through phase-mixing of the quiver motion, but by the slow scattering on the turbulent magnetic fields. Our calculation of the thermalization length confirms the basic idea of [55], albeit with a thermalization length that is one order of magnitude larger than their value.

Chapter 10

Computer simulations of the Weibel instability

To improve our understanding of the theoretical processes discussed in the previous chapters we have simulated the behavior of the charged particles in the Weibel instability with the help of computers. The simulations show how the Weibel instability causes the magnetic field strength to grow exponentially, stopping when the particles become trapped in the magnetic field. The simulations also show how the electrical currents continually merge to become larger and stronger and how the plasma shields the currents when they become strong. This supports the theory presented in the previous chapters.

This chapter will be submitted to Astronomy & Astrophysics [101].

10.1 Introduction

This chapter describes Particle-In-Cell (PIC) computer simulations of the evolution of the relativistic Weibel instability driven by two (symmetric) relativistic beams. The simulations consider the evolution of this instability in a 1D2V approach, where variations in one spatial dimension (x), transverse to the beam direction, are considered for a plasma with a two-dimensional momentum distribution, with momentum components p_x (p_z) transverse (along) the direction of the beams. We consider the linear properties of the beam-driven Weibel instability for this configuration, and show that its properties are virtually the same as in the fully three-dimensional case.

The beam-driven Weibel instability (or filamentation instability) is an important process in the shock front of relativistic collisionless shock waves [58, 9]. The mixing of pre- and post-shock plasma in collisionless shock fronts produces a plasma with an anisotropic velocity distribution. Such distributions are known to be unstable to the spontaneous generation of transverse electromagnetic waves [98].

The Weibel instability leads to filamentary, charge-separated electrical current channels that initially grow exponentially in strength. The exponential growth is terminated when wave braking and particle trapping in the wave-generated magnetic field occur (see chapter 9). After the exponential phase, the current channels merge to form larger units [52].

This merging process increases the transverse size of the current channels, amplifies the associated magnetic field and thereby suppresses diffusion of the magnetic field [59]. However, when the instability takes place in a stationary thermal background plasma, the background tends to shield the current channels and suppresses the merging process when the length scale grows beyond the skin depth of the background plasma, see the discussion in chapter 9. This is particularly important when one considers the instability in the shock transition layer of an electron-proton plasma: the Weibel instability in the electron component grows much faster than the proton-driven instability. As a result, the directed momentum of the electron beams is thermalized, and the electrons quickly form a very responsive quasi-thermal background plasma. The thermal electron background will lower the amplitude of the magnetic field that the slower proton-driven instability generates (see chapters 8 and 9). In this article we present a number of 1D2V PIC simulations to test and confirm the analytical estimates derived from instability theory in previous analytical models (chapter 9).

We note that a number of groups have reported fully two- and three-dimen-

sional computer simulations of the processes described in this article [21, 24, 69]. Such 2D and 3D simulations include phenomena, in particular turbulent behavior, that is suppressed by the one-dimensional nature of the simulations we present below. The primary goal of our simulations is not to provide a complete description of the long-term behavior of a realistic plasma, but to make it easier to compare simulation results with the analytical estimates for the behavior immediately following the phase of exponential growth, and so to confirm the underlying theory.

10.2 The simulated system

Our code computes the evolution of transverse perturbations in a collisionless plasma that contains both a hot background and two counterstreaming beams of particles. We allow the perturbations to be inhomogeneous in the direction perpendicular to the direction of propagation of the beams. In this situation the Weibel instability is purely electromagnetic, and involves growing transverse waves with a wave vector perpendicular to the direction of propagation of the beams: $\mathbf{E} \perp \mathbf{B}$ and $\mathbf{k} \cdot \mathbf{E} = 0$, with $\mathbf{k}$ the wave vector (see chapter 6). In the non-linear stage of the instability, there is a longitudinal component of electric field along $\mathbf{k}$.

In the unperturbed state, two homogeneous counterstreaming beams of charged particles travel along the z-direction through a background of stationary particles. When the motion of the beam particles is perturbed, the resulting charge density perturbations (charge bunching) lead to an advection current J_z^{adv} due to the bulk motion in the z-direction. This current perturbation will be the source for a magnetic field perturbation in the direction perpendicular to both the propagation direction of the beams and the direction of inhomogeneity.

We will assume that the perturbations vary along the x-direction, and that the magnetic field points in the y-direction. Consequently the electric field is in the x–z plane. We use a finite grid, and assume periodic boundary conditions in the x-direction in order to simulate a much larger plasma.

10.3 Basic equations

Consider a particle with velocity $\mathbf{v}$ and charge q, moving in an electric field $\mathbf{E}$ and a magnetic field $\mathbf{B}$. The particle position $\mathbf{r}$ and momentum $\mathbf{p}$ will evolve

according to:

$$\begin{aligned} \frac{\mathrm{d}\mathbf{r}}{\mathrm{d}t} &= \mathbf{v}, \\ \frac{\mathrm{d}\mathbf{p}}{\mathrm{d}t} &= q\big(\mathbf{E} + \frac{\mathbf{v}}{c} \times \mathbf{B}\big), \end{aligned} \tag{10.1}$$

where $\mathbf{v} = \mathbf{p}/\gamma m$ with $\gamma = (1 + |\mathbf{p}|^2/m^2c^2)^{1/2}$ the Lorentz factor, and m is the particle mass. In our configuration the momentum equations are

$$\begin{aligned} \frac{\mathrm{d}p_x}{\mathrm{d}t} &= q\big(E_x - \frac{v_z}{c}B_y\big), \\ \frac{\mathrm{d}p_y}{\mathrm{d}t} &= 0, \\ \frac{\mathrm{d}p_z}{\mathrm{d}t} &= q\big(E_z + \frac{v_x}{c}B_y\big). \end{aligned} \tag{10.2}$$

For simplicity, and without the loss of generality, we will assume that $p_y = 0$ in what follows.

The electric and magnetic fields follow from Maxwell's equations, with the charge and current densities in the system acting as a source for the fields. The charge and current density have contributions from the beam particles, as well as from any background plasma:

$$\begin{aligned} \rho_{\mathrm{tot}} &= \rho_{\mathrm{bg}} + \sum_i \rho_i \ , \\ \mathbf{J}_{\mathrm{tot}} &= \mathbf{J}_{\mathrm{bg}} + \sum_i \mathbf{J}_i \ , \end{aligned} \tag{10.3}$$

where the sum is taken over all beam particles with each particle contributing (*e.g.*, [41], equation 12.138)

$$\begin{aligned} \rho_i(\mathbf{x}, t) &= q\, \delta(\mathbf{x} - \mathbf{r}_i(t)), \\ \mathbf{J}_i(\mathbf{x}, t) &= q\mathbf{v}_i(t)\, \delta(\mathbf{x} - \mathbf{r}_i(t)). \end{aligned} \tag{10.4}$$

We denote the average density of simulated beam particles with n_0, and use a static neutralizing background so that the total charge density vanishes in the unperturbed system: $\rho_{\mathrm{bg}} = -qn_0$. We will assume that this neutralizing static background consists of very heavy (unresponsive) ions.

We will initialize the plasma in such a way that the average initial current density associated with the beams vanishes, so the background current

satisfies $\mathbf{J}_{\rm bg} = 0$. For our assumed geometry one has $\mathbf{E} = (E_x, 0, E_z)$ and $\mathbf{B} = (0, B_y, 0)$, and the full set of Maxwell's equations reduces to:

$$\frac{\partial E_x}{\partial x} = 4\pi\,\rho_{\rm tot}, \tag{10.5}$$

$$\frac{\partial B_y}{\partial x} - \frac{1}{c}\frac{\partial E_z}{\partial t} = \frac{4\pi}{c}\,J_{z,\rm tot}, \tag{10.6}$$

$$-\frac{\partial E_z}{\partial x} + \frac{1}{c}\frac{\partial B_y}{\partial t} = 0. \tag{10.7}$$

10.4 Particle in Cell method

We wish to investigate the behavior of the velocity distribution of the particles in a Weibel-unstable plasma. To that end we employ a Particle-In-Cell method [78, chapter 6], which computes the collective behavior of a plasma by describing the interaction of the particles in the plasma with the *average* electromagnetic fields on a grid, with (on average) many particles residing in each grid cell. In this approach, the position and momentum of the particles is calculated by solving the equation of motion (10.1). The charge and current densities are then calculated from the resulting distribution of particles and their velocities over the finite number of grid cells. This approach neglects the close (two-particle) interactions of the charges, but it is a valid approximation for a nearly collisionless plasma when the Coulomb collision time scale of the plasma is much longer than the duration of the simulation, and for phenomena occurring on a length scale that is larger than the Debye length of the plasma. The number of equations computed in such a simulation scales with the number of particles as N, instead of N^2 as is the case in a direct N-body calculation.

Limitations and strengths of this computational approach are discussed in [78]. In summary: the finite resolution of the grid on which we compute the electromagnetic fields and the finite time step used to compute the evolution of the system introduce numerical errors, which we minimize by taking small time steps and by using a sufficiently fine grid that resolves the typical wavelength of the instability. A more serious source of errors arises from the fact that the number of particles that we can include in the computation is much smaller than in a realistic plasma. Apart from statistical errors (noise), this usually means that the number of particles within a Debye sphere is not nearly as large as in real plasmas (typically one hundred instead of a hundred thousand). One consequence of this is that the effective Coulomb collision time scale of the simulated system is considerably shorter than the real collision time

scale. This must be taken into account in determining the maximum useful duration of the simulation.

The Appendix contains the details of our implementation of the simulation method.

10.5 Weibel instability theory

One of the goals of the code is to compare the behavior of the computed system to analytical estimates for the behavior of the system of beams and background plasma. In this section we will discuss how this system responds to small perturbations, based on a linearization of the governing equations presented in section 10.2.

We expect the Weibel instability to dominate the behavior of the plasma. The Weibel instability is a low-frequency ($\omega \ll kc$) transverse instability that occurs in plasmas with an anisotropic velocity distribution [98]. The associated electromagnetic field is mainly transverse and is dominated by the magnetic field, with field amplitudes scaling as $|B_y| \gg |E_z| \gg |E_x|$.

We will describe the electromagnetic fields using a scalar potential $\Phi(x,t)$, and the z-component of the vector potential $\mathbf{A}$: $A_z \equiv A(x,t)$. One has:

$$E_x = -\frac{\partial \Phi}{\partial x}, \qquad E_z = -\frac{1}{c}\frac{\partial A}{\partial t}, \qquad B_y = -\frac{\partial A}{\partial x}. \tag{10.8}$$

This way, Maxwell's equations reduce to:

$$\frac{\partial^2 \Phi}{\partial x^2} = -4\pi\rho, \tag{10.9}$$

$$\frac{\partial^2 A}{\partial x^2} - \frac{1}{c^2}\frac{\partial^2 A}{\partial t^2} = -\frac{4\pi}{c} J, \tag{10.10}$$

with J the z-component of the current density.

We will split the linear response into Fourier modes, e.g., for a physical quantity $A(x\,,\,t)$ we write

$$A(x\,,\,t) \rightarrow A_0 + \sum_k \tilde{A}(\omega\,,\,k)\,\exp(ikx - i\omega t)\,, \tag{10.11}$$

with $\tilde{A}(\omega\,,\,k)$ the corresponding Fourier amplitude, which satisfies $|\tilde{A}(\omega,k)| \ll |A_0|$, and $\sum_k$ a short-hand notation for a full Fourier integral. Unperturbed quantities are uniform and stationary: they satisfy $\partial A_0/\partial t = \partial A_0/\partial x = 0$. This implies $\partial A/\partial t \rightarrow -i\omega\,\tilde{A}$ and $\partial A/\partial x \rightarrow ik\,\tilde{A}$ in the Fourier domain.

The electromagnetic response of the plasma must satisfy equation (10.10):

$$\left(\frac{\omega^2}{c^2} - k^2\right)\,\tilde{A} = -\frac{4\pi}{c}\,\left(\tilde{J}_{\rm b} + \tilde{J}_{\rm bg}\right)\,, \tag{10.12}$$

where we have split the current density in contributions from the beams and the background. We will derive expressions for these contributions in the next two sections.

To describe the collective collisionless behavior of the simulated particles we will use a Vlasov approach. Let $f(\mathbf{p}\,,\,x\,,\,t)\,\mathrm{d}x\,\mathrm{d}p_x\,\mathrm{d}p_z$ be the fraction of particles in an infinitesimal volume of phase space around spatial coordinate x and momentum $\mathbf{p} = (p_x, p_z)$ (we will not need to consider the y-momentum). This distribution is normalized such that $\int \mathrm{d}^2p\, f(\mathbf{p}\,,\,x\,,\,t) = 1$. The Vlasov equation describes conservation of particles in phase space corresponding to the equations of motion (10.2)

$$\frac{\partial f}{\partial t} + v_x\,\frac{\partial f}{\partial x} + q\left(E_x - \frac{v_z}{c}\,B_y\right)\,\frac{\partial f}{\partial p_x} + q\left(E_z + \frac{v_x}{c}\,B_y\right)\,\frac{\partial f}{\partial p_z} = 0. \tag{10.13}$$

We can calculate the charge density (ρ) and the z-component of the current density (J) from f, given the number density n of the particles involved:

$$\begin{aligned} \rho(x\,,\,t) &= qn\int \mathrm{d}^2p\, f(\mathbf{p}\,,\,x\,,\,t) \\ J(x\,,\,t) &= qn\int \mathrm{d}^2p\, v_z f(\mathbf{p}\,,\,x\,,\,t)\ . \end{aligned} \tag{10.14}$$

We will separate the calculation for the stationary background plasma (which contributes a term $f_{\rm bg}$) and for the beams (which contribute a term $f_{\rm b}$).

Linearizing the Vlasov equation (10.13) and going to the Fourier-domain one obtains:

$$\tilde{f} = -\frac{qk}{\omega - kv_x}\,\left(\tilde{\Phi} - \frac{v_z}{c}\,\tilde{A}\right)\,\frac{\partial f_0}{\partial p_x} + \frac{q\tilde{A}}{c}\,\frac{\partial f_0}{\partial p_z}. \tag{10.15}$$

In the configuration considered here the linear stage the Weibel instability is purely electromagnetic, and $\tilde{\Phi} = 0$.

If one calculates the current perturbation $\tilde{J} = qn\int \mathrm{d}^2p\, v_z\tilde{f}$, and substitutes the resulting expression into (10.12), one finds that the reduced (linear) Maxwell equation becomes

$$\left[\omega^2 - k^2c^2 - \alpha_{zz}(\omega\,,\,k)\right]\,\tilde{A} = 0\,. \tag{10.16}$$

Here $\alpha_{zz} = -(4\pi c)\tilde{J}/\tilde{A}$ is the relevant component of the *polarization tensor* (see [62], [61], and also the discussion in chapter 6, in particular the Appendix of that chapter, where the same quantity is denoted by α_{33}). The Vlasov equation implies that it must satisfy

$$\alpha_{zz}(\omega\,,\,k) = -4\pi q^2 n \int \mathrm{d}^2 p\, v_z \left\{ \frac{k v_z}{\omega - k v_x} \frac{\partial f_0}{\partial p_x} + \frac{\partial f_0}{\partial p_z} \right\} . \tag{10.17}$$

In a multi-species plasma (the case considered here) one must sum over all species, $\alpha_{zz} \rightarrow \sum_s \alpha^s_{zz}$, where the index s enumerates the different species in the mixture.

10.5.1 Linear response of the beam particles

We model the beam configuration with the following momentum distribution (normalized to unity):

$$\begin{aligned} f_{\mathrm{b}0} \quad = \quad & \frac{\delta(p_y)}{4p_{\mathrm{th}}} \left[\{\delta(p_z - p_{\mathrm{b}}) + \delta(p_z + p_{\mathrm{b}})\} \times \right. \\ & \left. \{\Theta(p_x + p_{\mathrm{th}}) - \Theta(p_x - p_{\mathrm{th}})\} \right] . \end{aligned} \tag{10.18}$$

Here $\Theta(x) \equiv (1 + x/|x|)/2$ is the Heaviside step function. This so-called *waterbag distribution* (see for instance [21]) is mathematically convenient, and captures all the essential physics of the beam: the bulk motion of beam particles with associated momentum p_{b} defines a dimensionless drift velocity $u_{\mathrm{b}} \equiv p_{\mathrm{b}}/\gamma_0 m_{\mathrm{b}} c$, and the velocity dispersion along the wave vector due to the top-hat distribution with $|p_x| \leq p_{\mathrm{th}}$ defines the quantity $u_{\mathrm{th}} \equiv p_{\mathrm{th}}/\gamma_0 m_{\mathrm{b}} c$, where m_{b} is the mass of the beam particles and

$$\gamma_0 \equiv \sqrt{1 + \frac{p_{\mathrm{b}}^2 + p_{\mathrm{th}}^2}{m_{\mathrm{b}}^2 c^2}} = \frac{1}{\sqrt{1 - u_{\mathrm{b}}^2 - u_{\mathrm{th}}^2}} . \tag{10.19}$$

Substituting the beam distribution (10.18) in equations (10.15) and (10.14), we find the current density due to the beam and calculate the contribution of the beam to the polarization tensor:

$$\alpha^{\mathrm{b}}_{zz} = \hat{\omega}^2_{\mathrm{pb}} \left\{ \mathcal{G}(u_{\mathrm{b}}\,,\,u_{\mathrm{th}}) + \frac{k^2 c^2 u_{\mathrm{b}}^2}{\omega^2 - k^2 c^2 u_{\mathrm{th}}^2} \right\} , \tag{10.20}$$

where $n_{\rm b}$ is the number density of the beam particles,

$$\hat{\omega}_{\rm pb}^2 = \frac{4\pi q^2 n_{\rm b}}{\gamma_0 m_{\rm b}} \tag{10.21}$$

is the beam plasma frequency squared, and

$$\begin{aligned} \mathcal{G}(u_{\rm b}\,,\,u_{\rm th}) &\equiv \gamma_0 \int \frac{{\rm d}^2 p}{\gamma} \left(1 - \frac{{v_z}^2}{c^2}\right) f_{\rm b0} \\ &= \frac{1}{2u_{\rm th}} \ln\left(\frac{1+u_{\rm th}}{1-u_{\rm th}}\right) - \frac{\gamma_0^2 u_{\rm b}^2}{1+\gamma_0^2 u_{\rm b}^2} \\ &= \frac{1}{2u_{\rm th}} \ln\left(\frac{1+u_{\rm th}}{1-u_{\rm th}}\right) - \frac{u_{\rm b}^2}{1-u_{\rm th}^2}\ . \end{aligned} \tag{10.22}$$

This function follows from the term involving $\partial f_0/\partial p_z$ in expression (10.17), after partial integration with respect to p_z, and using $\partial v_z/\partial p_z = (1/\gamma m)(1 - v_z^2/c^2)$.

10.5.2 Linear response of the background particles

Because the background particles have an isotropic distribution with no bulk velocity the easiest approach to calculate their linear response to electromagnetic perturbations is to use a fluid description. From standard linear theory (chapter 6) we know that the linear current density perpendicular to **k** is given by

$$\tilde{J}_{\rm bg} = -\frac{\omega_{\rm p,fl}^2}{4\pi c}\,\tilde{A}, \tag{10.23}$$

where $\omega_{\rm p,fl}$ is the relativistic plasma frequency in the fluid model:

$$\omega_{\rm p,fl}^2 = \frac{4\pi q^2\, n_{\rm bg}}{h_{\rm bg} m}\ . \tag{10.24}$$

Here $n_{\rm bg}$ is the density of the background and $h_{\rm bg}$ is the enthalpy per unit mass, which is given by

$$h_{\rm bg} = 1 + \frac{e+P}{n_{\rm bg} m c^2}\ , \tag{10.25}$$

with P the pressure and e the internal (thermal) energy of the background plasma. For an N-dimensional Maxwellian plasma with temperature T, in the ultra-relativistic limit $k_b T \gg mc^2$, one has $e = NP = Nn_{bg}k_b T$ and $h_{bg} \approx (N+1)k_b T/mc^2$. In that case the plasma frequency (10.24) in the fluid approximation becomes:

$$\omega_{p,fl}^2 \approx \frac{4\pi q^2 n_{bg} c^2}{(N+1)\, k_b T} \,. \tag{10.26}$$

In this model the polarization α_{zz} is constant:

$$\alpha_{zz}^{fl} = \omega_{p,fl}^2 \,. \tag{10.27}$$

The simple fluid approach does not take account of the effect of the large velocity dispersion of the background plasma (in particular of the electrons or positrons) that arises when the background becomes relativistically hot, e.g., [55]. To take these effects into account we will use kinetic theory for the background plasma. In chapter 6 we found for the three-dimensional Weibel instability that the difference between the two approaches is small. Here we briefly derive the corresponding results for a two-dimensional thermal background plasma.

In the two-dimensional case considered here one can use a two-dimensional ultra-relativistic Maxwellian distribution, approximating the particle energy by $\mathcal{E} \approx pc$, which is

$$f_{bg0}^{Maxw}(p) = \frac{1}{2\pi \left(p_{bg}^{th}\right)^2} e^{-p/p_{bg}^{th}} \,. \tag{10.28}$$

Here $p = \sqrt{p_x^2 + p_y^2}$, and

$$p_{bg}^{th} \equiv k_b T/c \tag{10.29}$$

is the typical thermal momentum, with T the temperature of the background plasma and k_b Boltzmann's constant. In that case the background contribution to α_{zz} for a purely growing mode, with $\omega = i\tilde{\sigma}$ equals:

$$\alpha_{zz}^{bg} = \tilde{\omega}_{pbg}^2 \left(\frac{\tilde{\sigma}}{kc}\right) \left[\sqrt{1 + \frac{\tilde{\sigma}^2}{k^2c^2}} - \frac{\tilde{\sigma}}{kc}\right] \,. \tag{10.30}$$

The background plasma frequency squared in this case equals

$$\tilde{\omega}_{pbg}^2 = \frac{4\pi q^2 n_{bg} c}{p_{bg}^{th}} = \frac{4\pi q^2 n_{bg} c^2}{k_b T} \,. \tag{10.31}$$

In the simulations we use, for computational convenience, a two-dimensional Gaussian momentum distribution for the background particles of the form

$$f_{\rm bg0}(p) = \frac{1}{2\pi(p_{\rm bg}^{\rm th})^2}\,\exp\Big(-(p/2p_{\rm bg}^{\rm th})^2\Big)\,, \tag{10.32}$$

This distribution leaves the functional form (10.30) of $\alpha_{zz}^{\rm bg}(\tilde{\sigma}\,,\,k)$ unchanged, and only leads to a small change in the value of the background plasma frequency, by a factor $\sqrt{\pi/2} \approx 1.25$:

$$\tilde{\omega}_{\rm pbg}^2 \;\longrightarrow\; \sqrt{\frac{\pi}{2}}\,\frac{4\pi q^2 n_{\rm bg} c}{p_{\rm bg}^{\rm th}}\,. \tag{10.33}$$

We assume once again that $p_{\rm bg}^{\rm th} \gg mc$.

10.5.3 Dispersion relation

Substituting $\alpha_{zz} \equiv \alpha_{zz}^{\rm bg} + \alpha_{zz}^{\rm b}$ into dispersion relation (10.16) gives the dispersion relation for the unstable electromagnetic mode. The resulting dispersion relation is very similar to results obtained in chapter 6 for the case of a fully three-dimensional thermal background. Following the conventions introduced in chapter 6, we define the dimensionless growth rate σ and the dimensionless wave number κ, measured in units of the background plasma frequency $\tilde{\omega}_{\rm pbg}$ and inverse skin depth respectively:

$$\sigma = \tilde{\sigma}/\tilde{\omega}_{\rm pbg}\;\;,\;\;\kappa = kc/\tilde{\omega}_{\rm pbg}\,. \tag{10.34}$$

If one uses a fluid model for the background (either 2D or 3D in momentum space), the dispersion relation is the one derived in chapter 6:

$$\sigma^4 + \mathcal{B}\,\sigma^2 - \mathcal{C} = 0, \tag{10.35}$$

with

$$\begin{aligned}\mathcal{B} &= \kappa^2\,\Big(1 + u_{\rm th}^2\Big) + (1 + \eta\,\mathcal{G}),\\ \mathcal{C} &= \kappa^2 u_{\rm th}^2\,\Big\{\eta\,\mathcal{M}^2 - \Big(\kappa^2 + \eta\,\mathcal{G} + 1\Big)\,\Big\}.\end{aligned} \tag{10.36}$$

Here

$$\eta \equiv \hat{\omega}_{\rm pb}^2/\tilde{\omega}_{\rm pbg}^2 \tag{10.37}$$

and

$$\mathcal{M} \equiv u_{\rm b}/u_{\rm th} = p_{\rm b}/p_{\rm th}. \tag{10.38}$$

are the two fundamental parameters that determine the growth rate and the range of unstable wavenumbers of the instability, see chapter 6.

This mode is has an unstable solution (with $\sigma > 0$) when $\mathcal{C} > 0$. The growth rate σ is then given by

$$\sigma^2 = \frac{\sqrt{\mathcal{B}^2 + 4\mathcal{C}} - \mathcal{B}}{2}. \tag{10.39}$$

The instability condition $\mathcal{C} > 0$ leads to the condition $\kappa < \kappa_{\rm max}$ on the wavenumber, where

$$\kappa_{\rm max}^2 = \eta(\mathcal{M}^2 - \mathcal{G}) - 1. \tag{10.40}$$

For ultra-relativistic shocks ($\gamma_0 \gg 1$) the expression simplify because $u_{\rm th} \ll u_{\rm b} \sim 1$ and $\mathcal{G} \ll 1$. We then get

$$\begin{aligned} \mathcal{B} &\simeq 1 + \kappa^2, \\ \mathcal{C} &\simeq \frac{\kappa^2}{\mathcal{M}^2}\left(\eta\,\mathcal{M}^2 - \kappa^2 - 1\right), \\ \kappa_{\rm max}^2 &\simeq \eta\mathcal{M}^2 - 1. \end{aligned} \tag{10.41}$$

The dispersion relation of the instability in the fluid model is characterized by the two parameters η and $\mathcal{M}$, see chapter 6. The parameter η measures the strength of the beam plasma compared to the background plasma, the parameter $\mathcal{M}$ measures the importance of the thermal motions in the beams. As such, η determines the (maximum) growth rate of the instability, and η and $\mathcal{M}$ together determine the range of wavelengths that are unstable, as is illustrated in figures 10.1 and 10.2.

The 2D kinetic model for the background response yields a dispersion relation that can be written as

$$\sigma^2 + \kappa^2 + \left(\frac{\sigma}{\kappa}\right)\left[\sqrt{1 + \frac{\sigma^2}{\kappa^2}} - \frac{\sigma}{\kappa}\right] - \frac{\eta\kappa^2}{\sigma^2 + \kappa^2/\mathcal{M}^2} = 0\,. \tag{10.42}$$

This will give an instability with $\sigma > 0$ for $\kappa < \sqrt{\eta}\mathcal{M}$. Dispersion relation (10.42) can only be solved numerically. In the low-frequency limit, $\sigma^2 \ll \kappa^2$, one can expand the square root, and the leading terms give an approximate dispersion relation of the form

$$\kappa^2\left(\sigma^2 + \frac{\kappa^2}{\mathcal{M}^2} - \eta\right) + \frac{\sigma}{\kappa}\left(\sigma^2 + \frac{\kappa^2}{\mathcal{M}^2}\right) = 0\,. \tag{10.43}$$

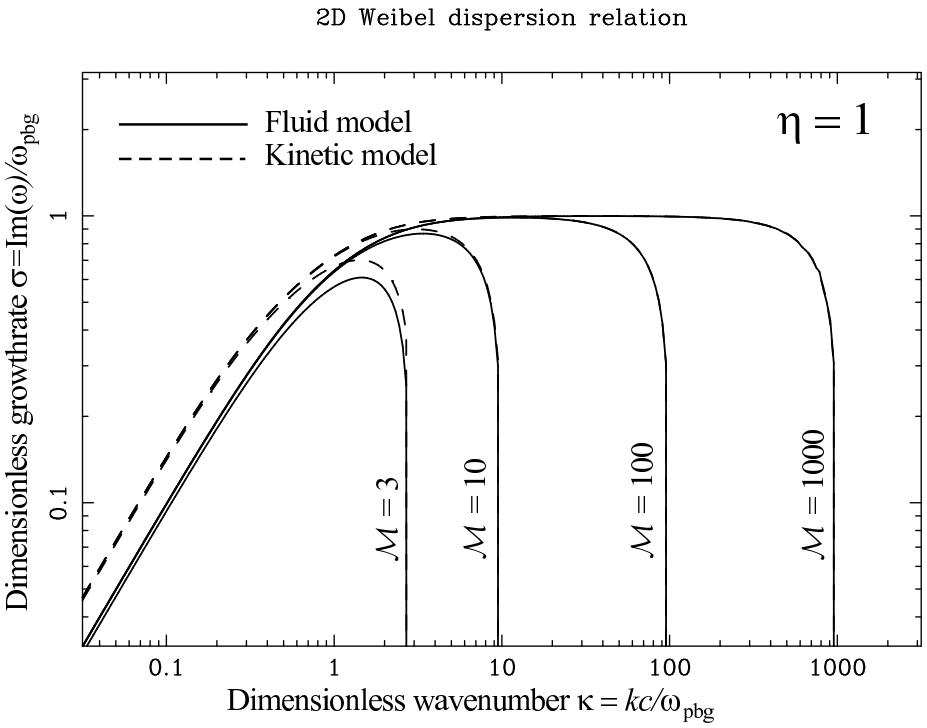

Figure 10.1: Theoretical growth rate of the Weibel instability in dimensionless units. Shown is the dimensionless growth rate $\sigma = \mathrm{Im}(\omega)/\tilde{\omega}_{\mathrm{pbg}}$ as a function of the dimensionless wavenumber $\kappa = kc/\tilde{\omega}_{\mathrm{pbg}}$ for $\eta = 1$, $\mathcal{M} = 3, 10, 100, 1000$, the parameters as used in the simulations of figure 10.4. Both the fluid background model and the kinetic model growth rates are shown.

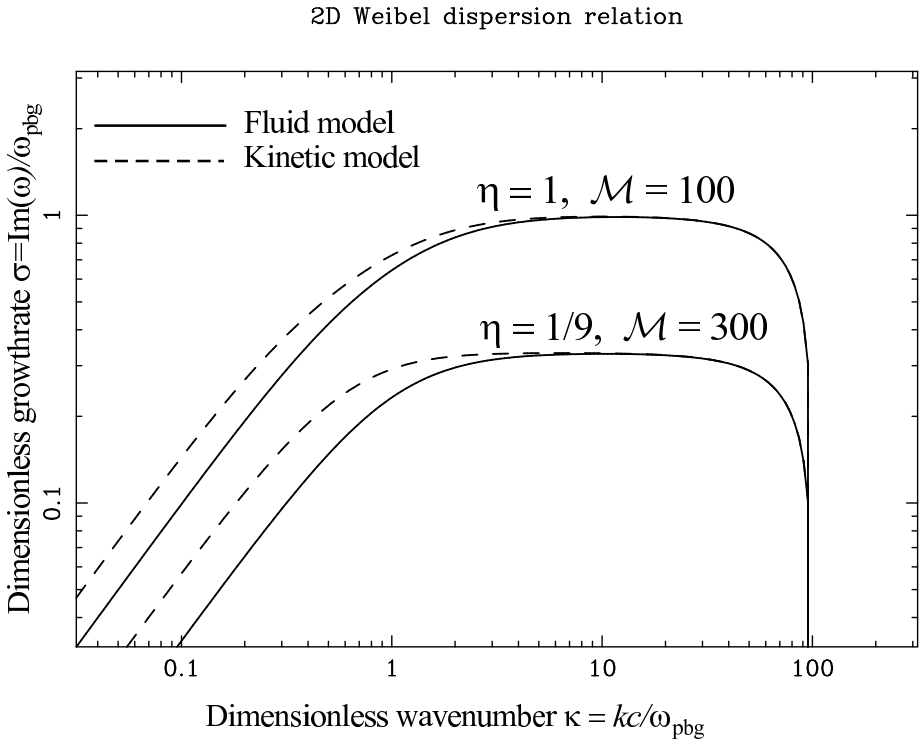

Figure 10.2: The dimensionless growth rate for $\eta = 1, \mathcal{M} = 100$ (the same two curves as in figure 10.1), and for $\eta = 1/9, \mathcal{M} = 300$: the parameters used in the simulations of figure 10.6.

For $\sigma \ll \sqrt{\eta}$ and $\kappa \ll \sqrt{\eta}\mathcal{M}$ the solution is

$$\sigma = \eta^{1/3}\kappa \; . \tag{10.44}$$

If $\sigma^2 \sim \eta$ and $\sigma \ll \kappa^3$ one has

$$\sigma \approx \sqrt{\eta - \frac{\kappa^2}{\mathcal{M}^2}} \; . \tag{10.45}$$

The solution of the unstable mode is approximated quite well over the whole range of unstable wavenumbers by the interpolation formula (see chapter 6)

$$\sigma^2 \simeq \frac{\kappa^2 \; \left(\kappa_{\rm max}^2 - \kappa^2\right)}{\mathcal{M}^2 \; \left(\kappa_{\rm s}^2 + \kappa^2\right)} \; , \tag{10.46}$$

where, in the limit $\eta\mathcal{M}^2 \gg 1$, one has $\kappa_{\rm max}^2 = \eta\mathcal{M}^2$ and

$$\kappa_{\rm s} = \begin{cases} 1 & \text{fluid background model, 2D or 3D;} \\ \\ \eta^{1/6} & \text{2D kinetic background model.} \end{cases} \tag{10.47}$$

For comparison: for a fully three-dimensional Maxwellian background model one finds $\kappa_{\rm s} = (\pi/4)^{1/3}\eta^{1/6} \approx 0.92\eta^{1/6}$.

The conclusion of these calculations is as follows: in both the kinetic and the fluid model the background plasma produces screening currents that slow the instability at sufficiently small k (large wavelengths), leading to a growth rate $\sigma \propto \kappa$. In the fluid case the relevant length scale (screening length) is the classical skin depth, $\lambda_{\rm sk} = c/\tilde{\omega}_{\rm pbg}$, with screening important for $k\lambda_{\rm sk} < 1$. In the kinetic case, the screening is due to the *anomalous skin effect* [e.g. 7], with a skin depth $\lambda_{\rm sk} = c/\tilde{\omega}_{\rm pbg}\,\kappa_{\rm s} \sim c/\tilde{\omega}_{\rm pbg}^{2/3}\omega_{\rm pb}^{1/3}$. For wavelengths shorter than the screening length ($\kappa > \kappa_{\rm s}$) the growth rate saturates quickly to the maximum value, $\sigma_{\rm max} \approx \sqrt{\eta}$ if $\eta\mathcal{M}^2 \gg 1$. The differences between the two-dimensional case (as employed in the simulations) and the fully three-dimensional case are small.

10.5.4 Saturation of the instability

As discussed in detail in chapter 9, following earlier work of Gruzinov [31], the exponential phase of the Weibel instability (where $B \propto e^{\tilde{\sigma}t}$) saturates when the motion of the beam particles in the direction transverse to the beam exhibits

trapping in the non-linear Lorentz force. After trapping occurs, the amplitude of the magnetic field grows much more slowly.

We characterize the trapping amplitude of the field by the parameter

$$\varepsilon_B \equiv \frac{B_{tr}^2}{8\pi n_b \gamma_b mc^2} \,, \tag{10.48}$$

the ratio of the magnetic energy density and the density of the beam kinetic energy, where $\gamma_b = (1 + p_b^2/m^2c^2)^{1/2} = \gamma_0(1 - u_{th}^2)^{1/2}$. Trapping creates the largest field amplitudes at a wavenumber where σ^2/κ has its maximum value, *cf.* Hoshino et al. [38], see also chapter 8. For the Weibel dispersion relation this occurs at $\kappa \approx \kappa_s$, and the typical amplitude of the magnetic field, the *trapping field*, is equal to (see chapter 9):

$$B_{tr} \approx \frac{2\pi q n_b c}{\tilde{\omega}_{pbg}\kappa_s} \,. \tag{10.49}$$

This leads to a ratio of magnetic to beam energy equal to:

$$\varepsilon_B \sim \frac{\gamma_0}{\gamma_b}\,\frac{\eta}{8\kappa_s^2} \,. \tag{10.50}$$

For an ultra-relativistic beam, with $\mathcal{M}^2 \gg 1$ and $\gamma_0 \approx \gamma_b$, the exponential phase of the Weibel instability therefore saturates when (see chapter 9 for the 3D case):

$$\varepsilon_B \simeq \begin{cases} \dfrac{\eta}{8} & \text{fluid background, with } \kappa_s = 1; \\ \\ \dfrac{\eta^{2/3}}{8} & \text{2D kinetic background, with } \kappa_s = \eta^{1/6}. \end{cases} \tag{10.51}$$

After trapping occurs, the current channels left by the quasi-exponential Weibel instability will keep merging, [59]. This merging of current filaments mostly transports field energy from scales smaller than the plasma skin depth to scales of order of the skin depth. The field amplification that results from this process slows down appreciably when considering current filaments with a transverse dimension much larger than the (anomalous) skin depth (see chapter 9). As a result, the extra field amplification resulting from this process is rather modest.

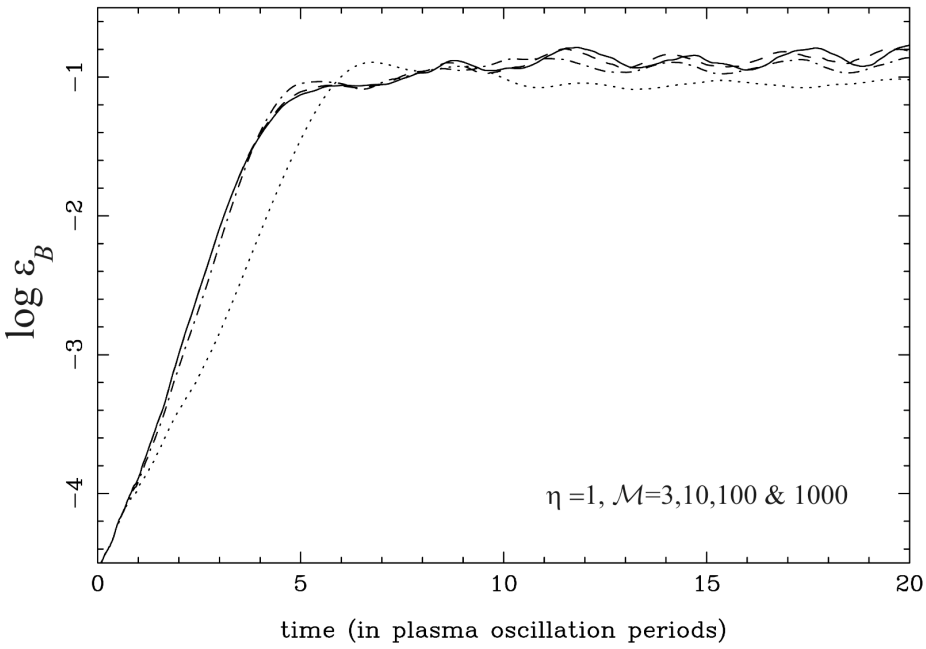

Figure 10.3: The magnetic energy density, plotted in terms of the dimensionless quantity ϵ_B, as a function of time for the four different simulations shown in figure 10.4, which all have $\eta = 1$. Solid curve: the case $\mathcal{M} = 1000$, dashed curve: the case $\mathcal{M} = 100$, dot-dash curve: the case $\mathcal{M} = 10$, dotted curve: the case $\mathcal{M} = 3$.

10.6 Simulation results

The simulation results that we have obtained confirm the basic properties of the Weibel instability as outlined in the preceding sections. We have performed simulations for a strong beam (with $\eta = 1$) and for a weak beam with $\eta = 1/9$, and for different values of $\mathcal{M}$, both relatively small ($\mathcal{M} = 3$) and large ($\mathcal{M} = 100$). These simulations have been performed with a sufficiently long duration, so that a full saturation of the magnetic field growth associated with this instability is obtained (see, for example, figure 10.3): saturation of magnetic field growth occurs roughly halfway through the simulations.

The development of the Weibel instability shows several phases (see figure 10.4). In the initial phase, random density concentrations in the beam plasma are enhanced, producing small-scale electrical currents. The minimum transverse size of the exponentially growing current perturbations, $\lambda_{\min}/\lambda_{\rm sk} \sim 2\pi/\kappa_{\max} \sim 2\pi/\sqrt{\eta}\mathcal{M}$, is determined by the temperature of the beam plasma (through the parameter $\mathcal{M}$), as predicted by linear theory, see equation (10.40). These small-scale electrical currents merge continually, until they produce current channels whose centers are separated by a distance of a few background plasma skin lengths, $\lambda_{\rm sk} \sim c/\tilde{\omega}_{\rm pbg}$, and which have a comparable transverse size. Having reached this size, the separation of the current channels persists for many plasma oscillation periods. Only the simulations with a large thermal spread in beam velocities show a last merger just before the end of the simulations shown in figure 10.4, but this is a rare event. We have checked with longer simulations that further mergers do not occur for at least another 20 plasma oscillation periods.

Note that the currents do not merge smoothly: instead they form an oscillating bunch of current wires, a behavior that was already noted by [52] in their simulations. In the simulations with a large thermal spread, which have $\mathcal{M} = 3$ or equivalently $p_{\rm th}/mc = 10/3$, the instability does not enhance the small-scale current perturbations, but from the start forms current channels at the largest scale. In contrast: in the simulations with a large value of $\mathcal{M}$ (the bottom two figures in figure 10.4) there is still a lot of fine-structure in the bunches of current filaments that form in the merger process.

The development of the instability is most conveniently represented by the behavior of the magnetic energy density in units of the beam energy density, $\varepsilon_{\rm B}$, as a function of time (figure 10.3). The growth rate in the exponential phase is largely independent of $\mathcal{M}$ for large $\mathcal{M}$, as predicted by linear theory. The simulation with smallest value of $\mathcal{M}$ (the case $\mathcal{M} \sim 3$) has a noticeably smaller growth rate, reflecting the fact that the larger thermal spread suppresses the

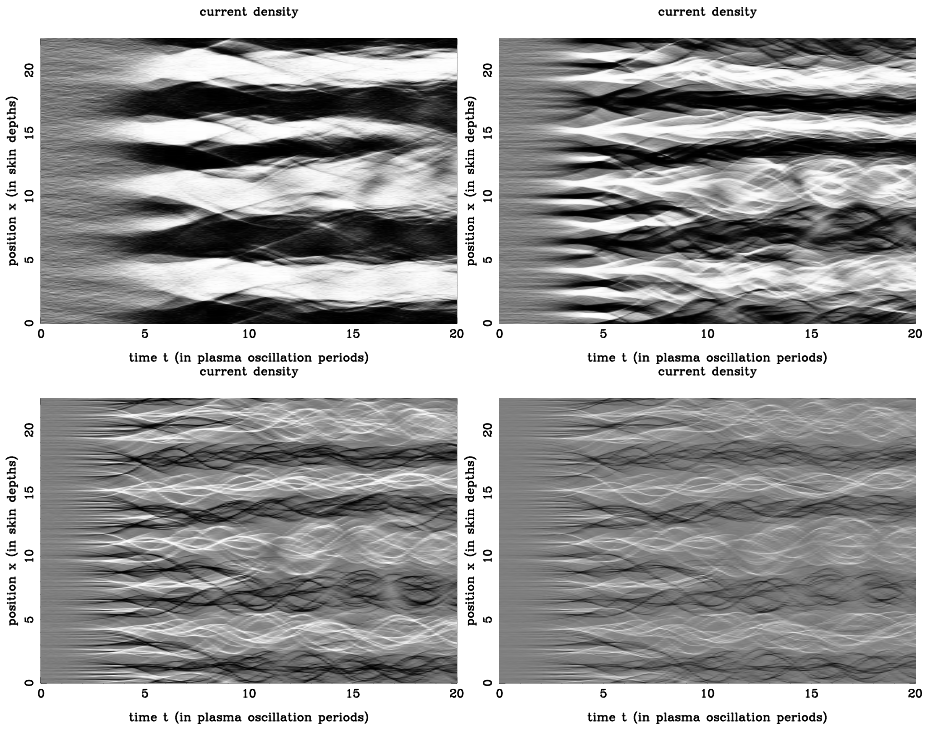

Figure 10.4: Current density as a function of the transverse position x, measured in units of the background plasma skin depth $c/\tilde{\omega}_{\rm pbg}$, and of time, measured in units of $2\pi/\omega_0$, with $\omega_0^2 = 4\pi q^2 n_0/m$ the plasma frequency based on the total number density of particles. From upper left to lower right we show the cases with $\mathcal{M} \equiv p_{\rm b}/p_{\rm th} = 3, 10, 100$ and 1000. The other parameters used in these simulations are: $r_{\rm bg} \equiv n_{\rm bg}/n_{\rm b} = 1$, $p_{\rm b}/mc = 10$, $p_{\rm th}^{\rm bg}/mc = 5.32$, $\omega_0\,\Delta t = (2\pi/512)$ and $n_0 = 30$, where n_0 is the number of simulated particles per grid cell. According to equations (10.37), (10.21) and (10.33) this corresponds to $\eta \simeq 1$. The simulations are initialized with a random (but on average uniform) spatial distribution of particles across the grid.

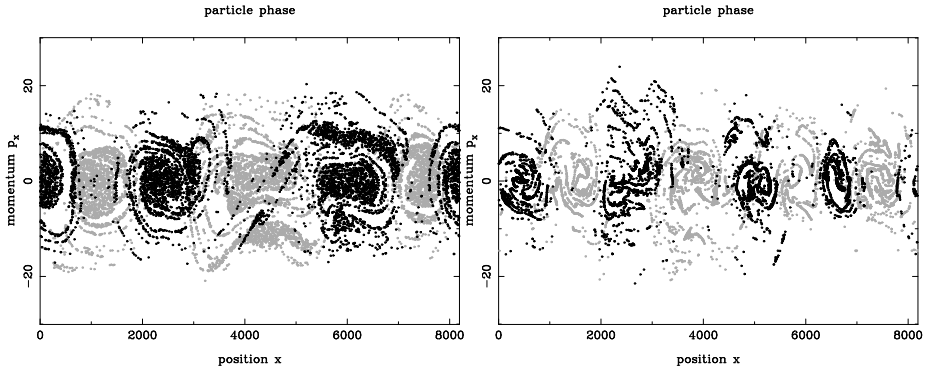

Figure 10.5: Particle phase plots for the situation as it occurs at the last time step of two of the simulations shown in figure 10.4. Left: the case $\mathcal{M} = 3$, right: the case $\mathcal{M} = 100$. Gray dots represent particles with positive p_z, i.e. particles moving in the direction of the forward beam, the black dots represent particles with negative p_z.

short-wavelength modes which have the largest growth rate (figure 10.1). In all cases, the saturated ε_B is slightly below the theoretical estimate (10.51), and independent of M as predicted by theory for $\mathcal{M} \gtrsim 1$.

The phase plots of momentum component p_x vs. x show how the particles become magnetically trapped into separated current channels, with particles moving alternately in positive or negative z-direction (figure 10.5). Most of the particles move in stable oscillating orbits (rings in phase space) that are confined within each current channel, although the edges of the channels overlap slightly. The rings in the simulation with the large thermal spread (the case $\mathcal{M} = 3$) are less distinct: they fill up because of the relatively large initial thermal spread in momentum in the x-direction.

We also performed simulations with only one in ten simulated particles belonging to the beams, instead of half the particles (figure 10.6). This results in $\eta = 1/9$. The weakness of the beams slows down the instability. The growth of the magnetic field amplitude again comes to an end when the size of the current channels reaches a few background skin lengths. This behavior is in accordance with the theoretical prediction for a Maxwellian plasma, which predicts a wave number $\kappa_s \approx 0.78$, corresponding to a length scale ~ 1.3 times larger than for $\eta = 1$. The saturation amplitude of the magnetic field (figure 10.7) is significantly weaker than in the case $\eta = 1$ (figure 10.3).

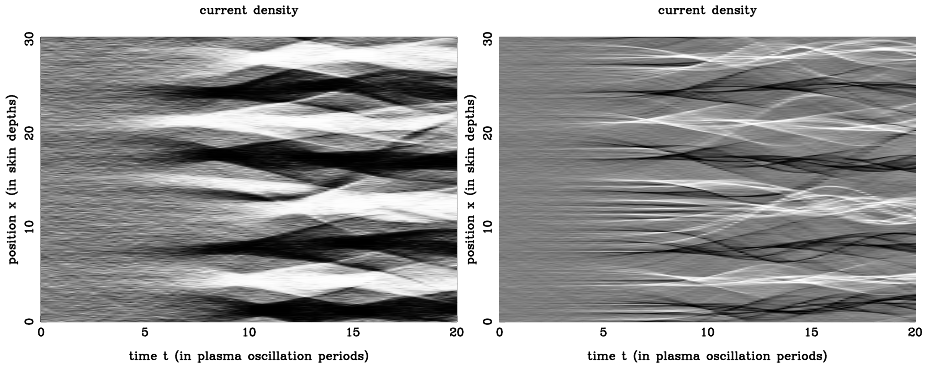

Figure 10.6: Current density for simulations with $\mathcal{M} = 10$ (left) and $\mathcal{M} = 300$ (right), for a relatively weak beam with $r_{\mathrm{bg}} = 9$ so that $\eta \simeq 1/9$. Other simulation parameters are the same as in figure 10.4 except: $\omega_0 \Delta t = 2\pi/256 \sim 0.0245$ and $n_0 = 200$. Note that the length-scale on the axes of these figures is different from figure 10.4.

By making the thermal momentum $p_{\mathrm{bg}}^{\mathrm{th}} \sim k_{\mathrm{b}} T/c$ of the background smaller, we have also performed simulations with a smaller effective inertia of the background plasma, so that its effect on the development of instability is larger: a cold plasma is more responsive. If we keep the same number of particles per grid cell, then a smaller $p_{\mathrm{bg}}^{\mathrm{th}}$ will mean that the background plasma frequency $\tilde{\omega}_{\mathrm{pbg}}$ becomes larger, and as a consequence the background skin depth becomes smaller. Changing $p_{\mathrm{bg}}^{\mathrm{th}}$ does not strongly influence the maximum growth rate of the instability, which is mostly determined by the density ratio $n_{\mathrm{b}}/n_{\mathrm{bg}}$ of the beam and background plasma. The smaller background skin depth *does* mean that the diameter of the current channels is smaller, as is immediately obvious from figure 10.8. The responsive background plasma will stall the merging of current channels by surrounding the current channels with reverse shielding currents. The shielding currents are visible in figure 10.8 as clouds of opposite color that surround the strongest current channels associated with the beams. As a result, the saturated magnetic field is also weaker than in the $\eta = 1$ case (figure 10.9).

The simulations confirm that the strength of the beams, as parameterized by η, influences the magnetic field strength that the instability reaches: lower η means a lower magnetic field strength at saturation. Although theory predicts

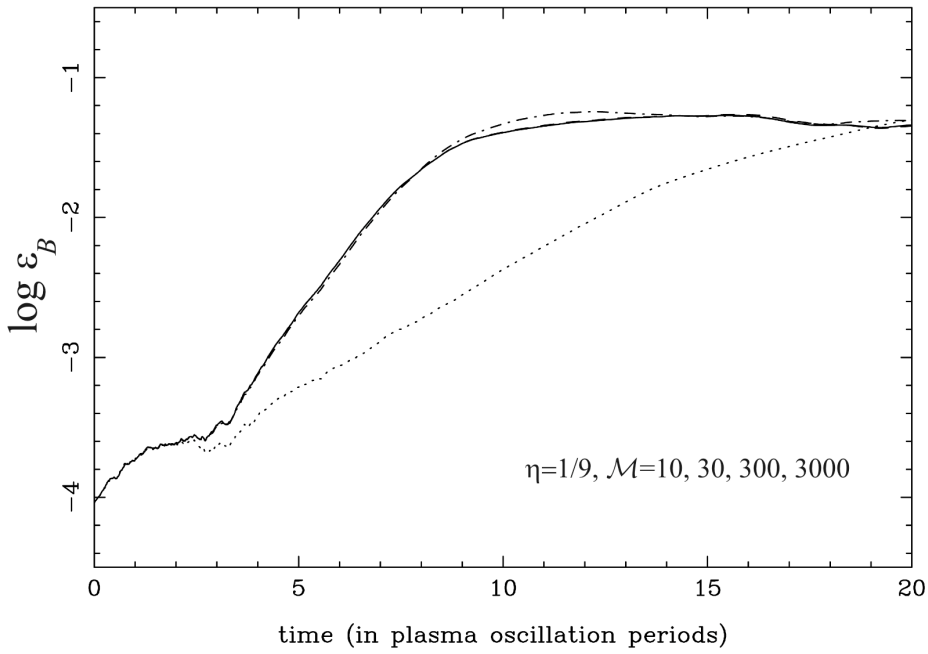

Figure 10.7: The magnetic energy density, plotted in terms of the dimensionless quantity ϵ_B, as a function of time for the set of simulations shown in figure 10.6, which have $\eta = 1/9$. Solid curve: the case $\mathcal{M} = 3000$, dashed curve: the case $\mathcal{M} = 300$, dot-dash curve: the case $\mathcal{M} = 30$ and the dotted curve: the case $\mathcal{M} = 10$. Note that the growth of the magnetic field in this case with $\eta = 1/9$ is slower than in the case $\eta = 1$ of figure 10.3: the exponentiation time of the field increases by a factor $\sim \sqrt{1/\eta} = 3$, as predicted by theory.

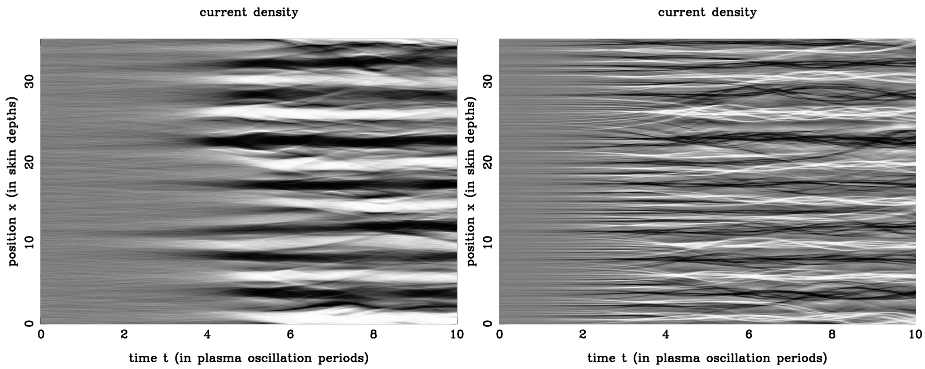

Figure 10.8: Current density for simulations with $\mathcal{M} = 10$ (left) and $\mathcal{M} = 300$ (right) for $p_{\rm bg}^{\rm th}/mc = 0.01$. All other simulation parameters are the same as those employed in the simulations shown in figure 10.4. Note that the scale on the axes is again different.

that $\varepsilon_{\rm B}$ increases with η (cf., equation 10.51), the effect of lowering η by using a more responsive background with smaller thermal momentum $p_{\rm bg}^{\rm th}$ is less strong. We attribute this behavior to the fact that the theoretical estimate does not take into account that the background plasma gets heated by its interaction with the electromagnetic fields generated by the bunching of the beam plasma: an effect of the phase mixing of the quiver motion of background particles in the wave electromagnetic field. This affects the plasma most strongly when the background plasma is initially cold. The subsequent heating of the background plasma lowers its plasma frequency, thereby suppressing its ability to shield the current channels. The current channels in the simulations with a cold background plasma therefore quickly reach a transverse length-scale comparable to the background skin depth of the heated background plasma, which is larger than the *initial* background skin depth of the cold background plasma.

10.7 Conclusions

By performing a number of 1D2V simulations of the Weibel instability we have confirmed the basic properties of this instability, as predicted by one-dimensional theory (see chapters 6 and 9). We have shown that the restriction to two-dimensional (rather than three-dimensional) momentum space in these simulations does not influence the properties of the linear (exponential)

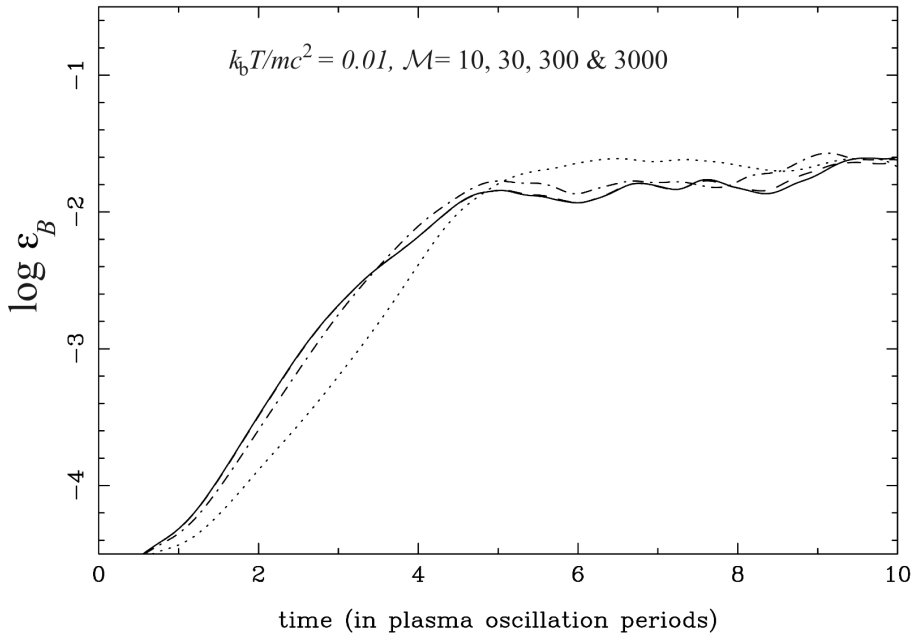

Figure 10.9: The magnetic energy density, plotted in terms of the dimensionless quantity ϵ_B, as a function of time for the set of simulations shown in figure 10.8. Solid curve : the case $\mathcal{M} = 3000$, dashed curve: the case $\mathcal{M} = 300$, dot-dash curve: the case $\mathcal{M} = 30$ and the dotted curve: the case $\mathcal{M} = 10$.

phase of the instability: the growth rate σ and range of unstable wavenumbers behave the same as in the case where the background has three degrees of freedom in momentum space. The waterbag model for the beam plasma, on which our analytical estimates are based, is intrinsically two-dimensional in momentum space.

The Weibel instability produces electrical current channels, whose strength is limited by the magnetic trapping of the particles inside the current channels. A dense and hot (stationary) background plasma inhibits the merging of the the parallel electrical currents produced by the instability due to its screening action, thereby reducing the magnetic field strength that the instability ultimately produces.

The influence of a strong background plasma is particularly important for the development of the Weibel instability for proton beams in a background plasma containing electrons. The low mass of the electrons implies that they form a very responsive background plasma, so that effectively $\eta \ll 1$. This will inhibit the merging of proton currents by shielding of the current channels as in our simulations with a cold background plasma.

10.8 Appendix: Numerical approach

10.8.1 Dimensionless form of the equations

In this Appendix, we briefly review the computational method used in our PIC simulations. The PIC Code employs dimensionless time, position and field variables. Given the grid size Δx we choose $\Delta t = \Delta x/c$ as our unit of time, which is a natural choice in this particular case since we consider ultra-relativistic beams with velocity $V_\mathrm{b} \approx c$. We measure time and the particle position on the grid in units of the timestep Δt and grid spacing Δx respectively:

$$\bar{t} = t/\Delta t, \qquad \bar{x} = x/\Delta x, \tag{10.52}$$

We define a dimensionless particle velocity and momentum as:

$$\bar{\mathbf{v}} = \frac{\mathbf{v}\,\Delta t}{\Delta x} = \frac{\mathbf{v}}{c} \;\;,\;\; \bar{\mathbf{p}} = \frac{\mathbf{p}\,\Delta t}{m\Delta x} = \frac{\mathbf{p}}{mc}\;, \tag{10.53}$$

The dimensionless equation of motion of a PIC particle in the x-direction is then

$$\frac{\mathrm{d}\bar{x}}{\mathrm{d}\bar{t}} = \bar{v}_x = \frac{\bar{p}_x}{\sqrt{1+\bar{p}^2}}\;. \tag{10.54}$$

Here we have used that the Lorentz factor is $\gamma = \sqrt{1+\bar{p}^2}$, with $\bar{p}^2 = \bar{p}_x^2 + \bar{p}_z^2$. If we define dimensionless electromagnetic fields $\bar{\mathbf{E}} = (\bar{E}_x\,,\,0\,,\,\bar{E}_z)$ and $\bar{\mathbf{B}} = (0\,,\,\bar{B}_y\,,\,0)$ by

$$\bar{\mathbf{E}} = \frac{q\,\Delta t^2}{m\Delta x}\,\mathbf{E} \;\;,\;\; \bar{\mathbf{B}} = \frac{q\,\Delta t^2}{m\Delta x}\,\mathbf{B}\;, \tag{10.55}$$

the momentum equation for $\bar{\mathbf{p}} = (\bar{p}_x\,,\,\bar{p}_y\,,\,0)$ becomes

$$\frac{\mathrm{d}\bar{\mathbf{p}}}{\mathrm{d}\bar{t}} = \bar{\mathbf{E}} + \bar{\mathbf{v}} \times \bar{\mathbf{B}}\;. \tag{10.56}$$

In these variables, the set of Maxwell's equations (equations (10.5 - 10.7) of the main paper) read:

$$\begin{aligned}
\frac{\partial \bar{E}_x}{\partial \bar{x}} &= \theta\,\bar{\rho}\;; \\
\frac{\partial \bar{B}_y}{\partial \bar{x}} - \frac{\partial \bar{E}_z}{\partial \bar{t}} &= \theta \bar{J}\;; \\
\frac{\partial \bar{B}_y}{\partial \bar{t}} - \frac{\partial \bar{E}_z}{\partial \bar{x}} &= 0\;.
\end{aligned} \tag{10.57}$$

Here the dimensionless charge- and current density (in the z-direction) are defined by

$$\bar{\rho} = \frac{\rho}{q n_0} \ , \ \bar{J} = \frac{J}{q n_0 c} \ , \tag{10.58}$$

where n_0 is the mean density of particles on the grid. The parameter θ follows from

$$\theta = \omega_0^2 \, \Delta t^2 \ , \ \omega_0^2 \equiv \frac{4\pi q^2 n_0}{m} \ . \tag{10.59}$$

In practice, we replace the equation for $\bar{E}_x$ by the Poisson equation for the electric scalar potential $\bar{\Phi} \equiv q\Phi/mc^2$:

$$\bar{E}_x = -\frac{\partial \bar{\Phi}}{\partial \bar{x}} \ , \ \frac{\partial^2 \bar{\Phi}}{\partial \bar{x}^2} = -\theta \, \bar{\rho} \ . \tag{10.60}$$

10.8.2 Solution method: particles

We employ a variant of the Leapfrog Scheme [78, p. 144], with a four-step Runge-Kutta time-integrator, to advance the equations of motion (10.54) and (10.56) in time. The stability of this explicit numerical solution scheme requires $\theta < 1/2$. In practice, we choose a much smaller value for θ for reasons of computational accuracy.

We calculate the electromagnetic field on a grid, but we permit the particles to move freely so, in general, their position will not coincide with a grid point. To find the electromagnetic fields at a given intermediate position x between grid points j and $j+1$ we use a linear interpolation scheme, for instance:

$$\bar{E}_z(\bar{x} = \bar{x}_j + \mathrm{d}\bar{x}) \simeq \mathrm{d}\bar{x} \ \left(\bar{E}_z\right)_{j+1} + (1 - \mathrm{d}\bar{x}) \ \left(\bar{E}_z\right)_j \ , \tag{10.61}$$

with $\left(\bar{E}_z\right)_j \equiv \bar{E}_z(\bar{x} = \bar{x}_j)$.

10.8.3 Solution method: electromagnetic fields

For the first order spatial derivatives in Maxwell's equations for $\bar{B}_y$ and $\bar{E}_z$ (the last two equations in 10.57) we use a space-centered approximation:

$$\left(\frac{\partial g}{\partial \bar{x}}\right)_j = \tfrac{1}{2} \ \left(g_{j+1} - g_{j-1}\right) \ , \tag{10.62}$$

where g is either $\bar{B}_y$ or $\bar{E}_z$. Here we use that in the dimensionless variables employed here the grid size is unity: $\Delta\bar{x} = 1$.

We calculate the charge and current densities (apart from the neutralizing background) that appear in Maxwell's equations at each gridpoint from the position of the particles near that grid point. We attribute the charge/current density of each particle to the two nearest grid points, weighted by its distance to each respective grid point. That is, a particle at position $\bar{x}_j + \mathrm{d}\bar{x}$ between grid points j and $j+1$ contributes $(1 - \mathrm{d}\bar{x})$ to the density at grid point j and $\mathrm{d}\bar{x}$ to the density at grid point $j+1$, and likewise for the current density.

We use a two-step Lax-Wendroff method [78, p. 67], modified to include the current density as a source term, to advance $\bar{E}_z$ and $\bar{B}_y$ in time at each (fixed) time step. The first (auxiliary) step calculates the fields at the half time-step:

$$\begin{aligned} \left(\bar{E}_z\right)_{j+1/2}^{n+1/2} &= \tfrac{1}{2}\left[\left(\bar{E}_z\right)_j^n + \left(\bar{E}_z\right)_{j+1}^n + \left(\bar{B}_y\right)_{j+1}^n - \left(\bar{B}_y\right)_j^n - \theta\left(\bar{J}_j^n + \bar{J}_{j+1}^n\right)\right], \\ \left(\bar{B}_y\right)_{j+1/2}^{n+1/2} &= \tfrac{1}{2}\left[\left(\bar{B}_y\right)_j^n + \left(\bar{B}_y\right)_{j+1}^n + \left(\bar{E}_z\right)_{j+1}^n - \left(\bar{E}_z\right)_j^n\right]. \end{aligned} \tag{10.63}$$

Here the indices n and j enumerate the time step and grid position respectively. These values are then used in the main time step to obtain an approximated time- and space-centered derivative, and to update the values of the field components:

$$\begin{aligned} \left(\bar{E}_z\right)_j^{n+1} &= \left(\bar{E}_z\right)_j^n + \left[\left(\bar{B}_y\right)_{j+1/2}^{n+1/2} - \left(\bar{B}_y\right)_{j-1/2}^{n+1/2}\right] - \theta\,\bar{J}_j^n, \\ \left(\bar{B}_y\right)_j^{n+1} &= \left(\bar{B}_y\right)_j^n + \left[\left(\bar{E}_z\right)_{j+1/2}^{n+1/2} - \left(\bar{E}_z\right)_{j-1/2}^{n+1/2}\right]. \end{aligned} \tag{10.64}$$

Poisson's equation (10.60) is discretized in the standard fashion [78], *i.e.*, by writing

$$\left.\frac{\partial^2 \bar{\Phi}}{\partial x^2}\right|_{\bar{x}=\bar{x}_j} = \bar{\Phi}_{j+1} - 2\bar{\Phi}_j + \bar{\Phi}_{j-1}, \tag{10.65}$$

where $\bar{\Phi}_j$ is the value of the function $\bar{\Phi}$ at gridpoint $\bar{x} = \bar{x}_j$. The periodic boundary conditions imply that $\bar{\Phi}_{M+1} = \bar{\Phi}_1$ and $\bar{\Phi}_0 = \bar{\Phi}_M$ where M is the number of grid points. The field equations at $\bar{x} = \bar{x}_j$ now take on the form

$$B\,\bar{\Phi}_{j+1} - C\,\bar{\Phi}_j + A\,\bar{\Phi}_{j-1} = -\theta\,\bar{\rho}_{j,\mathrm{tot}}, \tag{10.66}$$

where

$$A = B = 1, \qquad C = 2. \tag{10.67}$$

Poisson's finite-difference equation (10.66) for the scalar potential $\bar{\Phi}$ can be solved with the Forward Elimination–Backward Substitution Method [54, section 13.2.2]. For stability, this method requires

$$A > 0, \qquad B > 0, \qquad C > A + B \,. \tag{10.68}$$

Formally, the last requirement is not satisfied by our equations because $C = A + B = 2$. To remedy this, we have added a small positive quantity to C, in effect putting $C \implies 2 + \epsilon$ with $\epsilon \ll 1$. The effect of this replacement is to slightly enhance the Debye shielding of the electric field. As such, it is equivalent with adding a massive background plasma with a Debye length much larger than that of the gas of simulated particles. This 'fix' does not influence the solution on the scale that we are interested in: the skin depth of the simulated plasma.

Part III

Discussion and summary

Chapter 11

Discussion and conclusions

In this thesis I have presented an in-depth look at the physical processes that we expect to be at work in shock fronts that move with a speed very close to the speed of light. These shock waves only occur in deep space near extremely violent phenomena such as the explosion of stars many times heavier than the Sun or near compact objects such as neutron stars or black holes. The conditions in these environments are very different from conditions on Earth. In shock waves in normal air, such as the sonic boom of a jet plane traveling faster than sound, the physical processes producing the shock wave are dominated by collisions of the particles in the air. In most astrophysical situations, the gas density is so low that particle collisions are too rare to be of any importance.

We can still say something about the global properties of the shock transition if we assume that there are other processes than particle collisions that can produce the shock transition (chapter 5). However, because the particles in astrophysical gases (plasma) are electrically charged, we have to allow for the influence of electromagnetic fields. This introduces an uncertainty that we have now partly resolved.

Electromagnetic interaction plays a crucial role in these shock waves. Imagine a charged particle flying freely in deep space, part of the interstellar material that pervades all of space. When such a particle is overtaken by a relativistic shock wave it will be practically unaffected at first because the density of particles is so low, and they are so far separated from each other, that the particle hardly feels the electromagnetic field of the particles in the shock wave. However, if a concentration of charges occurs in the plasma, and this could happen purely by chance, then the cumulative electromagnetic field could be strong enough to influence the particle.

Because we are talking about relativistic shock waves the particles move very fast and a moving concentration of charges constitutes an electrical cur-

rent. If the particle that we are considering is moving in such a way that it would contribute to the electrical current of the random concentration of charge then it will be attracted by it (and repelled if it is moving in the opposite direction). The existence of this process of self-enhancing electrical currents was already proven by Erich S. Weibel in 1959 [98] and is therefore commonly referred to as the Weibel instability. The bulk of this thesis has dealt with a theoretical study of the role of the Weibel instability in relativistic shock waves.

When the instability starts from random variations in the plasma, then the electrical currents will grow most quickly at the smallest length scales. The smallest length scale on which the instability can grow is determined by the randomness of the velocities of the particles: a larger velocity spread inhibits growth at the smallest scales (chapters 6 and 10).

From the point of view of the shock wave the Weibel instability has the tendency to concentrate the charged particles that the shock sweeps up into electrical current channels directed mostly perpendicularly to the shock front (chapter 7).

The instability creates concentrations of electrons and protons, but the electron concentrations grow much quicker. Because electrons are almost two thousand times lighter in mass than protons, they react much more quickly than the protons. The protons, however, possess much more kinetic energy than the electrons because they are heavier, but the Weibel instability cannot use the energy of the protons as efficiently as the energy of the electrons (chapters 8 and 9).

When a particle gets incorporated in the electrical currents produced by the Weibel instability, it can become trapped in the magnetic field that the current channel produces (chapters 9 and 10). Because the particle picks up a velocity perpendicular to the electrical current as it moves towards the current, it will initially just move *through* the current channel. However, when the particle is about to leave the current channel, the magnetic field produced by the current channel will deflect it back. The oscillations that the particle undergoes in this way take on the nature of a thermal velocity spread (also referred to as 'fake diffusion' or 'quiver motions'; chapter 9). Such thermal motions inhibit further growth of the instability.

As the electrical currents grow stronger they will start to attract other current channels as a whole instead of only attracting individual particles. This merging process provides an additional way for the current channels to grow in strength (chapters 9 and 10).

An important factor to take into account when considering the Weibel instability in a shock front is that particles that have already undergone the shock

transition (in particular electrons) form a background of charged particles that also react to the electromagnetic fields that the instability produces. This slows the instability down and puts an upper limit on the size of the electrical currents (chapters 6 and 10). It will also limit the distance between the current channels: the background plasma acts as a conducting material that tends to shield the electromagnetic fields of the current channels in such a way that merging of the current channels is slowed down dramatically when the distance between them becomes larger than the skin depth of the background plasma (chapters 9 and 10).

Magnetic field generation through the Weibel instability is an inevitable process in relativistic shock waves, but it produces *small-scale* magnetic fields. The typical size and distance of the electrical currents that the instability produces and the typical length-scale of the associated magnetic field are limited by the skin depth of the plasma in the shock wave. This limitation is particularly important when we consider the electrical currents that the protons in the shock wave can produce. Because the protons have a much larger mass than the electrons, they could in theory produce much larger and, therefore, stronger electrical currents than the electrons. Our results show that the electrons in the plasma suppress this because they will serve as a background plasma that only allows much smaller current channels to form (chapters 8 and 9).

We have studied the Weibel instability from its initial exponential growth to the end of the merging of the electrical currents produced by the instability. However, the development of the shock wave does not stop there. The instability provides the reason why the charged particles inside the shock transition bunch together. The collective electromagnetic interaction of these groups of particles can then provide the dissipation needed to complete the shock transition. This collective interaction provides 'effective collisions' between groups of particles, which play the same role as particle collisions play in shock waves in normal air.

We expect this dissipation to take the form of a turbulent process. Preliminary computer simulations presented by Hededal [35] in chapter 4 of his PhD thesis show that a hot, dense thermalization region develops behind the Weibel-unstable region. In these simulations the magnetic field that the Weibel instability produces survives through the turbulent region to end up frozen into clumps of material left behind by the shock front. There are no theoretical models for these processes yet and the implications for the radiation produced by relativistic shock waves are unclear.

Another challenge is the application of this knowledge to models for Gamma-ray Burst sources (chapter 4). The Weibel instability produces magnetic fields with a strength that is a fraction of equipartition (the ratio of magnetic energy density to total energy density is $\varepsilon_B \sim 10^{-4}$; chapter 8). This is lower than the value that is obtained in some studies, for example by Wijers and Galama [102], that fit observations of Gamma-ray Bursts and their afterglows to models explaining the radiation with the synchrotron mechanism. However, from what I have seen in the literature and from talking to those researchers that do these fits, I have got the impression that there is a large scatter in the estimates for ε_B and that this parameter is not very tightly constrained by the observations [20, for example]. We can therefore say that the Weibel-produced magnetic fields could well be consistent with the observations.

Particles moving through the Weibel-produced magnetic field in relativistic shock waves could produce this synchrotron radiation. However, whether this would be sufficiently strong to explain Gamma-ray Bursts is still unclear. This point has caused some debate in the astrophysical journals with some authors, like Gruzinov [31], arguing that the Weibel produced fields are too small-scale and short-lived, and others, like Jaroschek et al. [42] arguing for the opposite point. The resolution of this issue requires a better understanding of what happens after the end of the Weibel instability. Another possibility is that dynamo processes on a larger scale produce additional magnetic fields (see the work by Milosavljević and Nakar [67], for example).

In conclusion, our understanding of the physical processes in relativistic shock waves is far from complete. Therefore, I believe that new developments such as new observations of Gamma-ray Bursts, theoretical advances, advances in computing power, and application to other astronomical phenomena, such as Active Galactic Nuclei and Pulsar Winds, will ensure that the interest in this field of research will remain high for many years to come.

Jorrit Wiersma
May 7, 2007
Utrecht

Hoofdstuk 12

Samenvatting in het Nederlands

12.1 Inleiding

Dit proefschrift bevat de belangrijkste resultaten van het onderzoek dat ik de laatste vijf jaar heb gedaan naar natuurkundige theoriën over schokgolven met een snelheid in de buurt van de snelheid van licht. Hierbij heb ik vooral bekeken hoe sterke elektrische stromen kunnen ontstaan in het schokfront. Dit is van belang voor de verklaring van explosieve sterrenkundige fenomenen zoals *Gamma-ray Bursts*.

Omdat dit soort schokgolven alleen voorkomen op grote afstand van de aarde en het zonnestelsel kunnen we ze niet van dichtbij bestuderen. Bovendien zijn dit soort schokgolven zo groot en energetisch dat we ze niet in een laboratorium kunnen opwekken. Om deze redenen kunnen we onze kennis van deze schokgolven alleen vergroten door de voorspellingen van theoretisch onderzoek, zoals het onderzoek dat in dit proefschrift wordt beschreven, te vergelijken met de waarnemingen van sterrenkundige objecten zoals Gamma-ray Bursts.

12.2 Gamma-ray Bursts

Gamma-ray Bursts (Gammaflitsen) zijn uitbarstingen van zeer intense gammastraling waarvan er ongeveer elke dag één door speciale satellieten wordt geregistreerd. Veel van deze uitbarstingen zijn waarschijnlijk afkomstig van de ontploffing van zeer zware sterren: een *hypernova*. Dit zijn ontploffende sterren waarvan de kern zo zwaar is dat hij instort door zijn eigen zwaartekracht (een *Core Collapse Supernova*). Alleen als de massa van de oorspronkelijke

Figuur 12.1: Illustratie van hoe een Gamma-ray Burst bron eruit zou kunnen zien. Binnenin een zeer zware ster vormt zich een zwart gat dat een jet materie uitspuwt.

ster zeer hoog is en als deze snel om zijn as draait leidt dit type supernova waarschijnlijk tot een Gamma-ray Burst.

Bij een hypernova is zoveel energie betrokken dat de modernste theoriën uit de natuurkunde nodig zijn om te verklaren wat we zien. Waarschijnlijk is de kern van deze sterren zo zwaar dat hij uiteindelijk tot een zwart gat instort, maar door de rotatie van de ster duurt het relatief lang voordat dat ook echt gebeurt: dit wordt het *collapsar* scenario genoemd. Een deel van het gas van de instortende ster kan daardoor aan het zwarte gat ontsnappen langs de rotatie-as van de ster en wordt de ruimte ingeblazen in de vorm van twee *jets*: straalstromen met een stroomsnelheid die bijna gelijk is aan de lichtsnelheid (zie figuur 12.1 ter illustratie). De straalstromen hebben zoveel energie dat ze heel sterke schokgolven in en rond de ster veroorzaken. Hierbij wordt de energiedichtheid zo hoog dat spontaan nieuwe deeltjes gevormd worden. Relativiteitstheorie, plasmafysica en deeltjesfysica komen zo samen.

Gamma-ray Bursts verschijnen in allerlei richtingen aan de hemel en duren over het algemeen maar een tiental seconden. Het is niet te voorspellen wanneer en waar ze verschijnen, dus we kunnen ze alleen waarnemen als een satelliet toevallig de juiste kant op kijkt. Met de komst van speciale satellieten die een groot beeldveld hebben en snel automatisch kunnen reageren op een flits hebben we echter steeds meer kunnen ontdekken over dit fenomeen.

Zo blijkt dat de flitsen van gammastraling vaak gevolgd worden door een

soort nagloeien van de bron waardoor we ook röntgenstraling, zichtbaar licht en zelfs radiostraling kunnen opvangen. Dit nagloeien nemen we lang niet altijd waar, waarschijnlijk door de grote afstand waarop de Gamma-ray Bursts plaatsvinden. Het nagloeien verschaft ons echter veel informatie over de bronnen van Gamma-ray Bursts. Uit de verdeling van de straling over de verschillende golflengten hebben we kunnen afleiden dat de straling gevormd wordt onder de invloed van magnetische velden: het stralingsspectrum lijkt meer op dat van synchrotronprocessen, waarbij snel bewegende elektronen door een magnetisch veld gaan, dan op het Planckspectrum van thermische stralingsprocessen. Waarom de straling deze eigenschappen heeft blijkt echter moeilijk te verklaren.

Een eerste probleem is de hevigheid van de gammastraling. Een Gamma-ray Burst zendt in een paar seconden evenveel energie uit in gammastraling als een supernova in totaal uitstraalt. Supernovae zijn ook ontploffende sterren en vertonen ook een explosieve groei in helderheid, maar ze stralen gedurende een periode van weken en hun straling is verdeeld over een veel groter golflengtebereik. Bij een Gamma-ray Burst explosie verwacht je dat een nog veel hetere en compacte vuurbal wordt gevormd dan bij een supernova waardoor thermische straling compleet overheerst in plaats van de synchrotron straling die we waarnemen. De verklaring waarom dit niet gebeurt is dat de straling niet afkomstig is van de explosie zelf: deze is waarschijnlijk zo compact dat het niet lukt om efficiënt gammastraling te produceren. In plaats daarvan wordt de gammastraling gevormd in de schokgolven die de explosie in zijn omgeving veroorzaakt. Dit model voor de bron van Gamma-ray Bursts wordt het *fireball model* genoemd[1].

Een tweede probleem is waar het benodigde magnetische veld vandaan komt dat nodig is voor de stralingsprocessen die we waarnemen. Een mogelijke verklaring waar de laatste paar jaar veel onderzoek naar is gedaan is dat het magnetische veld spontaan ontstaat door de elektromagnetische wisselwerking van de deeltjes in de schokgolf. Dit proefschrift beschrijft wat ik uit de theorie van deze wisselwerking heb kunnen afleiden.

Overigens bestaat er ook een klasse Gamma-ray Bursts die gemiddeld korter duren (enkele seconden in plaats van tientallen seconden). De eigenschappen van deze kortdurende Gamma-ray Bursts kunnen we beter verklaren met een model waarbij twee neutronsterren (sterren zo zwaar als de zon met de omvang van de aarde) samensmelten nadat ze lange tijd om elkaar heen gedraaid hebben in een dubbelster systeem. Dit gebeurt omdat deze dubbelster-

[1] Het idee voor het fireball model is van Rees and Mészáros [79].

systemen langzaam ineenstorten doordat ze energie verliezen via het uitzenden van zwaartekrachtstralen. Deze Gamma-ray Burst bronnen zijn dus heel anders dan de instortende zware sterren die de lángdurige Gamma-ray Bursts veroorzaken. In dit proefschrift heb ik me alleen bezig gehouden met de modellen voor de langdurige Gamma-ray Bursts.

12.3 Schokgolven en magnetische velden

Schokgolven ontstaan in een gas door grote drukverschillen, bijvoorbeeld bij explosies. Een schokgolf is ook eigenlijk niets anders dan een scherpe verandering in druk die zich voortplant door het gas. Doordat de druk achter de schokgolf zo hoog is sleurt de schokgolf gas met zich mee en daarbij wordt de stromingsenergie omgezet in warmte. In de schokgolf zijn de druk, de dichtheid en de temperatuur dan ook veel hoger dan ervóór.

Het gas waar de schokgolven die ik heb bestudeerd doorheen gaan is grotendeels geïoniseerd: het bestaat vrijwel geheel uit geladen deeltjes. Dit wordt een *plasma* genoemd. De geladen deeltjes zorgen ervoor dat het plasma een goede elektrische geleider is. Vanwege deze eigenschap leidt de verhoging van de plasmadichtheid in de schokgolf ook tot een verhoging van de magnetische veldsterkte. Het probleem is echter dat de magnetische veldsterkte in de ruimte rond Gamma-ray Bursts over het algemeen niet zo hoog is, en dat de schokgolfcompressie van dit interstellaire magnetische veld niet voldoende is om de synchrotronstraling die we waarnemen te verklaren. Bij ons onderzoek willen we daarom bepalen of er ook een ander mechanisme is dat het magnetische veld kan versterken.

Het is namelijk niet zo vreemd dat magnetische velden een belangrijke rol spelen. Dit ligt aan de grote snelheid die de schokgolven bereiken (bijna de lichtsnelheid). De snel bewegende, geladen deeltjes kunnen namelijk sterke elektrische stromen vormen die weer sterke magnetische velden in het plasma veroorzaken. Bovendien is de magnetische Lorentzkracht op een geladen deeltje ook nog eens evenredig met de snelheid.

Het idee is nu dat het plasma onstabiel is: dat wil zeggen dat kleine verstoringen van het plasma in de schokgolf snel uit zullen groeien tot veel sterkere verstoringen. Instabiliteiten komen in allerlei situaties voor. Een makkelijk te begrijpen voorbeeld is een auto die zonder handrem op de top van een heuvel is geparkeerd. Zolang de auto stilstaat is dat geen probleem, maar als iemand hem een heel klein zetje geeft zal de auto ineens heel snel van de heuvel afrollen. Op dezelfde manier zijn schokgolven die met zeer hoge snelheid door de ruimte bewegen onstabiel in de zin dat kleine verstoringen van het magneti-

sche veld snel in kracht zullen groeien.

Het proces dat op deze manier magnetische velden op kan wekken staat bekend als de *Weibel instabiliteit*[2]. Bij deze instabiliteit vormt een toevallige concentratie van ladingen in de schokgolf een sterke elektrische stroom door de hoge stroomsnelheid van het plasma. Deze stroom zal door magnetische wisselwerking naburige deeltjes met dezelfde lading die in dezelfde richting bewegen aantrekken: parallelle stromen trekken elkaar namelijk aan (en antiparallelle stromen stoten elkaar af). Hierdoor wordt de stroom dus steeds sterker. Dit zichzelf versterkende proces kan in zeer korte tijd tot sterke maar kleinschalige magnetische velden leiden.

12.4 Simulaties

Om de Weibel instabiliteit beter te begrijpen hebben we onder andere een computercode ontwikkeld om deze situatie te simuleren. De achterliggende natuurkunde van deze code is redelijk simpel: voor een grote hoeveelheid geladen deeltjes worden de bewegingsvergelijkingen numeriek opgelost om te berekenen hoe de deeltjes onder invloed van elektrische en magnetische velden bewegen. Deze elektrische en magnetische velden worden opgewekt door de deeltjes zelf. Omdat het teveel tijd kost om voor elk deeltje uit te rekenen wat de kracht is ten gevolge van alle andere deeltjes (voor N deeltjes kost dat N^2 berekeningen waarbij N ongeveer honderdduizend tot een miljoen is) rekenen we op elk moment de elektromagnetische velden uit op een netwerk van duizend tot tienduizend discrete punten. De kracht op ieder deeltje wordt dan berekend door een gewogen gemiddelde te nemen van de veldsterkte op de dichtstbijzijnde netwerkpunten.

We simuleren de interactie van twee plasmastromen die tegen elkaar in bewegen zoals gebeurt wanneer het schokfront van een Gamma-ray Burst het omringende plasma tegenkomt. Omdat de dichtheid van deeltjes heel erg laag is, is de kans erg klein dat de deeltjes op elkaar botsen en bewegen de plasmastromen in eerste instantie door elkaar heen. Echter, doordat ze geladen zijn zullen ze elkaar wel aantrekken en afstoten zoals hierboven ook beschreven. Figuur 12.3 toont als voorbeeld de evolutie van de stroomdichtheid tijdens een simulatie. Aan het begin van de simulatie zijn de deeltjes willekeurig verdeeld over de ruimte waarbij de helft van de deeltjes in de positieve z-richting beweegt en de andere helft in de negatieve z-richting. Door de willekeurige deeltjesverdeling is er op sommige plaatsen een overschot aan deeltjes die de ene of

[2]Het bestaan van dit proces werd bewezen door Weibel [98]. De toepassing in de context van Gamma-ray Bursts werd voorgesteld door Medvedev and Loeb [58].

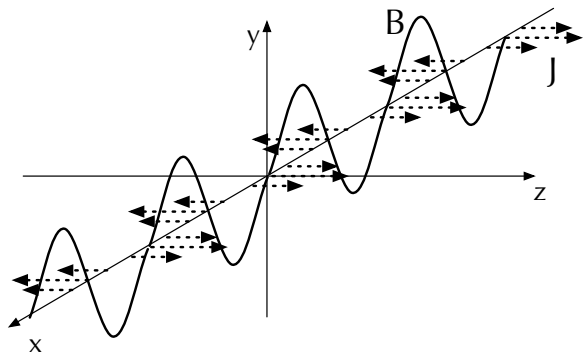

Figuur 12.2: Schematische weergave van de typische situatie aan het einde van een simulatie. De dikke lijn geeft de sterkte B en de richting van het magneetveld aan: bij de pieken wijst het magneetveld in de positieve y-richting, bij de dalen in de negatieve y-richting. De stippellijnen geven de richting van de netto elektrische stromen aan die veroorzaakt worden door de geladen deeltjes.

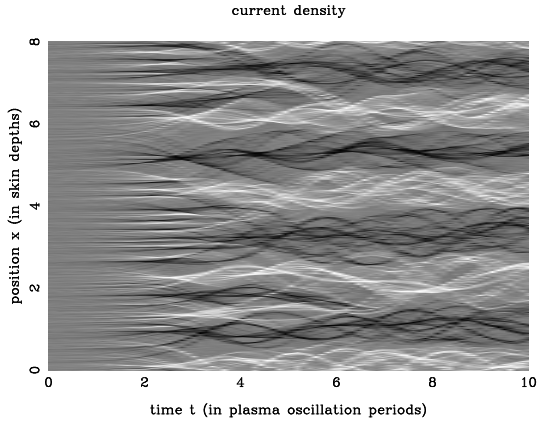

Figuur 12.3: Stroomdichtheid tijdens een simulatie. De grijswaarden geven de elektrische stroomdichtheid in de z-richting (zie figuur 12.2) aan, waarbij wit een netto stroom in de positieve richting aangeeft en zwart een netto stroom in de negatieve richting. Langs de verticale as is de ruimtelijke coördinaat x uitgezet en langs de horizontale as varieert de tijd met links het begin van de simulatie. Deze figuur is gekopiëerd uit hoofdstuk 10.

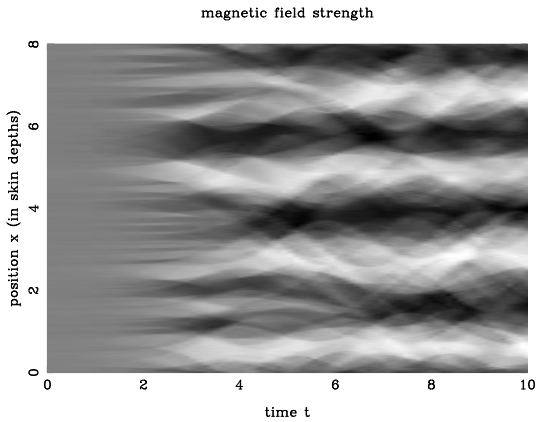

Figuur 12.4: Magnetische veldsterkte tijdens een simulatie. In de witte regionen wijst het magnetische veld in de positieve y-richting (zie figuur 12.2), in de zwarte regionen in de negatieve y-richting. Deze figuur is gekopiëerd uit hoofdstuk 10.

de andere kant op bewegen. Daarom bestaan er in het begin van de simulatie al wat fluctuaties in de stroomdichtheid.

Zoals ik hierboven heb uitgelegd is deze situatie instabiel: de kleine fluctuaties in de stroomdichtheid versterken zichzelf naarmate de tijd verstrijkt doordat de stroompjes deeltjes aantrekken die dezelfde kant op bewegen. Naarmate ze sterker worden zie je ook dat de stromen elkaar gaan aantrekken en afstoten waardoor ze samensmelten of verdwijnen. Uiteindelijk ontstaat een min of meer stabiel systeem van stromen die om elkaar heen oscilleren. Dit proces duurt in werkelijkheid ongeveer een paar milliseconden waarbij de simulatie ongeveer een gebied van een paar kilometer beslaat.

Het belangrijkste effect van de elektrische stromen is dat er een magnetisch veld gevormd wordt in het plasma. Dit is weergegeven in figuur 12.4. Als je de twee figuren met elkaar vergelijkt zie je dat het magnetische veld het sterkst is tussen de elektrische stromen in.

12.5 De sterkte van het magnetische veld

Om een schatting te maken van de straling die relativistische schokken kunnen produceren willen we graag weten hoe sterk de magnetische velden maximaal kunnen worden. Om een antwoord op deze vraag te vinden heb ik bij mijn

promotie-onderzoek een gedetailleerde analyse uitgevoerd van de hierboven beschreven processen. Ik zal deze hier kort samenvatten.

Om te beginnen kunnen we een grove schatting maken gebaseerd op elementaire natuurkunde. De Biot-Savart wet vertelt ons dat het magnetische veld rond een elektrische stroom I met straal d een sterkte B heeft met

$$B = \frac{2I}{cd}, \tag{12.1}$$

waarbij c de lichtsnelheid is. Omdat de deeltjes maximaal met de lichtsnelheid kunnen bewegen is de maximale stroomsterkte ongeveer $I = qn\pi d^2 c$ waarbij q de lading van de deeltjes is en n de dichtheid. De factor $n\pi d^2 c$ geeft het maximum aantal deeltjes dat per seconde door een doorsnede met straal d heen beweegt. De magnetische veldsterkte wordt dan

$$B = 2\pi qnd. \tag{12.2}$$

Hoewel dit een heel grove schatting is, blijkt de waarde die uit vergelijking (12.2) volgt wel ongeveer overeen te komen met wat we in de simulaties zien. We hebben dus onder andere gezien dat de geschatte magnetische veldsterkte evenredig is met de typische lengteschaal d. Naarmate de processen op grotere schaal plaatsvinden kan er dus (theoretisch) een sterker magnetisch veld gevormd worden. Door het gedrag van de geladen deeltjes volgens de plasmatheorie te bestuderen hebben we echter nog betere schattingen gemaakt van de verwachte magnetische veldsterkte.

Bij ons onderzoek hebben we deze processen wiskundig beschreven door de stroomdichtheidsverdeling te modelleren met een som van golfmodes (een *Fourier*-som). De stroomdichtheid van elke golfmode variëert als $\sin 2\pi x/\lambda$ met verschillende golflengte λ voor verschillende modes (de golflengte is de afstand tussen de pieken in figuur 12.2). Aan het begin van het proces groeien de fluctuaties in de stroomdichtheid onafhankelijk van naburige fluctuaties. In de wiskundige beschrijving komt dat overeen met golfmodes die onafhankelijk van elkaar in sterkte groeien (hoofdstukken 6 en 7). Zodra de fluctuaties elkaar echter gaan beïnvloeden komt dat er in de wiskundige beschrijving mee overeen dat de golfmodes met elkaar wisselwerken (hoofdstuk 9).

Uit onze berekeningen blijkt dat de in vergelijking (12.2) gegeven schatting voor de magnetische veldsterkte een bovengrens is. De geladen deeltjes raken namelijk gevangen in het magnetische veld dat ze zelf opwekken waardoor de instabiliteit en de bijgebehorende groei van de magnetische veldsterkte op een gegeven moment stopt.

Door de magnetische aantrekkingskracht kunnen de geproduceerde elektrische stromen echter nog wel groeien door met elkaar samen te smelten en zo de magnetische veldsterkte nog verder te vergroten. Toch zal dit samensmelten niet heel lang doorgaan. Het plasma werkt als een elektrische geleider die de neiging heeft de magnetische aantrekkingskracht af te schermen. Dit is met name van belang voor elektrische stromen die uit protonen bestaan. Door hun hoge massa kunnen protonen heel veel energie met zich mee dragen. Deze energie kunnen ze echter niet efficiënt omzetten in magnetische velden omdat de veel lichtere elektronen in het plasma heel sterk reageren op de magnetische velden die de protonen produceren. De elektronen schermen zo het magnetische veld van de protonbundels af en vertragen het samensmelten (zie hoofdstukken 8 en 9). Ook de protonbundels kunnen daardoor geen grote doorsnede bereiken en dat beperkt de magnetische veldsterkte, zoals gegeven door vergelijking (12.2).

In hoofdstukken 8 en 9 bespreken wij ook een belangrijk verschil tussen onze resultaten en die van eerdere onderzoeken zoals van Medvedev & Loeb [58]. In modellen zoals die van Medvedev & Loeb wordt aangenomen dat het magnetische veld uiteindelijk zo sterk wordt dat het de dynamica van de deeltjes in het plasma gaat overheersen en daaruit wordt dan een schatting voor de magnetische veldsterkte afgeleid. Onze resultaten tonen aan dat de effecten die ik in de vorige paragrafen heb beschreven al optreden voordat het magnetische veld totaaloverheersend wordt. Dit is een belangrijk gegeven alhoewel het de theorie van deze schokgolven wel complexer maakt: de door ons afgeleide effecten zullen er namelijk voor zorgen dat de deeltjes in het plasma turbulent of chaotisch gedrag gaan vertonen. Toekomstig onderzoek zal een uitgebreide analyse van dit laatste gedrag moeten uitvoeren.

12.6 Vergelijking met waarnemingen

Uit de waarnemingen van Gamma-ray Bursts en hun nagloeien kunnen we iets afleiden over de magnetische veldsterkte die in de relativistische schokken moet heersen. De intensiteit van de straling en de verdeling over de verschillende golflengten hangt daar namelijk mee samen. Het blijkt dat de schattingen op basis van de waarnemingen en die op basis van de theorie heel redelijk met elkaar overeenkomen.

Toch kunnen we nog niet zeggen dat we het probleem helemaal opgelost hebben. Naast de sterkte van het magnetische veld is ook de typische lengteschaal van belang voor de stralingsprocessen. Hoewel de processen die wij gesimuleerd hebben plaatsvinden op een schaal van kilometers, is dat in de

context van de sterrenkunde nog steeds heel klein.

Een tweede probleem is dat het magnetische veld, nadat het gevormd is, waarschijnlijk ook weer zal vervagen door chaotische processen in het plasma. Het is op dit moment nog niet duidelijk of dat zo snel gebeurt dat er niet genoeg straling gevormd kan worden om de waarnemingen te verklaren.

Een laatste open vraag betreft het effect van de aanwezigheid van deeltjes met verschillende massa's. Het meeste onderzoek op dit gebied heeft zich geconcentreerd op elektronenplasma's omdat de berekeningen het simpelst zijn als alle deeltjes dezelfde (elektron)massa hebben. In een realistisch model zouden echter ook zwaardere deeltjes zoals protonen opgenomen moeten worden. Deze gedragen zich echter heel anders dan de elektronen doordat zwaardere deeltjes trager reageren op de elektromagnetische krachten (zie ook hoofdstuk 8).

De oplossing voor deze problemen zal meer gedetailleerde simulaties en betere theoretische modellen vereisen voor de complexe processen die plaatsvinden na de eerste toename in magnetische veldsterkte. Om een echte schokgolf te vormen moet de kinetische energie van de deeltjes omgezet worden in warmte (en magnetische velden). Door de Weibel instabiliteit raken de deeltjes samengeklonterd in groepen en door de elektromagnetische interactie van deze groepen deeltjes kan warmte opgewekt worden. Dit is waarschijnlijk een turbulent proces en er zijn nog geen theoriën voor de details hiervan.

Er zouden misschien ook grootschaligere dynamoprocessen in de schokgolf op kunnen treden ten gevolge van turbulentie. Daarbij leiden wervelingen in het plasma tot de groei van magnetische velden.

Meer begrip van de rol van magnetisme in schokgolven is hoe dan ook nodig om de vorming van de straling die wij als Gamma-ray Bursts aan de hemel zien te begrijpen. Daarnaast zal deze kennis ook belangrijk zijn voor het onderzoek naar andere sterrenkundige fenomenen, zoals actieve sterrenstelsels (Active Galactic Nuclei) en pulsar winden, waarvan we ook vermoeden dat ze relativistische schokgolven veroorzaken. Om deze redenen verwacht ik dat dit onderzoeksveld nog lange tijd actief zal blijven.

Chapter 13

Curriculum Vitae

I was born in Bilthoven, in the centre of the Netherlands, on the seventh of May 1977, a mother's day gift to my mother. For a few years we continued living in Bilthoven and then moved to Hilversum, a few kilometers to the north. In Hilversum I attended the Gemeentelijk Gymnasium. My interest in astronomy started in those teen years.

In 1995 I started as a student at the faculty of Physics and Astronomy at the University of Utrecht. My intention was to take physics as my major because of the career prospects, but already in my second year I was pulled towards astrophysics mainly because astrophysics so elegantly blends multiple fields of physics. In January 2001 I graduated cum laude with a Master's degree in both Theoretical Physics and Theoretical Astrophysics neither of which has particularly good (commercial) career prospects :-).

I continued in Astrophysics as a PhD student until January 2006 and this thesis is the result of my research. During those years I also attended several conferences, two of which were held outside of the Netherlands: in Santa Fe (sunny, empty desert and thunderstorms) and in Rome (sunny, good food and wine, much traffic and soot). I also got married and was blessed with a daughter (chronologically in the opposite order).

At the time of printing this thesis I am no longer working in the field of astrophysics. Instead I am working as a software developer at a medium-sized software company in Utrecht that develops business-critical software for large insurance companies and banks.

Bibliography

[1] M. Abramowitz and I. A. Stegun. *Handbook of Mathematical Functions*. Dover Publications, New York, 1970.

[2] A. Achterberg. Covariant ponderomotive hamiltonian. *J. Plasma Phys.*, 35:257, 1986.

[3] A. Achterberg and J. Wiersma. The Weibel instability in relativistic plasmas I: Linear theory. Submitted to A&A, 2007.

[4] A. Achterberg, Y. A. Gallant, J. P. Rachen, C. A. Norman, and D. B. Melrose. Submitted to MNRAS, 2003.

[5] A. Achterberg, J. Wiersma, and C. A. Norman. The Weibel instability in relativistic plasmas II: Nonlinear theory and stabilization mechanism. Submitted to A&A, 2007.

[6] A. I. Akhiezer, I. A. Akhiezer, R. V. Polovin, A. G. Sitenko, and K. N. Stepanov. *Plasma Electrodynamics, v. 1. Linear theory*, volume 68 of *International series of monographs in natural philosophy*. Pergamon Press, Oxford, 1975. ISBN 0-08-017783-2.

[7] A. F. Alexandrov, L. S. Bogdankevich, and A. A. Rukhadze. *Principles of Plasma Electrodynamics*. Springer, 1984.

[8] R. D. Blandford and C. F. McKee. Fluid dynamics of relativistic blast waves. *Physics of Fluids*, 19(8):1130–1138, Aug. 1976.

[9] J. J. Brainerd. A plasma instability theory of Gamma-ray Burst emission. *ApJ*, 538:628–637, Aug. 2000.

[10] A. Bret, M.-C. Firpo, and C. Deutsch. Bridging the gap between two stream and filamentation instabilities. *Laser and Particle Beams*, 23:375–383, 2005.

[11] F. Califano, F. Pegoraro, S. V. Bulanov, and A. Mangeney. Kinetic saturation of the Weibel instability in a collisionless plasma. *Physical Review E*, 57(6):7048–7059, June 1998.

[12] F. Califano, T. Cecchi, and C. Chiuderi. Nonlinear kinetic regime of the Weibel instability in an electron-ion plasma. *Physics of Plasmas*, 9(2):451–457, Feb. 2002.

[13] J. R. Cary and A. N. Kaufman. Ponderomotive effects in collisionless plasma: a Lie transform approach. *Physics of Fluids*, 24:1238–1250, July 1981.

[14] E. Costa, F. Frontera, J. Heise, M. Feroci, J. in 't Zand, F. Fiore, M. N. Cinti, D. dal Fiume, et al. Discovery of an X-ray afterglow associated with the gamma-ray burst of 28 February 1997. *Nature*, 387:783–785, June 1997.

[15] S. Dado, A. Dar, and A. D. Rújula. On the optical and X-ray afterglows of gamma ray bursts. *A&A*, 388:1079–1105, 2002. On the cannonball model.

[16] R. C. Davidson, D. A. Hammer, I. Haber, and C. E. Wagner. Nonlinear development of electromagnetic instabilities in anisotropic plasmas. *Physics of Fluids*, 15 (2):317–333, Feb. 1972.

[17] R. J. Davidson. *Methods in Nonlinear Plasma Theory*. Academic Press, New York, Feb. 1972.

[18] R. L. Dewar. Energy-momentum tensors for dispersive electromagnetic waves. *Aust. J. Phys.*, 30:533–575, 1977.

[19] B. T. Draine and C. F. McKee. Theory of interstellar shocks. *ARA&A*, 31:373–432, 1993.

[20] D. Eichler and E. Waxman. The efficiency of electron acceleration in collisionless shocks and Gamma-ray Burst energetics. *ApJ*, 627:861–867, July 2005.

[21] R. A. Fonseca, L. O. Silva, J. W. Tonge, W. B. Mori, and J. M. Dawson. Three-dimensional Weibel instability in astro-physical scenarios. *Physics of Plasmas*, 10 (5):1979–1984, May 2003.

[22] D. B. Fox, D. A. Frail, P. A. Price, S. R. Kulkarni, E. Berger, T. Piran, A. M. Soderberg, S. B. Cenko, et al. The afterglow of GRB 050709 and the nature of the short-hard γ-ray bursts. *Nature*, 437:845–850, Oct. 2005.

[23] D. A. Frail, S. R. Kulkarni, L. Nicastro, M. Feroci, and G. B. Taylor. The radio afterglow from the γ-ray burst of 8 May 1997. *Nature*, 389:261–263, Sept. 1997.

[24] J. T. Frederiksen, C. B. Hededal, T. Haugbølle, and Å. Nordlund. Magnetic field generation in collisionless shocks: pattern growth and transport. *ApJ*, 608:L13–L16, June 2004.

[25] B. D. Fried. Mechanism for instability of transverse plasma waves. *Physics of Fluids*, 2:337, 1959.

[26] Y. Fujita and T. Kato. A possible origin of magnetic fields in galaxies and clusters: strong magnetic fields at $z \sim 10$? *MNRAS*, 364:247–252, 2005.

[27] T. J. Galama, P. M. Vreeswijk, J. van Paradijs, C. Kouveliotou, T. Augusteijn, H. Bohnhardt, J. P. Brewer, V. Doublier, et al. An unusual supernova in the error box of the gamma-ray burst of 25 April 1998. *Nature*, 395:670–672, 1998.

[28] A. A. Galeev and R. Z. Sagdeev. Nonlinear plasma theory. In M. A. Leontovich, editor, *Reviews of Plasma Physics*, volume 7, page 1. Consultants Bureau, New York, 1979.

[29] N. Gehrels, G. Chincarini, P. Giommi, K. O. Mason, J. A. Nousek, A. A. Wells, N. E. White, S. D. Barthelmy, et al. The Swift Gamma-Ray Burst Mission. *ApJ*, 611:1005–1020, Aug. 2004.

[30] J. Granot and A. Königl. Radiative hydromagnetic shocks in relativistic outflow sources. *ApJ*, 560:145–159, Oct. 2001.

[31] A. Gruzinov. Gamma-ray Burst phenomenology, shock dynamo, and the first magnetic fields. *ApJ*, 563:L15–L18, Dec. 2001.

[32] A. Gruzinov and E. Waxman. Gamma-ray burst afterglow: Polarization and analytic light curves. *ApJ*, 511:852–861, Feb. 1999.

[33] T. Haruki and J.-I. Sakai. Generation of magnetic field and electrostatic shock wave driven by counterstreaming pair plasmas. *Physics of Plasmas*, 10(2):392–397, Feb. 2003.

[34] T. Haugbølle. *Modelling Relativistic Astrophysics and the Large and Small Scale*. PhD thesis, University of Copenhagen, Denmark, May 2005.

[35] C. B. Hededal. *Gamma-ray Bursts, Collisionless Shocks and Synthetic Spectra*. PhD thesis, University of Copenhagen, Denmark, May 2005.

[36] C. B. Hededal and K.-I. Nishikawa. The influence of an ambient magnetic field on relativistic collisionless plasma shocks. *ApJ*, 623:L89–L92, Apr. 2005.

[37] J. Hjorth, J. Sollerman, P. Møller, J. P. U. Fynbo, S. E. Woosley, C. Kouveliotou, N. R. Tanvir, J. Greiner, et al. A very energetic supernova associated with the γ-ray burst of 29 March 2003. *Nature*, 423:847–850, June 2003.

[38] M. Hoshino, J. Arons, Y. A. Gallant, and A. B. Langdon. Relativistic magnetosonic shock waves in synchrotron sources: shock structure and nonthermal acceleration of positrons. *ApJ*, 390:454–479, May 1992.

[39] K. Hurley, S. E. Boggs, D. M. Smith, R. C. Duncan, R. Lin, A. Zoglauer, S. Krucker, G. Hurford, et al. An exceptionally bright flare from SGR 1806-20 and the origins of short-duration γ-ray bursts. *Nature*, 434:1098–1103, Apr. 2005.

[40] S. Ichimaru. *Basic Principles of Plasma Physics: A Statistical Approach*. W.A. Benjamin Inc., Reading, Ma., USA, 1973. ISBN 0805387536.

[41] J. D. Jackson. *Classical Electrodynamics*. John Wiley & Sons, New York, second edition, 1975. ISBN 0-471-43132-X.

[42] C. H. Jaroschek, H. Lesch, and R. A. Treumann. Self-consistent diffusive lifetimes of Weibel magnetic fields in Gamma-ray Bursts. *ApJ*, 616:1065–1071, Dec. 2004.

[43] B. B. Kadomtsev. *Plasma Turbulence*. Academic Press, London, 1965.

[44] T. N. Kato. Saturation mechanism of the Weibel instability in weakly magnetized plasmas. *Physics of Plasmas*, 12:080705, Aug. 2005.

[45] Y. Kazimura, J. I. Sakai, T. Neubert, and S. V. Bulanov. Generation of a small-scale quasi-static magnetic field and fast particles during the collision of electron-positron plasma clouds. *ApJ*, 498:L183–L186, May 1998.

[46] C. F. Kennel and F. V. Coroniti. Confinement of the crab pulsar's wind by its supernova remnant. *ApJ*, 283:694–709, Aug. 1984.

[47] J. G. Kirk and P. Duffy. Particle acceleration and relativistic shocks. *J. Phys. G: Nucl. Part. Phys.*, 25:R163–R194, 1999. Topical Review.

[48] D. Q. Lamb, G. R. Ricker, J.-L. Atteia, C. Barraud, M. Boër, J. Braga, N. Butler, T. Cline, et al. Scientific highlights of the HETE-2 mission. *Nuclear Physics B Proceedings Supplements*, 132:279–288, June 2004.

[49] L. D. Landau and E. M. Lifschitz. *Fluid Mechanics*. Pergamon Press, Oxford, 1975. ISBN 0-08-091040-8.

[50] L. D. Landau and E. M. Lifschitz. *The Classical Theory of Fields*. Pergamon Press, Oxford, fourth edition, 1975. ISBN 0080181767.

[51] D. Lazzati. A certain flare. *Nature*, 434:1075–1076, Apr. 2005.

[52] R. Lee and M. Lampe. Electromagnetic instabilities, filamentation and focusing of relativistic electron beams. *Physical Review Letters*, 31(23):1390–1393, Dec. 1973.

[53] A. Lichnerowicz. *Relativistic Hydrodynamics and Magnetohydrodynamics*. W. A. Benjamin, Inc., New York, 1967.

[54] A. S. Lipatov. *The Hybrid Multiscale Simulation Technology*. Springer, 2002. ISBN 3-540-41734-6.

[55] Lyubarsky and Eichler. Are gamma-ray burst shocks mediated by the weibel instability? *ApJ*, 647:1250–1254, 2006.

[56] M. V. Medvedev. Theory of "jitter" radiation from small-scale random magnetic fields and prompt emission from gamma-ray burst shocks. *ApJ*, 540:704–714, 2000.

[57] M. V. Medvedev. Weibel turbulence in laboratory experiments and GRB/SN shocks. Astrophysics and Space Science, Online First, Jan. 2007.

[58] M. V. Medvedev and A. Loeb. Generation of magnetic fields in the relativistic shock of gamma-ray burst sources. *ApJ*, 526:697–706, Dec. 1999.

[59] M. V. Medvedev, M. Fiore, R. A. Fonseca, L. O. Silva, and W. B. Mori. Long-time evolution of magnetic fields in relativistic Gamma-ray Burst shocks. *ApJ*, 618: L75–L78, Jan. 2005.

[60] D. Melrose. *Instabilities in Space and Laboratory Plasmas*. Cambridge University Press, 1986. ISBN 0-521-30541-1.

[61] D. B. Melrose. Quantum plasma dynamics, 2001. URL `http://www.physics.usyd.edu.au/~melrose/qpd.html`.

[62] D. B. Melrose. A covariant formulation of wave dispersion. *Plasma Phys.*, 15: 99–106, 1973.

[63] D. B. Melrose. *Plasma Astrophysics: Nonthermal Processes in Diffuse Magnetized Plasmas*, volume 1. Gordon and Breach Publ., New York, 1980. ISBN 0677034903.

[64] P. Mészáros. Gamma-ray bursts: Accumulating afterglow implications, progenitor clues, and prospects. *Science*, 291:79–84, Jan. 2001.

[65] P. Mészáros. Theories of gamma-ray bursts. *ARA&A*, 40:137–169, 2002. Review of fireball shock model.

[66] P. Mészáros. Gamma-ray bursts. *Rep. Prog. Phys.*, 69:2259–2321, 2006.

[67] M. Milosavljević and E. Nakar. The cosmic ray precursor of relativistic collisionless shocks: a missing link in Gamma-ray Burst afterglows. *ApJ*, 651:979–984, Nov. 2006.

[68] M. Milosavljević, E. Nakar, and A. Spitkovsky. Steady state electrostatic layers from Weibel instability in relativistic collisionless shocks. *ApJ*, 637:765–773, Feb. 2006.

[69] K.-I. Nishikawa, P. Hardee, G. Richardson, R. Preece, H. Sol, and G. J. Fishman. Particle acceleration in relativistic jets due to weibel instability. *ApJ*, 595:555–563, Sept. 2003.

[70] N. Okabe and M. Hattori. Spontaneous generation of the magnetic field and suppression of the heat conduction in cold fronts. *ApJ*, 599:964–970, Dec. 2003.

[71] A. Pais. *Subtle is the Lord: The Science and the Life of Albert Einstein*. Oxford University Press, 1983. ISBN 0-19-520438-7.

[72] A. Panaitescu and P. Kumar. Properties of relativistic jets in Gamma-ray Burst afterglows. *ApJ*, 571:779–789, June 2002.

[73] P. O. Petrucci, G. Henri, and G. Pelletier. Pair creation at shocks: Application to the high energy emission of compact objects. *A&A*, 374:719–732, 2001.

[74] T. Piran. Gamma-ray bursts – a puzzle being resolved. *Physics Reports*, 333: 529–553, 2000.

[75] T. Piran. The physics of gamma-ray bursts. *Rev. Mod. Phys.*, 76:1143–1210, Oct. 2004.

[76] T. Piran. Gamma-ray Bursts and the fireball model. *Physics Reports*, 314:575–667, 1999.

[77] L. Piro. Short-burst sources. *Nature*, 437:822–823, Oct. 2005.

[78] D. Potter. *Computational Physics*. John Wiley & Sons, New York, 1973. ISBN 0-471-69555-6.

[79] M. J. Rees and P. Mészáros. Relativistic fireballs: energy conversion and time-scales. *MNRAS*, 258:41P, Sept. 1992.

[80] M. J. Rees and P. Mészáros. Unsteady outflow models for cosmological gamma-ray bursts. *ApJ*, 430:L93–L96, Aug. 1994.

[81] P. H. Roberts. *An Introduction to Magnetohydrodynamics*. Longmans, Green and Co. Ltd, London, 1967.

[82] R. Z. Sagdeev. Cooperative phenomena and shock waves in collisionless plasmas. *Reviews of Plasma Physics*, 4:23–91, 1966.

[83] R. Sari, T. Piran, and J. Halpern. Jets in gamma-ray bursts. *ApJ*, 519:L17–L20, July 1999.

[84] U. Schaefer-Rolffs, I. Lerche, and R. Schlickeiser. The relativistic kinetic weibel instability: General arguments and specific illustrations. *Physics of Plasmas*, 13: 012107, 2006.

[85] R. Schlickeiser. Nonthermal radiation from jets of active galactic nuclei: Electrostatic bremsstrahlung as alternative to synchrotron radiation. *A&A*, 410:397–414, 2003.

[86] R. Schlickeiser. Covariant kinetic dispersion theory of linear waves in anisotropic plasmas. I. *Physics of Plasmas*, 11(12):5532–5546, Dec. 2004.

[87] R. Schlickeiser and P. K. Shukla. Cosmological magnetic field generation by the Weibel instability. *ApJ*, 599:L57–L60, Dec. 2003.

[88] R. Schlickeiser, R. Vainio, M. Böttcher, I. Lerche, M. Pohl, and C. Schuster. Conversion of relativistic pair energy into radiation in the jets of active galactic nuclei. *A&A*, 393:69–87, 2002.

[89] L. O. Silva, R. A. Fonseca, J. W. Tonge, W. B. Mori, and J. M. Dawson. On the role of the purely transverse Weibel instability in fast ignitor scenarios. *Physics of Plasmas*, 9(6):2458–2461, June 2002.

[90] A. Spitkovsky and J. Arons. Time dependence in relativistic collisionless shocks: theory of the variable "wisps" in the Crab nebula. *ApJ*, 603:669–681, Mar. 2004.

[91] R. C. Tautz and R. Schlickeiser. Counterstreaming magnetized plasmas. II. perpendicular wave propagation. *Physics of Plasmas*, 13:062901, 2006.

[92] D. A. Tidman and N. A. Krall. *Shock Waves in Collisionless Plasmas*. Wiley-Interscience, New York, 1971.

[93] B. T. Tsurutani and R. G. Stone, editors. *Collisionless Shocks in the Heliosphere: Reviews of Current Research*, volume 35 of *Geophysical Monograph*. American Geophysical Union, 1985.

[94] J. van Paradijs, P. J. Groot, T. Galama, C. Kouveliotou, R. G. Strom, J. Telting, R. G. M. Rutten, G. J. Fishman, et al. Transient optical emission from the error box of the gamma-ray burst of 28 February 1997. *Nature*, 386:686–689, 1997.

[95] J. Vink. Shocks and particle acceleration in supernova remnants: observational features. *Advances in Space Research*, 33(4):356–365, 2004.

[96] E. Waxman. Gamma-ray-burst afterglow: supporting the cosmological fireball model, contraining parameters, and making predictions. *ApJ*, 485:L5–L8, Aug. 1997.

[97] M. S. Wei, F. N. Beg, A. E. Dangor, A. Gopal, M. Tatarakis, K. Krushelnick, E. L. Clark, P. A. Norreys, et al. Experimental observations of the Weibel instability in high intensity laser solid interactions. *Annual Report of Central Laser Facility, Rutherford Appleton Laboratory*, pages 7–9, 2001/2002.

[98] E. S. Weibel. Spontaneously growing transverse waves in a plasma due to an anisotropic velocity distribution. *Physical Review Letters*, 2(3):83–84, Feb. 1959.

[99] J. Wiersma. *Magnetic fields inside extremely fast shock waves*. PhD thesis, University of Utrecht, The Netherlands, May 2007.

[100] J. Wiersma and A. Achterberg. Magnetic field generation in relativistic shocks - an early end of the exponential weibel instability in electron-proton plasmas. *A&A*, 428:365–371, Dec. 2004.

[101] J. Wiersma and A. Achterberg. Particle-In-Cell simulations of the Weibel instability. To be submitted to A&A, 2007.

[102] R. A. M. J. Wijers and T. J. Galama. Physical parameters of GRB 970508 and GRB 971214 from their afterglow synchrotron emission. *ApJ*, 523:177–186, Sept. 1999.

[103] R. A. M. J. Wijers, M. J. Rees, and P. Mészáros. Shocked by GRB 970228: the afterglow of a cosmological fireball. *MNRAS*, 288:L51–L56, 1997.

[104] T.-Y. B. Yang, J. Arons, and A. B. Langdon. Evolution of the Weibel instability in relativistically hot electron-positron plasmas. *Physics of Plasmas*, 1(9):3059–3077, Sept. 1994.

[105] P. H. Yoon and R. C. Davidson. Exact analytical model of the classical weibel instability in a relativistic anisotropic plasma. *Physical Review A*, 35(6):2718–2721, Mar. 1987. Brief report.

Index